Development of Fluorescent Nanoparticles 'Quantum Dots' for Biomedical Application

Shirin Ghaderi

UCL Center for Nanotechnology and Regenerative Medicine
Division of Surgery & Interventional Sciences
University College London

Submitted in fulfillment of the requirements for the

degree of Doctor of Philosophy for the University College London

2012

Declaration of Originality:

I, Shirin Ghaderi, certify that the work presented in this thesis is my own. Where information has been derived from other sources, I confirm that this has been indicated in the thesis.

Signature:

Abstract

Quantum dots (QDs) are semiconductor nanocrystals (<100 nm), which are emerging as a novel class of multifunctional fluorescent probes for many potential biological and medical applications. In comparison to conventional organic fluorescent probes (organic dyes), QDs have substantial advantages, such as, bright fluorescence, narrow emission, broadband excitation, photostability and extended half-life. Imaging with diagnostic assessment, plays an important part in clinical settings for determining disease (cancer) progression and therapy. However, current imaging techniques have certain limitations, and they include insufficient sensitivity to detect low numbers of cancer cells at primary or metastatic sites and appropriate probes to detect specific cancer cell surface markers.

To address these limitations, studies were conducted (1) to develop an aqueous synthesis of a series of near infrared (NIR) QDs, incorporating cadmium (Cd), tellurium (Te), cobalt (Co) and mercury (Hg) in its core (2) to minimize its potential toxicities, by developing coating strategies with a novel coating nanomaterial, mercaptopolyhedral oligomeric silsequioxane (MPOSS) while maintaining strong emission, stability and biocompatibility, (3) to apply conjugated NIR QDs as probes in targeting and detecting immunogenic apoptosis in cancer cells *in vitro* and mapping biodistribution *in vivo.*

The inclusion of mercury (Hg $(ClO_4)_2$) and cobalt (Co) to the QD core resulted in NIR emission at 800 nm with paramagnetic properties. Characterization by transmission electron microscopy (TEM) confirmed size of the QDs. Detoxification of QDs was demonstrated, by toxicity studies, using two different vital stains, Alamar Blue and Neutral Red on human umbilical vein endothelial cells (HUVECs), human breast cancer cells (MCF-7), colorectal cancer cells (SW620) and prostate cancer cells (PC3). A short synthetic peptide to calreticulin (CRT) was chemically synthesised and antibodies generated against the peptide (Anti-CRT) with specificity to the native CRT protein (a cancer cell immunogenic apoptosis marker). The presence of functional groups on the coatings of QDs provided an additional advantage for conjugation to Anti-CRT for targeting, and carbon nanotubes (CNT) for thermal strategy.

QDs conjugated to Anti-CRT showed specificity to cancer cells *in vitro* undergoing apoptosis when exposed to the following: 1) Doxorubicin (an anticancer drug), 2) cadmium and 3) QD-CNT (photothermal effect). Characterization by Fourier Transform Infrared Spectrophotometry (FTIR) confirmed conjugation of QDs to Anti-CRT. Confocal microscopy images further confirmed targeted and non-targeted QDs *in vitro*, and NIR sensitive camera for *in vivo* imaging.

These studies and findings demonstrate the feasibility of applying these engineered nanocrystals for clinical diagnostics, drug delivery and therapy.

Acknowledgements

Writing this thesis has certainly been a long and arduous journey, but it would not have ‘been’ at all possible were it not for the help and support of a rather special group of people.

I would like to begin by thanking my supervisor Professor Alexander Seifalian for his expert supervision, guidance and support throughout the length of this study.

I would also like by thanking Dr. Bala Ramesh for his encouragement and continuous expert, advice and help throughout the many experiments undertaken. My thanks also extend to Dr. Marilena Loizidou for her guidance and above all, moral support.

Many thanks also go to, all my friends and fellow colleagues in the Department of Surgery and Interventional Science for the help and support they have given me. I would like to mention Mr Behfar Moghaddam in particular, with whom I spent many long hours to format this thesis.

Finally, I would like to dedicate this thesis to my family, without their endless love, support and encouragement, the completion of this thesis would have not been possible.

Table of contents

List of Abbreviations:

Å	Angstrom
Ab	Absorption
AFP	Alpha-fetoprotein
ATCC	American type cell culture
BBB	Blood brain barrier
BRET	Bioluminescence resonance energy transfer
CaF_2	Calcium fluoride
CCM	Cell culture medium
Cd	Cadmium
$CdCl_2$	Cadmium chloride
CdSe	Cadmium selenide
CdTe	Cadmium telluride
CLSM	Confocal laser scanning microscopy
CNT	Carbon nanotube
CO_2	Carbon dioxide
CRT	Calreticulin
D_2O	Deuterium oxide
DCCI	N-(3-Dimethylaminopropyl)-N´-ethylcarbodiimide hydrochloride
DIC	Differential interference contrast
DLS	Dynamic light scattering
DMEM	Dulbecco's modified eagle medium
EBR	Exciton bohr radius
EDTA	Ethylenediaminetetraacetic acid
EPR	Enhanced permeability retention
FISH	Fluorescence *in situ* hybridization

FRET	Fluorescence resonance energy transfer
FTIR	Fourier transform infrared
FWHM	Full width half max
HCl	Hydrogen chloride
hMSC	Human mesenchymal stem cell
HPLC	High-performance liquid chromatography
HUVECs	Human umbilical vein endothelial cancer cells
ICP-MS	Inductively coupled plasma mass spectrometry
IHC	Immunohistochemistry
IVD	Intravenously delivered
LPS	Lipopolysaccharide
MCF-7	Michigan cancer foundation - 7
MMP	Methyl morpholine
MPOSS	Mercaptopolyhedral oligomeric silsesquioxanes
MRI	Magnetic resonance imaging
MSA	Mercaptosuccinic acid
MUA	Mercarptoundecanoic acid
$Na_2B_4O_7$	Sodium borate
Na_2TeO_3	Sodium telluride
$NaBH_4$	Sodium borohydride
NaHTe	Sodium hydrogen telluride
ng	Nanogram
NIR	Near infrared
nm	Nanometre
PBS	Phosphate buffered saline
PBS/T	PBS/Tween20
PC3	Prostate cancer cells

PCD	Programmed cell death
PDT	Photodynamic therapy
PEG	Poly ethylene glycol
PET	Positron emission tomography
PL	Photoluminescence
PMT	Photomultiplier
PS	Photosensitiser
PTD	Protein transduction domain
PU	Polyurethane
QC	Quantum confinement
QD	Quantum dot
QY	Quantum yield
RES	Reticuloendothelial system
ROS	Reactive oxygen species
SD	Standard deviation
Se	Selenium
Si	Silicon
SLN	Sentinel lymph node
SPECT	Single photoemissions computed tomography
SPIO	Superparamagnetic iron oxide
SSA	Sheep serum albumin
SW620	Colorectal cancer cells
Te	Tellurium
TEM	Transmission electron microscopy
TFA	Trifluoroacetic acid
TGA	Thioglycolic acid
TOPO	Trioctylphosphine oxide

UV	Ultra violet
XRD	X-ray diffraction
ZnS	Zinc sulphide

List of Figures:

List of Tables:

Chapter 1

Introduction: Applications of semiconductor nanoparticles in biology and medicine

1.1. Nanoparticles: An overview

Nanomaterials are at the cutting edge of the rapidly developing field of nanotechnology. Nanoparticles (Appenzeller, 1991, Shirin Ghaderi, 2012) specifically have great potential in medical diagnostics and targeted therapeutics since they have unique characteristics that can be used in medicine, biological products, pharmaceutics, industries and cosmetics. Nanoparticles can be organic or inorganic and examples include fullerenes, buckyballs, carbon nanotubes (CNT), liposomes, nanoshells, dendrimers, quantum dots (QDs), superparamagnetic, gold, and silver nanoparticles. These nanoparticles are expected to bring great benefits as applied to biomedicine in areas as diverse as diagnosis and treatment of disease. Potential applications in the field of medicine include drug delivery, clinical diagnostics, diet industry and improved biocompatible materials. Nanomaterials are potential tools that can facilitate some of these applications (Alivisatos et al., 2005).

Semiconductor and metal nanoparticles in the 2-10 nm size range have aroused great interest due to their unique size-dependent properties, which happen to also have similar dimensions to biological macromolecules (e.g. proteins and nucleic acids) (de Mel et al., 2012). This has added advantages in that, the similarities allow integration of nanotechnology and biology, thus promoting great advances in cell biology, molecular biology, targeted therapeutics and medical diagnostics. Current development in this field has allowed the linking of colloidal nanoparticles to nanoparticles (e.g. QDs, CNTs) (Bifeng Pan, 2006) and to biomolecules such as proteins (John P. Zimmer, 2000) peptides (Whaley et al., 2000) DNA (Pathak et al., 2001). These nanosized bioconjugates are used in the construction of hybrid materials for the development of multicolour fluorescent probes and bioassays (Dubertret et al., 2001) for ultrasensitive detection and imaging (Bentolila et al., 2005). This brief introduction will highlight recent developments of nanomaterials as applied to biology and medicine and the associated synthesis, optical properties, and biological applications.

Semiconductor nanocrystals are also known as QDs and are often assembled from atoms from groups II-VI or III-V elements in the periodic Table. These particles when compared to their bulk have smaller exciton Bohr radius (EBR) that describes their definition (Zhou and Ghosh, 2007). This imposes what is described as quantum confinement (QC) when special optical and electronic properties are produced

compared to bulk. Major development in the past has concentrated on the photophysics of nanostructures mainly in microelectronics and optoelectronics (Alivisatos, 1996). However there has been great interest in developing nanoparticles for biological and medical applications (Klarreich, 2001, Rizvi et al., 2010). The key development that has allowed these applications are the advances in the synthesis of highly luminescent QDs with high yields, comprehending complex surface chemistry, adaptation to water solubility, biocompatibility and multicolour emission for multiplex optical detection of biomolecules. Recent developments have introduced multifunctional QDs for molecular and cellular imaging, nanoparticle drugs for targeted therapy, disease screening, detection and diagnosis (Shirin Ghaderi, 2012). Figure **1.1** illustrates the basic structure of a semiconductor based QD (cadmium–telluride, CdTe).

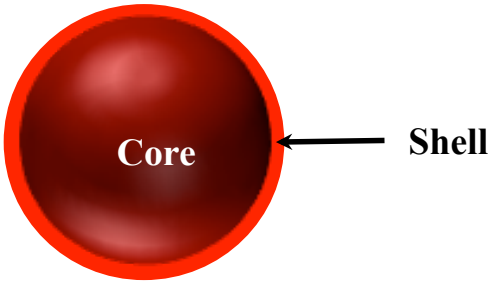

Figure 1.1: Basic structure of an uncoated QD.

1.2. Optical properties

QDs have demonstrated significant advantages over traditional organic dyes and fluorescent proteins. As the QDs are assembled from semiconductor materials, their optical properties are influenced by the interactions between electrons, holes and environments. Semiconductor materials absorb photons when the energy of absorbance exceeds the difference of the valence and conduction band energy (band gap) (details in chapter 2). During this stage, electrons in the valence band are elevated to the conduction band leaving a 'hole'. Light emission arises from the recombination of the returning electron and hole (exciton). By controlling the size, coating and composition of QDs, the emission wavelength can be tuned from the blue (ultraviolet) to the near infrared (NIR) region (Alivisatos et al., 2005, Aswathy et al., 2010). They can be stimulated to emit multicolour fluorescence with a single light source, with minimal spectral overlap, contributing to significant advantage for molecular multi-target imaging.

1.2.1. *In vitro* and *in vivo* imaging

The above-described properties of QDs are most promising for enhancing the sensitivity and the multiplexing capabilities of molecular histopathology and disease diagnosis. Recent developments in QDs have produced very bright and stable probes that have found applications in profiling genetic and protein biomarkers in intact cells and clinical tissue specimens. Because of inherent potential toxicity QDs have been generally excluded from a *in vivo* imaging applications. However, the use in immunohistological studies has found favour on *in vitro* or *ex vivo* clinical specimens. The utilization of multicolour QD probes in immunohistochemistry (IHC) will be a major contribution in clinical diagnostics in the coming years.

In vivo imaging has traditionally used contrast agents as imaging probes that include radioisotope small molecules in positron emission tomography (PET) and single photoemissions computed tomography (SPECT), gadolinium compounds in magnetic resonance imaging (MRI), and isotope conjugated antibodies. The unique features of bioconjugated targeted QDs however can provide extraordinary capabilities that could enhance the sensitivity and specificity of diseased tissues and improve diagnosis. The inherent, size dependent optical and electronic features of QDs can be manipulated continuously by altering the particle size. This tunability feature facilitates the use of a broadband range of QDs, for simultaneous detection of multiple cancer cell surface biomarkers. Additionally the large surface to volume ratio of QDs allows multifunctional groups suitable for conjugation with multiple diagnostic (magnetic, NIR and radioisotope) and therapeutic (e.g. anticancer) ligands. This allows the development and design of multifunctional "intelligent" nanocrystals for multi-modal imaging combining therapy. There is evidence that nanoparticle in the range of 10-100 nm preferentially concentrate at tumour sites through a phenomena defined as enhanced permeability retention (EPR) (Sinha et al., 2006).

1.3. Nano-drugs

Developing QDs as drugs and additional to drug delivery carriers and targeting probes is challenging and important in the arena of nanotechnology. Introducing nanosize range has improved the efficacy and toxicity profile of chemotherapeutic drugs by virtue of their desirable surface properties. Additionally it facilitates dispersibility of drugs that are otherwise poorly soluble in aqueous medium. Traditional drug formulations suffer from bioavailability with poor release mechanisms.

1.4. Synthesis

Various approaches to synthesis of QDs have been attempted. Traditionally their synthesis has been carried out in organic solvents such as toluene or chloroform at high temperatures in the presence of surfactants (Shirin Ghaderi, 2012). This method produced hydrophobic nanocrystals due to surface modifications, which are incompatible with aqueous biological environment (Smith et al., 2006). In biological environment, water is the main solvent and water-soluble nanocrystals will be an attractive proposition. To take full advantage of their optical properties for biosensing and bioimaging applications, they must possess minimum toxicity and monodispersible in aqueous biological environments. Novel strategies have been developed to make them water soluble and biocompatible, whereby the surface layer is exchanged or additional layer added with hydrophilic properties. These include the adsorption of small molecules such as mercaptoacetic acid or cysteine to QD surface (Jin et al., 2008) silica (Bharali et al., 2005) or wrapping within micelles (Maysinger et al., 2007), liposomes (Schroeder et al., 2007) and amphiphilic polymers. To overcome, the bioincompatibility and instability, development in hybrid coatings have been investigated in the followings studies. The hydrophilic coatings may have reactive functional groups for binding to the core at one end and for conjugation at the other end. These allow conjugation to specific molecules for *in vitro* and *in vivo* targeted delivery and imaging.

1.5. Conclusions

In summary, the advent of semiconductor fluorescent nanocrystals QDs as a new class of molecular imaging agents has made a great impact in medical research and new applications are continually developed. With suitable novel coatings the QD is now presented as a basic building block for further fabrication of multifunctional nanostructures and nano-devices. Multifunctional imaging probes can be constructed by incorporating QDs with NIR emission, paramagnetic or super-paramagnetic nanomaterials. Indeed, this laboratory has incorporated into its NIR QD core, cobalt (Co) for imaging purposes. Imaging deep tissues with suitable ultrasensitive optical imaging, tiny tumours could be visually identified with complete removal by surgeons. Medical imaging technology such as PET and X-ray can locate tumour and disease noninvasively and also provide visual guidance during surgery. The optimistic success currently observed with QDs in terms of toxicity reduction, and added multimodality can only further progress biomedical applications in order to understand the entire aspect of QDs for clinical usage.

This thesis presents an in depth background chemistry of QD synthesis and its applications, followed by specific aims and description of the work undertaken. Results and relevant discussions are presented in specific chapters and an overall discussion outlines the way forward in this exciting field.

Chapter 2

A critical review on development of 'Quantum Dot' nanoparticles and their biomedical applications

Published papers relating to this chapter:

GHADERI, S., RAMESH, B. & SEIFALIAN, A. M. 2011. Fluorescence nanoparticles "quantum dots" as drug delivery system and their toxicity: a review. *Journal of drug targeting*, 19, 475-86.

RIZVI, S. B., GHADERI, S., KESHTGAR, M. & SEIFALIAN, A. M. 2010. Semiconductor quantum dots as fluorescent probes for in vitro and in vivo bio-molecular and cellular imaging. *Nano Rev,* 1, 5161-76.

2.1. Introduction (quantum dots and nanotechnology)

The primary aim of this introduction is to explain key concepts of nanoscience and nanotechnology with its basic theoretical underpinnings. Many of scientists will see the tremendous applications of such technologies within our lifetimes, and various technologies are already on the market today. Because of their impact, a basic understanding of nanoscience and nanotechnology and how it affects our lives is presented.

Nanoparticles ('The Science') as nanoscience is defined as the study of materials at length scales smaller than those where conventional physics (classical) apply (less than 1 μm) but larger than those where atomic physics dominate (more than a few tenths of a nanometer). It incorporates contributions from many scientific disciplines, including biology, chemistry, physics, optics, engineering, computer sciences and mathematics.

Nanoparticles ('The Technology') as nanotechnology are defined as the application of nanoscience by practical engineering of structures at the nanoscale level and integrating them into materials, devices and products. There is not a definite length scale defining nanoscience and nanotechnology, but it typically ranges from several tenths of a nanometer to several hundred nanometers.

Currently, nanoparticles in the size range of 0.1 nm to 500 nm have received enormous attention from both science and industry, as new information about these particles and their potential benefits are established. Nanoparticles can be classified into three major groups, namely (1) natural, (2) incidental and (3) engineered (**Table 1**).

Table 2.1: Some major groups of nanotparticles.
They can be divided into three groups: (1) nanoparticles occurring naturally such as volcanic, (2) nanoparticles happening accidently such as mining and (3) engineered nanoparticles such as quantum dots.

Natural	Ocean spray, meteorite, volcanic ash, Biogenic magnetite: mollusks, bacteria, arthropods, fish, birds and brain
Incidental	Combustion products, frying, cooking, sandblasting, mining, metal working, biomaterial degradation
Engineered	QDs, CNTs, fullerenes, semiconductor wires, sun screen pigments

Naturally-occurring nanomaterials such as volcanic ash, ocean spray, magnetotactic bacteria, mineral composites, and others are ubiquitously found in the environment. Incidental nanoparticles are often the end-products of the manufacturing industries. The

engineered nanoparticles include materials that are specifically designed for function, such as fullerene (C_{60}) used in fuel cell technology and semiconductors for the electronic and solar cell technology.

As mentioned earlier, nanotechnology has a broad description, in that the processes and the technologies applied produce materials that are deliberately engineered by the manipulation of atoms. The main criterion for nanotechnology is that any chemically stable structure that does not violate existing laws of physics can be manipulated and engineered. By exploiting the basic properties of atoms, products with less bulkiness, with strong structure have been created and applied appropriately.

There are four basic groups of nanoscale materials that are commercially available. They are metal oxides, nanoclays, nanotubes and QDs or nanocrystals. The metal oxides include ceramics from oxides of zinc, iron, cerium and zirconium. Also chemical polishing material from semiconductor wafers; including scratch resistant coatings for glass, cosmetics and sunscreens are the major products incorporating nanomaterials.

Nanoclays are naturally found as plate-like clay particles that enhance strength, hardness, heat resistance and flame retardant of materials, also barrier films in plastic beverage bottles, paper juice cartons and tennis balls.

Nanotubes are incorporated in coatings to dissipate and reduce static electricity in fuel lines and hard disk handling trays. They are also part of flame retardant fillers for plastics, and field emitter sources in flat panel displays.

QDs are currently used in exploratory medical diagnostics and pre-clinical therapeutics and solar cells and nanoeletronics.

There has been vast growth and expansion of research and applications in the fields of nanoscience and nanotechnology. The outcomes in these disciplines are materials emphasized earlier, which are known as Nanoparticles. Engineered nanoparticles include fullerenes, buckyballs, carbon tubes (CNT), liposomes, nanoshells, dendrimers, QDs, ultra-small paramagnetic iron oxide, gold and silver nanoclusters (Chaloupka K, 2010, Iga et al., 2007, Malam et al., 2009). Furthermore, their applications extend to fast growing fields ranging from aerospace, military, energy, electronic, food, medicine and many others. It is expected that the application of nanoparticles will bring great benefits

to biomedicine in areas as diverse as diagnosis and treatment of disease. Potential applications in the field of medicine include drug delivery, clinical diagnostics, diet industry and development of materials for surgical implants. This introduction will highlight nanoparticles derived from semiconductor materials, which act as fluorophores known as QDs or nanocrystals.

In recent years, research in semiconductors has developed quite literally new dimensions. Their numbers are two, one and zero. Electrons in recently developed devices and materials can be confined to planes, lines and mathematical points i.e. QDs. In general, the energy of electrons in a semiconductor is limited by their temperature and by their properties of the material. When electrons are confined in a thin enough layer, however, the requirements of the uncertainty principle in effect override other considerations. That is to say, as long as the electrons do not have enough energy to break out of confinement, they become effectively two dimensional. Compared to bulk (three-dimensional) and quantum well (two-dimensional) structures, QDs are zero-dimensional (Su et al., 2002) with their electronic states fully quantized, which are similar to a single atom or atomic system. This fully quantized system is stable against any thermal perturbation (**Figure 2.1**).

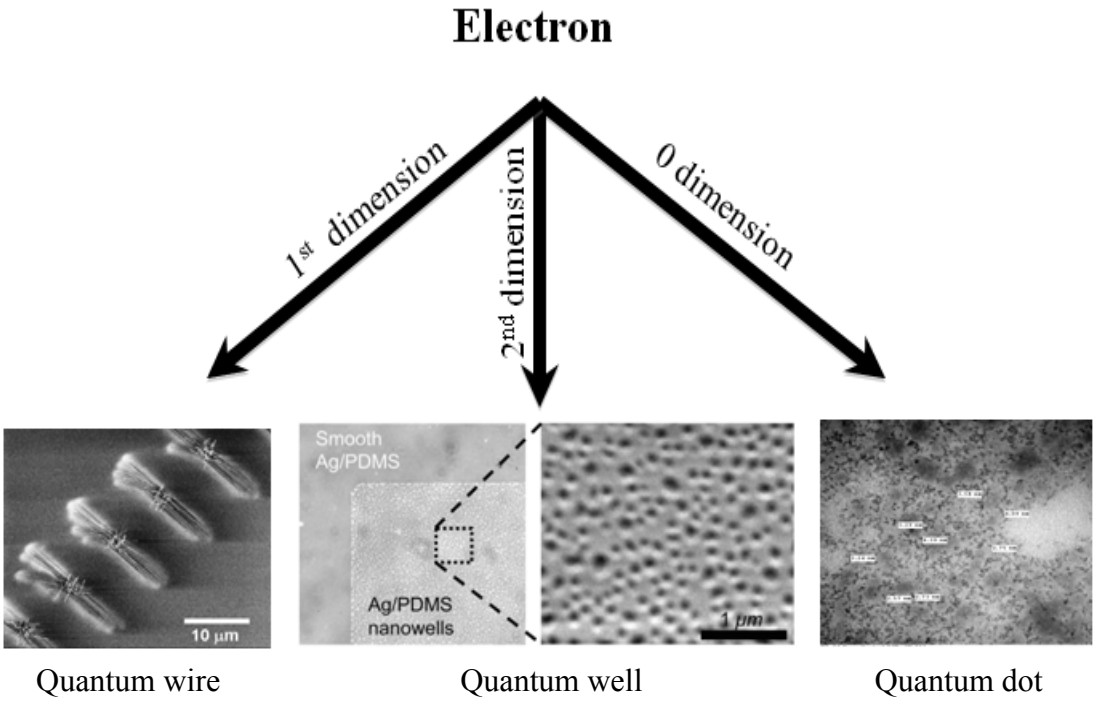

Figure 2.1: Different forms of nanomaterials with different dimensions.

2.2 Historical perspective

Earliest known nanoparticles (gold colloids) were already used in ancient times to colour glass (ruby glass) without scientific understanding. The first who scientifically investigated gold colloid formation was Michael Faraday in the mid-nineteenth century. He reduced a solution of $HAuCl_4$ with elemental phosphorus resulting in the formation of ruby-red gold sols. Subsequently, the reason for this colour was explained: it was due to the interaction of visible light with surface electrons of the gold nanoparticles and also the influence of size, shape and surrounding medium.

Colloidal semiconductor QDs were first prepared by Professor Louis Brus in 1982 (R. Rossetti, 1982, Alivisatos, 2008) and this marked the birth of a nanoscience building block. Their photophysical properties have been explored in great detail over the last two decades. Weller first described the quantum confinement effects of the colloidal semiconductor Q-particles in 1993 (Weller., 1993). During the same period, the Bawendi's group developed a novel, reproducible method for the synthesis of high quality, monodisperse nanocrystals (C. B. Murray, 1993).

Fluorescence QDs have great potentials in the field of electronics especially in photonics. In 1932, Rocksby found that the red or yellow colour of some silicate glasses could be linked to microscopic inclusions of CdSe and CdS (Rocksby, 1932) and in 1985, Ekimov and others discovered that these changes in colour were linked to the energy states determined by quantum confinement in CdSe or CdS "QDs".

The term "QDs" refers to crystal structures with extremely small dimensions. When the size of the semiconductor nanocrystal becomes this small, the electronic structure of the crystal is governed by the laws of quantum physics. Due to its very small size, group (II-VI) semiconductor nanoparticle QDs, in the order of 2-10 nm, exhibit significantly different optical and electronic properties from their bulk counterparts self-organized QDs (Woll AR, 2002). Due to unique properties of QDs, considerable efforts have been made to fabricate QDs for use in different research fields. The desire to identify, understand and explore the size-dependent properties of QDs at the nanometre scale has literally been stimulated since 1985 and has accelerated QDs research development.

2.3 Quantum dot technology

Research and development have focused on the synthesis, solubility and bioconjugation of highly luminescent stable QD.

QDs are light emitting nanocrystals assembled from semiconductor materials, from the elements in the periodic groups of II-VI, III-V or IV-VI, for example cadmium telluride (Cd from group II and Te from group VI) and Indium Phosphamide (In from group III and P from group V). In nanotechnology, the main precursors used in the assembly of QDs is cadmium and tellurium forming the core which they are range in size from 2-10 nm in diameter containing approximately 200-10000 atoms (Green and Howman, 2005). Due to the effects of quantum confinement QDs posses unique optical properties such brighter, highly photo and chemical stable, with broad absorption, narrow and symmetric emission spectrum. An outstanding feature of QDs is that their emission wavelength can be tuned by adjusting their size and chemical composition.

2.4 Structure of quantum dots

Structurally, QD possess a metalloid crystalline core, which ultimately depending on its composition and size will confer the type of fluorescence it will emit. A bare nanocrystal core is highly reactive and toxic resulting in a very unstable structure that is prone to photochemical degradation. Also the core crystalline structure has surface irregularities that may lead to emission irregularities like blinking. The core is composed of materials such as cadmium–selenium (CdSe), cadmium-tellurium (CdTe), indium-phosphate (InP) or indium-arsenate (InAs)(Jamieson et al., 2007) (**Figure 2.2**).

Semiconductor shells or coatings typically using zinc sulphide (ZnS) or mercaptosuccinic acid (MSA) not only stabilize the core, but further improves the optical, physical properties and bioavailability of the material but also reduce the toxicity of the core by shielding reactive Cd^{2+} and Te^{2-} ions from being exposed to photo-oxidative environments e.g. exposure to UV and air (Jamieson et al., 2007). Additional capping or coatings with biocompatible material or polymer layers such as functionalised silica, phospholipid micelles, amphiphylic polymers (polyacrylic acid) have been introduced to render them soluble in aqueous media. Further coatings with POSS-PCU (Polyhedral Oligomeric Silsesquioxane-Polycarbonateurethane, (Kidane et al., 2009) or PEG (Polyethylene Glycol) to the QD core-shell promotes water solubility,

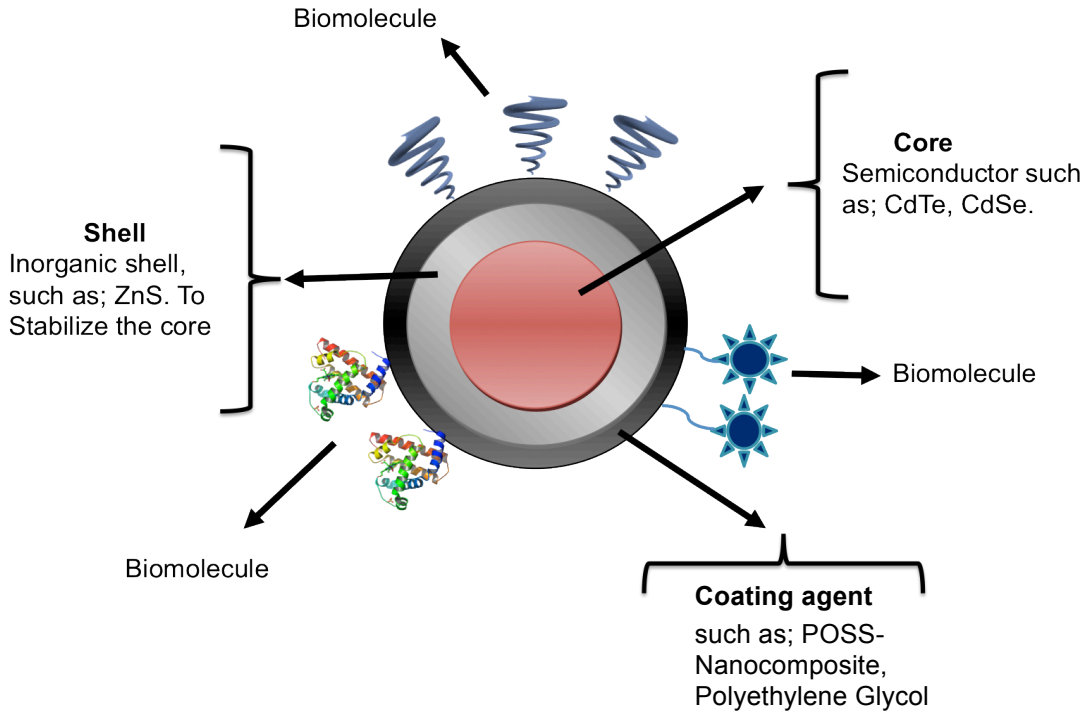

Figure 2.2: Structure of QDs modified with bioactive agents.
Materials such as zinc sulphide (ZnS) have been used to coat QDs to reduce its toxicity and facilitate covalent conjugation to bioactive molecules such as antibodies and peptides.

biocompatibility and desired bioactivity. The aqueous coating can then be tagged with various biomolecules of interest e.g. antibodies, peptides, nucleic acids with available methods of conjugation chemistries (Iga et al., 2007).

2.5 Optical and electronic properties

In natural semiconductor bulk material, the electrons (larger than 10 nm) exist in a range of energy levels. The energy levels are so compact that they can be described as continuous, meaning there is negligible energy difference between them. Also there is region where electrons do not reside or go and in known as "band gap". This band gap is different for each type of bulk semiconductor material. Electrons in energy level below this band gap are known to be in the valence band while those occupying above are known to be in the conduction band. Also, the maximum amount of electrons resides in the valence band whilst a minimum amount of electrons in the conduction band. On acquiring a stimulus such as photon, voltage or heat can push the electrons from the valence band beyond the band gap to conduction band. By leaving the valence band the space left vacant is known as a "hole" which happens to be positively charged. This elevated electron and the hole as a pair, is known as an "exciton". Conduction electrons and valence holes have an average physical distance and this is referred to as

the Exciton Bohr radius (EBR). These can vary with different materials. In bulk the distance is much larger than the EBR, which expands beyond its limit. This property also applies to QDs at the nanoscale level when it becomes equal to the EBR or less when the energy level is said to be discrete and not continuous anymore. This imposition of discrete energy is known as quantum confinement (QC) and at this stage the semiconductor material loses all resemblance to the bulk and adopts the structure of QD. This now alters the absorptive and emissive properties of the semiconductor material (Arya et al., 2005). Once excited to the conduction band, the electron falls back down across the band gap towards the valence band, in doing so electromagnetic radiation with a wavelength corresponding to the energy it loses in the transition is emitted (**Figure 2.3**).

This emission frequency is perceived as fluorescence and depends on the size of the band gap, which can be altered by changing the size of the QD by changing the surface chemistry. It is important to note that the band gap in a QD will always be energetically higher and the radiation emitted is referred to being "blue shifted" thus producing a shorter wavelength. Hence, with QD, the size of the band gap is dependent on the size of the dot and wavelength of the emitted photons. Because the emission frequency of QD depends on the band gap, it is possible to control the output wavelength of the QD with extreme precision (Alivisatos, 2004).

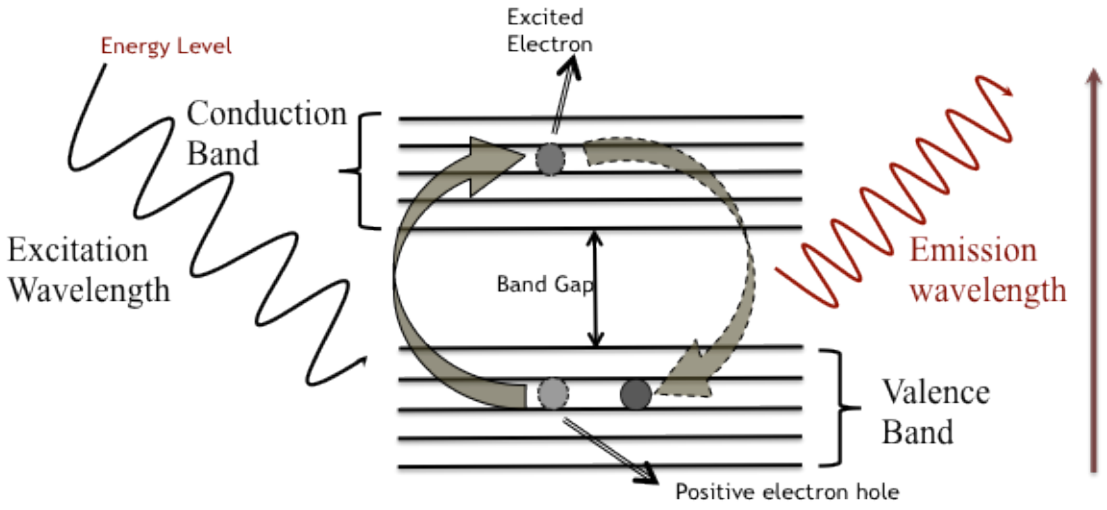

Figure 2.3: Schematic representation of the mechanism of emission by QDs.
Excited electron in the valence band is elevated across the band gap onto the conduction band. As the raised electron in the conduction band falls back across the band gap to its valence energy level, a wavelength of light is emitted in this process.

This size tunable absorption and emission property of QDs is an extremely valuable property for biological imaging as they can be tuned all the way from the ultraviolet (UV) to the NIR of the spectrum such that smaller dots emit in the blue range and the larger dots in the red and NIR region (**Figure 2.4**). QDs have a broad excitation and narrow, discrete emission spectra. The peak emission wavelength of the QD is slightly longer than the first exciton peak or absorption onset, and this energy separation is known as the "Stoke's shift". Also their peak emission wavelength is independent of the wavelength of excitation light. This means that variable sized QDs can be excited by a single wavelength of light, as long as this wavelength is shorter than the absorption onset. This can be used in multiplexed imaging where a number of different sized QDs with discrete emission peaks and hence different colours can be excited by a single wavelength of light.

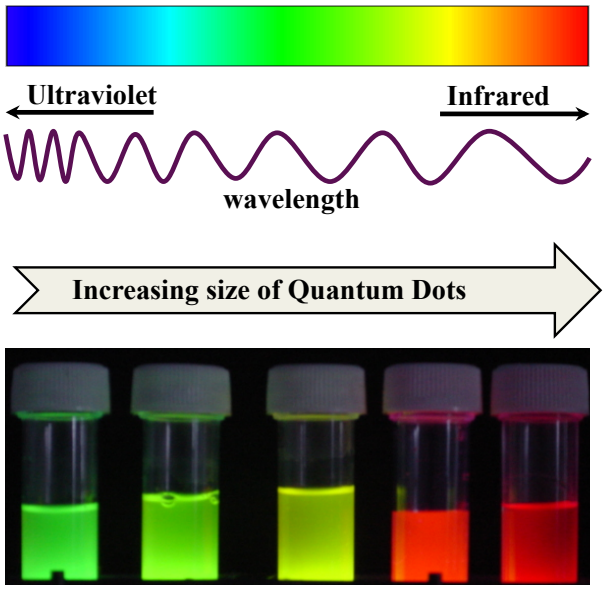

Figure 2.4: Shows size dependent multicolour fluorescence of QDs in aqueous solution.

With such small sizes, QD show some unique and fascinating optical properties, such as sharp, symmetrical emission spectra, high quantum yield (QY), chemical and photostability and size dependent emission wavelength tunability. Their intrinsic brightness is often of many orders that observed for traditional organic fluorophores. Their large surface to mass ratio confers the particles the ability to absorb and carry many compounds. QDs have relatively large (functional) surface, able to bind, adsorb and carry compounds such as drugs, probes and proteins. Based on these desirable properties, QDs have the potential to improve the sensitivity of biological imaging at

the cellular level which includes cancer detection, progression and treatment, radio-and chemo- sensitizing agents, electron and x-ray contrast agent and targeted drug delivery. However, caution has to be exercised with these attractive applications as QDs contain substantial quantities of cadmium, which are reactive in an ionic state, and only limited studies are only available concerning the health risk of exposure to nanoparticles (Juzenas et al., 2008, Smith et al., 2008a).

2.6. Quantum dot synthesis

There are various ways of synthesis of colloidal QDs. Each method has its own challenges and involves the integration of quantum physics, materials science, synthetic chemistry and most importantly biology (**Figure 2.5**).

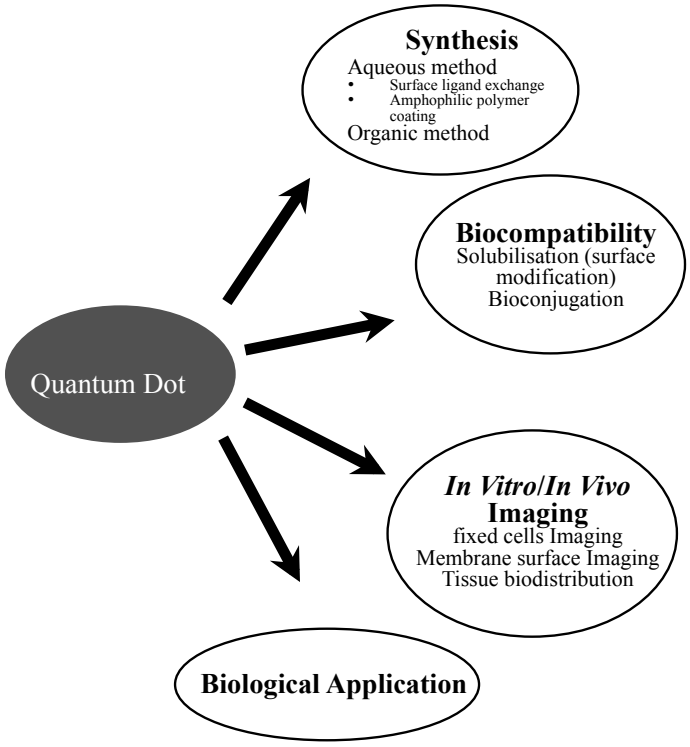

Figure 2.5: The multi-role applications of QDs in biomedicine

Currently, there are many methods for the synthesis of QDs including organic and aqueous synthesis in preparing highly luminescent nanocrystals. Additionally, there are reports of using microwave and hydrothermal methods (Yao He and Lian-Hui Wang, 2007, Junling Duan) for rapid synthesis of QDs . Traditionally high-quality nanocrystals were prepared in organic solvents and they cannot be used directly in biosystems due to their hydrophobicity. The use of high temperatures and in the presence of surfactants to yield monodisperse and stable particles are a drawback (C. B. Murray, 1993, Peng and

Peng, 2001). However, the QDs produced by the organic phase are insoluble in aqueous media and therefore not applicable to biological systems. Water dispersible QDs that sustain strong fluorescence can be prepared by ligand exchange with a hydrophilic moiety. However, it is a difficult procedure but direct synthesis in an aqueous environment is possible for use in biological applications. A number of successful methods to solubilise organically synthesised QDs in aqueous media have been developed. Aqueous synthesis, on the other hand, produces water soluble QDs through a simpler, inexpensive and reproducible method that can easily be scaled up. However, the aqueous route to the synthesis of QDs have good average crystallinity, with low QY and Full Width Half Maximum (FWHM), (**Figure 2.6**) and long reaction times, making preparation a time-consuming and tedious process (Weng and Ren, 2006). The Ren group (Li et al., 2005) has recently described a new method of QD synthesis based on microwave irradiation with controllable temperatures. This allowed rapid production of size tunable QDs in 5-45 minutes, based on the reaction between Cd^{2+} and NaHTe solution (Weng and Ren, 2006).

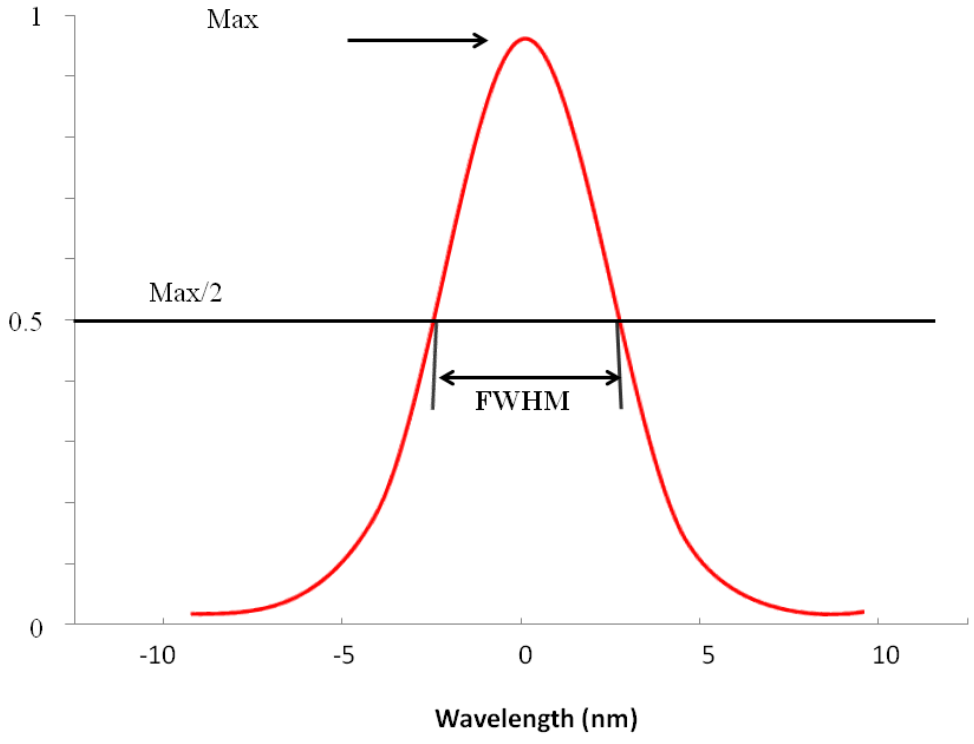

Figure 2.6: The bandwidth of the emission spectra,
denoted as Full Width at Half maximum (FWHM) stems from the temperature, natural spectral line width of the QDs, and the size distribution of the population of QDs within a solution or matrix material.

This method showed significant advantages over the traditional aqueous synthesis like reduced toxicity, good reproducibility, inexpensive, excellent water solubility, stability and biological compatibility and a comparable QY to the organic synthetic route (Rizvi et al., 2010).

2.6.1. Surface coatings and water-solubility

One of the biggest challenges to the biological application of QDs is their biocompatibility. This dilemma is due to their hydrophobic surface chemistry, which makes them insoluble in aqueous biological media. In order to render QDs biocompatible, they have to be soluble in biological buffer, and over the years many scientists have discovered a wide array of surface coatings for solubilisation of QDs (Pinaud et al., 2006). The aim is to achieve an ideal surface chemistry that is stable in biological media and not alter the photophysical properties of the QDs, while at the same time retaining a small QD size and providing free reactive surface groups for binding and recognition of biomolecules. The techniques used to achieve solubilisation include ligand exchange, surface silanization and phase transfer methods. The "ligand exchange" method is based on the exchange of the hydrophobic surfactant molecules with bi-functional molecules, which are hydrophyllic on one side and hydrophobic on the other, to bind to the ZnS shell on the QD (Alivisatos et al., 2005). Most often thiols (–SH) as functional groups are used to bind to the ZnS and carboxyl (-COOH) groups are used as hydrophyllic ends. The resulting QDs are soluble in both aqueous and polar solvents. This is by far the simplest method to achieve solubilisation. "Surface silanization" involves the growth of a silica shell around the nanocrystal. As silica shells are highly cross-linked they are very stable. However, the drawback is that the process is laborious and the shell may be hydrolysed (Alivisatos, 2004). The "phase transfer" method uses amphiphyllic polymers to coat the QDs surface (Nann, 2005, Wang et al., 2004). The hydrophobic alkyl chains of the polymer interdigitate with the alkyl groups on the QDs surface while the hydrophyllic groups orientate outwards to attain water solubility. However, coating with a polymer may increase the overall diameter of the QDs and this may reduce emission and limits their use biological applications (Uyeda et al., 2005). Various techniques of coating using phospholipids micelles, dithioretol, organic dendrons, and oligomeric ligands can be found in numerous publications (Benoit Dubertret, 2002, Kim et al., 2004).

2.6.2. Surface functionalization

Once solubilisation is achieved, QDs can be functionalized by conjugation to a number of biological molecules including avidin, biotin, oligonucleotides, peptides, antibodies, DNA and albumin (Alivisatos et al., 2005) through surface reactive groups for specific targeted action. Methods of bioconjugation broadly fall into two categories: noncovalent and covalent conjugation (Xing et al., 2009). Noncovalent interactions include absorption, electrostatic interaction and mercapto-exchange. Biomolecules like oligonucleotide and various serum albumins (Lakowicz et al., 2000) can be absorbed on the surface of the water-soluble QDs. This process is non-specific and depends on pH, temperature, ionic strength and surface charge of the molecule (Alivisatos et al., 2005). QDs may be cationic or anionic and may interact with biomolecules through electrostatic interaction. The surface charge plays an important role in the cellular interaction of QDs and is determined by the free surface reactive groups. It has been demonstrated that proteins engineered with positively charged domains, can interact with the negative charges on the QDs surface coated with dihydrolipoic acid (DHLA) through electrostatic interaction (Clapp et al., 2006). These conjugates have greater photoluminescence but are also more stable than unconjugated dots. However, electrostatic interactions are nonspecific and relatively weaker compared to covalent bonding and this may pose a problem in the biological environment. Many biological molecules have a thiol group, which can be tagged on to the surface of a QD by a mercapto-exchange process (Alivisatos et al., 2005). However, the resulting bond between thiol and Zn is not only weak but also dynamic and this may lead to precipitation of the biomolecules in solution as they easily detach from the QD surface. Covalent linkage is the most stable of all the bioconjugation methods and utilises functional groups on the QDs surface like primary amine, carboxylic acids, and thiols to form a covalent bond with similar groups present on biomolecules or through the use of cross-linker molecules (Alivisatos et al., 2005). The commonest and convenient method of bioconjugation is via the avidin-biotin interaction. This is based on the high affinity interaction between avidin and biotin through a generic key-lock mechanism. Avidin is attached to antibodies and biotin can covalently bind to the surface of QDs and vice versa. As most of the commercially available biomolecules are avidin or biotin linked, it makes this process most convenient as well (Clapp et al., 2006, Weng and Ren, 2006) (**Figure 2.7**).

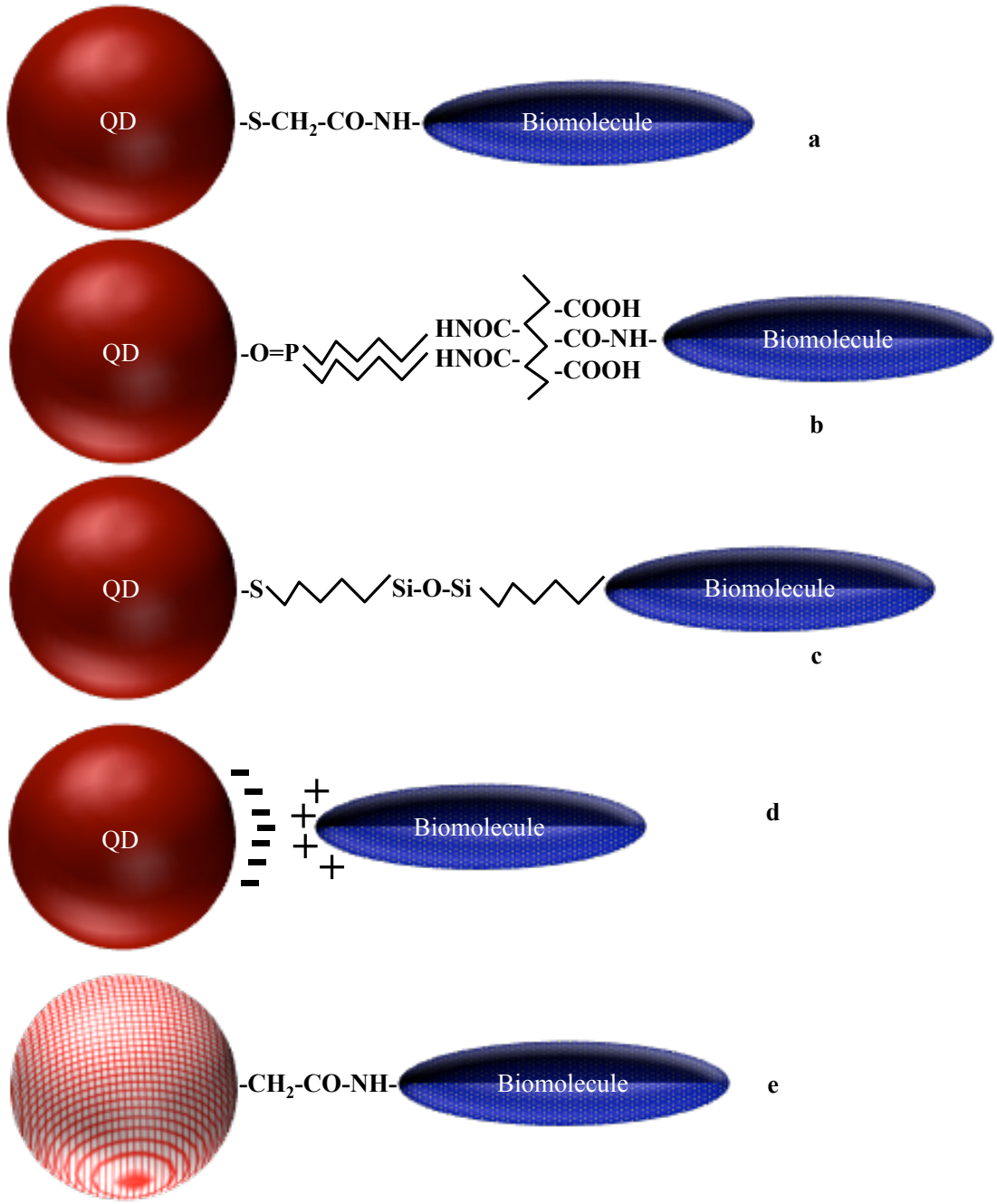

Figure 2.7: Schematic representation of different approaches to conjugation of QDs to biomolecules. (a) Use of a bifunctional ligand such as mercaptoacetic acid for linking QDs to biomolecules. (b) TOPO-capped QDs bound to a modified acrylic acid polymer by hydrophobic forces. (c) QD solubilisation and bioconjugation using a mercaptosilane compound. (d) Positively charged biomolecules linked to negatively charged QDs by electrostatic attraction. (e) Incorporation of QDs into microbeads and nanobeads.

2.6.3. Bioimaging applications

Microscopy especially fluorescence and confocal is an established technique of observing the microsructures and molecules within cells and QDs are increasingly being used as fluorescent labels for cellular and molecular imaging. QD application to this field is similar to that of organic fluorophores but with various advantages. They can facilitate in the visualization of cellular structures and receptors in both fixed and live cells. Although QDs have been used for a variety of biological applications (**Table 2.2**), their great potential for biomedical imaging and therapeutic remains unexplored.

Table 2.2: Several biological applications of QDs

Biological Applications of Quantum Dots			
Imaging	*In vitro* imaging	Fixed cell imaging	Immunofluorescent labeling of proteins, biomarkers Immunohistochemical detection Fluorescence *in situ* hybridization
		Live cell imaging	Single QD tracking of membrane receptors and signaling pathways Resonance energy transfer- fluorescence (FRET) Stem cell tracking
	In vivo imaging		Cancer studies and cancer localization
Labeling			As well as labeling, quantum dots have potential for detecting
Drug Delivery			Loading biological compounds on QDs such as; any types of drugs
Other Applications			Photodynamic Therapy Pathogen toxin detection

2.6.4. *In vitro* cell imaging

QD conjugates can substitute for several immunohistochemical applications and have various advantages over organic fluorophores, including increased photoluminescence, photostability, broad excitation and narrow emission spectra, also allowing multiplexed imaging (**Table 2.2**). Immunohistochemical detection of targeted molecules in fixed cells involves the use of primary antibodies that specifically interact and bind to the antigen of interest followed by the application of a labeled secondary antibody against the primary. Secondary antibodies are conjugated to organic fluorophores, radioisotopes or enzymes producing luminescence, counts or chemiluminescence at or near the site of the primary antibody, demonstrating amplification which can greatly increase the sensitivity of immunohistochemical detection (Akhtar et al., 2007).

Detection of targeted molecules in their natural distribution requires fixation followed by permeabilization of the cell wall by fluorescent conjugated probes. As QDs are larger than organic dyes they may require permeabilisation (Ornberg and Liu, 2007). The timing of cell fixation i.e. before or after exposure to QDs determines their stability, localization within the cell as well as emission properties. While in fixed permeabilised cells, QDs are readily taken up regardless of the cell type, whereas in live cells previously incubated with QDs, the choice of fixative influences the fluorescence characteristics. A comparative analysis of gluteraldehyde, methanol and paraformaldehyde demonstrated that 2% paraformaldehyde was the fixative of choice (Williams et al., 2008).

QD-Antibody conjugates have accurately and successfully identified membrane bound protein p-gp (glycoprotein) in fixed MCF7r breast adenocarcinoma cells (Weng and Ren, 2006). The localization of p-gp by confocal was reconstruction in a 3-D imaging which showed that QD-Antibody probe was highly sensitive and photostable compared to organic dyes like FITC, AlexaFluor488 and R-phycoerythrin. Using QD probes actin and microtubule fibres in the cytoplasm (Bruchez et al., 1998) and various nuclear antigens of fixed cancer cells have been located (Wu et al., 2003). Indirect immunofluorescence has been used to identify Her2, microtubules and nuclear antigens in fixed cancer cells by first incubating fixed cells with a primary antibody, then a biotinylated secondary antibody and finally with QD labeled streptavidin. This takes

advantage of the high affinity of streptavidin to biotin with amplification (Wu et al., 2003).

Fluorescence in situ hybridization (FISH) technology to evaluate DNA sequences in fixed biological specimens has been well established (Levsky and Singer, 2003). It uses fluorescently labeled DNA probes for gene mapping and probing subtle chromosomal abnormalities, which can provide diagnostic and prognostic results for particular chromosomal disorders. This technique adopts the concept of detection of a fluorescent signal at the site of hybridization of a fluorescent dye labeled probe with its matching chromosomal target (Rizvi et al., 2010). The disadvantage of using rapidly photo-unstable multicolour organic dyes are spectral overlap which can be solved with QDs with their high photostability and discrete spectra permitting multiplexed imaging (**Table 2.3**). Xiao et al. used a QD-FISH probe to analyse human metaphase chromosomes using organic dyes like Texas-Red and FITC and found QDs were more photostable and significantly brighter making them a more stable and quantitative mode of FISH for research and clinical applications (Xiao and Barker, 2004). QDs are also suitable to probe single DNA and RNA molecules and their interaction with proteins allowing the study of dynamic processes. The application of QD conjugates to visualize single copy sequence DNA probes as short as 1500 nucleotides in length has been demonstrated (Knoll, 2007).This should find application in rapid gene mapping and DNA-protein interactions and for automation (Weng and Ren, 2006).

Probing the molecular dynamics of various cellular processes poses great challenges in cell biology in live cells. This can contribute to the understanding of cellular and molecular interactions in real time over prolonged periods at high resolution. Applying QDs to live cells can function as a versatile tool in various applications especially in cell tracking leading to stem cell research and determining the metastatic potential of cancer cells. Their photostability permits long-term imaging applications like single molecule tracking in living cells exposing many cellular and molecular processes as have never been undertaken.

Labeling of live cells with QDs is an important step prior to various imaging applications. There is a possibility that QDs can be passively taken inside cells or be bound nonspecifically to the extracellular surface. However, intracellular labeling could

Table 2.3: Advances of QDs over organic dyes

Properties	Organic dyes	QDs	Advantages of QD
Excitation Spectrum	Narrow	Broad	Organic dyes can be excited only by light of a specific wavelength due to the narrow excitation spectrum whereas. QDs which may be excited by light of a range of wavelengths, allowing multi-colour QDs to be excited by a single wavelength of light.
Emission Spectrum	Broad and asymmetrical	Narrow and symmetrical	The broad emission spectra of organic dyes may overlap and this limits the number of fluorescent probes that can be tagged to biomolecules for simultaneous imaging in a single experiment. QDs have narrow emission spectra, which can be monitored by altering the size, composition and surface coatings of the dots. Therefore, multiple QDs emitting different colours can be excited by a single wavelength of light making them ideal for multiplexed imaging.
Photobleaching threshold	Low	High	Organic dyes bleach within a few minutes on exposure to light whereas QDs are extremely photostable due to their inorganic core, which is resistant to metabolic degradation and can maintain high brightness even after undergoing repeated cycles of excitation and fluorescence for hours. Hence they can be used for long-term monitoring and cell tracking studies.
Decay lifetime	Fast (<5 ns)	Slow (30-100 ns)	The fluorescence lifetime of QDs is considerably longer than typical organic dyes that decay within a few nanoseconds. This is valuable in overcoming the autofluorescence of background tissues hence improving signal to noise ratio.
Quantum Yield	Low	High	
Absorbance cross section	Low	High	QDs have higher quantum yields, large absorbance cross section and large saturation intensity than organic fluorophores in aqueous environments making them much brighter probes for *in vivo* studies and continuous tracking experiments over extended periods of time.
Saturation intensity	Low	High	

be encouraged by co-incubating cells with QDs via non-specific endocytosis (Hoshino et al., 2004b, Hanaki et al., 2003) or they may be linked to other biological compounds such as peptides or proteins on the cell surface that are specifically endocytosed (Chan and Nie, 1998). Alternatively, they can be introduced into the cell via electroporation or microinjection (Knoll, 2007, Dubertret et al., 2002, Jaiswal et al., 2003), which though complex and difficult, is the only technique that ensures uniform cytoplasmic distribution. Most convenient and efficient, peptide mediated intracellular delivery of QDs has been most commonly used. This approach relies on the fact that protein transduction domains (PTD) allow the passive delivery of drugs across the cell membranes as well as the blood brain barrier. There are documented studies of delivering a number of biomolecules including proteins, oligonucleotides, liposomes and magnetic nanoparticles into cells using PTDs (Lagerholm, 2007). It has been demonstrated that QDs can be delivered into cells using similar techniques. QDs have been coupled to PTDs via different approaches such as streptavidin-biotin link (Lagerholm, 2007), covalently (Hoshino et al., 2004a), by electrostatic adsorption or adsorption to synthetic PTDs like pep-1(Mattheakis et al., 2004). Of all the possible approaches for intracellular delivery, linking PTDs to QDs via a streptavidin-biotin bridge is most easily performed.

Targeting membrane receptors and proteins via QD probes can provide specific imaging. Various biological processes and pathways like chemotaxis, synaptic regulation, or signal transduction are dependent on the trans-membrane receptors and signaling pathways. Plasma membranes have a complex and dynamic construct with various components that modulate the diffusion of endogenous proteins, lipids and peptides. Successful application of biotinylated peptide coupled to QDs to study the organization of the plasma membrane and the influence of lipid raft microdomains on the diffusion of raft-associated proteins in HeLA cells (cervical cancer cells) and MCF-7 cells (Breast cancer cells) (Pinaud et al., 2009) were carried out. QD probes have also allowed high-resolution and long-term tracking of individual glycosyl-phosphatidyl-inositol-anchored avidin test probe (Av-GPI), and the classification of their various diffusive behaviors (Rosenthal et al., 2011).

2.6.4.1. Tracking biomolecules

This technique allows the tracking of single molecules in real time to visualise the actual molecular dynamics in biological environment. This can be used to follow various biological molecules like lipids, membrane associated proteins and cytosolic motor proteins, as well as detailed descriptions of the compartment sizes of micro-domains and the time that individual macromolecules reside in each compartment. Apart from genetic encoded fluorescent proteins and organic dyes, various materials have been used for single particle tracking studies including latex or fluorescent microspheres (~20-500 nm) and colloidal gold nanoparticles (40 nm). Fluorescent proteins and organic dyes have low photoluminescence in a background of high cell autofluorescence and a low photobleaching threshold making long-term tracking difficult. Gold nanoparticles are good agents for single particle tracking but do not allow multiplexed imaging however, with the synthesis gold nanoclusters.

2.6.4.2. Mapping stem cells

As one of the most fascinating areas of contemporary biology stem cell research has a vast potential to treat a myriad of medical conditions. Currently, magnetic and superparamagnetic iron oxide (SPIO) nanoparticles are being used to achieve this objective through the use of MRI. However, the gradual loss of the MRI cell signal due to cell division poses a hindrance to long-term imaging studies. The application of QDs as nanomaterials for monitoring stem cells survival, distribution, differentiation and regenerative impact either *in vitro* or *in vivo* due to their inherent mesenchymal stem cells (hMSC) with RGD peptide conjugated QDs during differentiation into osteogenic cell lineages has been carried out (**Figure 2.8**) (Unpublished).

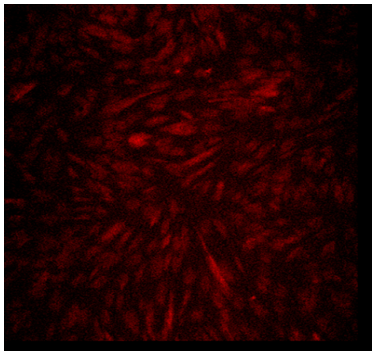

Figure 2.8: Bone marrow mesenchymal cells labeled with conjugated QD-RGD (Unpublished)

Another group has also demonstrated that RGD-conjugated QD labeled hMSCs remained viable following multilineage differentiation as did the unlabeled hMSCs (Shah et al., 2007). The regenerative potential of stem cells to repair damaged cardiac tissue is being investigated but attempts at tracking the differentiation and distribution of stem cells *in vivo* have been hampered by the inherent autofluorescence of damaged cardiac tissue. QD labeled human mesenchymal stem cells can illuminate stem cells in histological sections for at least 8 weeks following delivery allowing a 3-D reconstruction of the location of all stem cells following injection into the heart (Rosen et al., 2007). While QDs labeled tracking of stem cells promises great advancements in the field of stem cell research, the effects of QDs on stem cell self-renewal and differentiation are largely unknown and need to be explored.

2.6.4.3. Quantum dot uptake assays

QDs have been used to demonstrate the metastatic potential of cancer cells to distinguish between invasive and noninvasive cancer cell lines (Pellegrino et al., 2003). Gu et al. have demonstrated a two-dimensional *in vitro* cell motility assay based on the phagokinetic uptake of QDs by cells as the move across a homogenous layer of QDs leaving behind a fluorescence free trail. The ratio of the trail area to the cell area has been proposed to distinguish between invasive and noninvasive tumour cells (Gu et al., 2007, Gu et al., 2005).

2.6.4.4. Energy transformation assays

Fluorescence resonance energy transfer (FRET**)** is a process in which energy is transferred from an excited donor to an acceptor particle leading to a reduction in the donor's emission and excited state lifetime and an increase in the acceptor's emission intensity. This occurs whenever the distance between the donor and acceptor is minimal than the critical radius known as the Förster radius. FRET is sensitive to the distance between the donor and the acceptor and is used to measuring changes in distances rather than absolute distances. It is therefore suitable to study biomolecule conformation, dynamics and interactions e.g. monitoring protein conformational changes, protein interactions and assaying enzyme activity. Using organic dyes for FRET poses the problems of early photobleaching and significant emission overlap between the donor and acceptor and QDs provide an excellent alternative (Jamieson et al., 2007).

QD based FRET technology has found application in monitoring other biological processes like DNA replication and telomerisation for a fast and sensitive DNA detection and DNA array analyses (Patolsky et al., 2003). Most QDs based FRET probes are based on QDs as donors and organic fluorophores as acceptors. A single QD based nanosensor capable of detecting extremely low concentrations of DNA (50 copies) in a separation free format has been demonstrated. QDs were coupled to DNA probes to capture DNA targets. The target strand binds to a dye-labeled reporter strand thus forming a FRET donor-acceptor complex (Zhang et al., 2005).

Another application of QD-FRET is the detection of enzyme activity in particular protease sensing. This is based on the inserting peptide sequences of various proteases between QDs and quenchers (or acceptor dyes) (Medintz et al., 2003). The QD fluorescence is quenched by the acceptor dye but cleavage of the peptide sequences by specific proteases causes removal of these acceptor molecules, and hence the QDs are switched on. A good example is rhodamine Red-X-dye-labeled peptide linked to CdSe/ZnS QDs used as FRET probes to monitor proteolytic ability of collagenases in normal and cancer cells. Hydrolytic cleavage of the peptide linked dye by the collagenases restored QD fluorescence allowing detection of specific enzyme activity over short periods of time (Shi et al., 2006).

Bioluminescence resonance energy transfer (BRET) is a naturally occurring phenomenon, whereby a light emitting protein which acts as a donor (e.g. Renilla luciferase) non-radiatively transfers energy to a fluorescent protein as an acceptor (e.g. GFP) in close proximity. The process is similar to FRET except that the energy comes from a chemical reaction catalyzed by the donor enzyme (e.g. Renilla luciferase mediated oxidation of its substrate coelenterazine) rather than absorption of excitation photons. *So et al.* prepared self illuminating QDs by covalently coupling QDs (as acceptors) to a bioluminescent protein Renilla reniformis luciferase (as a donor). The protein emits a blue light at 480 nm upon addition of a substrate, coelenterazine. The QDs can be excited if they are in close proximity to the protein and emit at their emission maximum. These conjugates emit long-wavelength (from red to near infrared) bioluminescent light in cells and in animals, even in deep tissues, and are suitable for multiplexed *in vivo* imaging (So et al., 2006).

2.6.5. *In vivo* imaging

Fluorescence imaging of live animals is limited by the poor transmission of visible light through the living tissues as well as by the intense autofluorescence of tissue chromophores. QDs can overcome these limitations through their high photoluminescence, enhanced photostability under prolonged laser illumination and size tunability to emit at longer wavelengths like the NIR, which is not subjected to scattering and absorption as light in the visible range. Also QDs have a two photon absorption cross section several times greater than organic dyes and this property makes them more efficient at probing thick tissue specimens by multiphoton microscopy. Green emitting QDs were injected in living mice intravenously and dynamically visualised by two-photon microscopy as they perfused through the skin capillaries several micrometers deep. Two-photon excitation allows greater tissue penetration due to excitation in the NIR range (Larson et al., 2003). *Voura et al.* used spectral imaging to trace intravenously injected tumour labeled QDs into mice as they extravastated into lung tissue, and found that the behavior of QD-labeled tumour cells *in vivo* was indistinguishable from that of unlabeled cells. Also QDs and spectral imaging allowed the simultaneous identification of five different populations of cells using a sophisticated multiphoton laser excitation application (Voura et al., 2004).

2.6.5.1 Sentinel lymph node biopsy (SLNB) imaging

This is a means of detecting cancer metastasis and is now the standard of care in breast cancer surgery. It is based on targeting the first draining lymph node, also called the sentinel lymph node (SLN) of a lymphatic basin at the cancer site to determine the extent of disease spread. A negative detection of metastasis in the SLN means that the disease is contained and extensive surgery can be avoided. Available tracers for SLN biopsy include blue dye and radioisotope. However, these have various limitations that can be improved by the use of QDs that emit in the NIR range (>700 nm). The main problem with live animal imaging is to overcome the background tissue known as autofluorescence. NIR imaging can overcome this problem based on the concept that normal tissue chromophores do not absorb or scatter light in the NIR range. NIR light can therefore penetrate deeper tissues without being scattered and is ideal for imaging in real time. NIR QDs have successfully been used to demonstrate *in vivo* SLN biopsy in mice and pigs (Kim et al., 2004) (**Figure 2.9, 2.10**). A subdermal injection of picomolar

quantities of NIR QDs infiltrated the lymphatics and the fluorescence could be traced to the SLN in real time by using a NIR imaging system. This allowed an accurate and sensitive localization and biopsy of the SLN with minimal tissue dissection.

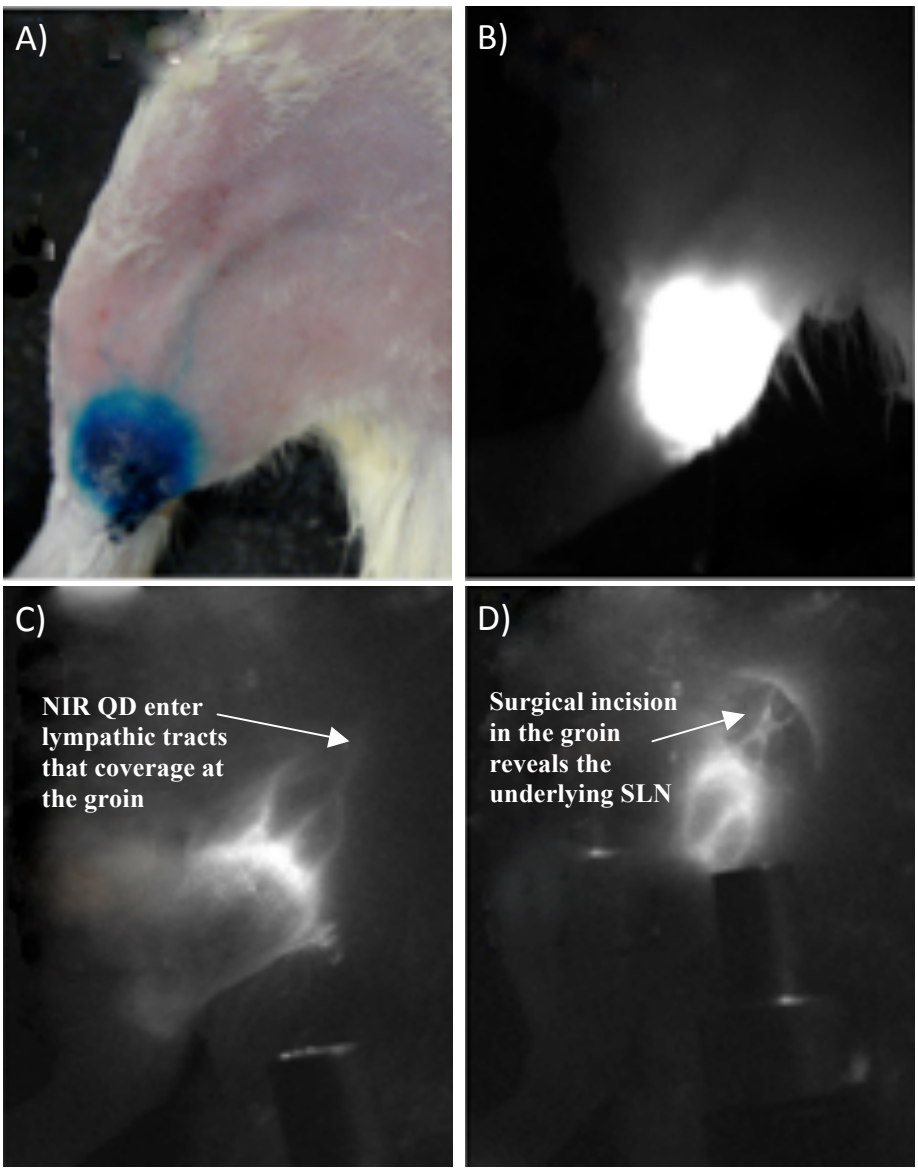

Figure 2.9: NIR QD at 800 nm upon excitation with a 630 nm light source.
Within 3 minutes of intradermal injection the NIR QD entered the lymphatic tracts. The lymphatics are seen to converge to the groin and a small surgical incision at this site revealed the underlying lymph nodes with minimal dissection. A) Colour image B) NIR image 0 minutes C) NIR image 3 minutes D) NIR image 5 minutes. (Collaborative studies with Dr Sarwat Rizvi of surgery and interventional sciences department)

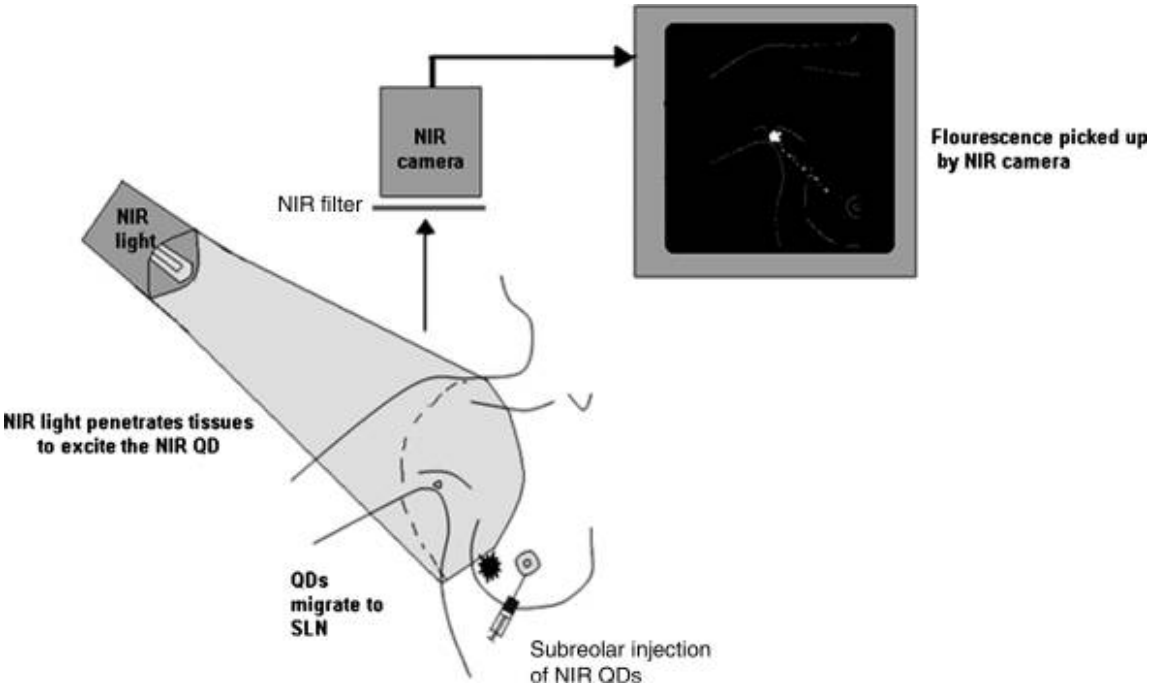

Figure 2.10: A schematic diagram of a NIR imaging system for SLNB in human breast cancer surgery. This has potential to be one of the major clinical applications of QDs in the future. The near-infrared light penetrates deep tissues with minimal scatter and excites the QDs that emit in the NIR range. A NIR camera detects the fluorescence from these dots, which is basically a regular camera with an infrared filter. These images can be superimposed with images from the colour camera on a PC to anatomically locate the exact position of the NIR QDs.

2.6.5.2. Tumour targeting and therapy

In vivo localization of cancer antigens using QDs bound to tumour-specific antibodies has been demonstrated in molecular imaging studies. Antibody specific to the prostate cancer cell marker PSMA was conjugated to QDs and injected into mice transplanted with human prostate cancer. This accurately homed in to the tumour, which was accurately imaged *in vivo*. Their bright luminescence and long lifetime allowed a more accurate and sensitive imaging compared to green fluorescent protein (GFP) (Gao et al., 2004). QDs linked to alpha-fetoprotein (AFP) monoclonal antibody were injected intravenously and successfully targeted human hepatocellular carcinoma xenograft growing in nude mice (Chen et al., 2008). QDs conjugated to anti-EGFR antibodies were able to detect increase expression of EGFR levels, which correspond to early change from cervical dysplasia to cancer (Nida et al., 2005). This can have a huge impact on the early diagnosis and treatment of cancer.

2.6.6. Other applications

2.6.6.1. Drug delivery

Targeted QDs may find a "drug delivery" application as an ultrasensitive tool for early cancer diagnosis by loading the chemotherapeutic agents, and at the same time overcoming systemic side effects. Drugs can be passively targeted to tumors by the EPR effect and this concept has been applied to anticancer agents (Iga et al., 2007). QDs as a probe can target and accumulate in tumors by both the EPR effect and recognition of cancer cell surface biomarkers (active targeting). QDs are one of the many nanoscale platforms being developed as novel drug delivery systems (Cuenca et al., 2006) based on their ability to target specific sites at a molecular level and unique photophysical properties (Hild et al., 2008).

2.6.6.2. Photodynamic therapy (PDT)

One of the major advances in minimally invasive therapies for cancer is photodynamic therapy (PDT). First discovered in the early 1900s, it is now an approved cancer treatment for various superficial malignancies including head and neck, basal cell carcinoma, oral, oesophageal and lung cancers (Hopper, 2000). It is based on the targeted localised destruction of diseased tissues via the generation of cytotoxic singlet oxygen ($^1O_2$) using a non-toxic photosensitizer (PS), activated by light of a specific wavelength in the presence of molecular oxygen ($^3O_2$). Singlet oxygen leads to cellular necrosis and apoptosis of target cells via oxidation and degradation of cellular components.

Photofrin is the most commonly used photosensitizer for PDT and suffers from various drawbacks like instability in aqueous solution, prolonged cutaneous sensitivity, chemical impurities, and weak absorption at therapeutic wavelengths of > 630 nm which is essential for deep tissue penetration (Samia et al., 2006, Ogawa and Kobuke, 2008). The application of QD-PS complexes as therapeutic PDT agents was first reported by Burda et al. (Samia et al., 2003). QDs can be used in PDT either indirectly as energy donors to conventional photosensitizers by FRET mechanism or directly as they react with molecular oxygen by energy transfer mechanisms to generate reactive oxygen species (ROS) (**Figure 2.11**). With their high photoluminescence quantum efficiency, prolonged photostability, high molar extinction coefficients, tunable emission spectra at NIR

wavelengths they form ideal donors for the FRET process in PDT. Additionally, functionalization of the QD surface gives the advantage of enhanced solubility, biocompatibility and localization of the QD-PS pair to the exact cancer site for specific targeted action (Yaghini et al., 2009).

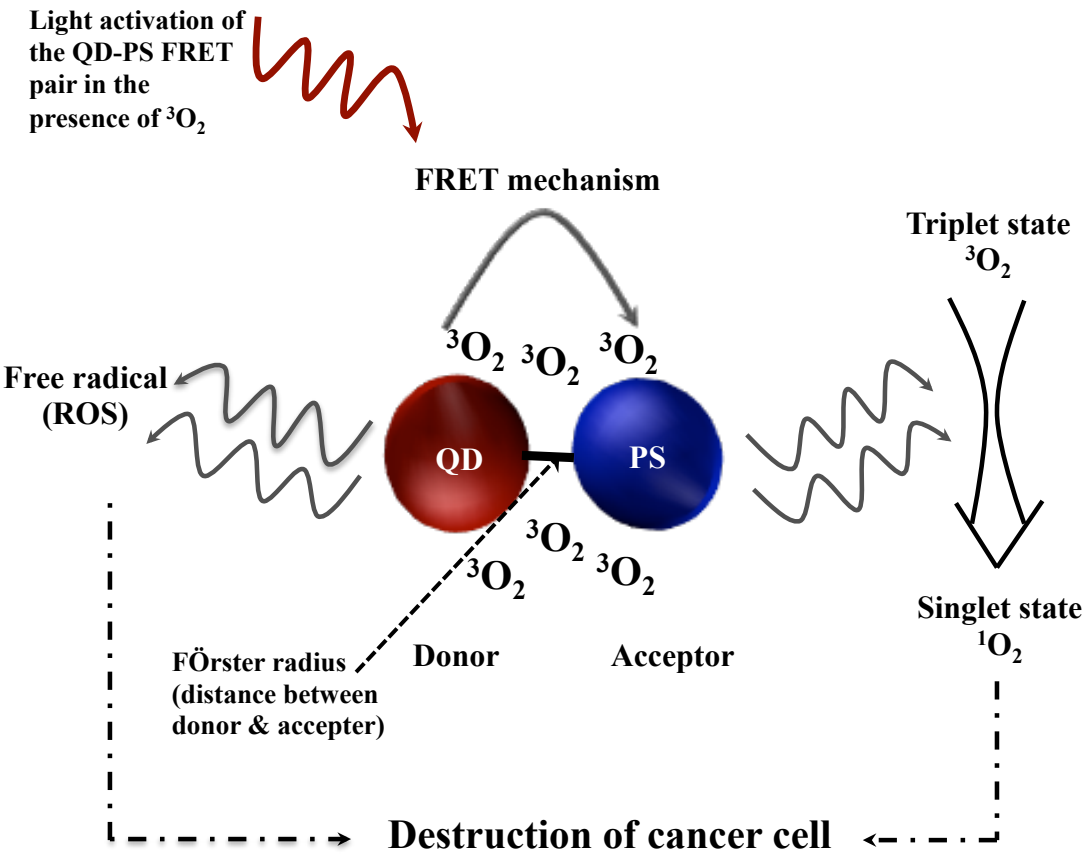

Figure 2.11: Mechanism of PDT using QD; QD-PS FRET pair localizes to the site of cancer, and is activated by light of a specific wavelength in the presence of molecular oxygen ($^3O_2$) to generate singlet oxygen, which is toxic to cancer cells. Free radical are also generated directly by activation of the QD by light

2.6.6.3. Medical microbiology and toxin detection

Using the concept of multiplexed imaging, different food borne pathogenic bacteria have been simultaneously detected at low concentrations of 10^{-3} cfu/mL (colony form unit/mL) within 2 hours by using antibody conjugated QDs and magnetic microparticles (Zhao et al., 2009). When compared with organic green dye fluorescein isothiocyanate, CdSe/ZnS core/shell bioconjugates displayed brighter fluorescence intensities, lower detection thresholds, and better accuracy in analyzing bacterial cell mixtures composed

of pathogenic *E. coli* O157:H7 and harmless *E. coli* DH5alpha using flow cytometry. A novel method for an ultrasensitive, fluorescent detection of DNA and antigen molecules based on self-assembly of multiwalled CNT and CdSe QDs via oligonucleotide hybridization has also been described. Overall, the QD technology demonstrates great potential for a rapid and cost effective detection of pathogen and toxin contamination of food samples (Cui et al., 2008).

2.7. Current status

QD technology holds great potential and promise for applications in nanobiotechnology and medical diagnostics where they can be used as probes. However, the use in a clinical setting requires extensive research and development to determine the long-term effects of its use. Introduction of QDs to the biological milieu involves complex parameters like composition, toxicity, thrombogenicity, immunogenicity as well as ADME characteristics (absorption, metabolism, distribution and excretion). QD toxicity can also occur at different levels including composition of the core, surface coating, size and surface charge (Kirchner et al., 2005, Lovric et al., 2005a, Shiohara et al., 2004).

2.7.1. Quantum dot and toxicity

There is no consistent data on QD toxicity as there are many varieties of QD synthesised. Each QD type possesses its own inherent physicochemical properties (as it was described earlier), which in turn dictates its potential toxicity or lack of it. There is no systematic body of data currently in literature regarding the toxicity of QD and this can be attributed to a number of factors: absence of proper toxicology-based studies, the many types of QD dosage/exposure concentrations reported in scientific literature, and the diverse physicochemical properties of individual QD (Hardman, 2006). Data from studies primarily designed for toxicological assessment (e.g. dose, duration, frequency of exposure and mechanism of action) are far and few. To summarize QD toxicity**,** the general concepts were discussed pertaining to core, core shell and coating toxicities and animal studies. Two tables are presented that summarises some recent publications on QD toxicity (**Table 2.4** and **2.5**).

Table 2.4. Summary of QDs toxicity studies *in vitro*.

QD Type	Shell	Coating Agent	QD Size (nm)	Concentration	Wavelength (nm)	Biological Model tested	Assay Used	Incubation time (h)	Evaluated toxicity	Outcome	Year
CdSe	ZnS	DHLA	NR	400-600 nM	NR	Dictyostelium discoideum and HeLa cells	NR	<1	Cell growth was unaffected	Not applicable. Absorbance is 350 nm	2003 (Jaiswal JK, 2003)
CdSe	ZnS	None	NR	10 pmol QD Approx 10 nM	E_x= 550	HeLa cells	NR	10 Day	10 nM had minimal effect on cell so no cytotoxicity.	Not applicable.	2004 (Chen FQ, 2004)
CdSe	ZnS	COOH, OH/COOH, OH, H_2/OH, NH_2, CdSe-MAA,TOPO	NR	1-2μM 62.5-1000μg/ml	E_x= 510-520	WTK1 cells Primary cultures of rat hepatocytes	NR	12 1-8	DNA damage was detected when exposed to 2mM QD-COOH at 2 h so there is a sign of cytotoxicity. Oxidative/photolytic influence was cytotoxic. There is no sign of cytotoxicity by capping the QD with ZnS.	Not applicable.	2004 (Hoshino A and Suzuki K, 2004)
CdSe	ZnS	MUA	NR	0-0.4 mg/ml	E_x= 640	Vero and HeLa cell culture, primary cultures of human hepatocytes	NR	24	Vero cells showed toxicity at 0.2 mg/ml, whereas, HeLa cells & hepatocytes at 0.1mg/ml.	Not applicable.	2004 (Shiohara A, 2004)
CdSe	ZnS	SSA	NR	0.1-0.4 mg/ml	E_x= 520	EL-4 cells (mouse lymphocytes)	NR	0-24	Cell growth was affected at 0.1 mg/ml.	Not applicable.	2004 (Hoshino A, 2004b)

Table 2.4. Continued

QD Type	Shell	Coating Agent	QD Size (nm)	Concentration	Wavelength (nm)	Biological Model tested	Assay Used	Incubation time (h)	Evaluated toxicity	Outcome	Year
CdTe	None	None	2.3, 2.2, 5.7, 5.2	0.01-100 µg/ml	E_λ= 605 A_λ= 518	rat pheochromocytoma &murine microglial cell line	MTT assay	2-24	At 10 µg/ml is cytotoxic.	Pre-incubation of cells with antioxident N-acetylcysteine & bovine serum albumin significantly reduced QD induced cell death, also size plays an important part in cytotoxicity.	2005 (Lovric et al., 2005a)
CdTe	None	None	2-green, 4-yellow, 6-red	0-100 µM	NR	Hep G2 (human hepatom) a cell line	MTT assay	48	Concentrations in the range of 3.0µM, 4.8 µM & 19.1 µM induced reduction of 50% in MTT activity respectively. Free Cd was implicated in the observed cell cytotoxicity.	Cytotoxicity is related to the size of QD. Higher cytotoxicity was related to smaller size than the larger QD in this particular experiment. Green 520 nm & yellow 519 nm	2005 (Lovric J, 2005)
CdSe	ZnS	PEG Silanized	NR	0, 8, 80 nM	NR	Human HSF-42 (skin fibroblast) & INR-90 (lung fibroblast) cell culture.	Cell proliferation, apoptosis and cell cycle distribution assays.	48	No cytotoxicity. Minimal effect on cells integrity & molecular response of QD exposed to cell lines.	Exposed QD was endocytosed by human skin & lung fibroblast. Gene expression was altered approximately 0.2% of genes QD stimulated skin fibroblast compared to controls.	2006 (Zhang T, 2006)
CdSe	ZnS	Peptide	NR	15-250 nM	E_λ= 510-550	HEK 239T/17 & COS-1 (African green Monkey) cell lines	Cell Titer 96- cell proliferation assay.	1 & 24	Low toxicity at 1 h High toxicity at 24 h	The toxicity is dependent on exposure duration and concentration.	2006 (Delehanty JB, 2006)

Table 2.4. Continued

QD Type	Shell	Coating Agent	QD Size (nm)	Concentration	Wavelength (nm)	Biological Model tested	Assay Used	Incubation time (h)	Evaluated toxicity	Outcome	Year
CdSe CdTe	ZnS	Cysteine, MPA, N-acetyl cysteine	NR	10 µg/ml	E_x= 517-554	MCF-7 (human breast cancer) cell culture.	MTT & Trypan blue cell assays.	1-24	Treatment of cells with all forms of CdTe QD resulted in significant cell death. Therefore, cytotoxicity has been shown.	The CdTe QD is more toxic than CdSe/ZnS QD. It was established that free Cd is from CdTe induces cell death by free radical production.	2007 (Cho SJ, 2007)
CdSe	None	None	2.38	1, 10,20 nM	NR	Primary rat cell culture (hippocampal neuron)	MTT assay	24	Cells exposed with QD: 1nM - no toxicity, 10, 20 reduced cell viability.	Reactive Oxygen species has been caused the toxicity.	2008 (Tang M, 2008)
CdSe	ZnS	PEG	NR	0.84-105 µM	NR	CaCo-2 (human colon carcinoma) cell culture.	MTT assay	24	There is low cytotoxicity	The toxicity of coated QD is increased with acid treatment due to the free Cd ions.	2008 (Wang L, 2008)
CdTe	CdS, CdS/ ZnS	None	NR	0.2-3.0 µM	NR	K562 & HEK 293T human cell lines	MTT assay	48	Cells exposed to CdTe & CdTe/CdS QD were mostly nonviable, hence cytotoxicity was seen. However, no sign of cytotoxicity in CdTe/CdS/ZnS QD.	ZnS shells may prevent the release of Cd^{2+} ions causing cytotoxicity. There is evidence that residual organic solvents in non-aqueous QD preparations may have resulted in QD independent cytotoxic effects in other reports.	2009 (Su Y, 2009)

Keys: MTT: 3-(4,5-dimethylthiazol-2-yl)-2,5-diphenyl tetrazolium bromide); MUA: Mercaptoundecanoic acid; NR: not reported.

Table 2.5: Summary of quantum dots toxicity studies *in vivo.*

QD Type	Shell	Coating Agent	QD Size (nm)	Concentration	Wavelength (nm)	Biological Model tested	Assay/s Used	Incubation time (h)	Evaluated toxicity	Outcome	Year
InAs	ZnSe	DHLA/ PEG	8.7	NR	No longer than 800	Subcutaneously & IV injected in to rats & mice.	NR	5 min	Toxicity was not observed.	QDs were accumulated to SLNs when they were applied subcutaneously. However, QDs injected intravenously were shown to extravagate from the vasculature.	2006 (Zimmer JP, 2006)
CdSe	ZnS	MAA/targeting peptides± PEG	3.5 & 5.5	NR	E_x= 750-920	IVD into the tail of mouse.	NR	20 min	Toxicity was not observed.	PEG prevents the nonspecific uptake of QD into the liver & spleen. Hence, PEG has an important role in QD.	2006 (Zimmer JP, 2006)
CdSe QD525 & QD800	ZnS	±PEG	21 & 12	25 pmol	E_x= 525	IVD in the mouse.	NR	15 min	There is no sign of toxicity in this paper.	QD/PEG coated had a 6 min circulation time & without the 2 min. Presence of QD in the liver & spleen. The size of QD had no effect on biodistribution.	2007 (Schipper ML, 2007)
CdTe	ZnS	Monoclonal antibody for lung	NR	NR	NR	IVD into the mouse.	NR	Up to 144	No acute toxicity was observed.	The QD was removed from the body in a slow pace.	2007 (Woodward JD and Avenell J, 2007)
CdSe	ZnS	LM BSA	25, 80	5 nmol	E_x= 430 A_x= 350	Intravenously injection into the rat.	NR	240	No toxicity was observed	BSA coated QD was almost distributed to the liver, spleen & other tissues in approximately less than 2 hours.	2006 (Fischer HC, 2006)

Table 2.5: Continued

QD Type	Shell	Coating Agent	QD Size (nm)	Concentration	Wavelength (nm)	Biological Model tested	Assay/s Used	Incubation time (h)	Evaluated toxicity	Outcome	Year
CdSe	CdS	PEG	37	NR	E_x= 610-621	Intradermal injection into the mouse.	NR	24	Not toxicity was assessed.	QD mainly stayed in the injected site, they were detected in Lymph nodes	2007 (Gopee NV, 2007)
CdSe	ZnS	SSA/MUA	NR	0.1 mg/ml	NR	EL-4 cells, injected into mouse.	NR	Up to 168 h	Not toxicity	NR	2004 (Hoshino A, 2004b)
CdTe	None	None	6	2 mM	NR	IVD into rat.	Physiological, locomotion, behavioural assessment with histopathology	24	According to this paper there are some signs of toxicity can be observed.	NR	2007 (Zhang Y, 2007)

Keys: IVD: Intravenously delivered.

2.7.1.1. Core material toxicity

The potential and main area of QD toxicity, especially the cadmium-based QD is from the cadmium located at the core of the nanocrystal. Data from uncoated QD and free Cd present in the colloid suspensions and core have affected cells intracellularly (Kirchner et al., 2005) concluded that CdTe QD were cytotoxic in rat pheochromocytoma cells (PC12) at 1 μg/mL level of concentration which induced apoptotic-type of cell death with chromatin condensation and membrane fragmentation. The toxicity effect observed in these studies resembled Cadmium ions (Cd^{2+}) toxicity. Data collected from incubation of uncoated nanocrystals in rat hepatocytes cells suggest that cadmium is released via surface oxidation by biodegradation (Derfus AM, 2003). This study suggests that cadmium toxicity is from the core and is likely to contribute significantly to QD toxicity.

QD derived from CdTe and CdSe are electronically active and as such are prone to photo and air oxidation (as it was described previously) which could potentially promote free radical formation which can instigate cytotoxicity (Ipe et al., 2005). There is evidence that free cadmium ions do not promote free radical formation but can increase oxidative stress, whereas the QD core does contribute to free radical generation. Studies have shown that using cadmium reactive dyes in cell culture, the cytotoxicity was not linked to cadmium release from QD but to free radical generation (Cho et al., 2007). There is also evidence that free radical generation promotes DNA damage in the absence and presence of light photon activation (Green and Howman, 2005). Photoactivation of QD by visible or UV light or air oxidation was shown to increase free radical formation. The mechanism involved in these environments is that a photon of light excites the QD generating an excited electron that migrates to molecular oxygen generating singlet oxygen. In the presence of water and biological molecules, singlet oxygen readily initiates free radical formation (**Figure 2.11**). This is the rationale behind photodynamic therapy in cancer applications when QD are the participating material and its toxicity needs assessing when distributed to normal tissues. When normal tissue takes up QD nanoparticles and when activated by photons of light or other oxidative stress, free radical production can have detrimental effects on the tissues.

To circumnavigate this problem, tissue culture studies can provide some understanding of the process but unfortunately correlating the outcome to *in vivo* scenarios can overestimate or underestimate toxicity effects. Uncoated QD have also contributed to cytotoxicity comparable to cadmium toxicity and oxidative damage. Perturbations in gene expression and biochemical processes have all been implicated with QD toxicity suggesting a need for more thorough long-term studies of the effects of QD on cell signalling. This is vital for future applications, as long transit times encountered by QD in tissues and cells may cause damage.

With the current knowledge based on fluorescent organic dyes to determine the fate of intracellular biomolecules, care has to be exercised. Numerous nanoparticles with their innate active electronic structure can interact with commonly used organic dyes. It is of utmost importance to conduct suitable controls to include data that nanoparticle activity is not due to its electronic interaction with organic dyes present in assays.

2.7.1.2. Encapsulated quantum dots and their toxicity

Studies have shown that encapsulation of the QD core with ZnS or alternative capping material tends to reduce toxicity, although more work in this area is needed investigating. Work on human breast cancer MCF-7 cells has shown that CdTe cadmium cellular damage is similar to cadmium toxicity, while CdTe/ZnS core-shells or CdTe capped with mercaptopropionic acid, cysteamine, and n-acetylcysteine minimized the effect, indicating that ZnS shells and capping materials are effective in the time scale studied (Bakalova et al., 2005). In the above studies, leaching of the free cadmium ion in the intracellular compartment was also minimized by ZnS, MSA and capping agents. The presence of ZnS shell not only reduced the process of apoptosis and biochemical activation of processes but also eliminated release of cadmium ions whilst in aqueous environment. It also showed that ZnS shells could also reduce free radical production generated by air oxidation. This clearly demonstrates that capping QD with ZnS or other capping material reduces toxicity implicated with free radical production or release of free cadmium. It is important to emphasize that to evaluate toxicity of shell or capped particles, the degradation of the shell or capping material, together with its cytotoxicity taken into consideration (Chan et al., 2006).

Previous studies have shown that fluorescence intensity of CdSe/ZnS decreased with time along with a shift towards the blue spectra within live cells over time. This indicates that ZnS core shell biodegrades within the intracellular milieu. Some studies have indicated that the ZnS shell did not fully eliminate cytotoxicity when air or photo-oxidation was involved and that CdSe/ZnS QD may have promoted free radical production. It has been proposed by some researchers that although the ZnS shell shielded the CdSe core from oxidation, it could not inhibit the electron-induced radical generation in the aqueous environment suggesting that the ZnS underwent slow oxidation in the presence of air or water generating the sulphite (SO^{2-}) radical (Kirchner et al., 2005).

Applying capping materials such as ZnS to insulate QD core to reduce toxicity has been undertaken in many applications. In one study, CdTe QD coated with mercaptopropionic acid or cysteamine required a higher concentration to become toxic in PC12 cells as compared to uncoated QD. Equally, using the amino acid derivative N-acetylcysteine as coating agent on CdTe a reduction in the induction of Fas upregulation involved in apoptosis (Lovric et al., 2005a) and a decrease in cytotoxicity in neuroblastoma cells. Using dihydroxylipoic acid (DHLA) coating on CdSe/ZnS (Voura et al., 2004) have shown reduction in toxicity of QD in several cell lines while maintaining the fluorescence for over a week with no adverse effects. Using a large protein such as bovine serum albumin coating on QD has also shown reduced toxicity.

The majority of the effective capping materials all belong to antioxidants and this demonstrates the existence of oxidative stress in cadmium based QD toxicity. Capping materials in themselves must also be taken into account as potential toxic substances and several groups have shown increased toxicity associated with mercaptoacetic acid and TOP-(o-tri-n-octylphosphine oxide) (TOPO). Accumulated data suggest that the stability of shell and capping materials as well as toxicity requires intensive investigation for different QD preparations (Smith et al., 2008a).

2.7.1.3. Functional coatings and toxicity of quantum dots

QD incorporating shell and capping materials contain functional groups in order to target specific cells or tissues. These functionalized QD will need their toxicity and physicochemical parameters investigated as they may reduce toxicity when targeted to

specific locations. The specificity of the targeting material needs evaluating, as migration to non-targeted tissue may generate toxicity especially when QD function as a photosensitizing agent or drug carrier. Despite many studies in the use of functionalized QD *in vitro* and *in vivo*, no detailed studies has been conducted to ascertain the toxicity of these nanoparticle derivatives or their presence in non-targeted tissues. Data as to the biostability of the coatings, their half-life *in vivo* and non-specific targeting needs investigating. All these queries need resolving before use of coated QD in human applications can be undertaken (Derfus AM, 2003).

2.7.1.4. Toxicity studies of quantum dots in vivo

Toxicity can be exploited for its benefit in regards to biomedical applications especially in directing cellular death of tumors or metastases (Juzenas et al., 2008). One can envisage QD being designed with a photoactivatable coating and a site-specific ligand. Toxicity induced by photoactivation is directed to specific sites (such as tumors). After excitation by a photon, QD can impart an excited electron to molecular oxygen in the vicinity thus initiating a chain reaction of free radical generation promoting cell death. Photodynamic therapy in oncology uses this rationale, and it must be borne in mind that non-specific distribution of QD to non-cancerous tissue such as skin or retina exposed to light taken into account.

QD pharmacology and toxicology pertaining to animal studies are incompletely investigated. Uncoated CdTe QD injected in rats produced inconclusive results relating to toxicity and organ damage, and a thorough histological evaluation was absent. Disturbances to the motor function, when post injection of QD, indicating potential toxic effect to neural function (Zhang et al., 2008a). Future investigation should focus in this area particularly using long-term exposure studies, needs addressing. Studies with injected amphiphylic polycyclic acid polymer and PEG-coated QD in mice of 20 $m^{-1}g^{-1}$ animal weight have indicated non-lethality up to the time of necropsy (133 days) and no indication of necrosis or damage at injection sites and no signs of QD degradation *in vivo*. Mice injected with 20 nM and 1 μM CdSe/ZnS showed no noticeable adverse effects (Larson et al., 2003). Absence of overt adverse effects is no indication that there is no toxicity. QD with polymer and amphiphilic coatings when injected was found to retard degradation of coatings over time *in vivo*, affecting fluorescence over time, indicating that toxicological effects can alter with residence time of QD in tissues.

Studies have shown depending on the coatings such as mercaptoundecanoic acid, lysine and BSA coated CdSe/ZnS QD when injected in rats show regional distribution. Interestingly detection of QDs in the urine or faeces were absent over the duration of 10 days, indicating long transit time in the body. The particles indicated non-toxicity but not eliminated from the system either. The existing few studies show the need for short and long-term toxicity assessment that monitors multi-organ systems before QD be evaluated accurately (Gao et al., 2004).

2.7.2. Parameters involved in the reduction of quantum dot toxicity

QDs in comparison with pharmaceutical drugs undergo similar toxicity evaluation in terms of size, dose and exposure emphasizing the importance of stringent physicochemical characterization of QD. Particle size evaluation is vital to biological actions of nanoparticles. Numerous studies have demonstrated that for QD, particle size influences toxicity at the intracellular and animal level. Some studies have indicated that in cellular studies, 2.2 nm CdTe QD had greater toxicity as compared to larger, 5.2 nm particles (Lovric et al., 2005b). Interestingly, smaller particles localized in and around the nucleus of the cell, while the larger particles (approximately 2.5 nm) were located within the cytoplasm.

At the nanoscale level, size and dose plays an important role, since surface area is critical for nanoparticle properties. In one study, it concluded that structure might play an important role in its activity when delivered via the dermal route. Relevant information needed for toxicological studies as applied to humans are, the level of exposure and dose (Zhang et al., 2008a). Studies done *in vitro* using milligram or microgram/ml quantities may indicate a high dose to correlate to physiological context, as QD used at low concentration when targeted. Until dosing parameters is standardized, current studies should include a wide range of concentrations, highest to the lowest and incorporate estimations of surface area and the number of particles delivered (Ryman-Rasmussen et al., 2007).

Finally, exposure parameters require further evaluation. Most nanoparticles including QD have a tendency to distribute widely in tissues unless targeted, and most have minimal level of metabolism or excretion. Evidence of long residence time in tissues,

and long-term studies are vital to establish toxicological risk (Zhang et al., 2008b). In relevance to QD, the presence of electronically active cadmium in the structure may reside in tissues for a long duration perhaps years. As has been established that QD promote toxicity via the effects of cadmium and free radical generation, alteration on transcription, DNA synthesis, and signal transduction can go on for a long time. Recent studies have shown how relevant, low levels of free radical formation are integral to signal transduction pathways, and hence low-level radical production from QD may participate and alter with these pathways over time, as the various layers coating the toxic cadmium core are biodegraded (Tonks, 2005).

2.8. Evaluating quantum dot location through blood brain barrier

The blood brain barrier (BBB) is a barrier, which prevents diffusion of any unwanted substances from entering the vasculature of the brain, due to tight junctions. The disadvantage of this is that therapeutic drugs cannot reach the brain. There are special receptors or specific transporters that depend on the integrity of the capillaries for the transport of compounds across the barrier (Lockman et al., 2002).

Nevertheless, the feasibility of the use of nanoparticles for drug delivery or even imaging of the brain through the BBB has great potential. Nanoparticles with appropriate ligands are able to cross the BBB to deliver therapeutic drug molecules into the brain, as well as maintaining their stability. Additionally, slow release of the drug may prevent or decrease the peripheral toxicity, which is the second desirable property of the nanoparticle. Due to lack of research in this area, there are many factors that have to be considered in order to use the nanoparticles for labelling purposes. In the late 19^{th} century BBB work was carried out using trypan blue dye injected into small animals intravenously and results showed that the blue dye had been absorbed into the entire body except the brain. In the 1950s, similar experiments done on bigger animals such as rabbits and dogs when injected directly into the cerebrospinal fluid and electron microscopy showed trace of the blue dye in the brain. Finally, there is lack of studies currently conducted on QD and BBB. The lack of data in this area is because of inability of QD to cross the BBB or uptake and clearance by the reticuloendothelial system (RES) from the circulation. More experiments in this area with QDs have to be explored and established (Longmire et al., 2008).

2.8.1. Transit time of quantum dots *in vivo*

It is important to consider the physiological aspect of nanoparticles in order to understand their clearance mechanism. Kidneys and liver are responsible for clearing the QD from different organs when taken up. It must be established that the injected QD have been removed from the body as they contain heavy metal such as cadmium and selenium. According to different reviews, QDs have varied half-life: for example one study has shown the existence of QDs in the liver and kidney for 28 days, and another study detecting the trace of QDs in the lymph node and bone marrow of mice for 133 days, after intravenous injection (Ballou et al., 2004, Hardman, 2006).

Generally, nanoparticles face several processes that eliminate them from the body through renal clearance. These processes involve of glomerular filtration, tubular secretion and finally elimination of the molecule (Deen et al., 2001). In addition to size, surface charge plays an important part in clearance of nanoparticles. The rate of filtration of nanoparticles depends on their hydrodynamic diameter in the glomerular filtration. Renal clearance of QDs has been studied in the past by monitoring the body fluid such as urine, bile and faeces (Choi et al., 2007). Nanoparticles with diameter less than 6 nm are freely filtered whereas size between 6-8 nm can be filtered depending on surface charge (Ohlson et al., 2001). Larger nanoparticles with size of 8 nm cannot be removed by the renal route however: studies have shown that RES may be involved in the uptake (Choi *et al.* 2007a). Additionally, the hepatobiliary system takes first priority in removing the large nanoparticles (> 8 nm). The renal system plays a vital part in the removal of QD from the body with hydrodynamic diameter ranging between 4 to 6 nm. It can be deduced that as the size of QD increases, the renal clearance decreases. One study has shown that the clearance of QD exhibited high level of QD conjugated with bovine serum albumin (BSA) in the liver (Schipper et al., 2007).

By analysing the amount of QD retained in the body, dimensions of the nanocrystal can be estimated (Pelley et al., 2009). Excretion of QD from body circulation is inversely linked to their toxicity. High amount of QD in the body causes significant toxicity. This was confirmed by work done by Lin et al (Lin et al., 2008).

Overall, more research is needed in order to gain a better understanding and thorough insight into fundamental issues of this topic. One needs to address a number of

fundamental issues. For instance, details as to how QDs are excreted from the human body need to be determined.

2.9. Future perspectives

QDs have found vast application in biological and biomedical research as the next generation fluorescent probes. They are a powerful tool for illuminating many of the mysteries that encompass signal transduction pathways and biomolecular interaction within cells. Through extrapolating their properties for *in vivo* molecular and cellular imaging, QDs have a potential to lead to major advances in nanomedicine. They can revolutionize cancer diagnosis and therapy through early pre-symptomatic diagnosis and image guided drug delivery of chemotherapeutic agents. NIR QDs may replace the current tracers for SLN biopsy. The most promising aspect of QD application is in their use as photosensitizers for PDT. This application is unique as it utilises their inherent toxicity via the generation of reactive oxygen species to target cancer cells and micro-organisms. Overall, there are relentless possibilities for the application of QDs in biology and nanomedicine. However, QD technology is still in its infancy and extensive research is still required to resolve many of the issues that are limiting their safe application in clinical medicine.

Nanotechnology is a rapidly expanding area of science and nanoparticles such as QDs have potential to revolutionize in the area of medicine and research. Once the potential toxicity is reduced or eliminated it has the potential for multifunctional applications in the field of biomedicine, which includes cancer detection, drug delivery, imaging and real time monitoring of cellular processes in a disease state. Explorative work in the area of toxicity and safe use of nanoparticles in a clinical setting will contribute to our understanding of its properties. In order to reduce toxicity more research and investigation on non-cadmium QD and novel biocompatible would be desirable.

2.10. Aims

Aims of this study were firstly to conduct and develop novel QDs using an aqueous synthesis method that would emit in the visible to NIR region. Secondly, to significantly reduce toxicities associated to traditional QDs by coating with new novel agents that are also biocompatible. Thirdly to conjugate QDs with suitable ligands so as to produce probes that can be targeted to biomarkers on cancer cells that can also function as therapeutic agents.

Chapter 3
General methods and materials

3.1. Introduction

An aqueous synthesis method to develop highly luminescent cadmium based nanocrystals and their characterizations are described in this chapter. A series of water-soluble semiconductor QDs with high photoluminescence quantum yield (QY) have been synthesised and the biocompatibility, toxicity and finally bioconjugation properties have been evaluated throughout this thesis.

Investigation of QD's properties is vital and necessary because of their potential biological applications. For instance, as described in chapter 2, the broad excitation wavelength and symmetric emission wavelength can help the clinician to obtain visible images of targeted sites whereas using the current organic dyes faint images with short half-life will be obtained. Additionally using NIR emitting QDs and exciting with NIR excitation can penetrate deep tissues for strong images avoiding autofluorescence from tissues (Rizvi et al., 2010).

In this chapter some useful and applied biophysical and biochemical techniques to characterize QDs are presented. Each of the techniques by itself provides direct and indirect information, however, the combined use of several of them can contribute to detailed size and structures of the fabrication methods used in the synthesis of QDs. The emphasis is on the biophysical nature of what is measured in each technique and the way in which the data are used to obtain spectral and biochemical information. These techniques exploit the interaction of electromagnetic radiation with the nanocrystals under investigation. The characteristic interactions in Fourier transform infrared (FTIR) are related to the energy and wavelength absorbed and hence the emission wavelengths related to the nanomaterials and size. Additionally, *in vitro* cell culture techniques are linked to the chemical interaction with uptake and membrane interaction and estimating viability.

Despite the growing importance of obtaining accurate estimates of size, size distribution and concentration of QD particles in an increasingly wide range of applications, existing techniques for obtaining such data (e.g. Electron Microscopy and light emission, absorbance and scattering) can prove time consuming and complex, thus results difficult to interpret, particularly in samples which are heterogeneous in composition or which contain a range of particle sizes, e.g. are polydisperse.

3.2. Materials

All reagents in this study were used directly without further purification whilst all other reagents were of analytical grade. Water for all reactions and solution prepared were of highly purified and filtered by reserve osmosis (EASYpure RO).

Materials	Sources
1-Ethyl-3-(3-dimethylaminopropyl)carbodiimide (EDC)	Sigma-Aldrich
Alamar Blue ™	Serotec, Kidlington, UK
Ammonium sulphate	Sigma-Aldrich
Cadmium chloride ($CdCl_2$) 99.99%	Sigma-Aldrich
Centricon	Sigma-Aldrich
Culture plastic ware	Costar
Dichloromethane (DCM)	Rathburn
Dimethyl sulfoxide (DMSO)	Sigma-Aldrich
Dulbecco's-modified eagle medium (DMEM)	Sigma-Aldrich
Duterium oxide (D_2O)	Sigma-Aldrich
Endothelial cell growth medium supplement mix C-39215 (HUVEC)	PromoCell GmbH
Endothelial cell growth medium with supplement mix 5% FBS supplemented with growth factors.	PromoCell GmbH
Ethanol	Sigma-Aldrich
Ethylenediaminetetraacetic acid (EDTA)	Sigma-Aldrich
Foetal calf serum (FCS)	Gibco BRL
Freund's adjuvant (FA)	Sigma-Aldrich
Glutaldehyde	Sigma-Aldrich
Keyhole limpet haemocyanin (KLH)	Sigma-Aldrich
Mercaptopropylisobutyl polyhedral oligomeric silsesquioxane (MPOSS)	Hybrid Plastics

Mercaptosuccinic acid MSA (98%)	Sigma-Aldrich
N-(3-Dimethylaminopropyl)-N´-ethylcarbodiimide hydrochloride (DCCI)	Sigma-Aldrich
N-hydroxysuccinimide (NHS)	Sigma-Aldrich
N-N-Dimetylformamide (DMF)	Sigma-Aldrich
Neutral Red assay	Sigma-Aldrich
Paraformaldehyde (powder 95%)	Sigma-Aldrich
PBS/Tween20	Sigma-Aldrich
Phosphate buffered saline (PBS)	Sigma-Aldrich
Rhodamine G	Sigma-Aldrich
Sodium borate $Na_2B_4O_7$ (98%)	Sigma-Aldrich
Sodium borohydride $NaBH_4$ (98%)	Sigma-Aldrich
Sodium citrate $C_6H_5Na_3O_7.2H_2O$	Sigma-Aldrich
Sodium sulphite Na_2SO_3 (98%)	Sigma-Aldrich
Sodium telluride Na_2TeO_3 (99.99%)	Sigma-Aldrich
Sodium tetraborate decahydrate, $B_4Na_2O_7$ (99.5%)	Sigma-Aldrich
TBTU, Fmoc-amino acids	Sigma-Aldrich
Tetrahydrofuran THF (99.9%)	Sigma-Aldrich
Trifluoroacetic acid (TFA)	Sigma-Aldrich

3.3. Analytical techniques and instruments

3.3.1. Transmission electron microscopy (TEM)

TEM (Phillips CM 120) was used for visualisation and to obtain the size of particles. The disadvantage of TEM is high costs and complex sample preparation procedure. Hence, TEM was used only to determine the size and shape of coated QDs and uncoated nanocrystals.

To determine the size and shape of the MPOSS coated QDs and uncoated QDs, a set of 1:100 serial dilutions were made of coated QD with PBS and the optimum dilution was chosen. A drop of the samples was mounted on to a Piloform (TAAB) coated G300HS copper electron microscopy grid (Gilder) and allowed to air dry. The grids were examined with a CM120 (Philips) TEM at 3.0 x 10^5 magnification.

3.3.2. Ultraviolet-Visible absorbance spectroscopy (λ_{ab})

This device is a very straightforward analytical device, which uses light in the visible and adjacent (UV and NIR) ranges. This device measures absorbance of samples, which are soluble in their respective solvents. The solvents for diluting samples are often distilled water from water-soluble compounds, or ethanol for organic-soluble compounds so not all solvents are suitable for use in UV spectroscopy.

In this study, UV-visible absorption spectra were recorded in a quartz cuvette with a 1 cm path length. Either Borate-citrate or PBS buffer or distilled water could be used as a blank and an absorption spectrum of the clear soluble QDs nanoparticles was obtained. Using "Jasco V-630 Spectrophotometer" absorption spectra were recorded from 400 nm to 750 nm using a bandwidth of 2.0 nm. Different types of synthesised QDs were measured and their absorbance obtained. All optical measurements were performed at room temperature under ambient conditions.

3.3.3. Emission spectrum (λ_{ex}) spectroscopy

The emission wavelength was conducted by USB 2000+ Ocean Optics spectroscopy. It is rapid and the evaluation of emission wavelength can be done promptly. The homogeneity of samples can be analyzed by its FWHM. This device is extremely sensitive for detecting emission of QDs.

Samples were placed in a 1 cm path quartz cuvette. Using an excitation wavelength (λ_{ex}) of 375 nm with slit width of 5.0 nm, spectra were recorded from 400 nm to 800 nm regions. The emission spectrum of all synthesised QDs was determined. In addition, using different excitation wavelength (λ_{ex}) allows studying the emission spectrum. This equipment is also designed to photostability of the QDs in aqueous solution in real time.

3.3.4. Fourier transform infrared spectroscopy (FTIR)

FTIR spectra were obtained using the Perkin-Elmer 1750 FTIR spectrometer equipped with a fast recovery TGS detector and spectra analysis program for data acquisition and analysis (**Figure 3.1**). QD samples were placed in specially designed micro-cell housing with specially cut calcium fluoride (CaF_2) windows with 5 μm spacer. QDs were equilibrated in Deuterium oxide (D_2O) and 1 mg/mL were used for measurement. The spectrometer was continuously purged with dry air to eliminate spectra from atmospheric moisture in the spectral region of interest. A sample shuttle was employed to permit the sample to be signal-averaged with the background. Measurements in D_2O at room temperature were recorded at a QD concentration of 1 mg/mL and 100 scans were signal averaged.

All spectra were recorded at a resolution of 4 cm^{-1} and aqueous D_2O spectra as blank were recorded under identical conditions as the sample spectra. Absorption spectra were obtained by digitally subtracting the solvent spectrum from the corresponding sample spectrum. Where appropriate, water vapour contributions were subtracted from the absorption spectrum using previously recorded water vapour spectrum. Resolution enhancement using second derivative were calculated over 13 data-point range ($13cm^{-1}$) using the DERIV function to assign features of the vibrational spectra present in the QD samples.

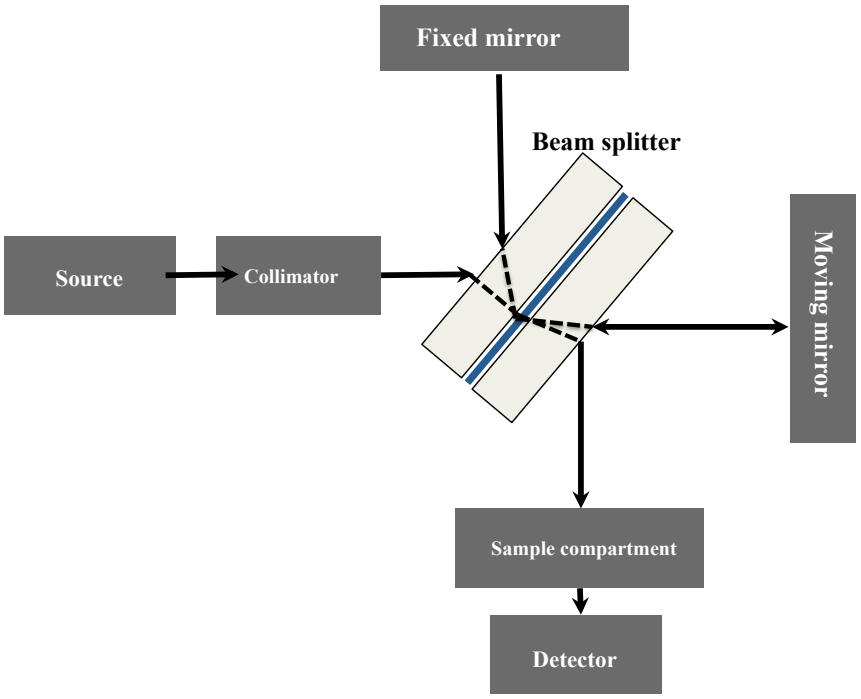

Figure 3.1: Schematic representation of a FTIR spectrometer.
FTIR is a technique, which utilizes an interferometer, originally designed by Michelson. The Michelson interferometer consists of two plane mirrors at right to each other and a beam splitter at an angle of 45° to the mirrors. One mirror is fixed in a stationary position and the other can be moved in a direction perpendicular to its front surface at a constant velocity. Between the fixed mirror and the movable mirror is a beam splitter, which divides the incoming light from the source, which is 50% is transmitted and 50% is reflected.

3.3.5. Confocal fluorescence microscopy

Images were acquired by fluorescent microscopy (Nikon Eclipse TE 300). The PCM scanning head is mounted on an inverted optical microscope (Nikon Eclipse TE 300), which can operate in fluorescence, reflection and phase contrast modes, and it is provided with Plan Fluor dry objective (20X/NA=0.5). A He-Ne blue laser at 488 nm and green at 543 nm are the sources, housed in a common module, providing the excitation beams that are delivered to the scanning head through a single-mode optical fiber. Photomultiplier (PMT) tubes are placed within the control unit, and the collected light arrives via high-transmission optical fibers. This means that electronic noise at the PMT output is greatly minimized.

3.3.6. Dynamic light scattering and X-ray diffraction

This technique produces fast results, high sample throughput and direct sample measurement as well as no need to dilute samples on column. However, there are some

weaknesses such as, evaluating data is complex, there is no any quantitative method and finally it is a poor devise for complex, polydisperse sample types (e.g. many biological sample types).

XRD is a rapid analytical technique primarily used for phase identification of a crystalline material and can provide information on unit cell dimensions. The analyzed material is finely ground, homogenized, and average bulk composition is determined. Further elemental composition was obtained with the use of XRD. The main application of X-ray powder diffraction is most widely used for the identification of unknown crystalline materials such as QDs. Determination of unknown solids is critical to studies in geology, environmental science, material science, engineering and biology. XRD information are normally obtained using aqueous solution of a prepared CdTe diluted with 1 volume of ethanol and centrifuged at 4000 rpm for 10 minutes. The precipitate is deposited onto a glass slide and dried at room temperature.

3.3.7. Zeta Potential

Measuring the zeta potential of particles in suspension is used to predict stability and behaviour when exposed to changes in ionic strength of the solution. Historically zeta potential measurement has required the sample to be diluted before measurements, which runs the risk of changing the zeta potential.

To characterize the size and charge on QD's surface, size distribution and zeta potential of QDs are determined with a Mastersizer 2000 Laser Particle Size Analyzer (Malvern, UK) equipped with a helium-neon laser (10 mW max, 633 nm). The laser light-scattering experiments were performed at a scattering angle of 90°. The available detection size ranged from 2 nm to 3 μm.

3.4. Methods

3.4.1. Cell culture techniques

3.4.1.1. Primary and secondary cultures

To propagate isolated or separated cells, specific tissues are first obtained and dispersed into its constituent cells, usually with the aid of a proteolytic enzyme such as trypsin. After removal of the trypsin the suspension is placed in a sterile plastic petri dish

together with a growth liquid medium containing required ions at isosmotic concentration, essential amino acids and vitamins, and an animal serum (usually foetal calf) in a proportion varying from a few percent to 50%. Sodium bicarbonate is commonly used as a buffer, in equilibrium with CO_2 (about 5%) in the air above the medium. After a variable lag phase the cells attach and spread on the bottom of the dish and start dividing mitotically, resulting in a primary culture. Attachment to a rigid support or substrate is crucial for the growth of most normal cells (anchorage dependence).

In many instances in the primary culture, the cells retain some of the characteristics of the tissue from which they were initiated, and are mainly of two varieties: thin and elongated (fibroblast like) or polygonal and tending to form sheets (epithelioid cells). The cells multiply or proliferate to cover the bottom of the flask with a continuous but thin layer, often one cell thick known as a monolayer. If they are fibroblastic they are regularly oriented parallel to each other (**Figure 3.2**).

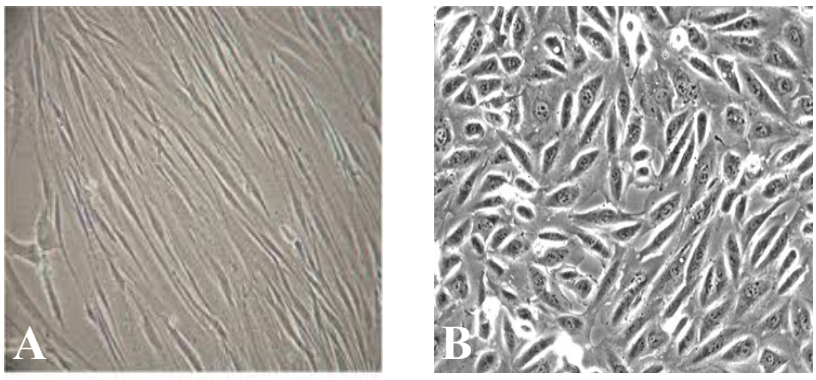

Figure 3.2: Cells arranged in two types: **A**, thin and elongated (fibroblast like) or **B**, polygonal and tending to form sheets (epithelioid cells)

Primary cell cultures derived from cancerous tissues usually differ from those of normal cells and are like transformed cells. The cultures are maintained by renewing the growth medium two or three times a week. When the cultures reach 90% confluence the cells are detached from the culture vessel wall by either trypsin or in combination with a chelating agent EDTA (Ethylenediaminetetraacetic acid, Sigma-Aldrich Company Ltd., Poole, UK), and a fraction of this is used to initiate new secondary cultures (transfer or splitting) to eventually establish cell strains or cell lines (**Figure 3.3**).

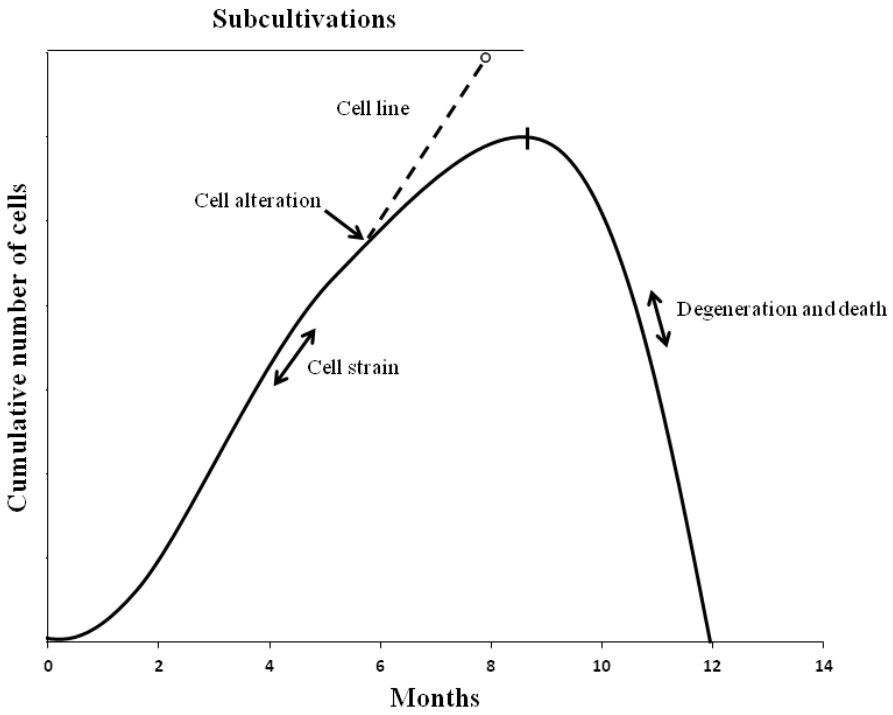

Figure 3.3: Multiplication of cultures of cells derived from normal tissues.
The primary culture gives rise to a cell strain, whose cells grow actively for many cells generations; then growth declines and finally the culture stops growing and dies. During multiplication of the cell strain altered cells maybe produced, which continued to grow indefinitely and originate a cell line. The cumulative number of cells is calculated as if all cells derived from the original culture had been kept at every transfer. (Adapted from Hayflick L: Analytic Cell Culture. National Cancer Institute Monograph, No. 7, 1962, p. 63)

Cells derived from primary cultures can often be passaged serially a number of times. This process usually causes a selection (cloning) for some cell types, which become predominant. The cells may then continue to proliferate at a constant rate over many successive transfers, and the primary culture is defined as having originated a cell strain (often called a diploid cell strain) whose cells appear unaltered in morphologic and growth properties. These cells must be transferred at a relative high cell density or split ratio to initiate a new culture. Despite this, the transferability of cell strains is limited: for example, with cultures of human cells the growth rate declines after about 50 duplications and the life of the strain comes to an end.

During the multiplication of cell strain some cells become transformed or altered, that is they acquire a different morphology, grow faster, and become able to start a culture from a small number of cells or high split ratio. The clone derived cells from one such cell, in contrast to the cell strain in which it originated, has unlimited or infinite life; it is designated as a cell line.

3.4.1.2. Cell transformation

Oncogenic viruses, radiations, and certain chemicals can induce mutation like changes in cultured cells that affect their growth and other properties. Such transformation (**Figure 3.4**) can also develop during the serial passage growth of cell lines without any exposure to the above, mentioned agents. Radiation and chemicals may induce transformation, as well as cancer *in vivo*, by initiating mutations (somatic mutations) because they were absent in the germ cells.

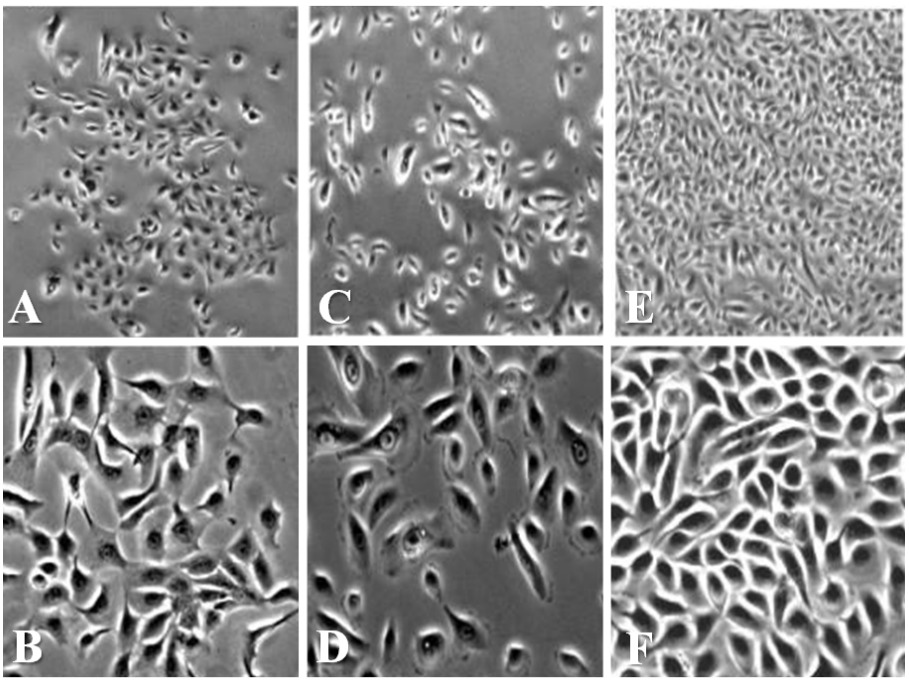

Figure 3.4: Transformation of cell lines during the serial passage.
Transformation can develop during the serial passage growth of cell lines without any exposure to the agents. A, C and E show cell proliferating with time whereas, B, D and F are amplified to show phenotypic changes after time. Radiation and chemicals may induce transformation, as well as cancer *in vivo*, by initiating mutations (somatic mutations) because they were absent in the germ cells.

3.4.1.3. Cell culture and treatments

3.4.1.3.1. Cell culture types

Human umbilical vein endothelial cells (HUVECs) originally isolated from umbilical cords. HUVECs the grown in cell culture medium (CCM) prepared using PromoCell Endothelial cell growth medium with supplement mix (PromoCell GmbH) at 37 $^{\circ}$C with 5% CO_2. Following confluences, cells were removed using 0.25% trypsin-EDTA and split in a 1:2 ratio. For this study the passage number 3 was selected. HUVECs originally were purchased from American type cell culture (ATCC) however, it was provided for this research from this department.

The supplement consisted of 5% inactivated foetal bovine serum (FBS), endothelial cell growth supplement 4%, epidermal growth factor 10 ng, basic fibroblast growth factor 100 ng, heparin 9 μg and hydrocortisone 100 μg. The medium has been developed for low serum for the *in vitro* cultivation of endothelial cells from large blood vessels. It has been optimized for human cells but can also be used in bovine, porcine and rat endothelial cells.

The prostate cancer cells (PC-3) were originally isolated from bone metastasis of a grade IV prostatic adenocarcinoma from a 62 year old male Caucasian. The cells exhibit low acid phosphates and testosterone-5-alpha reductase activities. Dr Ramesh of this department kindly provided this cell line for this toxicity experiment.

Colon cancer cells (SW620) were originally isolated from the tissue of a 52 year old Caucasian male (blood group A, Rh+). A recurrence of the malignancy resulted in a widespread metastasis from the colon to an abdominal mass. The established cell line consists mainly of individual small spherical and bipolar cells lacking microvilli.

Breast cancer cells (MCF-7) known as "Michigan Cancer Foundation-7" is a breast cancer cell line. This cell line is known to retain several characteristics of differentiated mammary epithelium including the ability to process estradiol via cytoplasmic oestrogen receptor and the capability of forming domes.

3.4.1.4. Cryopreservation of cells

For long-term storage of cells, trypsinized and neutralized in growth medium were re-suspended in 10% DMSO (dimethylsulfoxide, Sigma-Aldrich). Cells were dispensed in 1 mL cryotubes placed in polystyrene box and cooled to -70 ºC, followed by transfer to liquid nitrogen after 24 h.

To retrieve cells from cold storage, the cryotubes containing the cells were quickly thawed at 37 ºC, followed by one wash in complete appropriate growth medium before seeding into 25 cm^2 flasks in complete growth medium.

3.4.1.5. Subcultivation techniques

All cells were grown to 70-80% confluence in 75 cm^2 flask and maintained by subcultivation using the following protocol. All reagents and growth medium were

brought to room temperature. Medium from growing cell flask was aspirated and PBS solution 100 μL/cm^2 of vessel surface was added to wash the cells with gentle agitation for approximately 15 to 30 seconds.

The PBS solution was aspirated and Trypsin/EDTA solution 100 μL/cm^2 of vessel surface was added. The HUVECs were allowed to detach at room temperature (5 minutes) as recommended by the manufacturers. All other cells were incubated at 37 ºC to facilitate detachment (3-5 minutes). All flasks were examined under microscope for detachment. At the first sign of detachment, the flask was gently tapped on the sides of the vessel to loosen the remaining cells and then after, the cells were further dispersed by pipetting up and down for few times.

The trypsin neutralization solution (0.05%) trypsin inhibitor from soybean and 0.5% bovine serum albumin at 100 μL/cm^2 of vessel surface was added. This formulation of trypsin, neutralization solution was only used for the primary HUVECs cell as recommended by manufacturers. For all other cells the normal growth medium with 5% heat inactivated FBS were sufficient. The detached cells were aspirated and transferred to centrifugation tube. The cells were centrifuged for 3 minutes at 220 x g.

The supernatant were discarded, and 1 mL of the appropriate growth medium were added to the cells and re-suspended by pipetting up and down. The cells were plated at desired seeding density in new cell culture vessels containing appropriate growth medium pre-warmed to 37 ºC, 5% CO_2.

3.4.2. Cell Viability Assessment

3.4.2.1. Preparation of synthesised QDs preparation in MEM medium

The following QDs; CdHgCoTe, CdHgCoTe/MAS, CdHgCoTe/MAS/MPOSS were mixed with neat ethanol in a ratio of 1:2 v/v and centrifuged for 15 minutes at 4000 rpm separately. The supernatant was discarded and the precipitate were dried under vacuum and weighted. The resulting dried QDs were all suspended in MEM medium with HEPEs buffer at pH 7.4 and adjusted to contain 1 mg/mL as a stock for experimental use.

3.4.2.2. Preparation of precursor materials: Cadmium Chloride (Cd^{2+}) and Mercury Perchlorate (Hg^{2+}) ions for toxicity studies

Stock solutions of $CdCl_2$ and ($Hg(ClO_4)_2$), QD precursor materials were prepared at 1 mg and dissolved in 1 mL MEM medium in HEPEs buffer pH 7.4. Samples were kept at +4 ºC until further experiments where it was diluted to contain amounts in the range of QDs preparations.

3.4.2.3. Seeding of cells in the culture plates for toxicity evaluation

All cell cultures were incubated in standard growth conditions (37 ºC, 5% CO_2) cells lines PC3, MCF-7 and SW620 were all maintained in 75 cm^2 tissue culture flask in D-MEM supplemented with 10% foetal bovine serum (FBS) and 1% penicillin/streptomycin, 1 mM pyruvate, 2 mM glutamine and 10 mM HEPES. HUVECS were grown and maintained in PromoCell endothelial cell growth medium with supplement mix (PromoCell GmbH) 5% FBS supplemented with growth factors. All cells were suspended in their appropriate growth medium after they have been treated with trypsin and centrifuged at 1500 pm for 5 minutes at room temperature. The cell count was performed for the four types of cells respectively. Cells were counted using a hemocytometer and 1 x 10^4 cells were plated into each well of a 96-well culture plate (Corning USA) 200 μL/well (replicates of 6). All cell cultures were used for toxicity assessment after 48 h growth.

3.4.2.4. Cytotoxicity assays

The viability of the cells treated with the appropriate QDs was estimated with Alamar Blue (AB) and Neutral Red (NR) assays. After 48 h incubation, the growth medium were removed and washed 3 times with serum free growth medium. The prepared coated and uncoated QDs (CdHgCoTe, CdHgCoTe/MSA, CdHgCoTe/MSA/MPOSS) were prepared in MEM with reduced serum 2% to avoid interference of QDs with serum components to a final concentration range of 0.1-100 μg/mL at 200 μL were added to each well. The selected concentrations of coated and uncoated QDs are as following; 0, 0.1, 1.0, 10, 50 and 100 μg/mL where they were added in replicates of 6 wells in a 96-well plate. The incubated cells were monitored over the time course of 4, 8, and 24 h.

After different incubation periods, 20 μl of Alamar Blue solutions (10 X) was added to medium each well and incubated for another 4 h. The viability indicator that uses the natural reducing power of living cells to convert resazurin to the fluorescent/absorbing molecule, resorufin, indicates the amount of viable cells.

The amount of absorbance is proportional to the number of living cells and corresponds to the cell metabolic activity. The absorbance was read using a 96–well plate reader (Helena Biosciences, Sunderland, UK) in a Multiscan MS UV-visible spectrophotometer (Labsystems, Ashford, UK). The absorbance at 570 nm was monitored using 600 nm as a reference wavelength.

In parallel, viability was also monitored using an *in vitro* toxicology assay kit, Neutral Red based vital dye (Sigma-Aldrich). The procedures as above for Alamar Blue was duplicated for Neutral Red with 20 μL of a 0.33% of Neutral Red solution and added to the medium of each well and incubated for another 4 h. At the end of the incubation period, the medium was carefully removed and the cells quickly rinsed with PBS. The PBS was removed and the incorporated dye was solubilized in 200 μl of 1% acetic acid in 50% ethanol. The cultures were allowed to stand for 10 minutes at room temperature with gentle agitation. Viable cells take up the dye by active transport and incorporate the dye into lysosomes, whereas non-viable cells will not take up the dye. The liberated incorporated dye is proportional to the number of viable cells. The absorbance was read using a 96–well plate reader (Helena Biosciences, Sunderland, UK) in a Multiscan MS UV-visible spectrophotometer (Labsystems, Ashford, UK). The absorbance at 540 nm was monitored using 690 nm as a reference wavelength.

3.4.2.4.1. AlamarBlue assay

Alamar Blue™ (AB) (Serotec, Kidlington) is a commercially available assay, which aims to quantitatively assess cell proliferation, cytotoxicity and viability. Changing the colour from dark blue to light pink is the result of the cell metabolism. This color change is measured by monitoring absorbance at 570 nm and 630 nm. The advantages of this assay are that it is soluble in media, stable in solution, minimally toxic to cells and produces changes that are easily monitored (Seifalian et al., 2001).

Figure **3.5**, demonstrates the reduction reaction, which takes place in functional cells. The blue dye resazurin has negligible intrinsic fluorescence and absorbance while its reduced product, resorufin, emits a highly fluorescent, pink colour, which can be detected by means of a plate reader equipped with a 570 nm filter.

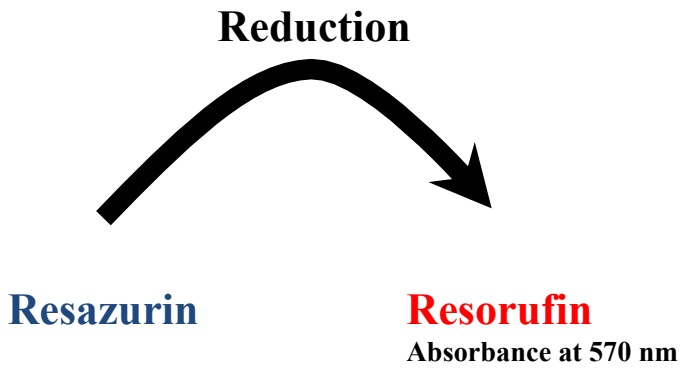

Figure 3.5: The blue dye resazurin is reduced to the fluorescent pink resorufin by viable, metabolically active cells only. The intensity of absorbance is proportional to the number of metabolically active cells.

3.4.2.4.2. Neutral Red Assay

The key component is the vital dye, Neutral Red (Basic Red 5, Toluylene Red). Viable cells will take up the dye by active transport and incorporate the dye into lysosomes, whereas non-viable cells will not take up the dye. After the cells have been allowed to incorporate the dye they are briefly washed or fixed. The incorporated dye is then liberated from the cells in an acidified ethanol solution. An increase or decrease in the number of cells or their physiological state results in a concomitant change in the amount of dye incorporated by the cells in the culture. This indicates the degree of cytotoxicity caused by the test material.

3.4.2.5. Statistical analysis

Means and standard deviation (SD) were calculated for all experiments. For comparison of data, one-way analysis of variance (ANOVA) was performed and the statistical significance determined to 0.05 confidence intervals ($P < 0.05$). To compare the difference of significance of different conditions Tukey's post hoc test was performed.

3.4.3. Solid-phase peptide (Calreticulin) synthesis

Calreticulin (CRT) peptides were synthesised manually, using an in-house designed glass reaction vessel, using Rink amide resin as the solid phase (**Figure 3.6**). All amino acids used were amino protected with Fmoc amino acid with side-chain protection.

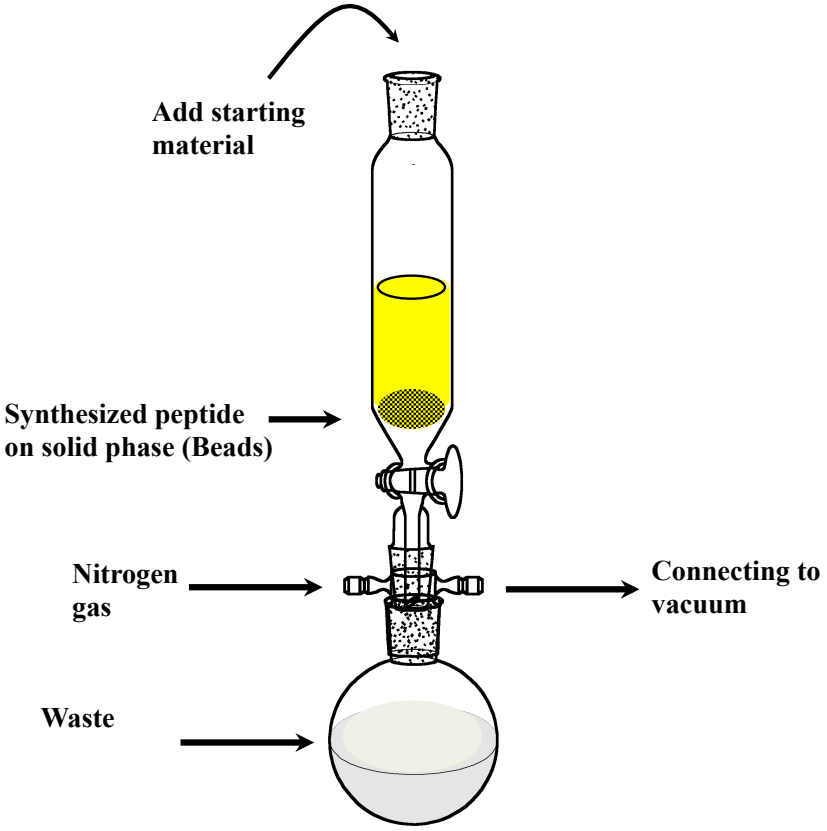

Figure 3.6: Schematic representation of a manual solid phase peptide synthesis

0.5 g of the Rink-amide resin derivatized with Fmoc-amide was placed into the glass reaction vessel and de-protection was carried out using 20% piperidine in DMF for 10 minutes. The resin was thoroughly rinsed with DMF (10 mL/g, 5 x 1 minutes). Acylation was initiated using pre-weighed Fmoc amino acids in the presence of HBTU in 5 mL bottles. A 2.5 –fold excess (based on the resin loading) of the acylating species in 0.2 M methyl morpholine (MMP) in DMF (5 mL) were added to the reaction vessel. The cycle for the addition of the activated protected amino acid and de-protection was repeated until the desired complete length of the CRT peptide was achieved. Complete detachment of the assembled peptide was carried out by adding 95% Trifluoroacetic acid (TFA) in H_2O (50 mL) containing EDT, phenol and thioanisol as scavengers for 2

h. The TFA and scavengers were removed by rotary evaporation and precipitated with cold diethyl ether to further remove any residual scavengers. The precipitated peptide was further rinsed in diethyl ether and vacuum dried until powder. The peptide was characterized by high performance liquid chromatography (HPLC) and calculated molecular weight was confirmed by matrix assisted laser desorption ionisation/ time of flight (MALDI/TOFF). The peptide was lyophilized and stored at +4 ºC until further use (**Figure 3.7**).

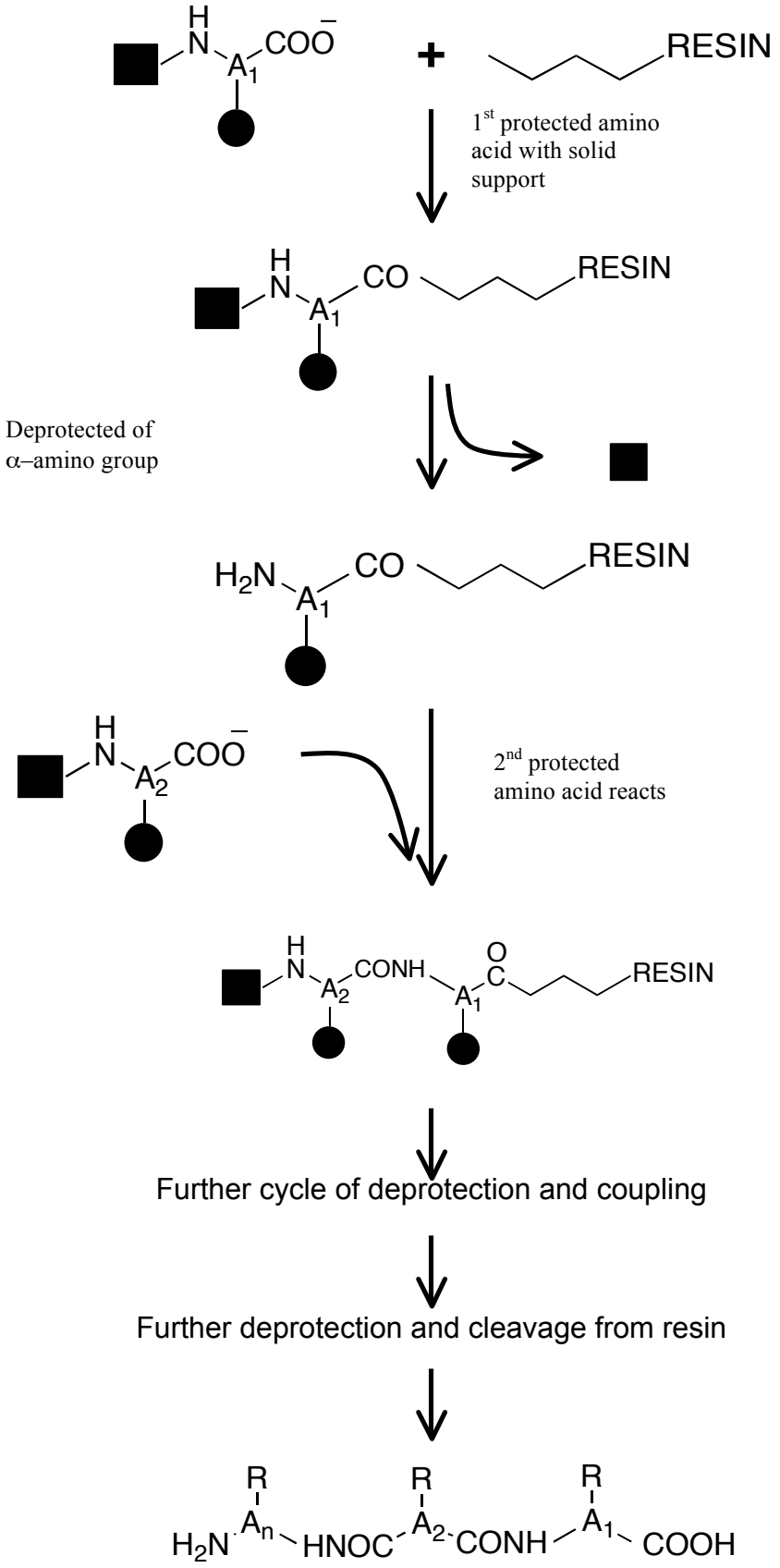

Figure 3.7: Reaction scheme of manual solid-phase synthesis of synthetic CRT peptide

3.4.4. Cell cultures treated with Doxorubicin (anticancer drug) and cadmium ions

All cells (HUVEC, MCF-7 and SW620) were seeded in 24-well flat culture plate (Corning). After culturing for 24 h, the cells were washed with FBS-free DMEM and incubated with Doxorubicin 50 µg/mL and Cd^{2+} 50 µg/mL in FBS-free culture medium at 37 ºC for 1 h. The cells were then washed gently with PBS (X 3 wash) and fixed with 4% formaldehyde for 20 minutes, and blocked with 1% BSA in PBS/Tween20 (PBS/T) for 30 minutes. The fixative was aspirated and washed three times PBS/T and conjugation complex (NIR QD-(Anti-CRT)) incubated at room temperature for 2 h. In the end, cells were washed three times with PBS/T for 5 minutes each. Cells were observed under confocal microscope for the localization of QD-(Anti-CRT) for evidence of apoptosis of cancer cells compared to untreated and primary cultures.

Seeded cells were also repeated this time with incubation with NIR QD-CNT. In this arrangement cells were exposed to 650 nm red light-source for 5 minutes. The cells were rinsed in PBS and fixed as above. The cells were blocked with 1% BSA in PBS/T for 30 minutes. The fixative were removed and washed with PBS and conjugated complex NIR QD-(Anti-CRT) incubated at room temperature for 2 h. Excess complex were removed with washing with PBS and observed for evidence of apoptosis with confocal microscopy.

3.4.4.1. In vivo detection of targeted NIR quantum dot and non-targeted with carbon nanotube

Six to eight weeks old BALB/c female mice (18-21 g) were provided by Pharmidex Ltd. All the experiments were carried out at Pharmidex pharmaceutical Ltd, adhered to the 1986 Scientific Procedures Act (UK) and in compliance with the guide for the care and use of laboratory animals in Pharmidex Ltd. The animal housing area was maintained at 24 ºC with a 12 h light/dark cycle, and animals fed adlibitum with water and standard laboratory diet. All animals were acclimatized to the animal facility for at least 48 h prior to experimentation. In the study involving *in vivo* imaging, mice were administered 10 mg/kg body weight of QD-CNT in PBS by intraperitoneal (IP) injection.

Mice treated with targeted LPS-QDs were imaged using the IVIS *in vivo* imaging system (Xenogen). The filter sets used to acquire the images were excitation, 590/30nm; emission, 730/80nm for targeted NIR QD.

However, for the biodistribution studies of non-targeted NIR QD-CNT, the Hamamatsu Orca R2 capture system/fire wire was used with the filter set of 705 nm.

3.4.4.2. Histological analysis

Coated CdHgCoTe/MSA/MPOSS QDs at a total dose of approximately 10 mg/kg were injected into mice by intraperitoneal (IP) injection for the histological studies. Liver, spleen, lung and brain were removed from sacrificed animals after 4 h and tissues were harvested and fixed in 10% formalin, embedded in paraffin, sectioned and observed under confocal microscope.

Chapter 4

Development and synthesis of a novel multifunctional water-soluble ‘Quantum Dots’ with biocompatible coatings

4.1. Introduction

The synthesis and application of semiconductor quantum dots (QDs) with high photoluminescence (PL) and especially water-soluble nanocrystals have generated great interest since the pioneering work of Alivisatos (Alivisatos, 2004). In comparison to traditional organic fluorescent labels, QDs are superior in performance due to numerous advantages (Rizvi et al., 2010) (refer to chapter 1). Currently, semiconductor colloidal nanoparticles are under intensive investigation for potential applications in multiplexed bioassays and in ultrasensitive optical detection and imaging (Alivisatos, 2004).

An additional main advantage is that the spectral properties of these nanocrystals can be conveniently tuned by manipulating particle size and multicolored fluorescence obtained with a single excitation light source. The NIR wavelength window (700-900 nm) is useful for biological imaging and detection as auto-fluorescence and absorbance from tissue is reduced in this range. By doping cadmium telluride (CdCoTe) QDs with mercury (Hg^{2+}) ions the range of the emission could be extended into the NIR region.

All synthesised fluorescent emitting QDs in this study are assembled with semi-conductive materials, which is cadmium-based. Although, cadmium is known to be toxic, presence of it in the QD's core in combination with other metals maybe a potential contributor of toxicity in clinical applications. Semiconductor based QDs with Cd^{2+} ions are essential in the formation of QDs as they emit stronger fluorescence with stable quantum confinement, compared to non-cadmium based QDs. However by using a novel biocompatible coating agent (MPOSS) has solved some of the toxicity issues in this proposed technique (chapter 5).

The complementary characteristics of optical techniques and magnetic resonance imaging (MRI), as combinatory probes, which exhibit both fluorescent and (super) paramagnetic properties were explored. A strategy employed in this study was to dope QDs with paramagnetic ion (cobalt) in the synthesis. Agar phantoms of QDs were developed and imaged with MRI.

The above properties were developed and are desirable in multiplexed labeling and simultaneous detection of markers on cells and tissues (refer to chapter 6). It is still a big challenge for many researchers to synthesis novel water-soluble QDs with ideal combinational optical properties (Yu, 2008).

It has been established that fluorescence emitted by QDs is affected by surface defects on the nanocrystals and by reducing these defects with an inorganic shell with higher band-gap materials or with suitable coatings, the fluorescence intensity can be increased and quantum confinement established. Many variations of cadmium (Cd) based QDs such as CdTe-CdS, core/shell, CdSe-CdS, core/shell and CdTe-CdS-ZnS, core/shell/shell structures have been synthesised and modified by many laboratories with a view of improving their photoluminescence and to reduce toxicity.

A number of water-soluble bifunctional molecules can replace the hydrophobic ligands on the surface of QD particles to make them water-soluble (**Figure 4.1**). Such molecules that have already been used in this study include mercaptosuccinic acid. Due to their high surface-to-volume ratio, they also can provide for the attachment of multiple different chemical/biological molecules (Delehanty et al., 2009). These molecules have one end anchored to the QD surface atoms such as –SH, while the other end extends outwards to provide water-solubility, as well as bioconjugation ability such as $–NH_2$, –OH and –COOH.

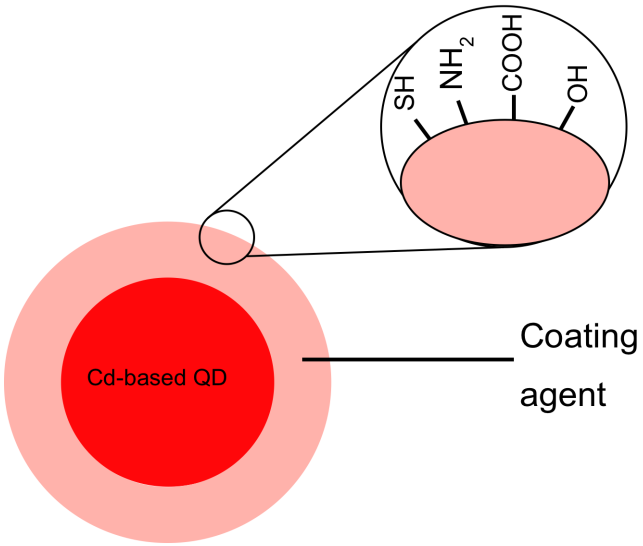

Figure 4.1: Coating layer provides multiple functional groups (amine, carboxylic acids and cysteines residuals) for covalent conjugation with biocompatible biological molecules.

In the present study, a selection of monodisperse, highly luminescent and NIR emitting water-soluble QDs was synthesised including: (1) uncoated CdTe (been used as control), (2) CdTe/MSA, (3) CdCoTe/MSA (4) CdHgCoTe/MSA and (5)

CdHgCoTe/MSA/MPOSS (**Table 4.1**). The synthesised QDs were characterized and results are presented and discussed.

4.2. Supplementary Materials and Methods

4.2.1. Materials

Sodium borohydrate ($NaBH_4$, 98%), Mercaptosuccinic acid (MSA), Mercuryperchlorate ($Hg(ClO_4)_2$), Cadmium chloride ($CdCl_2$), Sodium tellurite (Na_2TeO_3), Sodium borate ($Na_2B_4O_7$), Cobalt chloride, Sodium sulphite (Na_2SO_3), Tetrahydrofuran (THF) and Rhodamine G were all purchased from Sigma-Aldrich.

All other chemicals were all of reagent grade. Milli-Q grade water (> 18.2 MW) was used as the solvent for aqueous solutions.

Refer to section 3.2. of Chapter 3 for details.

4.2.2. Aqueous synthesis of quantum dots

4.2.2.1. Synthesis of MSA and MSA/MPOSS coated quantum dots

CdTe QDs were synthesised by an improved method of the procedure described in reference (Gao et al., 2002). Instead of a magnetic stirring, a homogenizer (KIKA T25 LABORTECHNIK) at 24000 rpm/min was used for vigorous mixing. Also, sodium sulphite ($NaSO_3$) was used as a mild reducing agent during the synthesis. All the starting materials were obtained from commercial suppliers and were used without further purification. All reactions were carried out in buffer solution composed of 15 mM $Na_2B_4O_7$ and 15 mM citrate acid, pH at different values adjusted with 1 M NaOH/HCL.

Synthesis of CdTe (control): For preparing uncoated CdTe QD, a precursor solution was prepared by mixing solutions of $CdCl_2$ (1 mM) and Na_2TeO_3 (0.25 mM). Mixing this solution with Na_2SO_3 (0.25 mM) in 50 mL of above buffers in a flask pre-chilled in ice for another 5 minutes. However, uncoated QDs are water insoluble.

Synthesis of CdTe/MSA: For preparing CdTe/MSA QD, a precursor solution was prepared by mixing solutions of $CdCl_2$ (1 mM), Na_2TeO_3 (0.25 mM) and MSA (3 mM).

Mixing this solution with Na_2SO_3 (0.25 mM) in 50 mL of above buffers in a flask pre-chilled in ice for another 5 minutes.

Synthesis of CdCoTe/MSA: The preparation is included precursors $CdCl_2$ (1 mM), Na_2TeO_3 (0.25 mM), $CoCl_2$ (1 mM) and MSA (3 mM) into Na_2SO_3 (0.25 mM) in 50 mL of above buffers in a flask pre-chilled in ice.

Synthesis of CdHgCoTe/MSA: The preparation of CdHgCoTe/MSA included precursors $CdCl_2$ (1 mM), Na_2TeO_3 (0.25 mM) with varying amounts of $Hg(ClO_4)_2$ (0.2, 0.3, 0.4, 0.5 and 0.6 mM) as above, MSA (3 mM) and $CoCl_2$ (1 mM), Na_2SO_3 (0.25 mM) in above buffers in a flask pre-chilled in ice.

Synthesis of CdHgCo/MSA/MPOSS: The preparation of CdHgCoTe/MSA/MPOSS included precursors $CdCl_2$ (1 mM), Na_2TeO_3 (0.25 mM), $Hg(ClO_4)_2$ (0.2, 0.3, 0.4 and 0.5 mM, MSA (2 mM), $CoCl_2$ (1 mM) and Na_2SO_3 (0.25 mM) and finally, MPOSS (0.1 mM in THF) into a flask pre-chilled in ice.

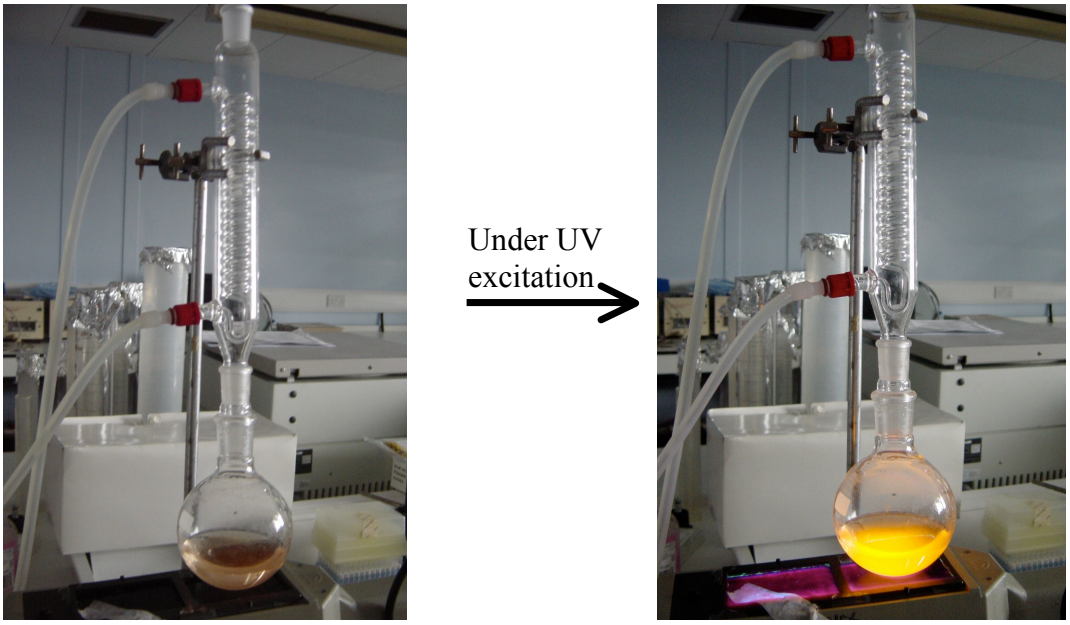

Figure 4.2: Images of reflux apparatus used for synthesising coated QD before and after excited by UV light with emission.

The above individual mixtures were subjected to vigorous mixing using a homogenizer for 5 minutes. After 5 minutes, 20 mg of solid $NaBH_4$ were added rapidly and mixed for a further 5 minutes. Finally, the mixture was transferred into a one-neck round bottle flask (250 mL) that was connected to a condenser and refluxed with mixing at 100 ºC under aerobic conditions (**Figure 4.2**).

4.2.3. Characterization of quantum dots

Fluorescence measurements were carried out at room temperature using (USB 2000+ Ocean Optics spectrometer). UV-VIS absorption spectra were recorded by Jasco V-630 spectrometer to detect the absorption wavelength by using the distilled water as a control. Irradiating at 365 nm with a LED-based light with QD samples placed in quartz cuvettes performed with a time-course study of photostabilities.

Transmission electron microscopy (TEM) images were obtained on a (Phillips CM 120). TEM samples were prepared by depositing nanoparticles on copper grid coated with Piloform (TAAB) and examined at 3×10^5 magnifications.

FTIR spectra were obtained using Perkin-Elmer 1750 FTIR spectrometer purged with dry air to eliminate atmospheric moisture absorbance from spectral region of interest. Dried QD samples were resuspended and equilibrated in D_2O and 100 scans were signal averaged in the range of 4000-400 cm^{-1} wavenumbers on calcium fluoride (CaF_2) cell with a 6 mm path length were carried out to improve signal to noise ratio.

FTIR vibrational spectroscopy was used to further characterize the mentioned QDs and the surface chemistry of them. All the cadmium based QDs synthesised were initially centrifuged to eliminate any insoluble material. The QD solution was then precipitated with equal volume of cold ethanol and air-dried. The dried samples were then dispersed in D_2O for FTIR analysis.

4.3. Results

4.3.1. Preparation of MSA and MSA/MPOSS stabilized quantum dots

The introduction of an improved method of synthesis with a homogenizer for mixing and $NaSO_3$ as a mild reluctant in precursor solutions, improved the formation of nanocrystals which showed strong luminescence and stability.

At the start of the synthesis the solution containing the precursors $CdCl_2$, Na_2TeO_4 and MSA showed a faint brown color at 5 minutes. Those containing cobalt (Co) and mercury (Hg) would appear as faint pink in appearance, which could be due to the mild reducing properties of MSA and Na_2SO_3. On adding solid $NaBH_4$ powder, the solution turned to strong pink color instantly for the precursor with Co depending on the pH value of the precursor solutions. However, in precursor solutions without the presence of Co it turned to a dark a light green color.

These initial crude solutions displayed no luminescence presumably due to very small nanocrystal formation. Lowering the pH value of the precursor solution or raising the reaction temperature accelerated the formation of the nanocrystals. As the heating to boiling progressed the crude solution turned to brown colour for all the precursor solution and after approximately 2 h, a weak brown luminescent could be observed when excited by UV light. Sustaining the boiling and refluxing for approximately 18 h, the absorption spectra of QD nanocrystals and emission shifted towards the longer wavelengths as an indication of increasing size and quantum confinement.

Finally, by controlling the reaction time (2-18 h), suitable CdTe QDs with fluorescence of different colors were harvested (**Table 4.1**). Below is the list of synthesised QDs:

Table 4.1: Range of fluorescent QDs were synthesised and coated with biocompatible materials

Quantum dot	Coating agent	Absorption wavelength (nm)	Emission Wavelength (nm)	Size (nm)
CdTe	Control	N/A	N/A	N/A
CdTe	MSA	425	600	2.96
CdCoTe	MSA	455	610	3.01
CdHgCoTe	MSA	495	630	4.67
CdHgCoTe	MSA/MPOSS	610	800	4.87

The sizes of the QDs could be influenced by controlling the duration of the reflux, which was monitored by sampling at time intervals as above for absorption and photoluminance (PL). At 18 h of refluxing, the emission peaks of the QDs shifted towards the NIR region (**Figure 4.3**).

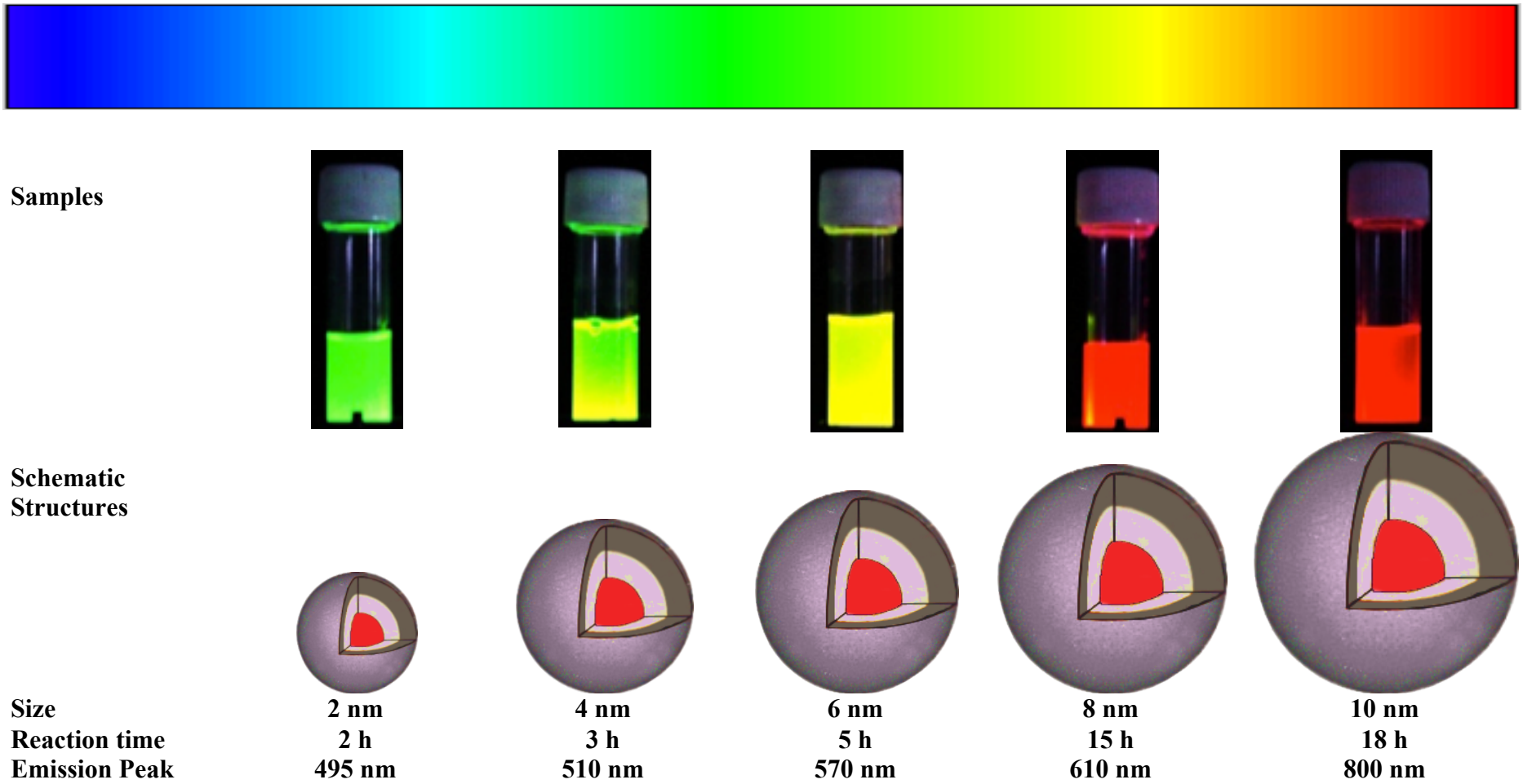

Figure 4.3: General description of monitoring the synthesis process of QD over the time course of 18 h showing increasing size and shifting the PL the towards NIR region

4.3.2. Characterization results

4.3.2.1. Absorption and emission spectra

Optical characterization of QDs is usually provided by UV-VIS and photoluminescence spectrometer, which offer fast and non-destructive option. The absorption and emission spectra of QDs were monitored during the reflux. The absorption and emission spectra of all synthesised QDs shown in figure **4.4** and **4.5** respectively at the end of the synthesis procedure, irradiated under the UV-light (375 nm).

After 18 h reflux the absorption and emission peak for CdTe/MSA, CdCoTe/MSA, CdHgCoTe/MSA and finally CdHgCoTe/MSA/MPOSS is (425, 600 nm), (455, 610 nm), (495, 630 nm) and (610, 800 nm) are respectively (**Figure 4.4**) and (**Figure 4.5**).

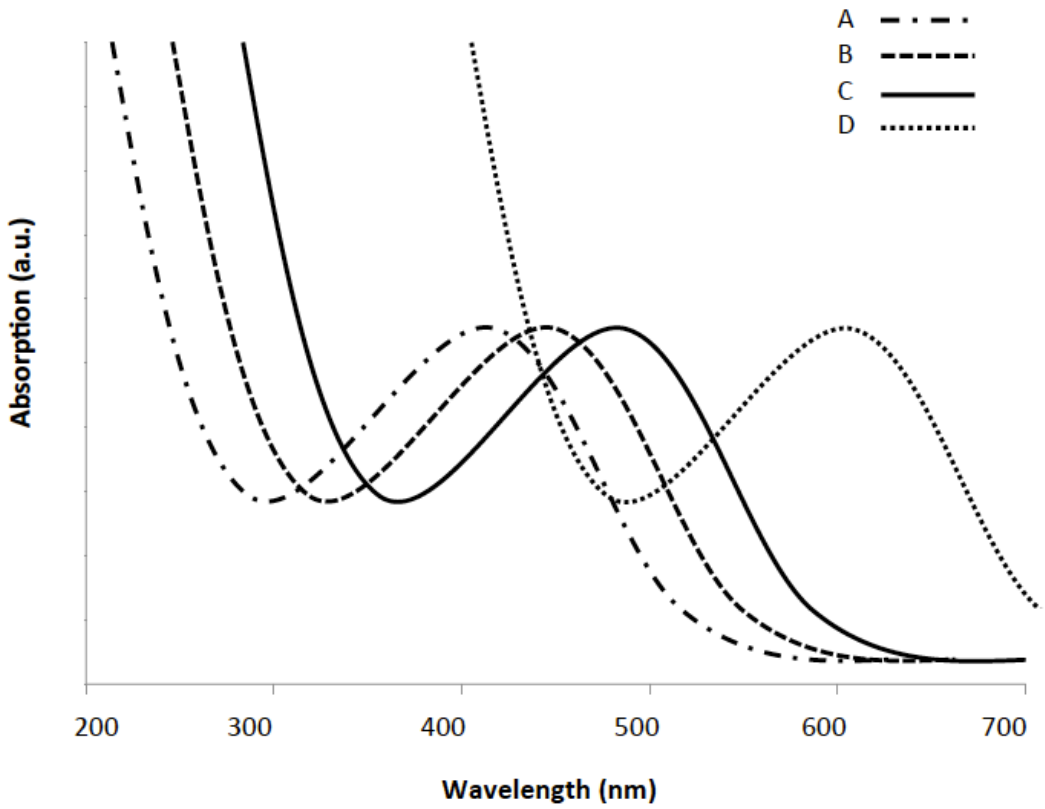

Figure 4.4: Absorption wavelengths of four different QDs dispersions.
The absorption of (A) CdTe/MSA QDs at 425 nm, (B) CdCoTe/MSA QDs at 455 nm, (C) CdHgCoTe/MSA QDs at 495 nm and (D) CdHgCoTe/MSA/MPOSS QD at 610 nm.

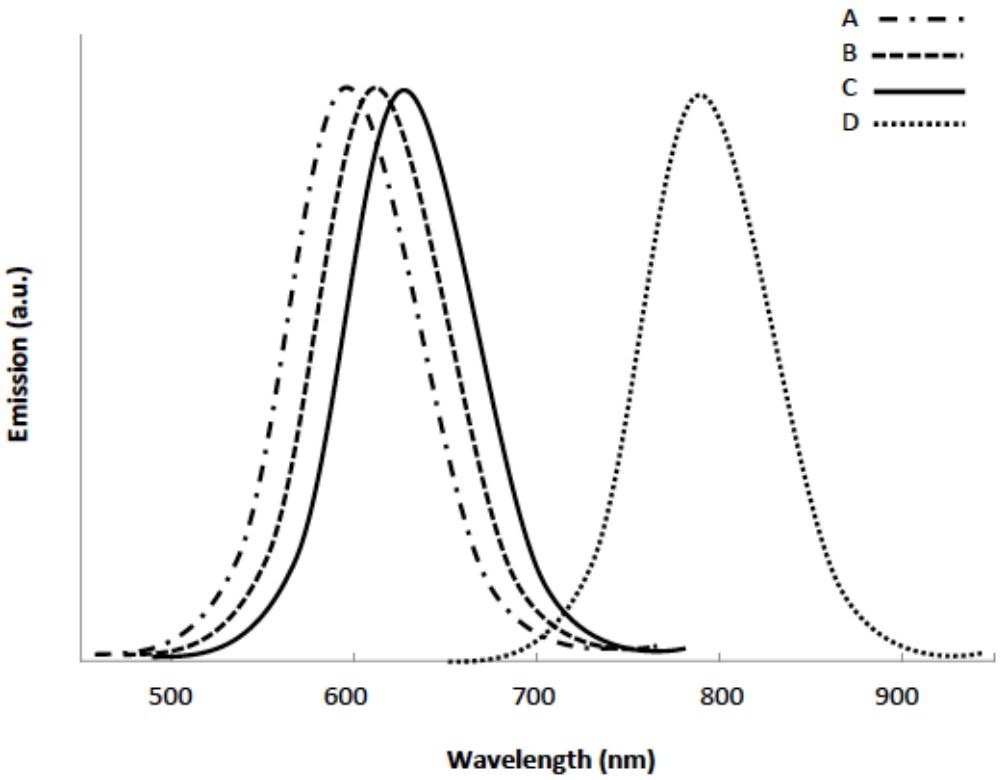

Figure 4.5: Emission spectra of four different QDs dispersions.
(A) CdTe/MSA QDs at 600 nm, (B) CdCoTe/MSA QDs at 610 nm, (C) CdHgCoTe/MSA QDs at 630 nm and (D) NIR CdHgCoTe/MSA/MPOSS QD approximately at 800 nm.

The progress of nanocrystal growth was obtained by evaluating the emission wavelength of CdHgCoTe/MSA/MPOSS NIR emitting QD at room temperature at different refluxing time of 2, 5, 18 h (**Figure 4.6**). Spectra were measured in as-prepared CdHgCoTe colloidal solutions, which were taken from the refluxing reaction mixture at designated intervals of time. The first emission peak was appeared at 650 nm after 2 h of reflux procedure started. The emission peaks shifted to longer wavelength at the nanocrystal grows in the course of heating. The peaks at 700 and 800 nm were obtained at 5 and 18 h respectively.

The symmetrical peaks show the homogeneous character of the QDs and nanoparticles. This experiment indicted that the no matter how long the refluxing time was, the emission peak cannot be extended over 800 nm.

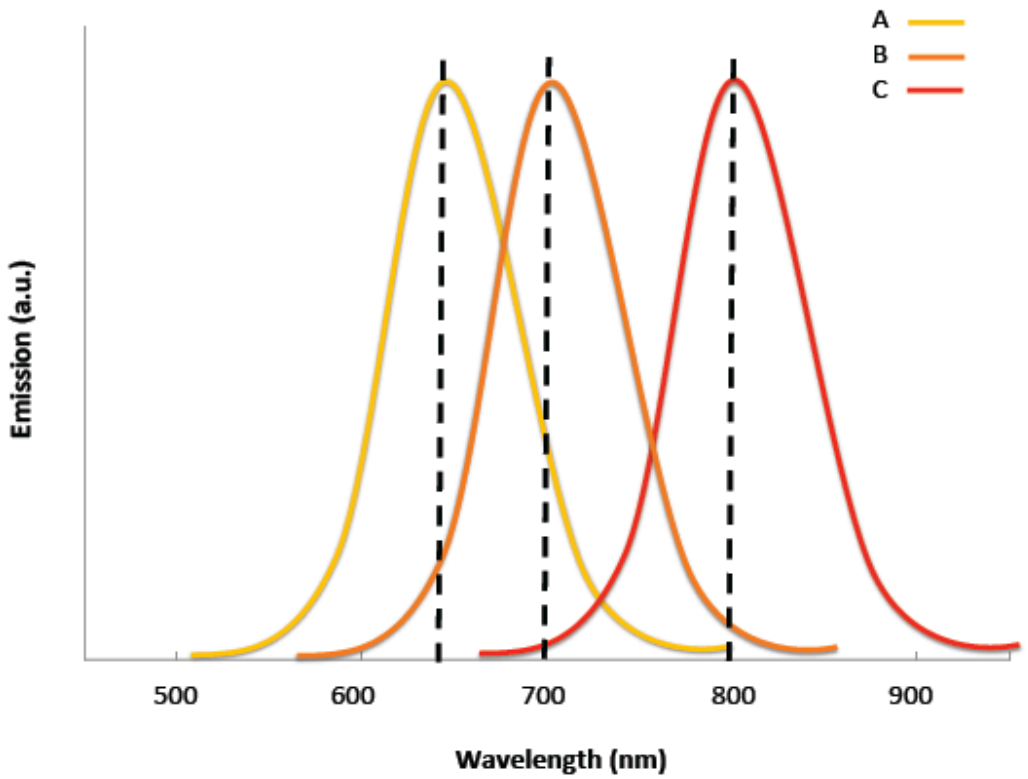

Figure 4.6: Photoluminescence spectra of CdHgCoTe/MSA/MPOSS QD of different times of reflux (2, 5, 18 h) at A) 650 nm, B) 700 nm and C) 800 nm respectively.

As previously mentioned, the optical properties of QDs can be fine-tuned by size of QD, which is a key parameter that determines the spectral position and purity of PL. The average size of QD's is generally estimated using TEM technique.

4.3.2.2. Transmission electron microscopy characterization

The TEM images of all water dispersed QDs reveal spherical morphologies. However, there is formation of aggregates from uncoated CdTe nanocrystals due to its hydrophobicity (**Figure 4.7 A**). TEM technique can accurately measure hydrodynamic diameter of QDs core in these preparations, as the cores are electron dense. Some moderately dispersed particles are also present in the MSA coated CdTe nanoparticles (**Figure 4.7 B**) which is intermediate between uncoated (**Figure 4.7 D**) and coated MSA/MPOSS QDs (**Figure 4.7 F**) with an average size of 3.0 nm in diameter. TEM of CdCoTe/MSA QDs dispersed in water showed fairly spherical particles at an average diameter of 4.0 nm (**Figure 4.7 C**). With the presence of MSA on the CdHgCoTe QDs, it can be observed that it facilitates dispersal in aqueous medium with average size of 4.5 nm in diameter (**Figure 4.7 E**). Interestingly the MSA/MPOSS coated QD

nanocrystals with average size of 5.0 nm in diameter (**Figure 4.7 F**) are well dispersed compared to other mentioned QDs.

Hence, the uncoated CdTe (**Figure 4.7 A**) and CdHgCoTe (**Figure 4.7 D**) images show some aggregation due to hydrophobicity. However, the coated CdHgCoTe QDs with MSA (**Figure 4.7 E**) and MSA/MPOSS (**Figure 4.7 F**) are well dispersed due to their hydrophilicity.

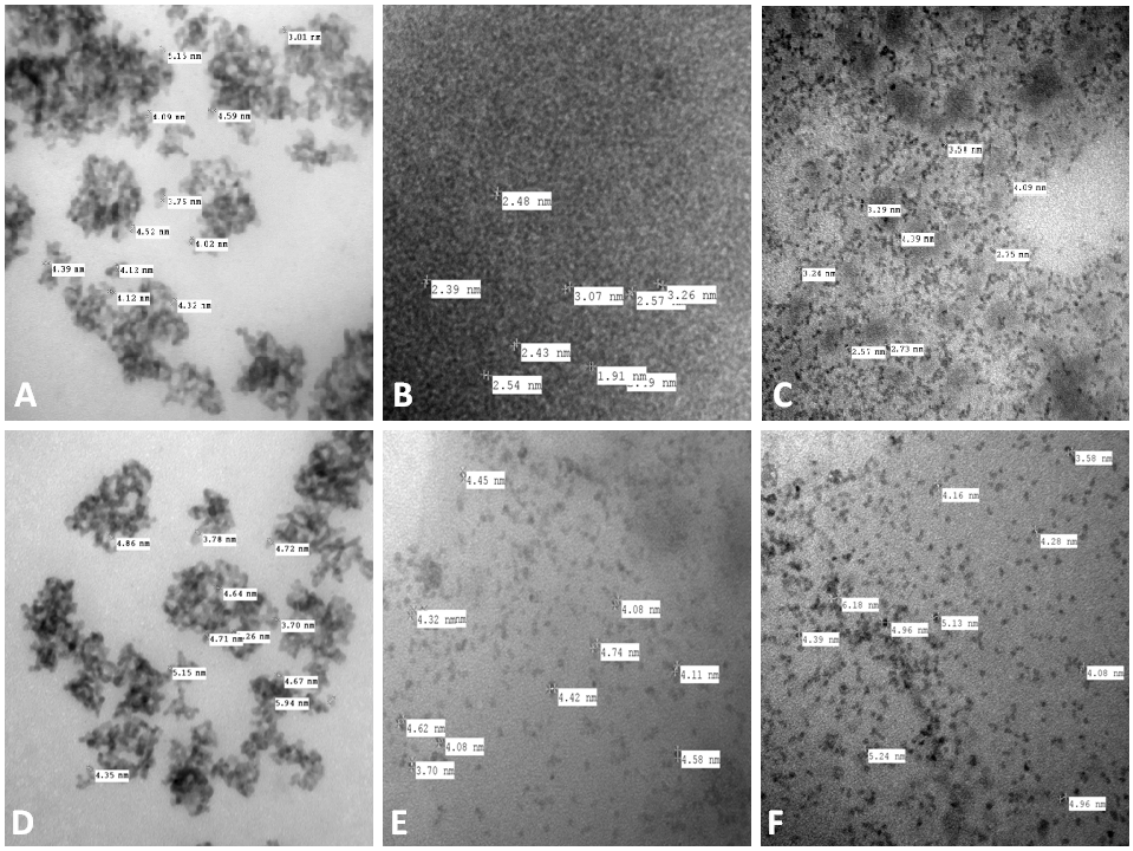

Figure 4.7: TEM images of different quantum dots.
(A) TEM image of uncoated CdTe QDs, (B) CdTe/MSA coated CdTe QDs with mean diameter of roughly 3.0 nm, (C) CdCoTe/MSA QDs diameter of roughly 4.0 nm (D) CdHgCoTe QDs, (E) CdHgCoTe/MSA QD with 4.5 nm, (F) CdHgCoTe/MSA/MPOSS QDs with 5.0 nm in diameter.

4.3.2.3. Fourier transform infrared spectroscopy (FTIR)

Figure **4.8** shows all possible vibrational and stretching movements around covalent bonds within molecules radiated with infrared. Thus, the presence of small molecules has potential to determine the presence of chemical bonds giving rise to characteristic infrared bands at a particular frequency. Infrared spectroscopy investigates the diverse, chemical bond-dependent vibrations, which can then be identified by a particular absorption band within the infrared spectrum.

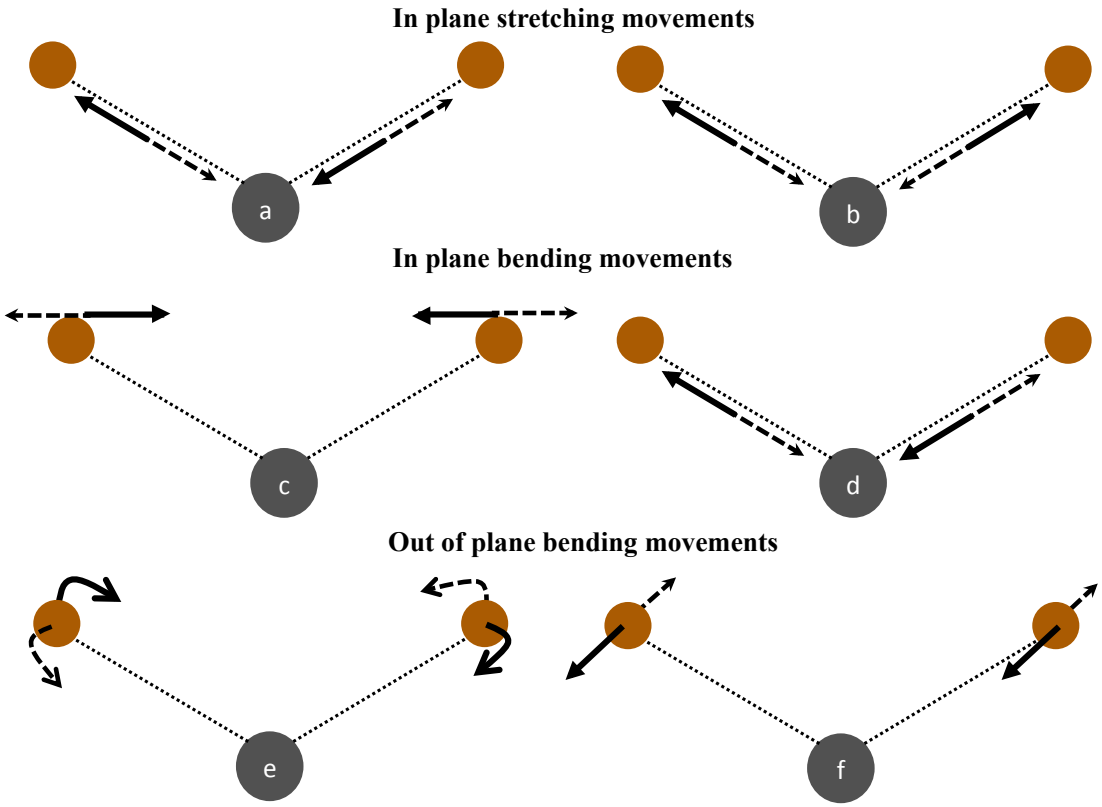

A

Bond		Frequency (cm^{-1})
Alkyl	C-H	2853-2962
Alcohol	O-H	3590-3650
Amine	N-H	3300-3500

B

Bond	Frequency (cm^{-1})
C≡C	2100-2260
C≡N	2220-2260
C=C	1620-1750
C=O	1690-1750

Figure 4.8: a: Asymmetric, b: Symmetric, c: Scissoring, d: Rocking, e: Twisting, f: Wagging.
On absorption of electrostatic energy within the IR spectrum, the covalent bonds connecting atoms as shown above undergo in-plane stretching and bending as well as out-of-plane bending movements. (A) and (B) show that the frequency and location of a given vibration in the IR spectrum has a specific range for a particular bond, although overlaps occur. The vibrational frequency is related to the atomic mass (lighter atoms such as hydrogen vibrate as a higher frequency) and the relative stiffness of the bonds (triple bonds are stiffer than double bonds which are stiffer than single bonds)

Figure 4.9 shows the FTIR spectra for all cadmium-based QDs merged in one graph with different vibrational absorptions for MPOSS coating with CdHgCoTe. All QD samples were equilibrated in D_2O for 1 h before assessing the spectra. For reference, the FTIR of uncoated CdHgCoTe and pure MPOSS were obtained. The peaks appearing at

2312 and 2316 cm^{-1} in (**Figure 4.9 purple and red**) represents the uncoated CdHgCoTe and CdHgCoTe/MSA respectively. There is a slight shift in the peaks, which is due to the presence of MSA in CdHgCoTe/MSA QD.

The QDs containing MPOSS were centrifuged in THF and precipitated to remove any unbound MPOSS. The vibrational band at around 2364 cm^{-1} can be assigned as emanating from Si-D bonds vibration after deuterium exchange. When bound to the surface of QDs there is a shift to the higher vibration band at around 2387 cm^{-1}. This indicates an open structure accessible to deuterium exchange as opposed to a close structure of the aggregated free MPOSS. The vibrational band at 2313 cm^{-1} of the MSA coated CdHgCoTe form of the crystal indicates interaction with deuterium. As the intensity is stronger than the uncoated CdHgCoTe QD it can be assigned to some interaction of the core/shell and deuterium. These assignments are unique for coated and uncoated QDs as they can assist in identifying coating interaction with their environment.

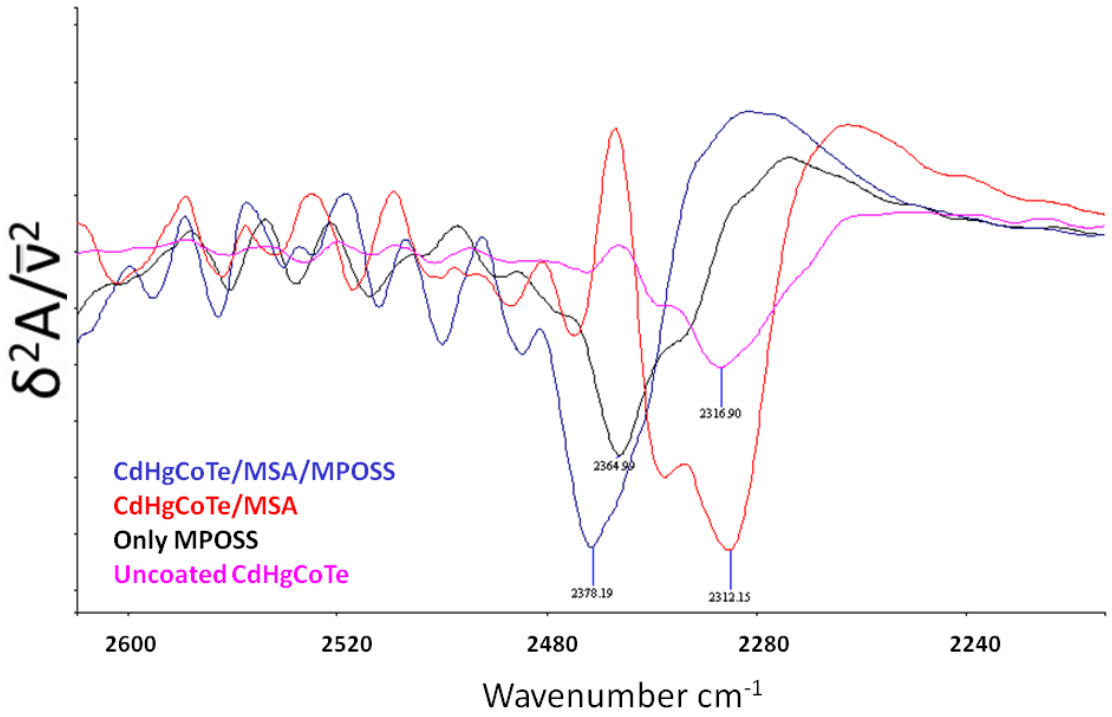

Figure 4.9: FTIR spectra of uncoated CdHgCoTe (purple), CdCoHgTe/MSA (red), CdHgCoTe/MSA/MPOSS (blue) and MPOSS only (black). A vibration peak at around 2387 cm^{-1} (Blue) indicates the presence of MPOSS around the core.

4.4. Further results and discussion

4.4.1. Synthesis of quantum dots

Traditionally, highly luminescent QDs are synthesised using the organometallic route whereby trioctylphosphine-trioctylphosphine oxide (TOP-TOPO) is utilized (Han et al., 2001). There are however, disadvantages in this method of synthesis as high reaction temperatures are needed and the end product is normally insoluble in aqueous medium unsuitable for biological applications.

The new improved method, has not only facilitated its production in an aqueous medium in one-pot synthesis but is very convenient, economical, and repeatable with a solution to alternative probes for *in vitro* and *in vivo* imaging.

4.4.2. Effects of pH values on synthesizing quantum dots

The influence of parameters such as buffer with different pH values on QDs has been investigated. Maintaining pH values during synthesis has shown to play an important part. A range of pH values were applied and investigated while maintaining the molar ratios of the precursors.

Experimental results indicated that pH values significantly influenced the optical properties of the QDs, especially the QY. Selecting an appropriate buffer system is crucial in the formation of highly luminescent QDs. It is postulated that during the evolution of QDs, the following chemical reactions are taking place (Ying et al., 2008).

(1) $TeO_3^{-2} + BH_4^- \longrightarrow Te^{2-} + B(OH)_3 + H_2O$

(2) $CdL + Te^{2-} \longrightarrow CdTe + L$, where L= MSA

The above reaction scheme is a simplified scheme, when the true reaction is a complex cascade. As Te^{2-} is oxygen sensitive, sodium sulphite was included in the reaction to exclude oxygen during the preparation, although the Na_2TeO_4 is oxygen stable used in this study. It is also postulated that the initially formed Te^{2-} may be completely reduced on addition of $NaBH_4$. In this instance, the Na_2SO_3 is only partially reducing and addition of the $NaBH_4$ is powerfully reducing, thus rendering the reaction atmosphere anaerobic, and preventing re-oxidizing Te^{2-}. As there is an excess of $NaBH_4$ (molar ratio of $NaBH_4/Cd^{2+}$ = 5/1) has been selected, most of the excess $NaBH_4$ is initially

hydrolysed or oxidized by the slow introduction of oxygen from the air according to the below reaction;

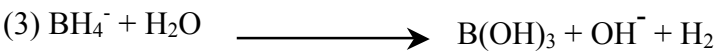

(3) $BH_4^- + H_2O \longrightarrow B(OH)_3 + OH^- + H_2$

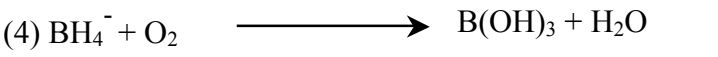

(4) $BH_4^- + O_2 \longrightarrow B(OH)_3 + H_2O$

As depicted by reaction scheme (1), (2), (3) and (4), a substantial amount of $B(OH)_3$ can act as a weak acid or OH^- will be evolved when water without buffering capacity is used, resulting in precipitation. This can be contributed by $NaBH_4$, which shifted the pH wildly with no buffering capacity with subsequent low QY and even absence of luminescence. It is found to be important that a suitable buffer system is employed with enough buffering capacity for the development of the nanocrystals to grow during heating and refluxing.

In this study the buffer system that was selected was one that included 15 mM sodium borate and 15 mM sodium citrate, which enabled to sustain enough buffering capacity and to accommodate the changes resulting to exogenous addition of $NaBH_4$ solid powder. It was observed that when the precursor materials $CdCl_2$, Na_2TeO_3, Co and Hg and MSA were added as a mixture to this buffer solution, there was a small drop in the pH (ΔpH ~ 0.5). On completion of the reactions, the pH values of the assembled CdTe containing nanocrystal solutions showed a slight increase (ΔpH ~ 0.6).

The pH range investigated was 6.0, 7.2, 8.0 and 9.0. When prepared at the stated range, the maximum QY obtained is illustrated in Figure **4.10** shows the pH effects of the precursor solution on the QY of the coated CdHgCoTe/MAS/MPOSS QD. It is evident that at pH value 7.2, the maximum QYs was greater than 70%. This indicates a great improvement compared to other studies where thioglycolic acid (TGA) (pH ~ 11) (Yao He, 2007) or MPA (pH > 8.0) (Liang Li, 2006), when present as thiol stabilizers for Cd^{2+} based QDs. It can be observed that when pH values were adjusted to 6, 8 and 9 there was a deterioration and reduction in QY. Lower pH values, may be desirable in some instances when visible fluorescence is required. In contrast, by using MSA it was found to stabilize doped CdHgCoTe QDs in physiological pH, which can be due to the dicarboxilic presence, and function in the structure of MSA. The explanation as to why

this is, has been described in previous studies whereby strong thiol complexation occurs on the surface of evolving CdS clusters *in situ* than Cd^{2+} ions in the formation of QDs.

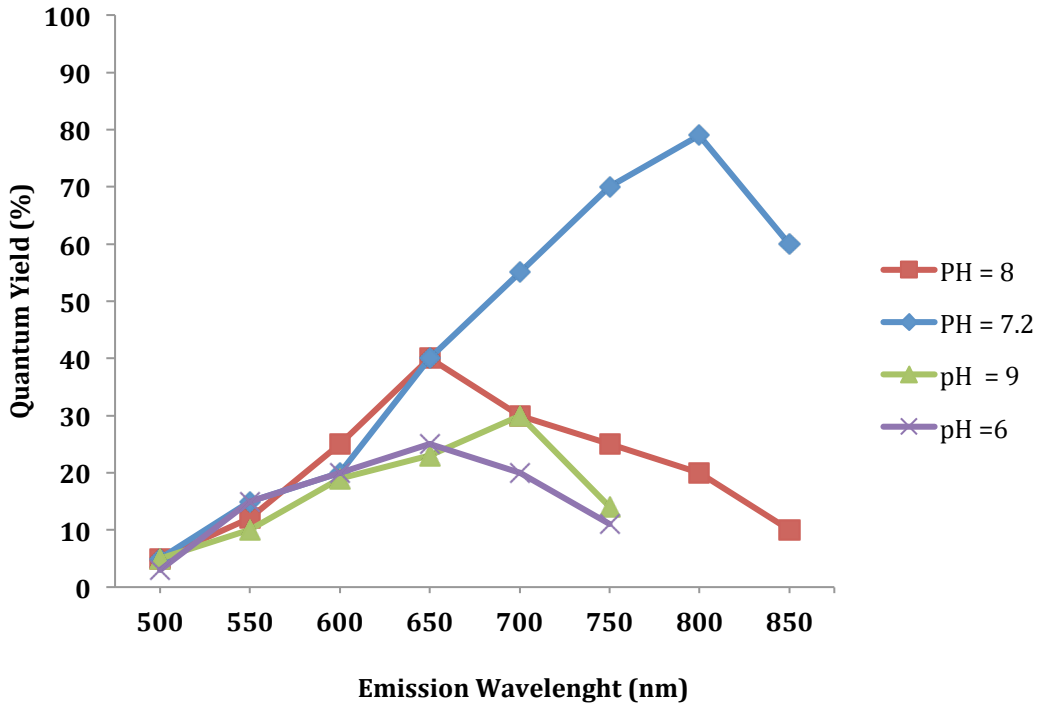

Figure 4.10: Optimising pH values of buffers in the synthesis with quantum yield. The optimum pH of 7.2 yielded a QY of > 70 %.

It can be postulated that a large number of free thiols and Cd^{2+} ions will be liberated from Cd-thiol complex in this buffer region. It can be assumed that the surface coverage with MSA is maximized when the QD solution is in this buffer range (7.0-7.2) and it can be concluded that available surface trap sites on the QDs surface will be occupied, thus increasing the fluorescence efficiency.

Considering all the above factors, the major contribution has to be the special structure of MSA and MPOSS, which occupies and reduces the surface traps of QDs. With the former contributing two carbonyl groups, this confers strong stability than other thiol compounds (TGA, MPA) and strong emission efficiency.

4.4.3. Effect of concentration of Hg^{2+} ions on quantum dots

By introducing different ranges of Hg^{2+} concentration (0.2, 0.3, 0.4 and 0.5 mM) into CdCoTe/MSA and CdCoTe/MSA/MPOSS QD, an optimum value of Hg^{2+} ion concentration has been evaluated. This is important for obtaining NIR QDs, as absence tends to inhibit the red shift.

The mercury amount included in the QDs is proportional to the Hg^{2+} ions initially added. Not only increasing the amount of mercury can precipitate the QDs, presumably of interaction with the precursors but also too low a concentration will produce faint fluorescent (**Figure 4.11**). Figure **4.11** shows the Hg^{2+} concentration and time dependent emission wavelengths (a) CdHgCoTe (0.2 mM) (b) CdCoHgTe (0.3 mM), (c) CdHgCoTe (0.4 mM) and (d) CdHgCoTe (0.5 mM) and (e) CdHgCoTe (0.6 nm).

As observed, when Hg^{2+} concentration increases from 0.2 mM to 0.5 mM the emission wavelengths shifted towards the NIR (800 nm) region. For instance with Hg^{2+} (0.2 mM) (**Figure 4.11 a**) the emission wavelength has moved from 495 to 540 nm. The optimum Hg^{2+} concentration at 0.5 mM gave an emission of 800 nm in NIR region. Increasing the concentration of Hg^{2+} beyond 0.5 mM to 0.6 mM, the emission wavelength can be seen to decrease (**Figure 4.11 d, e**).

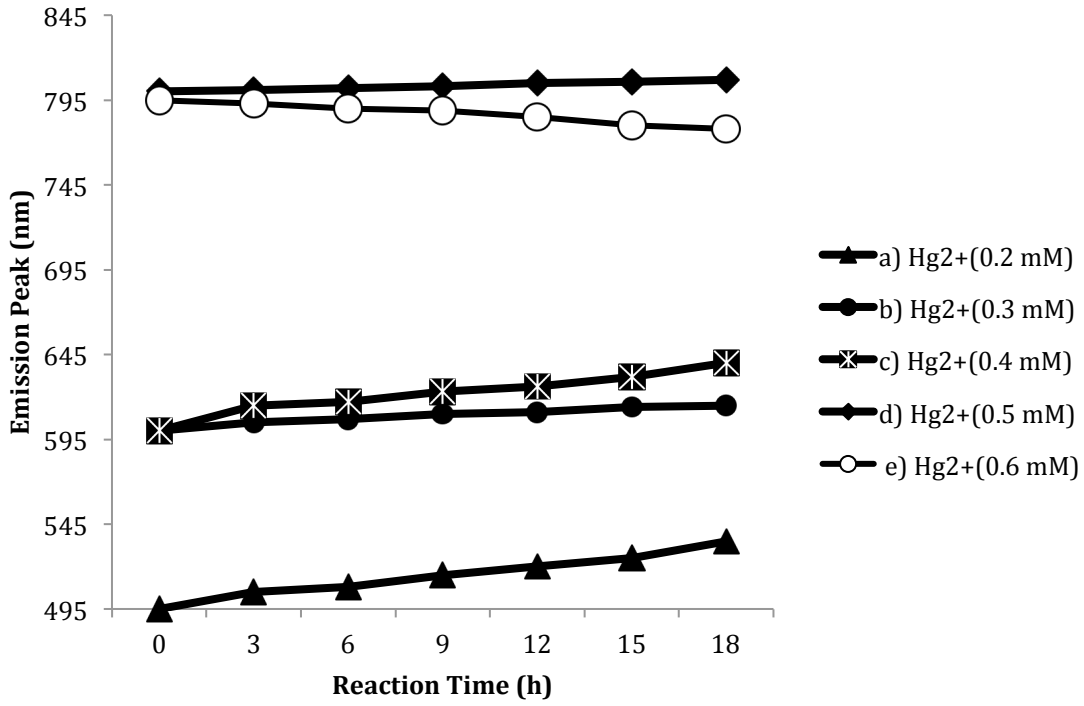

Figure 4.11: Optimising the concentration of Hg2+ in the core during synthesis to enable NIR emission in aqueous buffer.
The optimum concentration determined for Hg^{2+} is 0.5 mM with emission wavelength at 800nm in the NIR region.

4.4.4. Quantum dots and photostability

Figure **4.12** displays the photostability of all the synthesised QDs in this study. All QDs were exposed to UV illumination at 375 nm for period of 10 minutes. The photostability

of the QDs were compared with Rhodamine G. Rhodamine G as a reference fluorophores, loose approximately 80% of its photostability after 10 minutes of exposure under UV light (**Figure 4.12 E**). Under identical conditions, CdTe/MSA and CdCoTe/MSA QDs show photostability with a loss of approximately 30% and 40% respectively (**Figure 4.12 D, C**). On the other hand, CdHgCoTe/MSA QD maintained 50% of its photostability after 10 minutes (**Figure 4.12 B)**.

Remarkably, the CdHgCoTe/MSA/MPOSS QD was more resistant to photo-oxidation despite long exposure to UV illumination (375 nm) as compared to Rhodamine G and the other QDs (**Figure 4.12 A**). Although all the QDs photodegraded over the period of exposure, the rate of decline of the emission intensity of CdHgCoTe/MSA/MPOSS QD was considerably less than other QDs.

Current data shows, CdHgCoTe/MSA/MPOSS shows the highest photostability amongst the CdHgCoTe/MSA, CdCoTe/MSA and CdTe/MSA by approximately 80% (**Figure 4.12**). The results indicate that CdHgCoTe/MSA/MPOSS possesses better photostability than other QDs indicative of its novel coatings.

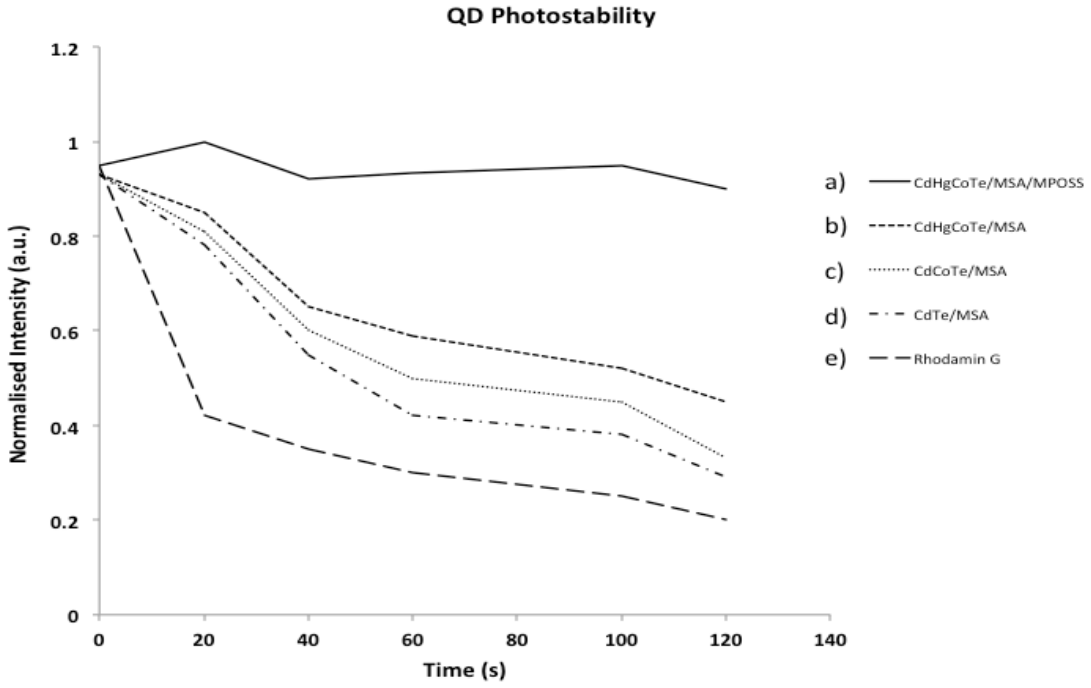

Figure 4.12: Photostability of QDs irradiate CdHgCoTe/MSA/MPOSS with better stability in aqueous buffer.
a) CdHgCoTe/MSA/MPOSS), b) CdHgCoTe/MSA, c) CdCoTe/MSA, d) for CdTe/MSA, e) for Rhodamin G

4.4.5. Hybrid MSA/MPOSS biocompatible coating of the CdHgCoTe quantum dot core

It has been reported by some researchers that coating a larger band gap nanocrystals onto a smaller band gap QD core can improve and increase the luminescence, photostability and chemical stability of the QDs. For instance, in the synthesis of CdSe/CdS core/shell structures (Huifeng Qian, 2007) it was found that PL and photostability were significantly enhanced compared to just CdSe core.

In this study, MSA and MPOSS were coated to the alloyed CdCoHgTe QDs core with *in situ* formation of CdS shell to improve the photostability. Below is the list of coating agents that other researchers have used for QD synthesis (**Table 4.2**):

Table 4.2: List of coating compounds that have been traditionally used for QD synthesis

Coating Compounds	Quantum Yield (QY)
Dihydroxylipid acid (DHLA)(Voura et al., 2004)	N/A
Octodecylamine (in hexane)	79.3%
Mercaptopropionic acid	63.4%
Polythylenimine	43%
Alkylated polycarboxylic acid	64.15%
Lipid-PEG	52.8%
Diblock copolymer (Smith et al., 2006)	20.9%(Smith et al., 2006)

As stated in the introduction chapter, cadmium or other heavy metals may cause cell death, if the QDs are damaged. Hence to overcome this probability the development of a novel coating of MSA/MPOSS has been introduced to the QD's core to provide water-solubility, stability, higher QY and PL and additionally to reduce possible toxicity.

It has been established that QDs coated with large molecules, such as mercaptoacetic acid, mercaptopropionic acid, 11-mercaptoundecanoic acid or 2-aminoethanethiol are less toxic than simple molecules. It can be shown from this study that by coating QDs with mercaptopolyhedral oligomeric silsesquioxanes (MPOSS), their toxicity can be

reduced dramatically (chapter 5). This extra layer can be protective and therefore greatly reduces the possible leaching of interior toxic cadmium or any other incorporated metal under physiological environment. Introducing MPOSS molecules further increases the stability and decreases the cytotoxicity of water-soluble QDs as shown by the results in the next chapter.

Applying appropriate coatings to QDs that is biocompatible and biostable will also play a vital role in reducing toxicity. In this study a novel coating has been introduced for the first time to QDs. POSS cages are extensively used as pendent to polyurethane (PU) polymer chain. POSS is known to molecularly reinforce and improve mechanical and physical properties of PUs. The chemical composition of POSS is a hybrid, intermediate between that of silica and silicone. The ability of polyhedral oligomeric silsesquioxanes (POSS) to serve as nanocomposites in polycarbonateurethanes as implant materials has been successfully shown to be biocompatible in human tracheal implant. With this promising outlook, POSS was applied as a coating for QDs so as to form a biocompatible and robust coating to otherwise toxic nanomaterials.

POSS units are three-dimensional, cubic shaped, building blocks that embody an inorganic inner siloxane core (6 $Å^3$) with the possibility of chemical modification at each of the eight corners of the POSS units (**Figure 4.13**). POSS based materials have been shown to resist thermal and chemical conditions and therefore should display high *in vivo* stability. In addition to acquiring chemical functionalization and chemical stability, POSS units display other properties that make them suitable as drug delivery agents. The small size of the POSS units allows this system as coatings on nanoparticles to biologically tissues. These units confer monodispersity when coated and prevents aggregation of nanomaterials.

To investigate the use of POSS as QD coatings, a thiol derivative (MPOSS) was incorporated during aqueous synthesis.

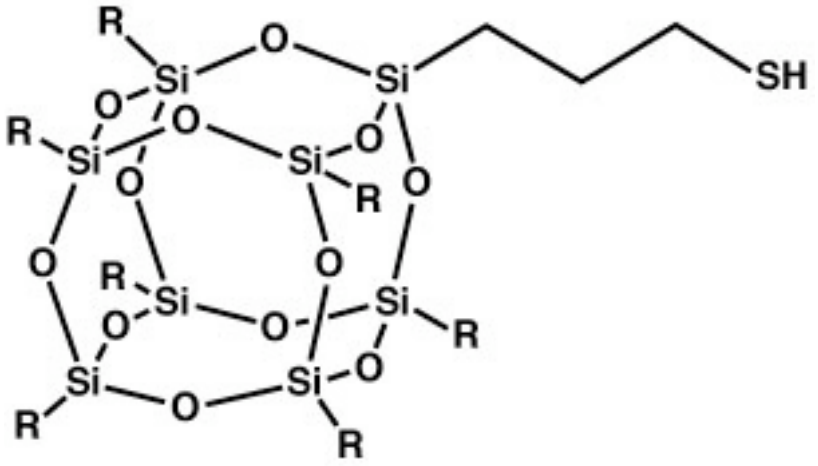

Figure 4.13: Structure of mercaptopolyhedral oligomeric silsesquioxanes (MPOSS)

It is very important to consider the characterization of QDs after any alteration on their surface. Because any changes on their surface alters the chemical and physical conditions of the QD surface atoms, and most cases have shown it dramatically decreases the quantum efficiency of the QDs. A combination of MSA and MPOSS has resulted in an elegant coating that not only confers stability but also biocompatibility.

4.5. Conclusion

In this study, NIR-emitting QDs were developed using novel materials such as the hybrid MSA and MPOSS, encapsulating the core of QD with biocompatible properties, which greatly improved stability. The NIR QDs are very useful for biological imaging and detection because autofluorescence and absorbance from tissues reach their minima in this range. Currently there are number of limited organic dyes available in the market such as Cy7, IRDye78 and Indocyanine green (Huifeng Qian, 2007).

The main part of this study was to synthesise highly luminescent, stable CdHgCoTe/MSA/MPOSS core/coating nanoparticles in aqueous method by one-pot technique. According to biophysical characterization of coated QDs, the presence of MPOSS can be verified by FTIR spectroscopy, while TEM micrographs indicate QDs with approximately 5.0 nm in diameter. The photostability of CdHgCoTe/MSA/MPOSS QD is high due to presence of MPOSS.

However, the toxicity of QDs must be solved before practical clinical applications. The next chapter will address toxicity issues with development to minimize the toxicity of synthesised NIR CdHgCoTe/MSA/MPOSS QD. The stable, unique and superior physical properties, and the multifunctionality are the major advantages of nanoparticles; through them we can integrate multiple diagnostic and therapeutic agents in one system theranostics.

With increasing research effort into materials synthesis, toxicity mechanisms and clearance from the body, QDs, together with other promising nanomaterials will be applied in imaging, detection and treatment in the near future.

Chapter 5

Toxicity assessment of the new near infrared ‘Quantum Dots’

5.1. Introduction

The potential toxicity and hazardous effects of QD nanoparticles are of great concern as previously mentioned in chapter 2. It is a well-known fact that QDs have the potential to cause greater effect of toxicity compared to the bulk counterparts at the same mass dose (Oberdorster et al., 2005). This knowledge can be referenced to their vast amount of research that has been carried out over the past two decades, mainly focused on the effects of exposure to nanoparticles in the environment as air pollution (Hardman, 2006). However there is a lack of knowledge on the effect of semiconductor based QDs either ingested or injected as drugs or fluorophores.

Semiconductor QDs have been developed and experimented as fluorescent tags for biological and potential medical applications, such as *in vitro* diagnostic, *in vivo* biological labeling, imaging, targeting, drug carriers and delivery. Despite many modifications, the issues of toxicity and clearance of QDs in bio-systems are of concern as they have not been fully investigated and there is a need for a comprehensive assessment, if QDs are to transcend from scientific curiosity to biomedical applications (Austin M. Derfus, 2003).

Several reports have been published about toxicity and clearance of QDs. One consistent common view for toxicity of cadmium containing QDs is that their toxicity is closely associated to the concentration of free Cd^{2+} ions. Current consensus is that toxicity of CdTe QDs is correlated to the leaching of free Cd^{2+} ions (Austin M. Derfus, 2003)

Many techniques by different laboratories have been applied to evaluate toxicity in cell culture studies. Considerable effort has been invested on development of short-term *in vitro* toxicity assays with cultured cells for the evaluation of acute toxicities of QDs or drugs. Such assays would be a first line rapid evaluation and screening of QDs that would allow the development and to measure the effectiveness of novel QDs and to assess the sensitivities to different cell types.

In this study, two different *in vitro* toxicity techniques, Neutral Red and Alamar Blue were adopted. The Neutral Red assay is based on the uptake of the dye, a supravital dye and its accumulation in the lysosomes of viable uninjured cells. The Alamar Blue assay is based on the reduction by viable cell resazurin to the fluorescent/absorbance

derivative (resorufin) molecule. Neutral Red assay uses colorimetric measurements whereas Alamar Blue assay uses fluorescence for the quantitation of viable cells after their incubation with different QD constructs. These results indicate that when QDs are appropriately coated with biocompatible coating materials, such as MSA and MSA/MPOSS (details in chapter 4) this can significantly reduce toxicity.

In this chapter, the emphasis is on toxicity of NIR QDs synthesised using the aqueous method with and without coatings, evaluated *in vitro* using human breast (MCF-7), prostate (PC3) and colon cancer cells (SW620), with human umbilical vein endothelial cells (HUVECs) as normal control cells. It can be shown that the NIR QDs developed with MSA/MPOSS have excellent biocompatibility with minimum toxicity for application in bio-labeling and imaging.

This demonstrates that QDs make excellent fluorophores and by introducing suitable coatings, cytotoxicity can be reduced to a significant point. With the resolution and comprehension of toxicity of QDs, the next chapter will focus on targeting via conjugation to antibodies, synthetic ligands and carbon nanotubes as imaging and delivery systems respectively (Liu et al., 2008) (**Figure 5.1**).

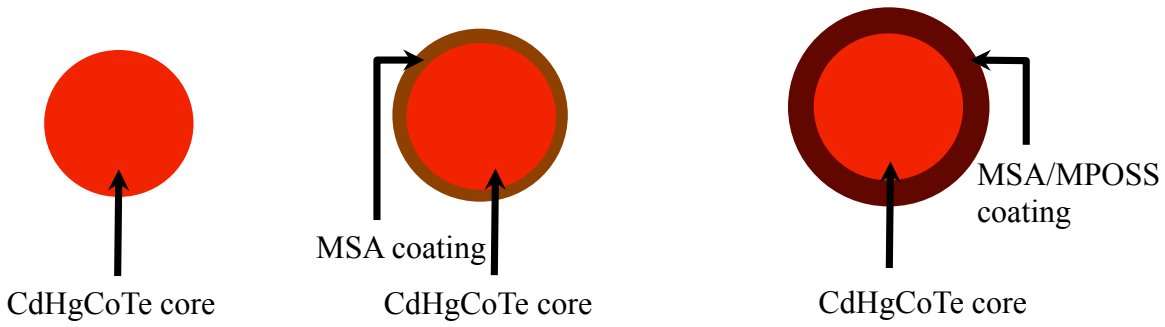

Figure 5.1: The schematic surface properties of three kinds of quantum dots: uncoated CdHgCoTe, CdHgCoTe/MSA core-shell and CdHgCoTe/MSA/MPOSS quantum dots synthesised in aqueous phase, with an aim to evaluate their toxicity study through this experiment.

5.2. Materials and Methods

5.2.1. Materials

Details have been described in chapter 3.

5.2.1.1. Cell types used for in vitro toxicity studies

Toxicity studies were conducted on four different cell cultures *in vitro*; three were established cancer cell lines that were derived from human breast, colon and prostate cancer. As a control for normal cells, HUVECs were chosen, as endothelial cells are the first line of tissues to encounter QDs *in vivo* (**Table 5.1**). Using different derived cancer cells for toxicity, would also establish their sensitivity to QDs in this study.

Table 5.1: This is the list of cell cultures have been used in this study

List of cell cultures	Full name of cell cultures	Kind
MCF-7	Breast cancer cells	Cell line
SW680	Colorectal cancer cells	Cell line
PC3	Prostate cancer cells	Cell line
HUVEC	Human umbilical	Primary cell

Briefly, MPOSS coated QDs incorporating Cobalt (Co) and Mercury (Hg) have emission wavelength in the NIR region. From the pool of synthesised QDs (chapter 4) two (CdHgCoTe and CdHgCoTe/MSA) was selected as comparison to NIR emitting CdHgCoTe/MSA/MPOSS QDs for toxicity in this study to highlight their protective properties.

5.2.2. Quantification of quantum dots concentration by serial dilution

Refer to chapter 3, section 3.4.2.4. for full details.

5.2.3. Preparation of precursor materials cadmium chloride (Cd^{2+}) and mercury perchlorate (Hg^{2+}) ions for toxicity studies

Refer to chapter 3, section 3.4.2.2. for full details.

5.2.4. Quantum dots preparation for toxicity assay

Briefly all three QDs were precipitated with ethanol, dried and accurately weighted for re-constitution in PBS and filter sterilized with membrane (0.2 μm). Initially, a desired number of all four different types of test cells were incubated for 48 h. Then after, concentrations of three different QDs, CdHgCoTe, CdHgCoTe/MSA and CdHgCoTe/MSA/MPOSS in PBS were added and incubated at 2, 8 and 24 h. The purified QDs were prepared at five concentrations of 0, 0.1, 1.0, 10, 50 and 100 μg/mL in HEPE buffered minimum essential medium (MEM).

5.2.5. Cell seeding and viability assay

Briefly, cells were seeded into 96-well plates at a density of 1 x 10^4 cells per well (200 μL), and allowed to equilibrate for 48 h at 37 °C in an incubator with 5% CO_2. After this period cells were washed thoroughly with PBS then exposed to serial dilutions of all three QDs at 200 μL and MEM as control. After addition they were incubated at 37 °C in 5% CO_2 for 2, 8 and 24 h. At the end of their respective period of exposure, the cells were thoroughly washed with PBS. At this stage the wells were replaced with MEM (200 μL) and 20 μL of Alamar Blue and Neutral Red were added in tandem to each well and incubated for further 4 h at 37 °C with 5% CO_2. Finally, the plates were read by a microplate-reader (Labsystems, Ashford, UK).

Cell viability data was obtained as the percentage of treated cells to untreated cells, using the following formula:

Cell viability (%) = Abs (treated)/Abs (control) X 100

5.3. Results and discussion

5.3.1 *In vitro* toxicity of QDs in cell cultures

Three different QDs, CdHgCoTe, CdHgCoTe/MSA and CdHgCoTe/MSA/MPOSS were compared to each other to assess their toxicity via cell viability, according to their appropriate coatings, on four different cell cultures (MCF-7, SW620, PC3 and HUVECs). Cancer cells have been widely used here because they are important in biomedical imaging using QDs, and they are accepted to be sturdier than normal cells to

assess for cytotoxicity. However, even with different normal cell lines, there are different levels of resistance to toxic environments and thus these results may not represent the maximum exposure time limits. The data obtained are useful, however, for setting a standard for toxic response to different types of coatings. In addition, some of their compositional materials such as Hg^{2+} and Cd^{2+} were also used for toxicity assessment.

5.3.1.1. In vitro toxicity of precursor material of CdHgCoTe/MSA/MPOSS

Figures **5.2-5.3** show the effect of precursor material (Cd^{2+} and Hg^{2+} ions) when incubated with four cell cultures at different concentrations, and viability evaluated using Alamar Blue and Neutral Red assays at time intervals of 2, 8 and 24 h. The 0 μg/mL concentration, which is growth culture medium (MEM), has been used as control throughout whole toxicity experiments, hence there is a high number of viable cells present (100 % cells).

In figure **5.2 a, b**, the graphs show that at 1 μg/mL of Cd^{2+} and Hg^{2+}, the cell viability have been reduced dramatically to approximately 50% for all cell cultures at 2 h incubations. It can also be seen that as the concentrations of Cd^{2+} and Hg^{2+} increase, there is further reduction of cell viability (approximately 30%).

A similar effect has taken place at 8 h incubations where at 1 μg/mL it has now reduce viability to approximately 40% (**Figure 5.2 c, d**). Again a similar pattern can be observed with increased concentrations where the cell viability is reduced to approximately 20% (**Figure 5.2 a, b**).

At 24 h incubation for both precursor materials, there is further reduction of cell viability at concentration of 1 μg/mL at approximately 30 %. At 24 h incubation, there is a dramatic reduction of cells (to approximately 10%) where we can assume maximum cell death had occurred at 50 μg/mL concentrations.

Although for Neutral Red similar results were obtained, it can be clearly seen that at 2 h incubation with 1 μg/mL the cell viability was at 50% approximately. Similarly, at increased concentrations there is reduction of cell viability at an average 30% (**Figure 5.3 a, b**).

Figure **5.3 c, d** shows that at 8 h incubation with both precursor materials (Cd^{2+} and Hg^{2+}) there is further reduction of cell viability from 45% to 25% at concentrations of 1 µg/mL and 50 µg/mL respectively. Likewise, the 24 h incubation also follows a similar pattern whereby at 1 µg/mL there is approximately 20% viability.

Although, the results follow a similar pattern there is a slight variation in cell numbers for the HUVEC cell culture (**Figure 5.3 b, d, f**). There appears to be an increase in cell numbers compared to the other cell lines and this could be due to overestimation using this particular assay system (Neutral Red). On the other hand, this could be due to HUVECs response to Neutral Red being different to that of the cancer cells used in this study.

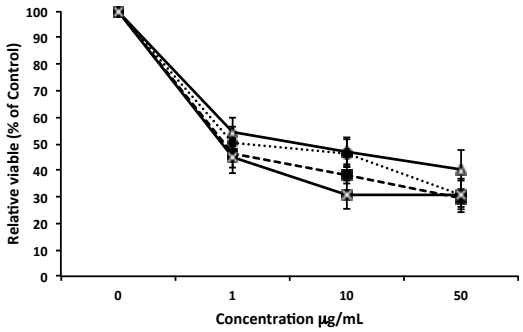

a. **Cd**$^{2+}$ toxicity at 2 h, assayed by Alamar Blue

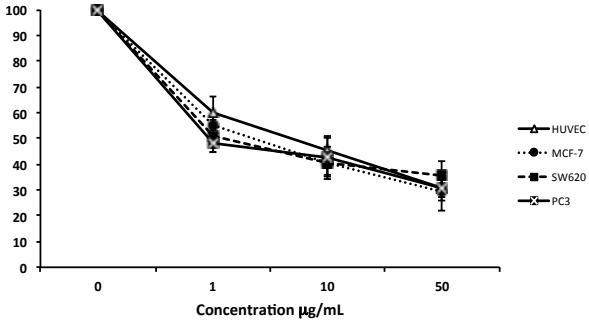

b. **Hg**$^{2+}$ toxicity at 2 h, assayed by Alamar Blue

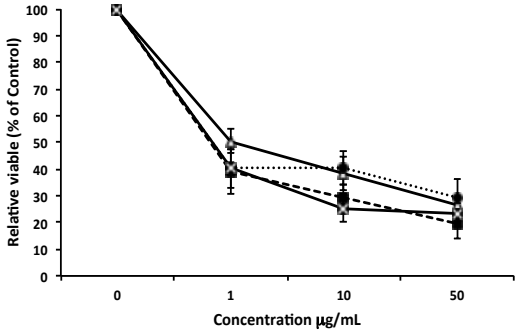

c. **Cd**$^{2+}$ toxicity at 8 h assayed by Alamar Blue

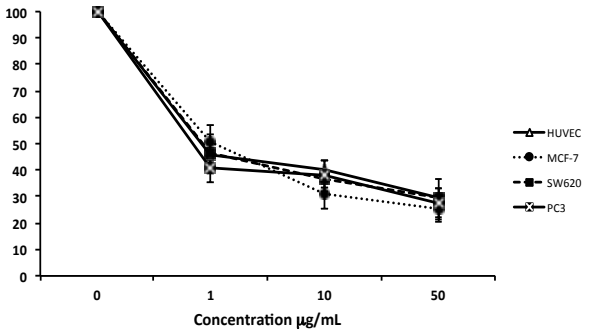

d. **Hg**$^{2+}$ toxicity at 8 h assayed by Alamar Blue

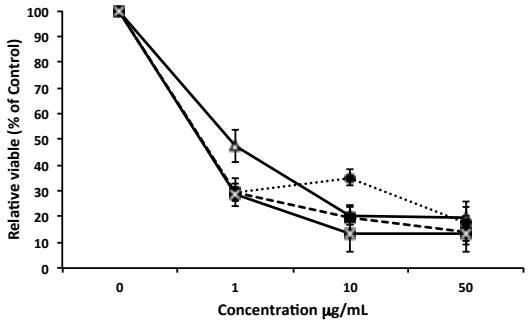

e. **Cd**$^{2+}$ toxicity at 24 h, assayed by Alamar Blue

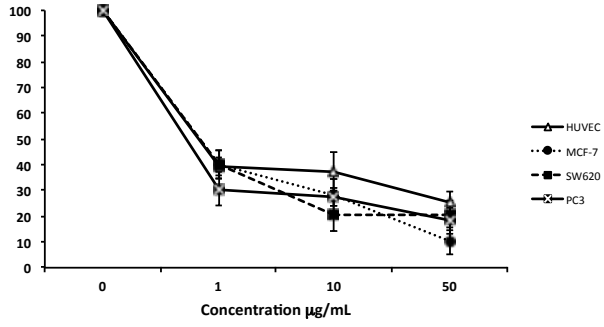

f. **Hg**$^{2+}$ toxicity at 24 h, assayed by Alamar Blue

Figure 5.2: Cd^{2+} and Hg^{2+} toxicity readings with Alamar Blue.
Toxicity results using Alamar Blue assay on four cell cultures (MCF-7, SW620, PC3 and HUVECs) exposed to Cd^{2+} and Hg^{2+} at different time frame at (2, 8 and 24 h) with concentrations ranging from 1 µg/mL to 50 µg/mL.

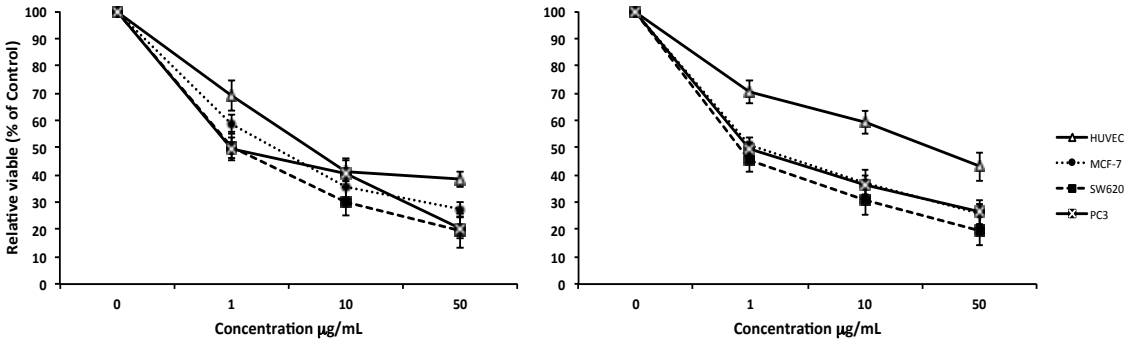

a. Cd^{2+} toxicity at 2 h, assayed by Neutral Red

b. Hg^{2+} toxicity at 2 h, assayed by Neutral Red

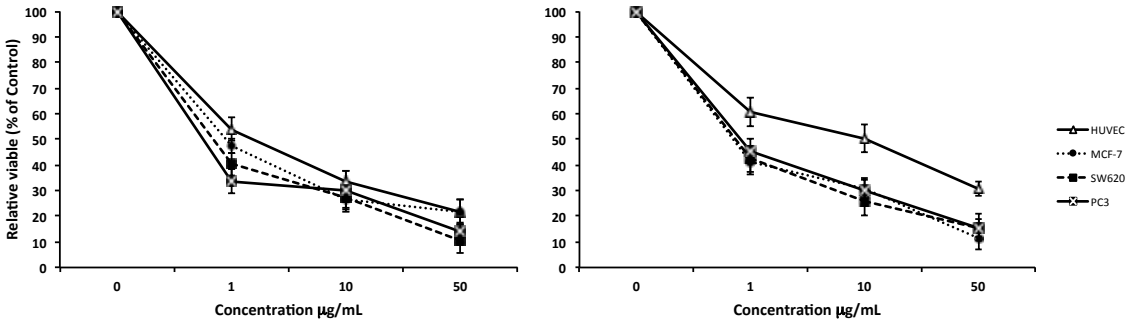

c. Cd^{2+} toxicity at 8 h, assayed by Neutral Red

d. Hg^{2+} toxicity at 8 h, assayed by Neutral Red

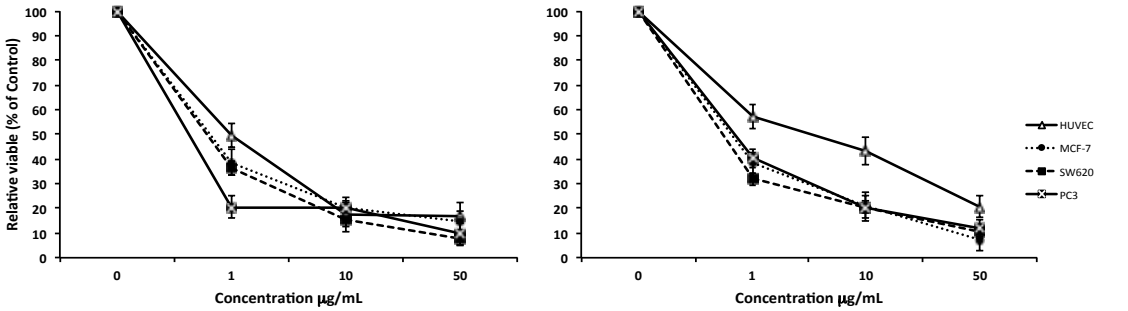

e. Cd^{2+} toxicity at 24 h, assayed by Neutral Red

f. Hg^{2+} toxicity at 24 h, assayed by Neutral Red

Figure 5.3: Cd^{2+} and Hg^{2+} toxicity readings with Neutral Red.
Toxicity results using Neutral Red assay on four cell cultures (MCF-7, SW620, PC3 and HUVECs) exposed to Cd^{2+} and Hg^{2+} at different time frame at (2, 8 and 24 h) with concentrations ranging from 1 µg/mL to 50 µg/mL.

The above results indicate the toxicity of Cd^{2+} ions and Hg^{2+} ions in solution, which as shown can have detrimental effects on cells. This is also a simulation of what may happen when these precursor materials are released from cadmium based QD cores.

5.3.1.2. In vitro toxicity of CdHgCoTe at 2, 8 and 24 hour

One primary and three different cell types were used for uncoated CdHgCoTe QD toxicity assessment. This essentially demonstrates the sensitivities of the different cell types to semiconductor coated and uncoated CdHgCoTe QDs.

Figure **5.4** shows the toxicity in tandem as above, using two types of assay system (Alamar Blue and Neutral Red) on all four cell cultures at varied times exposure (i.e. 2, 8, 24 h) for uncoated CdHgCoTe QDs. The 0 μg/mL concentration, which is growth culture medium (MEM), has been used as control throughout whole toxicity experiments, hence there is a high number of viable cells present (100 % cells).

Comparing toxicities using the two different assays, (**Figure 5.4**) the data in this study indicate a pattern that is similar, confirming the accuracy and consistency of the cell response. This mode of parallel toxicity study was applied to all the cell models used here. Figure **5.4 a, b** illustrates the effect of uncoated CdHgCoTe QD toxicity on MCF-7, SW620, PC3 and HUVECs cell cultures at 2 h exposure. The cell viability was in approximately at 70-90% at 0.1 μg/mL concentration for both assays for the four cell cultures. On increasing the concentration to 100 μg/ml of the uncoated CdHgCoTe, the cell viability has decreased to approximately 40-60%, which indicates that concentrations have significant effect on the cell viability. Similar results were also obtained at 8 h exposure time (**Figure 5.4 c,d**). The cell viability at 0.1μg/mL has decreased from approximately 70-90% to 60-70% from 2 h to 8 h exposure respectively (**Figure 5.4 a. c**).

However there are some unexpected observations at 0.1 μg/mL concentration at 24 h exposure, cell death is still occurring (**Figure 5.4 e, f**) at about 60-70%. This slowed decline could be to cells equilibrating or resisting the kill at this stage. The uncoated CdHgCoTe QD at high concentrations showed cell death within the time frame of 24 h. The low cell death at 100 μg/mL at 8 h with Alamar Blue can possibly be due to inefficient uptake of CdHgCoTe QD or Alamar Blue reduction by metabolic products or

possible operator error. However in the Neutral Red assay (**Figure 5.4 d**), this seems to be absent, as this is based on live cell uptake only.

The cell toxicity results for the uncoated CdHgCoTe QDs (**Figure 5.4**) indicates approximately 15% less than the free precursor materials (Cd^{2+} and Hg^{2+} ions) in figures **5.2** and **5.3** with high significance ($p < 0.05$). This could be due to the intactness of the uncoated complex that is temporarily stable with a CdS shell (formed *in situ*) that is hydrophobic. Whereas the precursor materials Cd^{2+} and Hg^{2+} are hydrophilic, and have free interaction with cells with toxic effects.

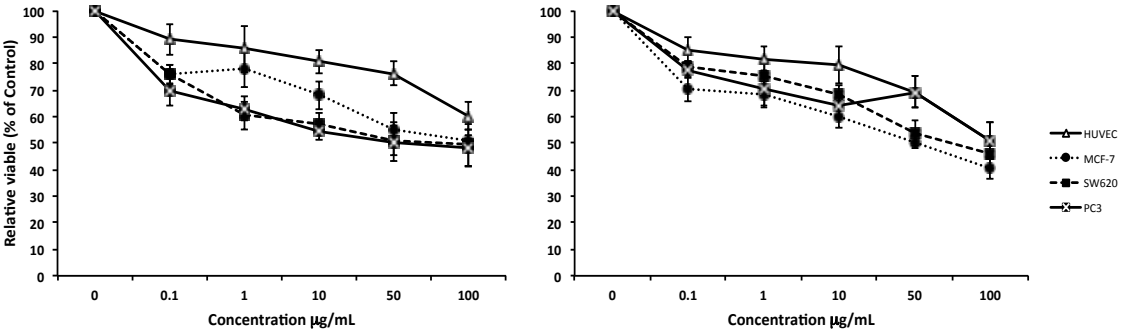

a. CdHgCoTe toxicity at 2 h, assayed by Alamar Blue

b. CdHgCoTe toxicity at 2 h, assayed by Neutral Red

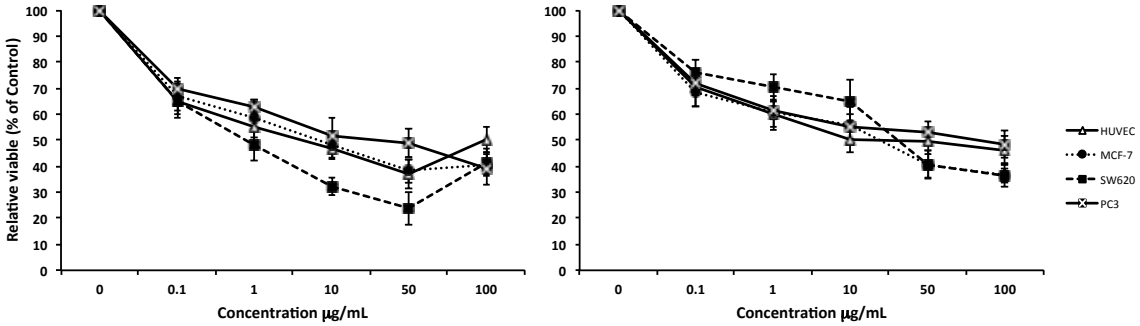

c. CdHgCoTe toxicity at 8 h, assayed Alamar Blue

d. CdHgCoTe toxicity at 8 h, assayed by Neutral Red

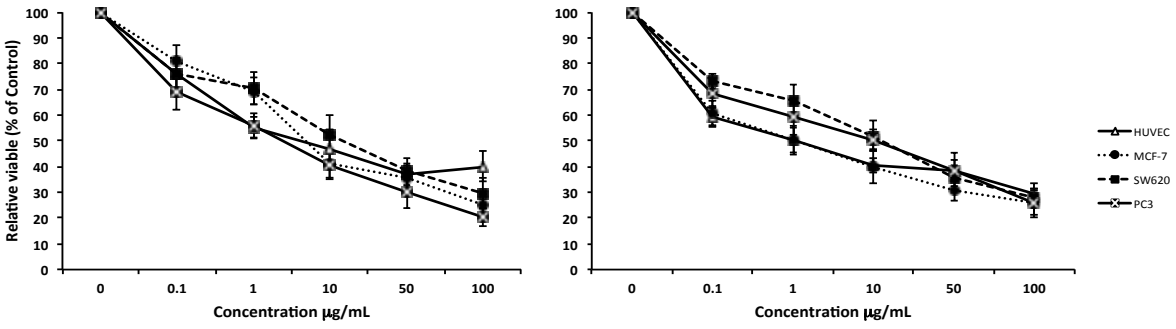

e. CdHgCoTe toxicity at 24 h, assayed by Alamar Blue

f. CdHgCoTe toxicity at 24 h, assayed by with Neutral Red

Figure 5.4: Toxicity of uncoated CdHgCoTe QDs using Alamar Blue and Neutral Red assay on four different cell cultures at different time exposure (2, 8 and 24 h) with different concentrations from 1 µg/mL to 100 µg/mL. It indicates that the uncoated CdHgCoTe QDs are highly toxic.

5.3.1.3. In vitro toxicity of coated CdHgCoTe/MSA at 2, 8 and 24 hour exposure

The toxicity assay was repeated as described as above.

Figure **5.5** indicates the toxicity evaluation CdHgCoTe/MSA QD at 2, 8 and 24 h exposure on four different cell cultures (MCF-7, SW620, PC3 and HUVECs). At 0 μg/mL concentration (culture medium) minus QD free control the cell population is defined at 100%.

The viability of cells decreased at 0.1 μg/mL CdHgCoTe/MSA QD from 70-90% to 65-80% at 2 h and 24 h exposure time respectively (**Figure 5.5 a, e**) for all four cell cultures, using the Alamar Blue assay. Similar results were observed for Neutral Red assay (**Figure 5.5 b, f**) at same concentration of 0.1 μg/mL. Using Alamar Blue, cell viability decreased from 50-70% to 30-50% at the highest concentration (100 μg/mL) at lowest (2 h) to highest (24 h) incubation time respectively (**Figure 5.5 a, e**).

There is a decreasing cell survival pattern in the overall results (**Figure 5.5**). However, there is increase cell viability for CdHgCoTe/MSA QD (**Figure 5.5**) as compared to uncoated CdHgCoTe QDs (**Figure 5.4**). As previously mentioned, two types of toxicity assay were carried out in this study. Although minor differences were noted in the toxicity rankings of the coated QDs in the Neutral Red and Alamar Blue assays, there was, for most part, good agreement between the two assays. Overall, both assays exhibited similar sensitivities to the QDs.

Generally, it can be shown that there is still significant toxicity for CdHgCoTe/MSA QDs at higher concentrations over longer exposure time. However, comparing the data of uncoated CdHgCoTe (**Figure 5.4**) with coated CdHgCoTe/MSA QD (**Figure 5.5**), the toxicity has been notably reduced to 20% on all four cell cultures ($p < 0.05$). This is significant improvement for CdHgCoTe/MSA QDs and can be attributed to the coating around the core preventing leaching of Cd^{2+} and Hg^{2+} ions form the core.

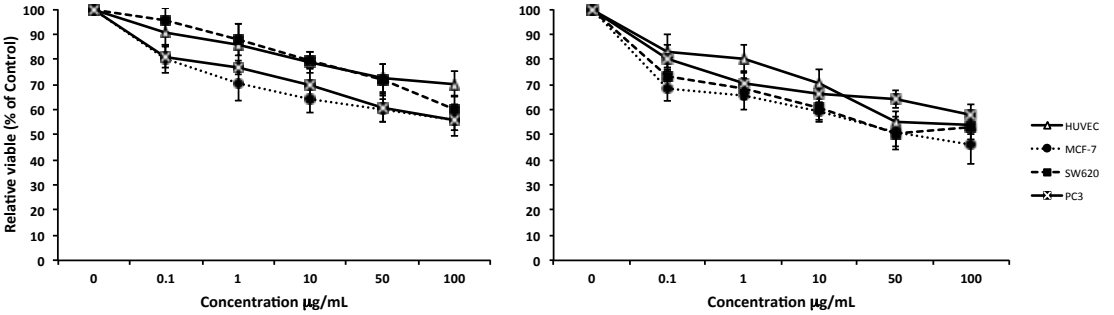

a. CdHgCoTe/MSA toxicity at 2 h, assayed by Alamar Blue

b. CdHgCoTe/MSA toxicity at 2 h, assayed by Neutral Red

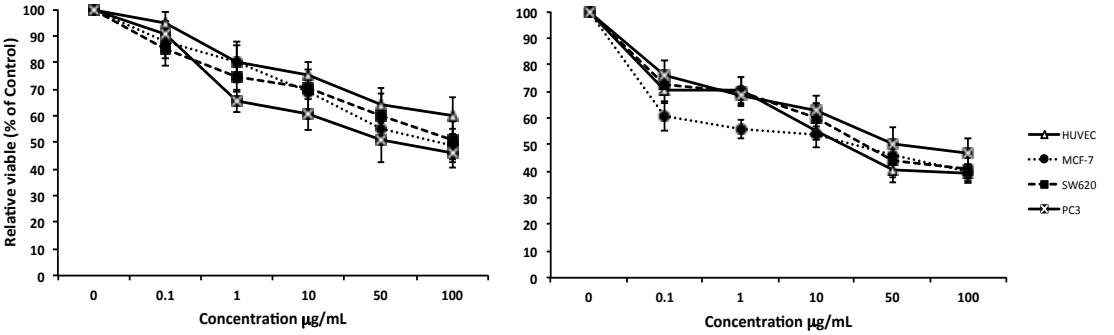

c. CdHgCoTe/MSA toxicity at 8 h, assayed by Alamar Blue

d. CdHgCoTe/MSA toxicity at 8 h, assayed by Neutral Red

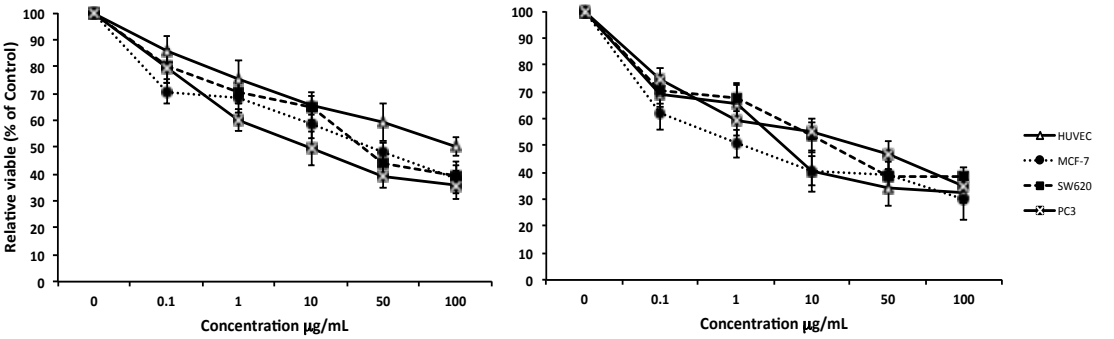

e. CdHgCoTe/MSA toxicity at 24 h, assayed by Alamar Blue

f. CdHgCoTe/MSA toxicity at 24 h, assayed by Neutral Red

Figure 5.5: Toxicity of CdHgCoTe/MSA QDs using Alamar Blue and Neutral Red assays on four different cell cultures at different time exposure (2, 8 and 24 h) with different concentrations from 1 µg/mL to 100 µg/mL. It indicates that the toxicity of CdHgCoTe/MSAQDs has reduced due to the coating of the core with MSA compared to uncoated CdHgCoTe QDs ($p < 0.05$).

5.3.1.4. In vitro toxicity of CdHgCoTe/MSA/MPOSS at 2, 8 and 24 hour exposure

This assay was carried out as described previously whereby the CdHgCoTe/MSA/MPOSS QDs were given to MCF-7, SW620, PC3 and HUVEC cell cultures at various concentrations over a time course of 2, 8 and 24 h and viability was assessed using Alamar Blue and Neutral Red assays.

Based on the observed changes in cell survivability, the toxicity of CdHgCoTe/MSA/MPOSS QDs was this time compared with uncoated CdHgCoTe and coated CdHgCoTe/MSA QDs at similar time course of 2, 8 and 24 h with concentrations from 0 to 100 μg/mL, using Alamar Blue and Neutral Red assays.

The cell viability using CdHgCoTe/MSA/MPOSS QDs at the lowest concentration (0.1 μg/mL) was approximately > 90% (**Figure 5.6 a, b**) in both assays at 2 h incubation. Even at maximum concentration (100 μg/mL) the cell viability was approximately over 80% at 2 h incubation time (**Figure 5.6 a, b**). The cell viability in this part of evaluation (50%), compared to CdHgCoTe/MSA (**Figure 5.5**) has increased significantly.

Higher cell viability was seen for longer incubations (8 and 24 h) at different concentrations of CdHgCoTe/MSA/MPOSS QDs. The cell viability was approximately over 80% for 100 μg/mL concentration of CdHgCoTe/MSA/MPOSS at 8 and 24 h incubations for both assays (**Figure 5.6 c, d, e, f**).

The graphs (**Figure 5.6**) demonstrate high percentage of cell survival of approximately over 75% on all culture cells and especially over 90% on HUVECs primary cells (**Figure 5.6**). Interestingly, at 100 μg/mL QD concentration, there was no significant toxicity at 24 h incubation, which indicates the excellent biocompatibility and stability of the CdHgCoTe/MSA/MPOSS QDs.

MSA is relatively non-toxic, chemically stable and often employed as the outer coating for QDs (Komarala et al., 2006, Zheng et al., 2007). Importantly, it has been shown that no free cadmium ions are found on the surface of such layers when used with cadmium based QDs, which should favor its use in cellular studies (Derfus AM, 2003, Kirchner et al., 2005). A highly fluorescent CdHgCoTe core stabilized with MSA/MPOSS coating, synthesised through one-pot aqueous method was introduced as a novel development

(Chapter 4).

Also QDs encounter and are exposed to vascular tissues first when injected systemically. The precursor materials Cd^{2+} and Hg^{2+} of QDs demonstrated dramatic cell loss in this cell culture study. This indicates that toxicological studies are important and encapsulating QD's core with biocompatible coating agents minimizes the toxicity level of QDs even at high concentrations. Thus in both assays the free heavy metals Cd^{2+} ion and Hg^{2+} ion were highly toxic, whereas the coated CdHgCoTe/MSA QD was moderately toxic with the CdHgCoTe/MSA/MPOSS QD nontoxic in the concentration range tested.

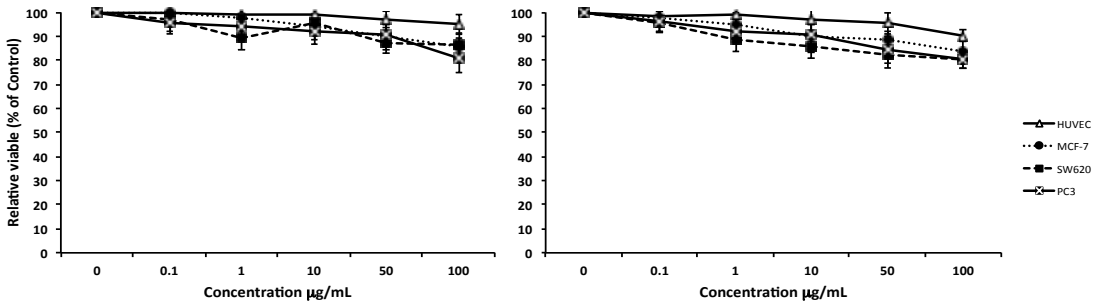

a. CdHgCoTe/MSA/MPOSS QD toxicity at 2 h, assayed by Alamar Blue

b. CdHgCoTe/MSA/MPOSS toxicity at 2 h, assayed by Neutral Red

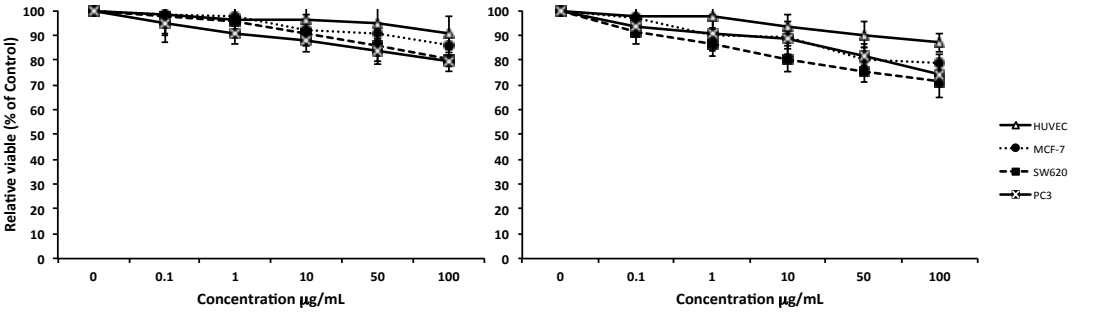

b. CdHgCoTe/MSA/MPOSS QD toxicity at 8 h, assayed by Alamar Blue

d. CdHgCoTe/MSA/MPOSS QD toxicity at 8 h, assayed by Red

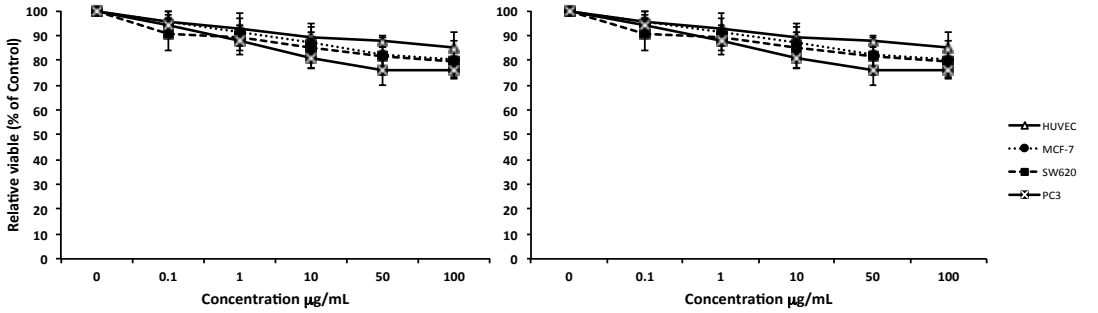

e. CdHgCoTe/MSA/MPOSS QD toxicity at 24 h, assayed by Alamar Blue

f. CdHgCoTe/MSA/MPOSS QD toxicity at 24 h, assayed by Neutral Red

Figure 5.6: Toxicity of CdHgCoTe/MSA/MPOSS QDs using Alamar Blue and Neutral Red assays on four different cell cultures at different time exposure (2, 8 and 24 h) with different concentrations from 1 µg/mL to 100 µg/mL. It indicates that the toxicity of coated CdHgCoTe/MSA/MPOSS QDs has improved significantly by biocompatible MSA and MPOSS coatings compared to coated CdHgCoTe/MSA ($p < 0.05$).

5.3.2 Overview of cell toxicity

Figures **5.7 a-5.9 b** represent the toxicity of CdHgCoTe, CdHgCoTe/MSA and CdHgCoTe/MSA/MPOSS QDs with different exposure times of (2, 8 and 24 h) using Alamar Blue and Neutral Red assays for each cell type for all experiments. Previous graphs represent concentrations at different time scale of exposure. The graphs below depict similar patterns as described earlier.

It can be observed from the Alamar Blue (**Figure 5.7 a**) and Neutral Red (**Figure 5.7 b**) results that the coated CdHgCoTe/MSA was moderately toxic and the uncoated CdHgCoTe QDs were highly toxic. It can also be observed that there are some unexpected growth properties of HUVECs using Alamar Blue for uncoated CdHgCoTe QDs. It was seen (**Figure 5.7 a**) that at concentrations 0.1, 1.0 and 10 µg/mL the cell viability has increased for HUVEC primary cells at longer incubation (24 h) when quantitated by Alamar Blue assays. This may be due to unusual metabolic property of HUVECs towards the uncoated CdHgCoTe QDs and overestimation of cell counts to Alamar Blue assay. However, there is absence of overestimation when using Neutral Red assay (**Figure 5.7 b**). Therefore, it can be concluded that despite this overestimation of HUVECs towards uncoated CdHgCoTe, the CdHgCoTe and CdHgCoTe/MSA QDs were still toxic compared relatively with the hybrid coated CdHgCoTe/MSA/MPOSS QDs.

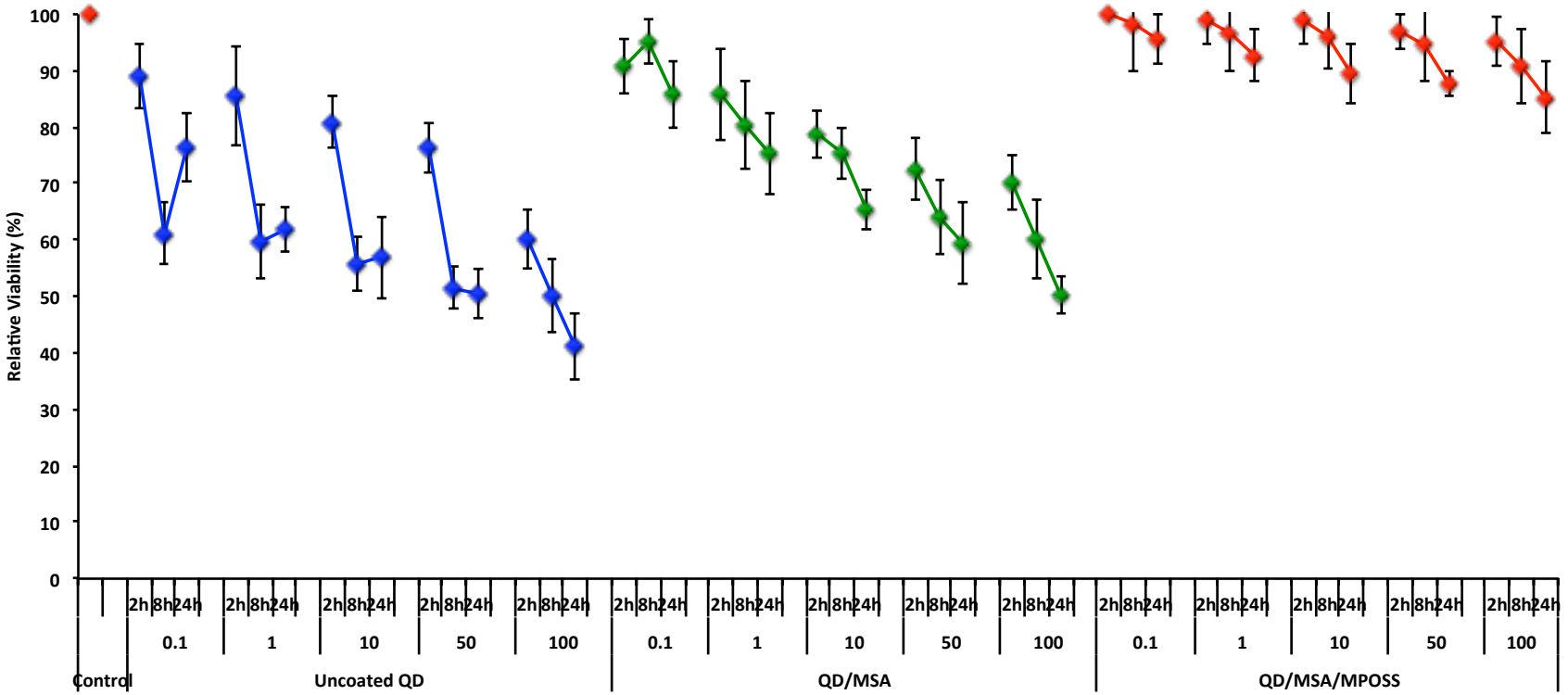

Figure 5.7: a) Comparison of three types of QDs (uncoated CdHgCoTe, coated CdHgCoTe/MSA, coated CdHgCoTe/MSA/MPOSS) induced toxicity on HUVECs, determined by Alamar Blue assay. The coated CdHgCoTe/MSA/MPOSS demostrates minimum toxicity amongst the uncoated CdHgCoTe and CdHgCoTe/MSA QDs.

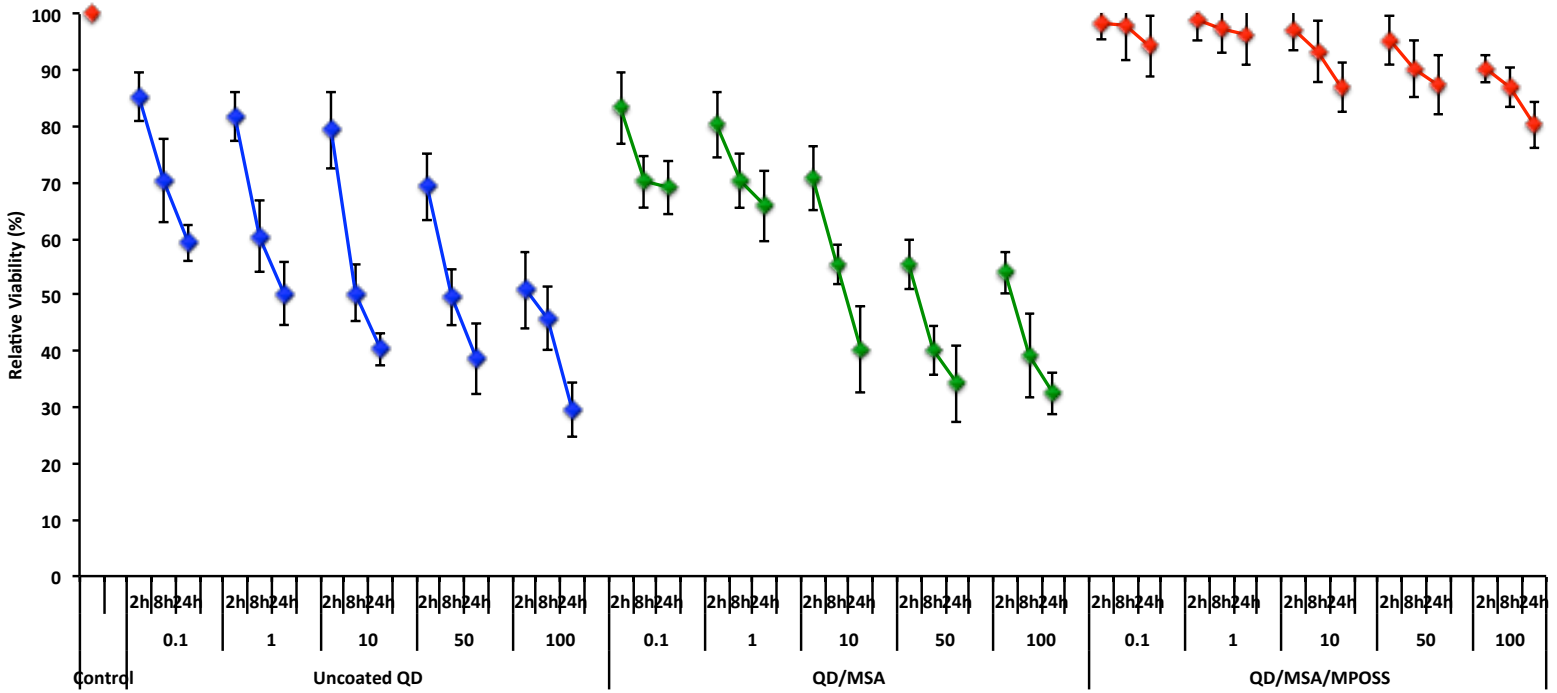

Figure 5.7: b) Comparison of three types of QDs (uncoated CdHgCoTe, coated CdHgCoTe/MSA, coated CdHgCoTe/MSA/MPOSS) induced toxicity on HUVECs, determined by Neutral Red assay. The coated CdHgCoTe/MSA/MPOSS demostrates minimum toxicity amongst the uncoated CdHgCoTe and CdHgCoTe/MSA QDs.

Figures **5.8 a** and **b** represent a comparison of toxicity level of all three types of QDs using Alamar Blue and Neutral Red respectively on MCF-7 breast cancer cells. MCF-7 cells have a similar pattern showing that the toxicity of CdHgCoTe/MSA/MPOSS QDs is relatively low compared with two other QDs. This may be attributed to the MSA/MPOSS preventing leaching of Cd^{2+} and Hg^{2+} from the core (**Figure 5.8 a,b**). It can be observed that the level of toxicity is relatively higher for MCF-7 than with HUVEC cells.

There are two very minor unexpected cell number increases seen in figure 5.8 a, b and is consistent with possible human error. Also, the extend of experimental variables tested makes it statistically possible that a few of the results would give unexpected results. The cell viability increased unexpectedly for uncoated CdHgCoTe QDs at concentration of 0.1 µg/mL using Alamar Blue (**Figure 5.8 a**), and CdHgCoTe/MSA QDs using Neutral Red assay at 24 h incubation respectively (**Figure 5.8 b**).

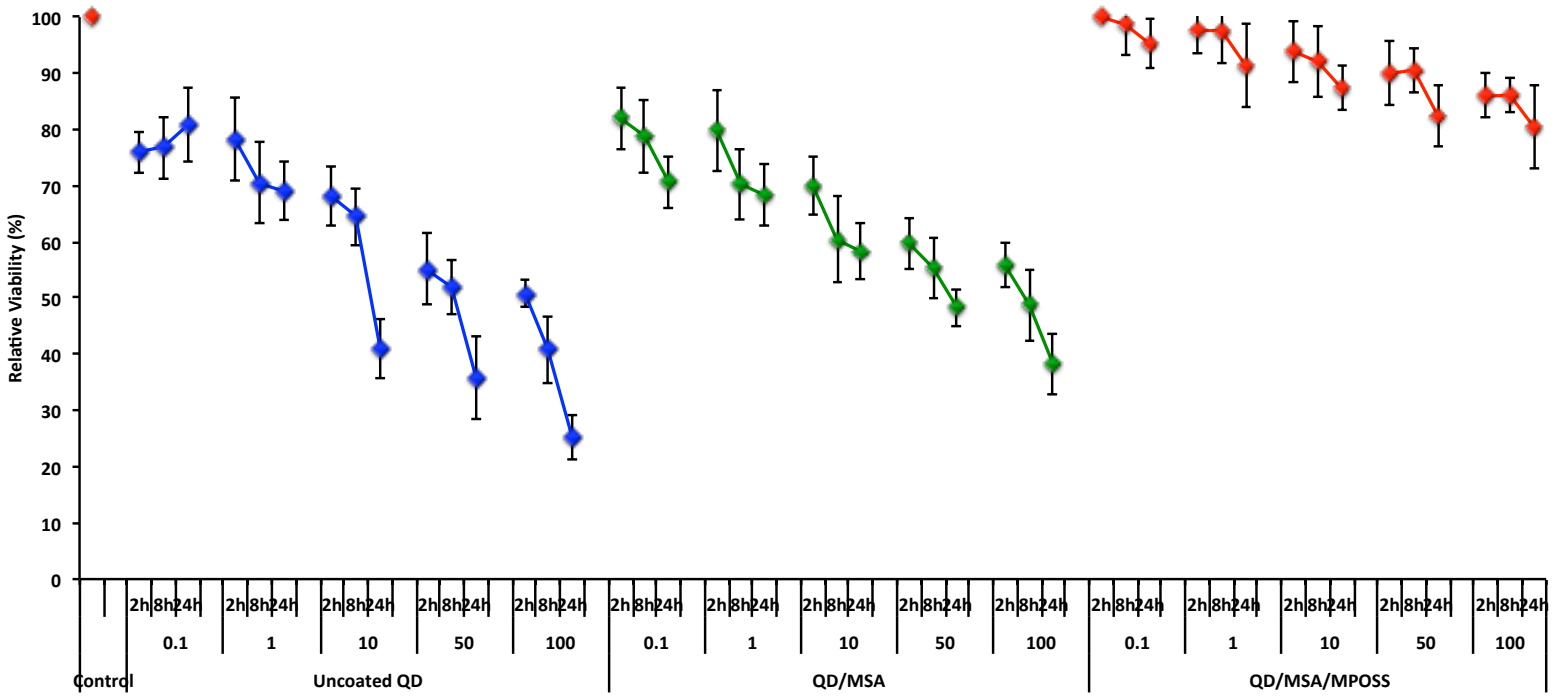

Figure 5.8: a) Comparison of three types of QDs (uncoated CdHgCoTe, coated CdHgCoTe/MSA, coated CdHgCoTe/MSA/MPOSS) induced toxicity on MCF-7, determined by Alamar Blue assay. The coated CdHgCoTe/MSA/MPOSS demostrates minimum toxicity amongst the uncoated CdHgCoTe and CdHgCoTe/MSA QDs.

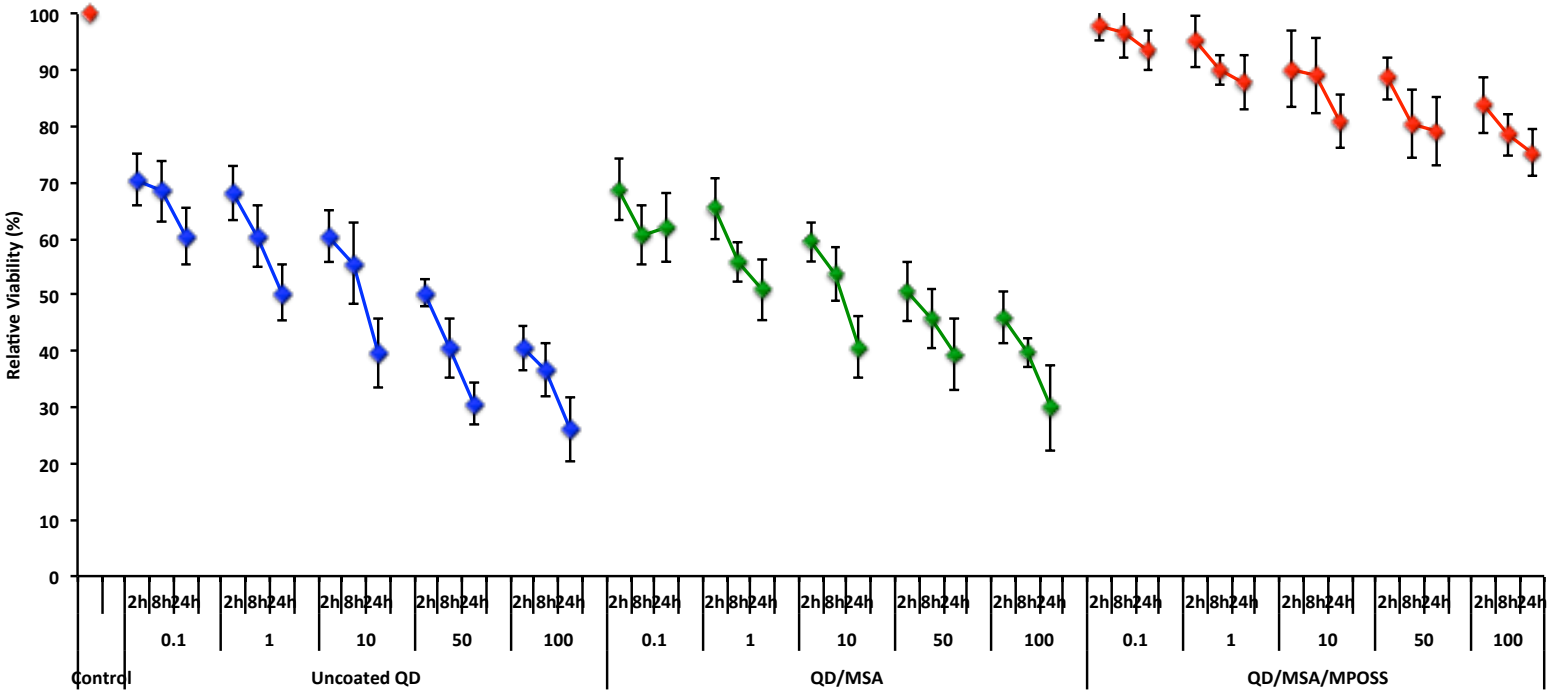

Figure 5.8: b) Comparison of three types of QDs (Uncoated CdHgCoTe, coated CdHgCoTe/MSA, coated CdHgCoTe/MSA/MPOSS) induced toxicity on MCF-7, determined by Neutral Red assay. The coated CdHgCoTe/MSA/MPOSS demostrates minimum toxicity amongst the uncoated CdHgCoTe and CdHgCoTe/MSA QDs.

Figure **5.9 a, b** represent a comparative toxicity level evaluation of all three QDs treated on SW620 colorectal cancer cells using Alamar Blue and Neutral Red assays respectively.

General toxicity can be evaluated in these two graphs illustrating that uncoated CdHgCoTe QDs have the highest toxicity followed by CdHgCoTe/MSA QDs and the least by CdHgCoTe/MSA/MPOSS QDs.

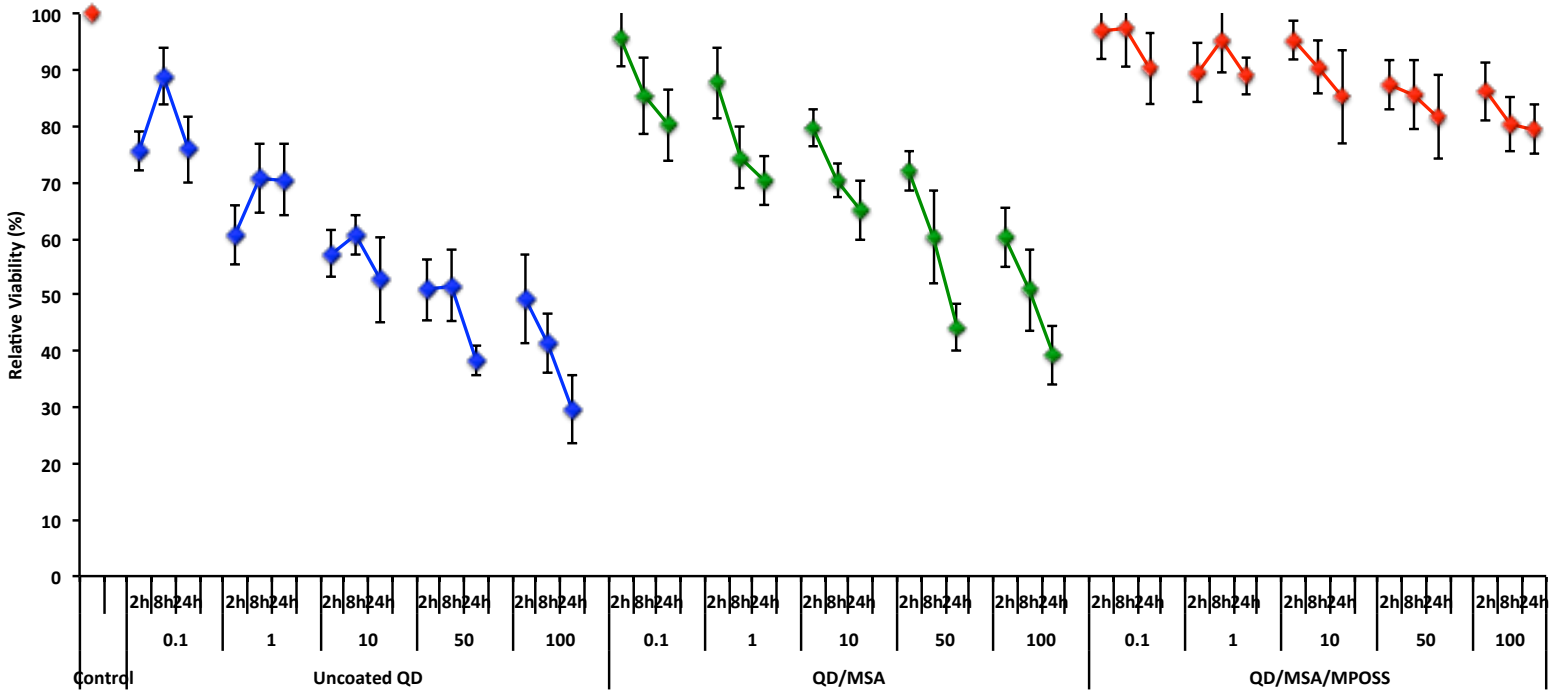

Figure 5.9: a) Comparison of three types of QDs (Uncoated CdHgCoTe, coated CdHgCoTe/MSA, coated CdHgCoTe/MSA/MPOSS) induced toxicity on SW620, determined by Alamar Blue assay. The coated CdHgCoTe/MSA/MPOSS demostrates minimum toxicity amongst the uncoated CdHgCoTe and CdHgCoTe/MSA QDs.

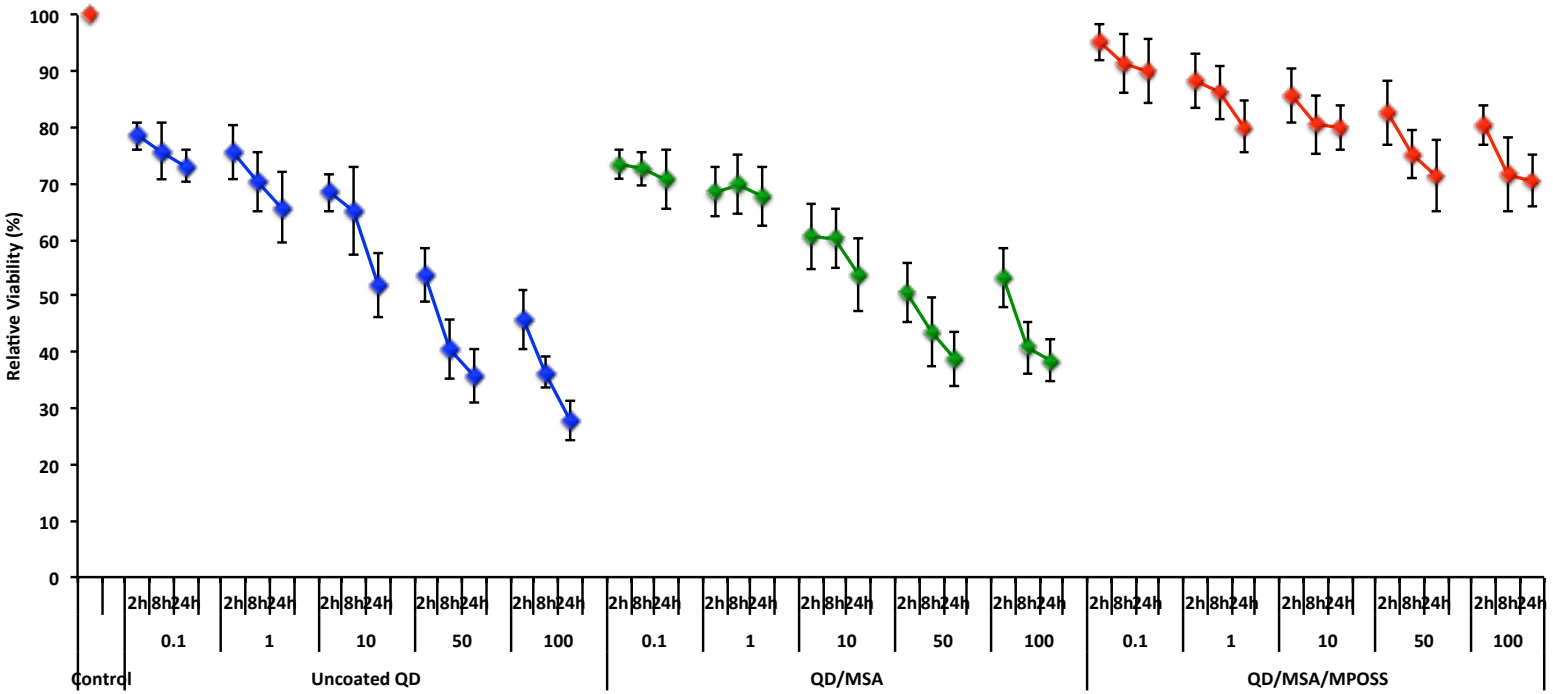

Figure 5.9: b) Comparison of three types of QDs (uncoated CdHgCoTe, coated CdHgCoTe/MSA, coated CdHgCoTe/MSA/MPOSS) induced toxicity on SW620, determined by Neutral Red assay. The coated CdHgCoTe/MSA/MPOSS demostrates minimum toxicity amongst the uncoated CdHgCoTe and CdHgCoTe/MSA QDs.

Additionally, prostate cancer cells (PC3) showed a similar pattern to all the cell cultures used (**Figure 5.10 a,b**). The toxicity evaluation showed similar results even though the cell cultures are of different origin. Minor changes can be observed figure **5.9 a** for uncoated CdHgCoTe QDs at 0.1, 1.0 and 10 μg/mL concentration at 8 h incubation, again using Alamar blue assay. However, the minor unexpected cell number increases may be accounted due to using these assays.

The cytotoxicity of CdHgCoTe, (core, uncoated) and water soluble CdHgCoTe/MSA, CdHgCoTe/MSA/MPOSS QDs (core, shell/coating,) respectively, directly synthesised in aqueous phase, was systematically studied for the first time in this type of coated QDs. It can be concluded that the uncoated CdHgCoTe and CdHgCoTe/MSA coated QDs were toxic, possibly due to the liberation of Cd^{2+} and Hg^{2+} ions from the core. In contrast, the CdHgCoTe/MSA/MPOSS QDs were less toxic than the MSA coated QDs, even at low concentration with long incubation for all cell cultures. This can be attributed to the novel hybrid coatings of MSA and MPOSS. This combination is likely to act by preventing the release of cadmium ions from the core. Current data indicates that the cytotoxicity of nanomaterials such as QDs could be effectively modified through novel surface coating techniques.

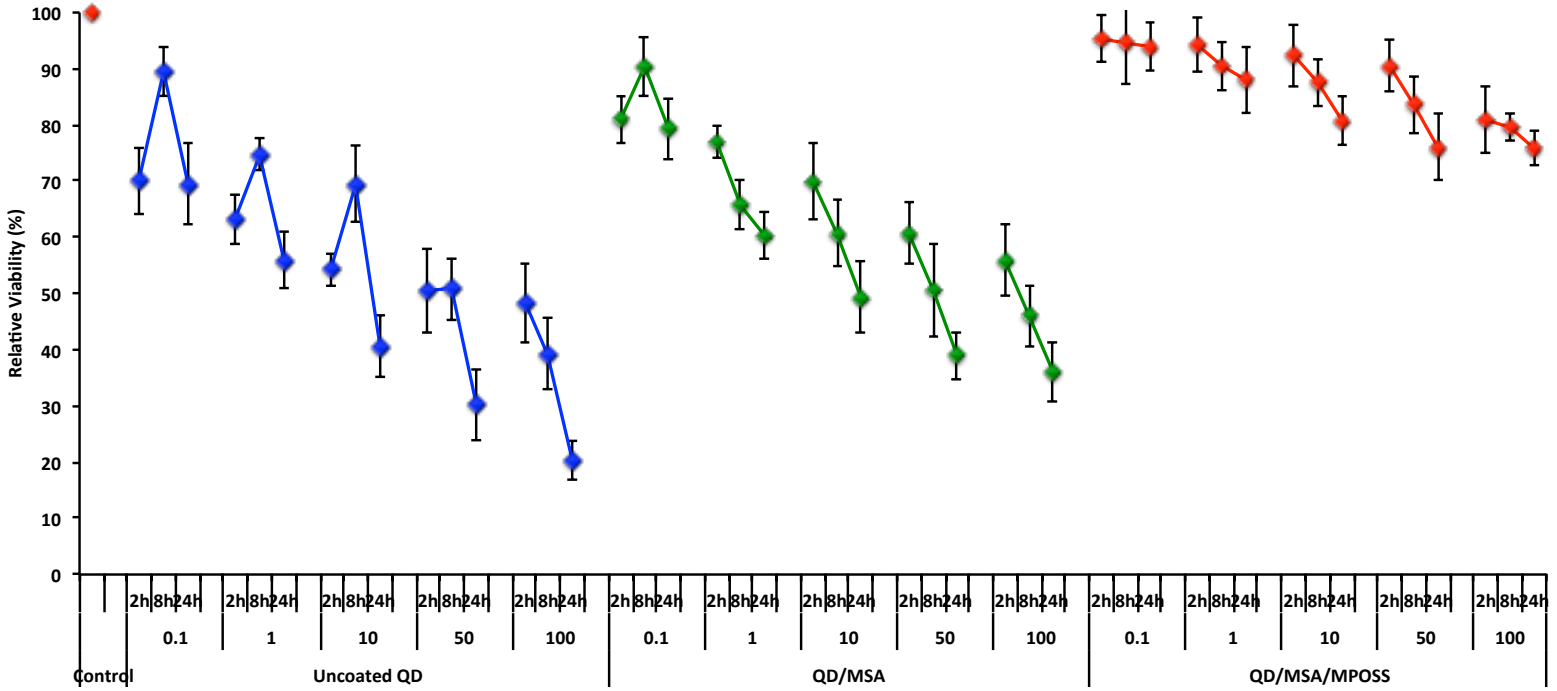

Figure 5.10: a) Comparison of three types of QDs (uncoated CdHgCoTe, coated CdHgCoTe/MSA, coated CdHgCoTe/MSA/MPOSS) induced toxicity on PC3, determined by Alamar Blue assay. The coated CdHgCoTe/MSA/MPOSS demostrates minimum toxicity amongst the uncoated CdHgCoTe and CdHgCoTe/MSA QDs.

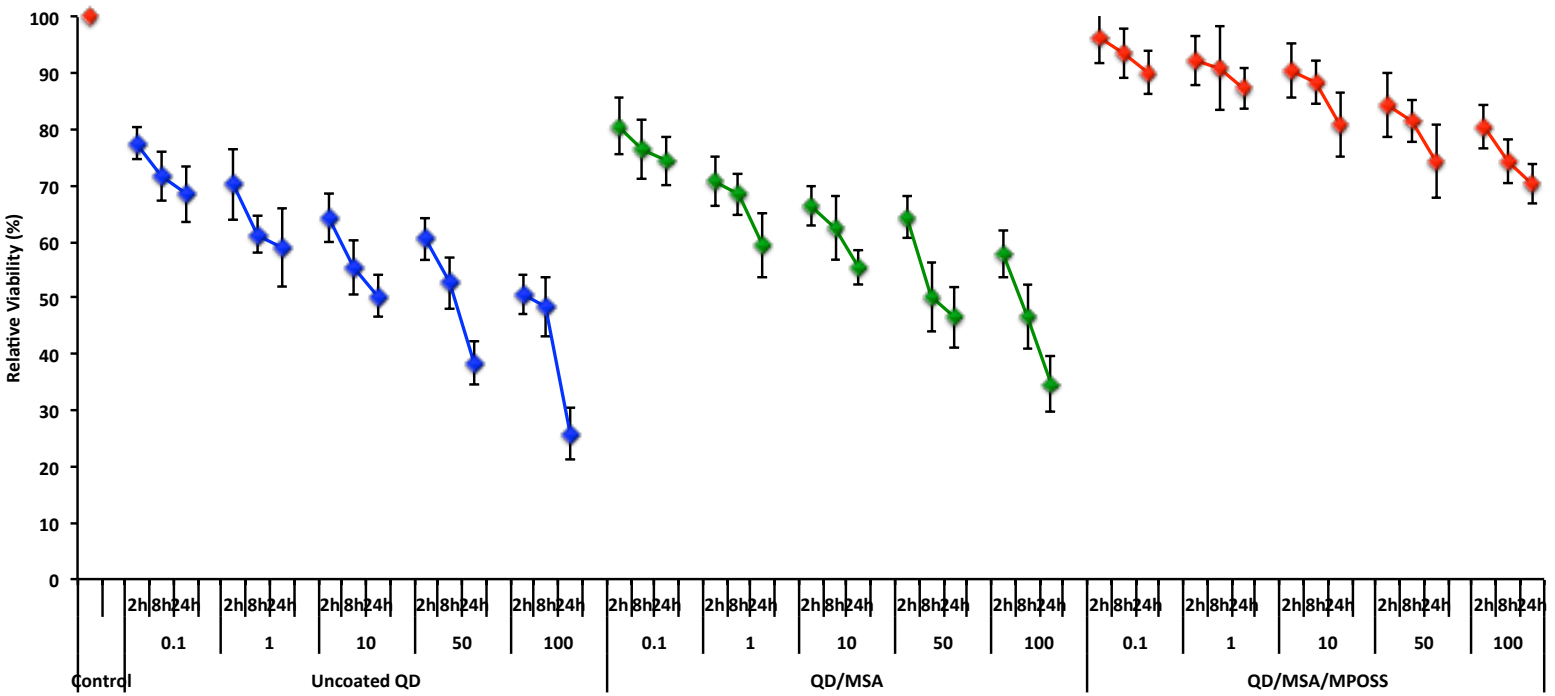

Figure 5.10: b) Comparison of three types of QDs (uncoated CdHgCoTe, coated CdHgCoTe/MSA, coated CdHgCoTe/MSA/MPOSS) induced toxicity on PC3 determined by Neutral Red assay. The coated CdHgCoTe/MSA/MPOSS demostrates minimum toxicity amongst the uncoated CdHgCoTe and CdHgCoTe/MSA QDs.

5.4. Overall discussion

Although QDs have great potential as probes for imaging in biology and medicine, certain limitations may restrict their usefulness. The introduction of NIR emitting QDs has solved some of the problem associated with autofluorecence by reducing the background fluorescence. This presents an attractive alternative for *in vivo* imaging. In this experiment the NIR emitting QDs had in its core, cadmium, telluride, mercury and cobalt (CdHgCoTe) with appropriate coatings (MSA and MSA/MPOSS).

It was first observed that Cd^{2+} ions could liberate from the surface of cadmium based QDs, which led to their cytotoxic effects (Austin M. Derfus, 2004). In another study, it was found that it was the capping molecule (TOPO, Trioctylphosphine oxide) of QDs that determined the cytotoxicity of QDs (Hoshino A, 2004a). More recently (this laboratory) a systematic toxicity investigation was carried out that employed CdHgCoTe/MSA and CdHgCoTe/MSA/MPOSS coatings *in vitro*. It was concluded that MSA coated QDs released Cd^{2+} and Hg^{2+} ions from the surface chemistry of QDs that were responsible for the toxicity of QDs. This can be correlated with toxicity studies carried out using the constituent material Cd^{2+} and Hg^{2+} *in vitro*.

The figures and graphs demonstrate toxicity of free Cd^{2+}, Hg^{2+} ions and uncoated and coated QDs in solution. The precursor studies simulate release of Cd^{2+} and Hg^{2+} from core and this establishes the lethal dose for the cells. Moderate levels of toxicity was demonstrated when QDs were coated only with MSA, compared with uncoated QDs. However, toxicity was reduced significantly when biocompatible MPOSS was included with MSA as coatings for the QD. It can also be concluded that the results indicate heavy metal ions especially Cd^{2+} and Hg^{2+} ions are very toxic to cells. The use of hybrid coatings such as MSA and MPOSS will ultimate lead to the potential applications in a clinical setting with minimal toxicity.

5.5. Conclusion

The aim of this study was to evaluate the toxicity of the NIR QDs with novel coatings for potential biomedical application. However, the issues of toxicity and clearance of QDs in biological systems are of concern as these two issues are not fully understood currently, and must be investigated if QDs are to move from scientific curiosity to biomedical applications. Some studies have indicated QDs have been retained inside the cells and cannot be eliminated after intravenous application (Fischer et al., 2006). This work needs further investigation.

From these results, it can be concluded that the uncoated CdHgCoTe QDs are significantly toxic to all four cell cultures. It can be observed that concentration and exposure duration plays a critical role in cell viability. This is possibly that the tri-metallic complex is breaking into its constituent parts with the release of Cd^{2+} ion or Hg^{2+} ion and hence the observed cell toxicity. This is most likely that biological degradation is occurring with subsequent release of the constituent metals. This clearly indicates that coatings are essential to contain the release of these heavy metals.

Further extensive studies, need to be performed on potential application of this type of QDs for *in vivo* imaging, distribution, and excretion in animal models. The use of suitable biocompatible coating agents with proper functional groups as used in this study, will offer a promising solution to the current limitations for different applications such as diagnostics and therapy of disease.

Chapter 6

Conjugation of the near infrared ‘Quantum Dots’ for *in vitro* and *in vivo* bio-imaging

6.1 Introduction

The interaction of nanotechnology with biology and medicine is expected to produce major advances in molecular diagnostics, molecular biology and bioengineering (Gao et al., 2002). To study these interactions, it is necessary to map the interactions of multiple proteins or drugs within an organism. Further, to fully understand and approach the complex clinical issues in disease (cancer) diagnosis and treatment, nanotechnologies have been developed in several key areas including cell targeting, drug delivery, hyperthermia and imaging by fluorescent nanocrystals.

Fluorescent imaging techniques, particularly NIR fluorescence imaging, with its unique advantages over other imaging modalities in sensitivity, multiplex detection capabilities and equipment cost, has attracted great attention as a vital tool in the field of tumor research (Rao et al., 2007). In the 700-900 nm spectra, the absorbance spectra for most biomolecules are low, which provides a clear window for *in vivo* optical imaging (Frangioni, 2003, Chen et al., 2011). However, current imaging techniques using NIR fluorescent organic dyes are known to suffer from rapid photobleaching which is not desirable for long-term molecular imaging (Frangioni, 2003) and are limited in terms of fluorophores conjugated per ligand.

Recent developments in nanotechnology have contributed significant contributions by means of NIR fluorescent nanomaterial based contrast agents (Farmer and Gordon, 2006). These include NIR dye-containing nanoparticles (Altinoglu et al., 2008), NIR fluorescent carbon nanotubes and upconversion fluorescent nanoparticles, have all shown superior brightness and photostability compared to organic dyes (Altinoglu et al., 2008, Xiong et al., 2009). Among the vastly studied NIR fluorescent nanoparticle based contrast agents, the NIR QDs are one of popular choice as imaging agents and have been successfully applied for cancer molecular imaging in small animal models of human cancer. Numerous studies have been conducted where non-targeted QDs were applied for cell trafficking (Dubertret et al., 2002), vasculature imaging (Larson et al., 2003, Stroh et al., 2005), sentinel lymph node mapping (SLN) and neural imaging (Stroh et al., 2005, Thorne and Nicholson, 2006, Zimmer et al., 2006).

To enable QDs to be useful for *in vivo* imaging and other biomedical applications, the required criteria are high sensitivity, biostability and specificity with accurate targeting

to a specific organ or disease site without being quenched. Specific targeting can be achieved by conjugating to targeting molecules to the QD surface. Site specific antibodies, peptides, peptidomimetics and small molecules make suitable targeting ligands, as large numbers of these molecules can be conjugated to the surface of a single QD and such conjugates may exhibit strong binding affinity with targeting efficacy due to the polyvalency effect (Hull et al., 1998).

Medical practice, especially in cancer diagnosis and treatment requires a series of clinical procedures to establish completion. In this clinical area, the potential of NIR QDs can play a vital part. For example, cell targeting is the primary step for nano-carriers to be localized in the tumor region. Using fluorescent nanocrystals, the targeted cancer cells or biopsy may be imaged *in vivo* or *in vitro* with high specificity and resolution. In addition, the nanoparticles *in vivo* may function as drug carriers with release mechanism in the vicinity of the tumor. Other development of cancer treatment may be applied such as hyperthermia when the nanocrystals are designed to be magnetic or photoactive.

In the field of drug delivery with nanoscale levels, various carriers have been evaluated (Wang and Marchant, 2004). Amongst the nano-carriers, multi-wall carbon nanotubes (MWCNTs) have been widely investigated for their potential advantages over metal nanoparticle systems, with their inherent high cargo loading, structural flexibility and biostability. Carbon nanotubes (CNTs) have been well studied in recent years to their interesting biological properties. The task was to promote surface functionalization and simultaneously provide colloidal stability to the resulting modified CNT in aqueous media. These properties as compared with suitably coated QDs could extend the circulation time and drug release. In this study, a new strategy to conjugate with QD is described. Previous studies have also shown strong optical absorbance of CNTs in the NIR region, which makes it a promising tool in photothermal therapy especially in cancer studies.

For a clinical application with simultaneous medical diagnosis and treatment, integrating functionalities into QDs, namely fluorescence for imaging, photo or magnetic for hyperthermia, and drug delivery would be ideal.

There are a variety of covalent and non-covalent strategies that have been developed for conjugating biomolecules (e.g. antibodies) and nanomaterials (e.g. carbon nanotubes) to QDs. Most materials including biomolecules can be conjugated covalently via cross-linkers, which form a bridge with functional groups such as;

$-NH_2$, -COOH or -SH (amino, carboxyl and thiol groups) introduced on the QD surface to the functional groups existing on nanomaterials or biomolecules. Currently many selective conjugation chemistries are available for introducing desirable functional groups for this purpose.

In this chapter, the design and development of QDs with integrated properties for simultaneous potential diagnosis, imaging and treatment are presented. Multifunctional QDs were conjugated to antibodies for targeting to cancer cell surfaces. Calreticulin (CRT) a calcium regulating protein was selected as a marker for cancer cells undergoing immunogenic or non-immunogenic depending on the presence of CRT on plasma membrane of the dying cell after toxic stimuli (Obeid et al., 2007).

Non-targeted multifunctional QDs were also conjugated to outer surface of the multi-wall carbon nanotubes (MWCNT) using PEG (Polyethylene glycol) as a linker. The assembled MWCNT which will be referred as CNT throughout this study, displayed unique functionalities due to surface conjugated NIR CdHgCoTe/MSA/MPOSS, making them potential probes for *in vivo* imaging and for introducing photohyperthermia simultaneously (**Figure 6.6**). Hyperthermia is a noninvasive approach to cancer treatment, whereby tissues are exposed to higher than normal temperatures to enable selective destruction of abnormal cells.

Photohyperthermia also induced immunogenic apoptosis of cancer cells *in vitro* by presence of CRT on cancer cell surface membrane. A short peptide corresponding to CRT was synthesised for generating antibodies (Anti-CRT) as a targeting ligand for cancer cell apoptosis detection. NIR fluorescent CdHgCoTe/MSA/MPOSS QD was conjugated to Anti-CRT for localization of cancer cells undergoing apoptosis when incubated in the presence of Cd^{2+} and doxorubicin, a known anticancer drug. Apoptosis was also detected using Anti-CRT in cancer cells *in vitro* when NIR CdHgCoTe/MSA/MPOSS QD conjugated CNTs when illuminated at 630 nm thus inducing NIR hyperthermia.

6.2. Supplementary methods

6.2.1. Materials

Refer to chapter 3, section 3.2 for further details.

6.2.2. Method

6.2.2.1. Solid-phase peptide (Calreticulin) synthesis

Refer to chapter 3, section 3.4.3 for full details.

6.2.2.2. Production of anti-peptide IgG antibodies

To generate anti-sera to human CRT protein, a peptide of 15 amino acid (NH_2-Met-Leu-Leu-Ser-Val-Pro-Leu-Leu-Gly-Leu-Ala-Val-Ala-Pro-Ala-NH_2) corresponding to the amino terminus (sequence numbers) of this protein was synthesised (described earlier). The peptide was conjugated to keyhole limpet haemocyanin (KLH) using glutaldehyde. The KLH conjugated peptide was injected into New Zealand white rabbits (1mg/rabbit) (Intra muscular, IM) for polyclonal antibody production. The IgG components were isolated from antiserum using 50% saturated ammonium sulphate solution. Antibody specificity was confirmed by antibody blocking experiments. Anti-CRT was use for conjugation experiment and for all detection *in vitro* studies.

6.2.2.3. Preparation of QD-(Anti-CRT) conjugation

Fluorescent CdHgCoTe/MSA/MPOSS QD solution was diluted with equal volume of cold ethanol and centrifuged at 4000 rpm for 30 minutes. The precipitated CdHgCoTe/MSA/MPOSS QD was vacuum dried to obtain as a powder. The precipitated dried QDs (Approximately, 1 mg) were re-suspended in 1 mL phosphate buffer saline/tetrahydrofuran (PBS/THF) (1:1 v/v) and centrifuged at 4000 rpm for approximately 10 to 15 min. The obtained coated QD (1 mL) solution was conjugated to the Anti-CRT using EDC as an acylating agent together with NHS. Briefly, 200 μL QD/MSA/MPOSS solution (1 mg/mL) was mixed with 200 μL EDC (1 mg/mL) and 200 μL NHS (1 mg/mL) in PBS for 30 minutes at room temperature. 100 μL of Anti-CRT solution (5 mg/mL) was added to the mixture and mixed for 2 h in ice. To separate the reagent and unconjugated CdHgCoTe/MSA/MPOSS QDs, membrane centrifugal

columns (centricon) with a cut off of 100 kDa with UV monitoring at 280 nm of the retained samples was used. The purified QD-(Anti-CRT) defines as CdHgCoTe/MSA/MPOSS conjugated to (Anti-CRT) were collected and stored at +4 ºC until further use. The sample was further characterized by NIR fluorescence and FTIR spectroscopy.

6.2.2.4. Application of conjugated QD-(Anti-CRT) for detection of apoptosis in vitro by confocal microscopy

Briefly, MCF-7 and SW620 were selected for its cancer cell characteristics and HUVECs were selected as a noncancerous control for this study. All three (HUVEC, MCF-7 and SW620) culture cells were plated in triplicates into a twelve well plate separately and incubated for 24 h in an incubator. The cells were allowed to grow to approximately 80% confluence for this study. Cadmium (50 μg/mL) from previous studies has been shown to be toxic and was investigated for its mechanism. Doxorubicin (50 μg/mL) is a well-known anticancer drug was also investigated and added in a twelve well plate with appropriate controls in each plate. After the addition, the plates were incubated for further 1 h at 37 °C. After 1 h incubation at 37 °C, the cells were rinsed 5 times with PBS and fixed with 1 mL of paraformaldehyde 4% in PBS for 20 minutes. The wells were aspirated and rinsed with 1 mL PBS (x 3) and blocked using bovine serum albumin (BSA) in PBS/Tween20 (PBS/T) (1 mL) for 1 h. The wells were aspirated and rinsed with PBS/T (x 1). QD-(Anti-CRT) (1 mL) in PBS/T was added to the fixed wells and incubated at room temperature for 2 h. Finally, they were rinsed with PBS (x 3). Fluorescence images were acquired using Nikon laser scanning confocal microscope (EZ C1) with a x 40 objective.

6.2.2.5. Functionalization of Carbon Nanotube

Crude CNTs (0.5 g) were added to H_2SO_4/HNO_3 = 3:1 (v/v). The mixture was dispersed in an ultrasonic bath (40 KHz) for 5 minutes and then stirred for 24 h at 100 °C under reflux. The mixture was then filtered under vacuum through a 0.22 μm Millipore polycarbonate membrane. The membrane was washed with distilled water until most of the acid mixtures have been diluted out. The CNT-COOH on the membrane was dried and weighted. The filter containing CNT was then suspended in PBS and eluted by ultrasonication to disperse the CNT-COOH.

6.2.2.6. Conjugation of CdHgCoTe/MSA/MPOSS quantum dot to functionalized Carbon nanotube

The functionalized CNT with carboxyl groups (CNT-COOH) (0.1 g/mL) was dispersed in PBS with CdHgCoTe/MSA/MPOSS QD (0.1 mg/mL) with brief sonication to further disperse the mixture. The dispersed MWCNTs and QDs were mixed with EDC solution (100 μl of 1 M in PBS) and NHS solution (100 μl of 0.5 M in PBS) for 30 minutes. At this stage the linker O,O'- Bis(2-aminopropyl)polyethylene glycol 1900 (PEG) was added to the mixture to form a peptide bond simultaneously with CNT and NIR CdHgCoTe/MAS/MPOSS thus forming (CNT-PEG-CdHgCoTe/MSA/MPOSS) species after 1 h. The solution was then centrifuged at 12000 rpm for 2 minutes and rinsed three times with PBS using centrifugation and decantation. The final re-suspended CNT-PEG-CdHgCoTe/MSA/MPOSS were filtered through a 0.22 μm Millipore polycarbonate membrane under vacuum to eliminate coupling reagents and unreacted QDs. Finally, presence of QDs on CNTs was confirmed by the TEM images (**Figure 6.10**).

6.2.2.7. Biodistribution study of conjugated NIR QD-CNT

The biodistribution of QD-CNT was studied in female 6-8 weeks old (18-21 g) BALB/c mice (Charles River, Margrate, UK). All the experiments were carried out at Pharmidex pharmaceutical Ltd, adhered to the 1986 Scientific Procedures Act (UK) and in compliance with the guide for the care and use of laboratory animals in Pharmidex Ltd.

The NIR QD-CNT solution for intraperitoneal (IP) injection was prepared by dissolving the mixture of QD-CNT in normal PBS buffer. Six mice were separated randomly into two groups (three mice in each group) and marked with No. 1 and No. 2. Normal saline solution as control named as group No. 1 and the conjugated QD-CNT in PBS (0.6 mL) was IP administrated into the mice (**Table 6.1**). Animals were sacrificed by CO_2 administration.

Table 6.1: Administration of conjugated QD-CNT in mice.

Group Number	Nanoparticles	Injection Type	Dosage (mL)	Time course (h)
No 1	Control (PBS)	IP	0.6	4
No 2	NIRQD-CNT	IP	0.6	4

After sacrificing the animals, fluorescence imaging was performed on each mouse. For each of them, a background image was collected. First, the images of the body, abdomen and dorsal region were captured by NIR camera with excitation at 640 nm by selecting emission, 730/80 nm long-pass filter. Subsequently, the ventral and dorsal skin of the mouse was removed and images were collected (**Figure 6.13**). Different organs were removed, dissected and frozen.

To continue the investigation, histopathological assessment of tissues was conducted to determine the presence of QD-CNT. Briefly, the control group (No. 1) and No. 2 group were dissected. Four representative organs (liver, spleen, lung, brain) were removed from the mice, fixed in 10% formalin overnight, and formalin-fixed tissues were sectioned at 8 μm using a cryostat and tissue sections prepared by the Histopathology Department, Royal Free Hospital, London. Confocal laser scanning microscopy was carried out using the filter set excitation at 488 nm and emissions at 800 nm long-pass filter and imaged via a computer. The NIR fluorescence images were acquired with the microscope at the same Pseudocolour (red) scale throughout.

6.2.2.8. Photothermal induced apoptosis induced in cancer cells by conjugated NIR QD-CNT

Similar to section 6.2.2.4, seeded cells were also repeated this time with incubation with NIR QD-CNT (5 μg/mL) and unconjugated CNT. In this arrangement cells (HUVECs as control) and (MCF-7 and SW620) were exposed to 650 nm laser red light source for 5 minutes. The cells were rinsed in PBS and fixed as above. The cells were blocked with 1% BSA in PBS/T for 30 minutes. The blocking solution was removed and rinsed in PBS/T. The NIR QD-(Anti-CRT) was incubated at room temperature for 2 h. Excess complex were removed with washing with PBS (X 3 washes) and observed for evidence of apoptosis in the presence of conjugated and unconjugated CNTs with confocal microscopy.

6.2.2.9. Confocal fluorescence microscopy

Details in section 3.3.5 in chapter 3

6.3. Results and Discussion

6.3.1. FTIR Characterization of QD-(Anti-CRT)

The amino terminus of CRT was synthesised and the anti-peptide antibodies (Anti-CRT) were generated in the rabbit and conjugated to CdHgCoTe/MSA/MPOSS QDs. FTIR spectroscopy was used to evaluate the Anti-CRT conjugation to NIR CdHgCoTe/MSA/MPOSS QD. FTIR spectroscopy spectra results confirmed the presence of amide I peak of Anti-CRT conjugated to CdHgCoTe/MSA/MPOSS QD (**Figure 6.1**). The region around 1645 cm^{-1} indicates the amide bond stretch of the protein. This region is assigned to the amide bond which is 80% C=O stretching and 10% from N-H bending and 10% C-N stretching region in deuterium oxide (D_2O). Additionally, when bound to QDs there is a shift to the higher vibration band, this indicates an open structure accessible to deuterium exchange as opposed to a close structure of QD to Anti-CRT. This indicates that the protein has maintained its native conformation despite the conjugation to the QD. Therefore, the QD conjugated to Anti-CRT has a strong peak at 1645 cm^{-1}.

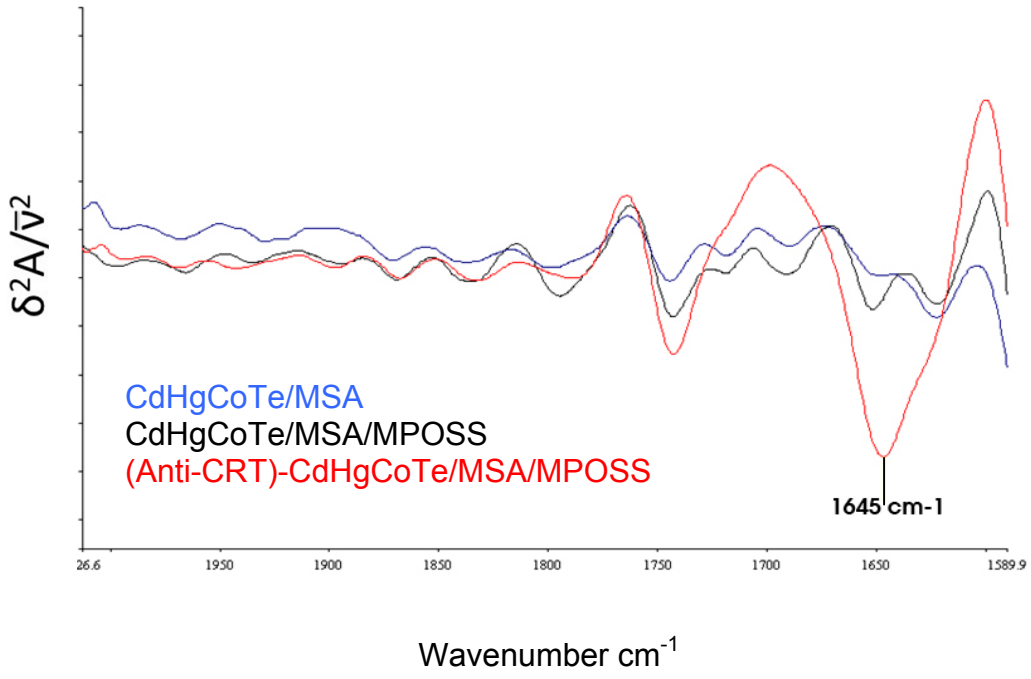

Figure 6.1: FTIR Spectra of CdHgCoTe/MSA QD (Blue), CdHgCoTe/MSA/MPOSS QD (Black) and (Anti-CRT)-CdHgCoTe/MSA/MPOSS (Red). The 1650 cm-1 indicates amide I region of the Anti-CRT protein.

6.3.2. Quantum dots in cell labeling applications

Semiconductor QDs have been developed as fluorescence tags in biological and medical applications such as *in vitro* and *in vivo* biological labeling, imaging, targeting therapeutic carriers and drug delivery, due to their exceptional fluorescent properties. To avoid QD aggregation, improve water-solubility and biocompatibility, and exert specific surface chemistry for targeting and delivery, various conformations of semiconductor QDs (Liu et al., 2008).

6.3.2.1. Chemical synthesis of proteins CRT

A linear, bifunctional peptide was synthesised called Calreticulin (CRT). Proteins and polypeptides with important structure-function interrelationship's isolated from animal, plants and microorganisms has been a subject of great interest for many years. Amongst them, there are the many membrane-associated proteins such as neuropeptides, toxins, growth factors, antibodies and hormones. The realisation that these naturally occurring biological molecules have peptide structures encouraged the development of techniques for the organic chemical synthesis of proteins and polypeptides with predetermined sequence.

Although subsequent rapid developments in genetic engineering made it possible to produce desired proteins, this process can be expensive and is generally unsuitable for obtaining desirable quantities with suitable rapidity. This remains attached to the solid support throughout the synthesis cycle (deprotection/coupling) and is separated from soluble reagents and solvents by simple filtration and washing without incurring manipulative losses. The repetitive steps are quick and simple. Once chain elongation has been accomplished, it is necessary to detach (cleave) the fully protected peptide from the solid support under conditions that are mild to labile residues in the sequence. Finally complete deprotection of the residues accompanied by purification and characterization are carried out in free solution. The main advantage of a solid-phase approach is that reactions are driven to completion by using excess soluble reagents promoting high efficiency and yields which can be recovered by filtration and washing without manipulative losses.

The essential feature, which distinguishes solid phases synthesis from other techniques is the solid support. The resin support is quite often a polystyrene suspension polymer

cross-linked with 1% of divinylbenzene as cross-linking agent. The resulting spherical beads when dry have an average diameter of 50 μm with a functional value of 0.2 to 1.0 mmol/g. These beads in solvents commonly used for peptide synthesis, namely DMF and DCM swell 2.5 to 6.2 fold their original volume. Furthermore, as peptide chains are extended the dry volume increases to accommodate the increased mass and most crucially the swollen volumes continue to increase.

6.3.2.2. Preparation of QD-(Anti-CRT) conjugation

Antibody molecules possess a number of functional groups that are suitable for QD conjugation. Crosslinking reagents can be used to target lysing primary amine and N-terminal amine groups. Keyhole limpet haemocyanin (KLH) plays an important role for raising antibody for producing Anti-CRT. Once prepared, the QD-(Anti-CRT) conjugates can be stored for about 4-6 weeks. Beyond this storage period, staining still works but the quality is fairly poor. The problem is that a lot of antibodies need to be stored at -20 °C while QD samples at 4 °C. If the QD-(Anti-CRT) conjugates are stored at 4 °C for long time, the antibodies lose binding affinity and specificity.

Unsuccessful conjugation is often due to the presence of other disulfide-containing molecules in the antibody medium or buffer. It can be the aggregate formation by too many QDs presented in buffer, too much of a reagent, e.g., EDC, wrong reaction buffer (e.g., buffer at an incorrect pH or using a free-amine containing buffer in EDC coupling reaction). QD conjugation should be confirmed by running FTIR.

6.3.2.3. Conjugating QD with Anti-CRT

Targeting tumor cells or tumor vascular by peptide technology is a promising strategy for delivering drugs or for labeling (Zitzmann et al., 2002). In this study, a novel method was developed for a novel surface coating and functionalization of QD. Anti-CRT was developed and conjugated to NIR QD as a probe for labeling applications. However, the specific labeling of target (cell surface integrin) on fixed cells *in vitro* was described. **Figure 6.2** shows the pathway from synthesizing CRT peptide and raising antibodies to CRT and applying to cell culture studies.

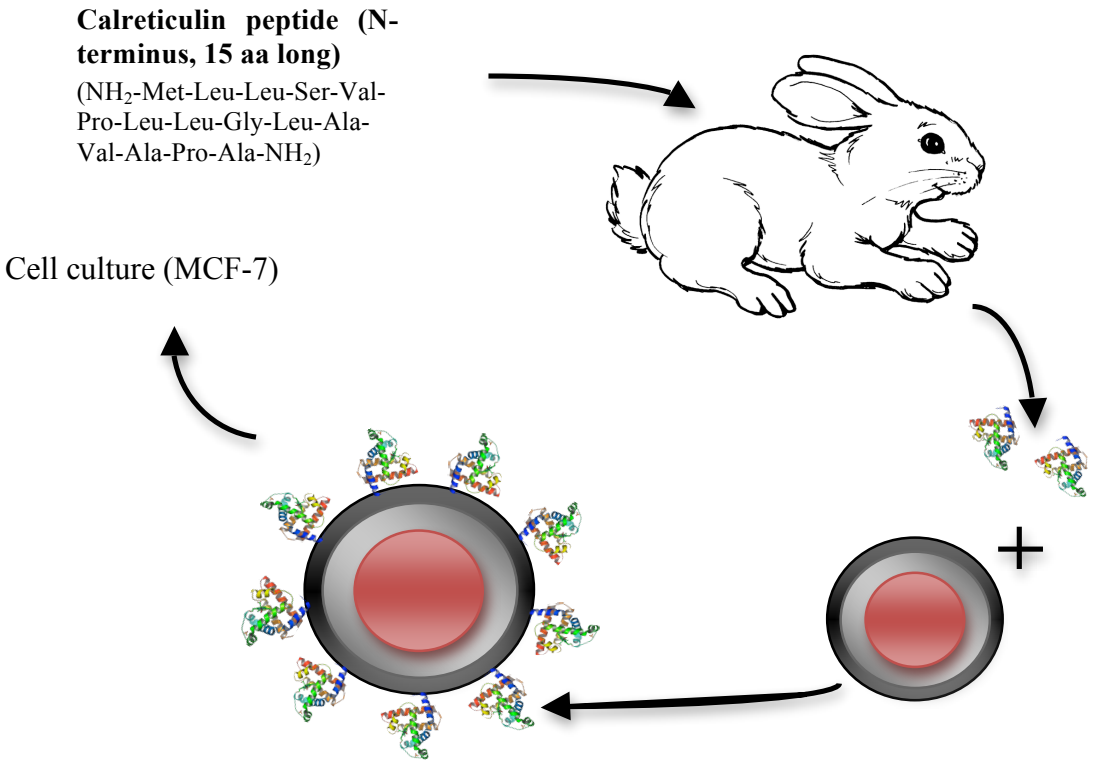

Figure 6.2: Schematic diagram of preparation of Anti-CRT followed by conjugation to quantum dot. Some anticancer drugs may increase immunogenic signal (calreticulin, CRT) on apoptosis. CRT expression also increases cancer immunogenicity. Synthetic calreticulin peptide was used to raise anti-peptide antibodies.

Anticancer therapies are being developed in which PCD is induced in cancer cells to halt or reverse tumour growth. As it has been established that PCD is involved in many diseases, imaging of this process would be of great value to diagnosis and guidance of therapy. Apoptosis is often described as a silent process whereby apoptotic cells are removed by phagocytosis without provoking an immune response i.e. non-immunogenic. It has been established in previous studies, that when tumours in *in vivo* models cells were exposed to anticancer drugs belonging to the anthracycline family, an anti-tumour immune response was initiated (Chakravarthy et al., 2011). Furthermore, in a recent study cancer cells when undergoing apoptosis became immunogenic by exposing CRT on their plasma membrane (**Figure 6.5**). It was concluded that only certain type of pro-apoptotic drugs (anthracyclines) induced immunogenic apoptosis while others induced non-immunogenic apoptosis. In the presence of recombinant CRT,

the non-immunogenic apoptosis could be converted to immunogenic apoptosis. In the present study, a synthetic peptide corresponding to the amino terminus of the CRT protein was synthesised and antibodies generated in a rabbit. In the course of this study it was discovered that cancer cell lines could also be induced to undergo immunogenic apoptosis by Cd^{2+} and photothermal induction by QD-CNT conjugate (more detail in this chapter). The anti-peptide (Anti-CRT) was conjugated to QDs to detect induced CRT in cancer cell surface when exposed to Doxorubicin, cadmium and thermal death QD-CNT. This study has shown for the first time that QD-(Anti-CRT) may enable in assessing the potential anticancer drugs that can induce immunogenic apoptosis in tissues or cells.

At this stage QD-(Anti-CRT) was incubated with three cell types for 2 hours at room temperature. In normal non-cancer cells, CRT is found predominantly in the endoplasmic reticulum, where it acts as a chaperone aiding proper folding of other proteins (Clarke and Smyth, 2007). Incubation of HUVEC with QD-(Anti-CRT) was used as control and indicated no evidence of its presence in surface membrane or intracellular uptake by confocal microscopy. Exogenous availability of CRT from neighboring cells cannot be dismissed as the control cells showed very low level of this protein. However, the other two cell lines had indicated a high level of CRT expressed when cells were exposed to the elemental forms of Cd^{2+} and Doxorubicin drug. Figures **6.3** and **6.4** have shown that Cd^{2+} could be used to as anticancer drug in this part of experiment due to similar results with doxorubicin results.

6.3.3. NIR emitting QD-(Anti-CRT) targeted to CRT on immunogenic apoptotic cancer cells

Triggering the body's natural immune response against tumours has great potential as alternative to cancer therapy. Many attempts have been tried in the past by others to immunize with tumour cells that have been modified deliberately, so as to use it as a vaccine. Unfortunately it has not worked as the body has not been sufficiently stimulated or tolerance has occurred. Recently a possible route to producing an anti-tumor vaccine was to treat isolated tumor cells with a particular class of chemotherapeutic drugs, the anthracyclines. This approach was shown to induce specific immune response of sufficient strength as to eliminate established tumors in

mice (Zhang et al., 2007). This work was further extended in demonstrating that tumor cells when exposed to anthracyclines produce specific protein marker, calreticulin (CRT), which marked them for removal by the immune system. These findings indicate that agents that can trigger CRT can be combined with conventional chemotherapy to provoke the immune system. For the first time, QDs conjugated to Anti-CRT have been employed to the study of cancer cells *in vitro* when exposed to cadmium ion (Cd^{2+}) or Doxorubicin. It can be shown from confocal fluorescence that it is feasible to apply this technology to the detection of cancer cell apoptosis (**Figure 6.3 and 6.4**). Doses of Cd^{2+} ion or Doxorubicin can be shown to stimulate CRT production. By extending these studies, antibodies directed against a selected region of CRT can be produced chemically and conjugated for imaging of cancer cells. This is illustrated below with confocal microscopy where the presence of CRT is evident after exposure to Cd^{2+} or Doxorubicin for 1 h. Figures **6.3 A** and **6.3 B** show the differential interference contrast (DIC) image of MCF-7 and fluorescence as control with absence of CRT on its surface respectively. This indicates that cancer cells do not produce CRT when not exposed to any toxic materials such as Cd^{2+} or Doxorubicin. Figures **6.3 C** and **6.3 D** show the contrast and fluorescence of MCF-7 cells after exposure to 50 μM of Cd^{2+} with production of CRT on surface. This is clear indications that cell are undergoing apoptosis as described in literature. In the following figures **6.3 E** and **6.3 F**, it can be seen that MCF-7 cell when exposed to Doxorubicin, an anticancer drug, there is strong indication that CRT

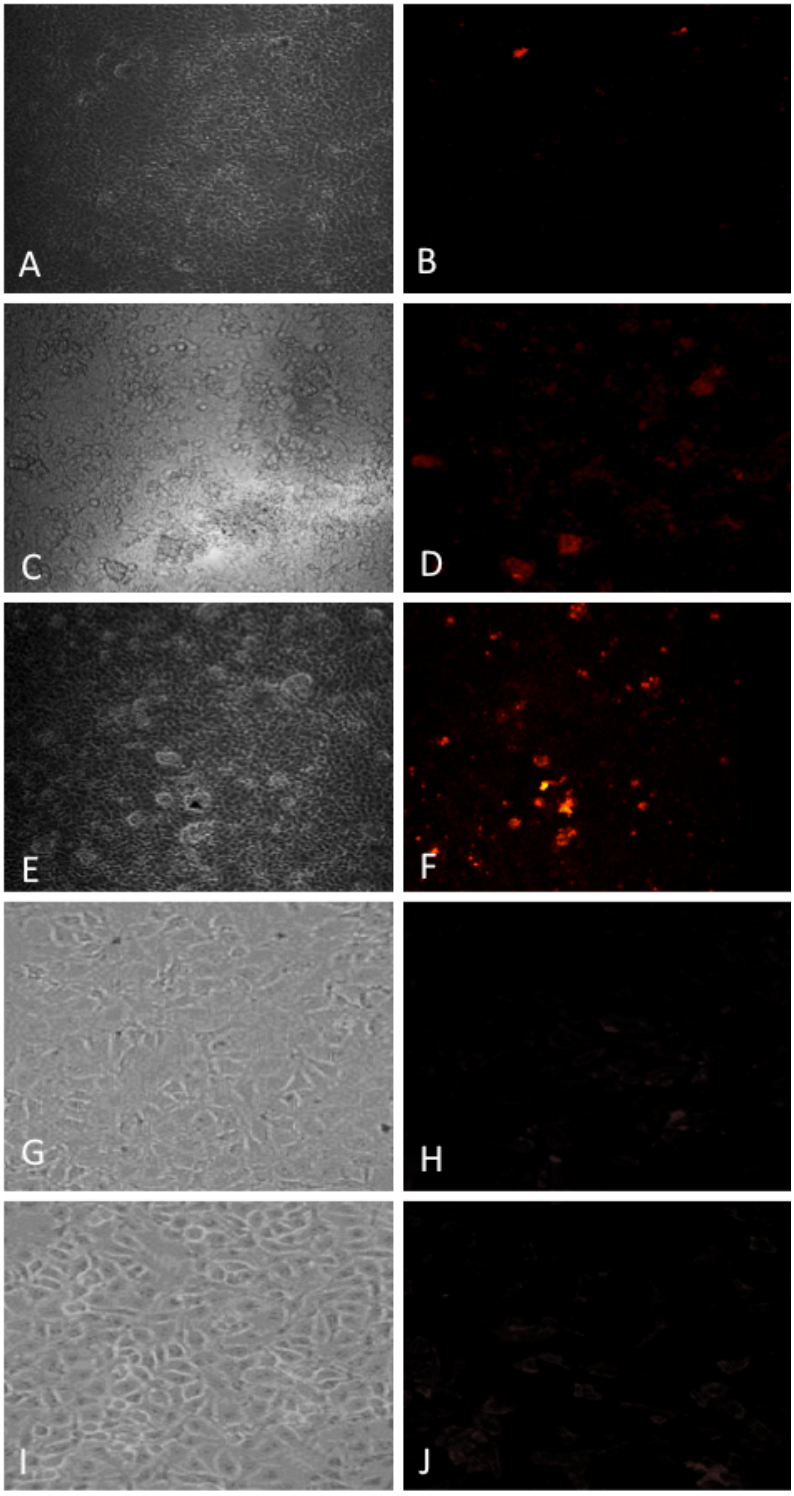

Figure 6.3: Images of MCF-7 cell exposed to Cd^{2+} and Doxorubicin to detect immunogenic apoptosis. **A, B)** DIC and fluorescent images of MCF-7, in the absence of Cd^{2+} or Doxorubicin (control). **C, D)** DIC and fluorescent images of MCF-7 cells exposed to Cd^{2+} ions at 1 h. QD-(Anti-CRT) fluorescence indicates presence of CRT protein (Apoptotic marker). **E, F)** DIC and fluorescent images of MCF-7 cells exposed to Doxorubicin at 1 h and CRT detected by QD-(Anti-CRT) **G,H**). DIC and fluorescent images of HUVECs primary cells exposed to Cd^{2+} for 1 h with absence of CRT with Anti-CRT. **I**, **J**) DIC and fluorescent images of HUVECs primary cells when exposed to Doxorubicin with absence of CRT protein by Anti-CRT.

are produced, which confirms previous *in vivo* studies. Figures **6.3** (G,H,I,J) illustrate HUVECs, which are primary culture as non-cancerous control to indicate that exposure to Cd^{2+} or Doxorubicin does not produce CRT despite undergoing cell death or apoptosis.

Similar procedure as above was carried out for SW620 cancer cells for detection of CRT on exposure to the compounds mentioned. The figures **6.4 A** and **B** illustrates SW620 cells as control, with no exposure to Cd^{2+} or Doxorubicin and hence absence of fluorescence. However, very weak fluorescence can be observed and is possibly due to non-specific binding. The figures **6.4 C** and **D** are the images of SW620 when exposed to Cd^{2+} ion for 1 h washed and fixed and incubated with QD-(Anti-CRT) for 2 h and examined with confocal microscopy. Clearly there is strong fluorescence for CRT due to apoptosis. Figure **6.4** are the images of SW620 cells when Doxorubicin under similar conditions, again showing that cells undergoing apoptosis with CRT expressed on surface of cell membrane detected by targeted QDs (QD-(Anti-CRT)). Similar procedure with exposure and detection shows that HUVCEs as non-cancerous control (**Figure 6.4 G-J**) do not produce CRT hence absence of strong fluorescence.

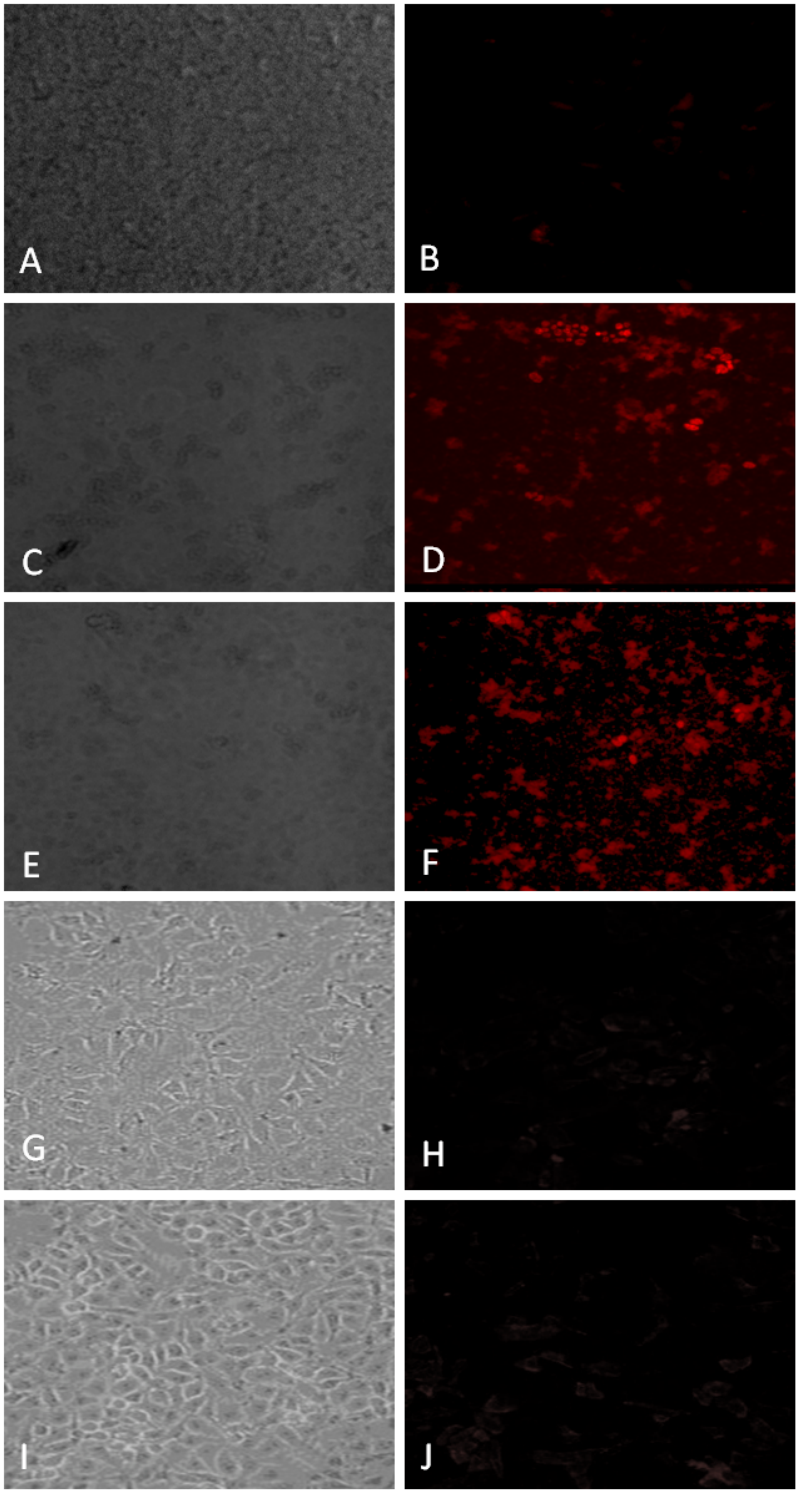

Figure 6.4: Images of SW620 cell exposed to Cd^{2+} and Doxorubicin to detect immunogenic apoptosis. **A, B)** DIC and fluorescent images of SW620, in the absence of Cd^{2+} or Doxorubicin (control). **C, D)** DIC and fluorescent images of SW620 cells exposed to Cd^{2+} ions at 1 h. QD-(Anti-CRT) fluorescence indicates presence of CRT protein (Apoptotic marker). **E, F)** DIC and fluorescent images of SW620 cells exposed to Doxorubicin at 1 h and CRT detected by QD-(Anti-CRT). **G, H**). DIC and fluorescent images of HUVECs primary cells exposed to Cd^{2+} for 1 h with absence of CRT with Anti-CRT. **I**, **J**) DIC and fluorescent images of HUVECs primary cells when exposed to Doxorubicin with absence of CRT protein by Anti-CRT.

6.3.3.1. Doxorubicin and Cadmium as inducers of apoptosis in cancer cells in vitro

Doxorubicin (Doxorubicin Hydrochloride, Sigma-Aldrich) is presently one of most successful and widely used anticancer drugs because of its broad spectrum of activity. The drug is given by injection into a fast running infusion for treating acute leukemias, carcinomas of the breast and ovary as well as soft-tissue carcinomas. Doxorubicin is mostly excreted by the biliary tract with an elevated bilirubin level is considered a marker for reducing the dose. Higher cumulative doses are associated with cardiomyopathy, and potentially fatal heart failure can occur (Thurston, 2006). Not only Doxorubicin anticancer drug was used for this study but also Cd^{2+} was used for inducing apoptosis in the cancer cells.

The novel coated QDs with MSA and MPOSS were used in the investigation of programmed cell death (PCD) in cancer cells. This phenomenon of organized cell suicide takes many forms, of which apoptosis is well known and studied. PCD is central in many biological roles such as physiology and pathology of multicellular organisms.

Cell proliferation and death are held in fine balance during homeostasis and are disturbed in a diseased state. However, in these conditions PCD is increased and in cancer it is polarized towards proliferation. The great challenges in cancer studies are to develop drugs that cannot only induce PCD but also the elimination by the immune system.

There are some cancer therapy drugs, which are available commercially such as the anthracyclines, which have been already shown to induce a specific immune response of sufficient strength to eliminate tumor cells. According to previous studies (Obeid et al., 2007), these drugs also cause tumor cells to expose on their surface a specific protein marker, called calreticulin (CRT), which tags them for removal by the immune system. CRT (calcium-binding protein) was used as a molecular target as it is known that certain anticancer drugs especially the anthracyclines such as Actinomycin, Cycloheximide and doxorubicin can induce necrotic apoptosis, which in turn can induce an immune response (Obeid et al., 2007). According to (Obeid et al., 2007) Doxorubicin induces apoptosis with an immunogenic clearance of cancerous cells. Similar behavior to Doxorubicin was detected when Cd^{2+} was used in cancer cells when immunogenic apoptosis was also detected by the presence of CRT on the cell surface (**Figure 6.5**).

It must be stated that in previous chapter on toxicity, Cd^{2+} ions were shown to kill cells and perhaps this could be a marker for future toxicity assay studies. There is clear evidence that exposure of Doxorubicin and free Cd^{2+} ion on the cancer cells stimulates the expression of the CRT as a marker on cancer cells (MCF-7, SW620) but not with HUVECs). Below is a simple depiction towards the path of an immunogenic apoptosis.

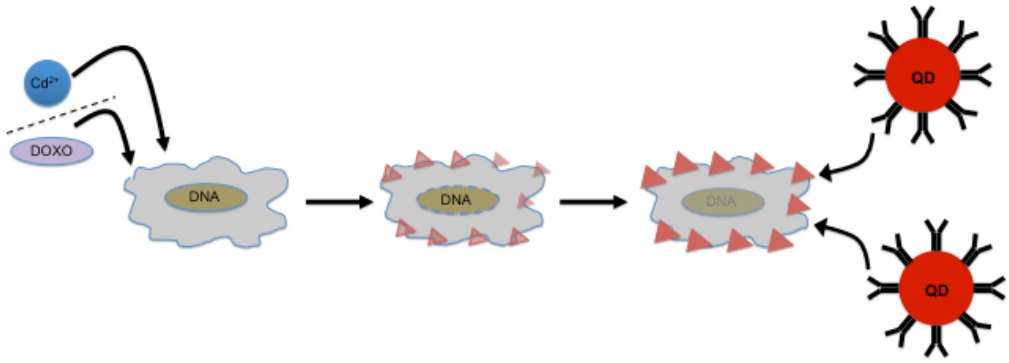

Figure 6.5: Schematic diagram showing process of programmed cell death (PCD).
Induction of apoptosis using drugs, heat or light may promote tumour elimination via the immune system. The ideal aim is to develop a cancer vaccine with production of CRT as a modulator for the immune response.

6.3.4. Surface modification of carbon nanotube

Water-soluble QDs and CNTs can be prepared by surface modification by many methods. Thiol molecules are the first choice and commonly used to modify the QD surface because of ease and speed. As for the CNTs the method is slightly different in that the nanotubes are refluxed at boiling in the presence of sulphuric and nitric acid.

In addition in this study, a new strategy to derivatize CNT with CdHgCoTe/MSA/MPOSS QD is described. This offers the possibility to predefine the size, shape, and amount of the nanoparticles attached on CNTs, depending on the specific application (**Figure 6.6**).

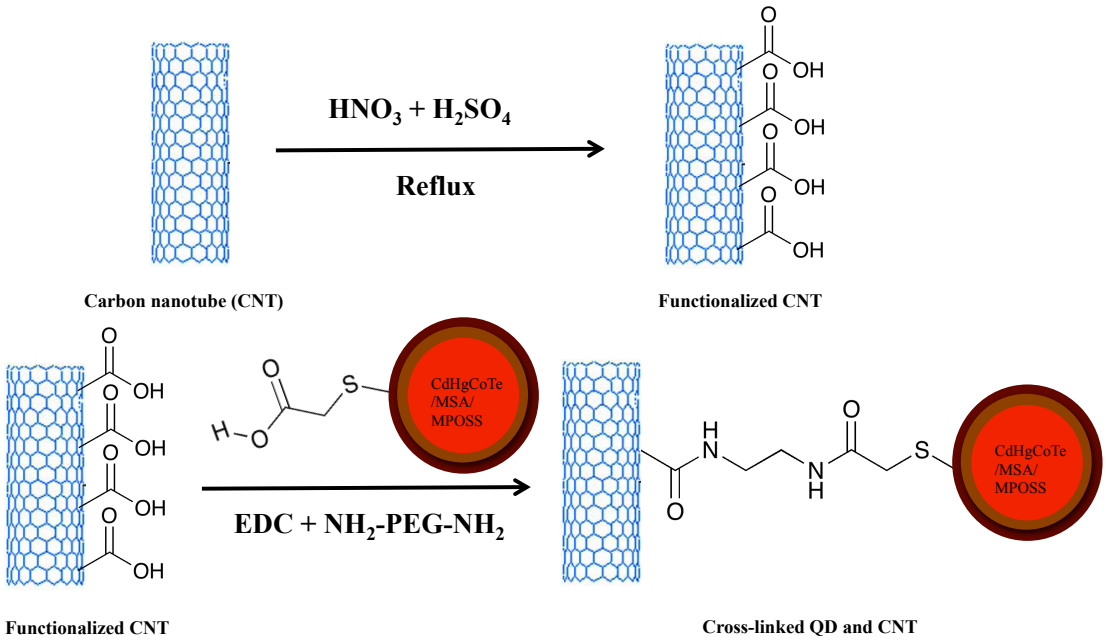

Figure 6.6: Schematic representation of QD-CNT conjugation.
This shows the reaction mechanism of conjugation of the NIR CdHgCoTe/MSA/MPOSS to carbon nanotube (CNT) via a linker NH2-PEG-NH2

Immobilization of biomolecules on CdHgCoTe/MSA/MPOSS QD and CNT is an area of great interest. Such hybrid materials have numerous applications in the areas of biotechnology, immunosensing, and biomedical applications.

All these modifications not only allow the nanomaterials to be water-soluble or water dispersible but also allow the presence of the functional group such as –COOH to be linked to other biomolecules or nanomaterials. The coupling agent of choice 1-Ethyl-3-(3-dimehylaminopropyl)carbodiimid hydrochloride (EDC) commonly known as water soluble carbodiimide is a versatile coupling agent that can form an amide, ester or thioester bond and thus to cross-link proteins, nuclei acids or to bind molecules to solid surfaces in aqueous or organic media.

6.3.4.1. Mechanism of reaction of the functional group (COOH) with coupling agent (EDC)

The carboxyl group on the QD and CNTs surfaces when activated proceeds similarly to other carbodiimide couplings. An o-acylurea intermediate is formed by the reaction of a carboxylic acid and the carbodiimide. The o-acylurea is a highly reactive species that readily reacts with primary amines, peptide coupling additives or reducing agents. For

the coated water-soluble QDs with MSA/MPOSS-capped water soluble in this study, the change in CdHgCoTe/MSA/MPOSS QD size was ~ 5 nm (refer to chapter 4). Fluorescence-labeled biomolecules are applied widely in the life science arena. Proteins, DNA and synthetic peptides are all involved in biochemical processes and therefore for their mapping, conjugation with water-soluble QDs or CNTs is used extensively. In this study, tagging was focused on the rabbit Anti-CRT immunoglobulin as they possess lysine residues on their constant region, which facilitates coupling of carboxyl groups to the amino residues of the lysines. After coupling, the specificity can be tested with the CRT peptide.

Equally using the above method, coupling of the QDs to CNTs was carried out by crosslinking with O,O'-Bis(2-aminopropyl)-polyethylene glycol 1900 (Fluka) (diaminoPEG). Examples of few coupling reagents were used for conjugating the QDs with other biological compounds (**Figure 6.7**).

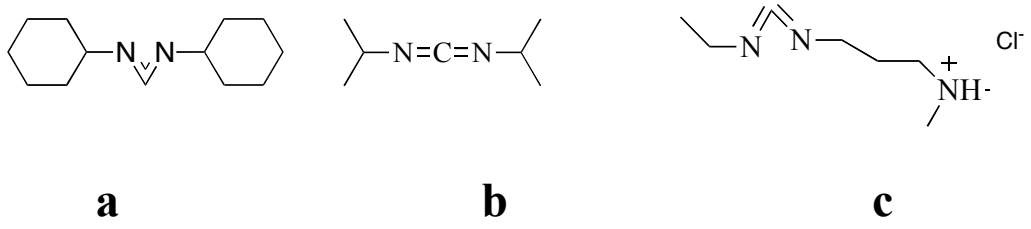

Figure 6.7: list of some of the coupling agents
a) DCC: efficient low racemization when used with HOBt forms insoluble byproduct b) DIC: efficient low racemization when used with HOBt. Most efficient at elevated temperatures. c) EDC: byproducts are water-soluble when used to conjugate proteins with linkers and labels.

In Solid-phase mode an efficient and unambiguous peptide bond formation requires chemical activation of the carboxyl component of the protected amino acid. The classical component of the protected amino acid *in situ* has been DCCI. Reactions were carried out at room temperature but the principle limitation is the formation of the insoluble DCU during the activation and acylation reaction. Recently, new reagents for *in situ* activation have become widely accepted because of ease, fast reaction even between amino acids and side reactions. This is also adaptable for conjugation in solution between QDs and antibodies or with cross-linkers such as PEG. A mechanism for conjugation scheme is shown in figure **6.8**.

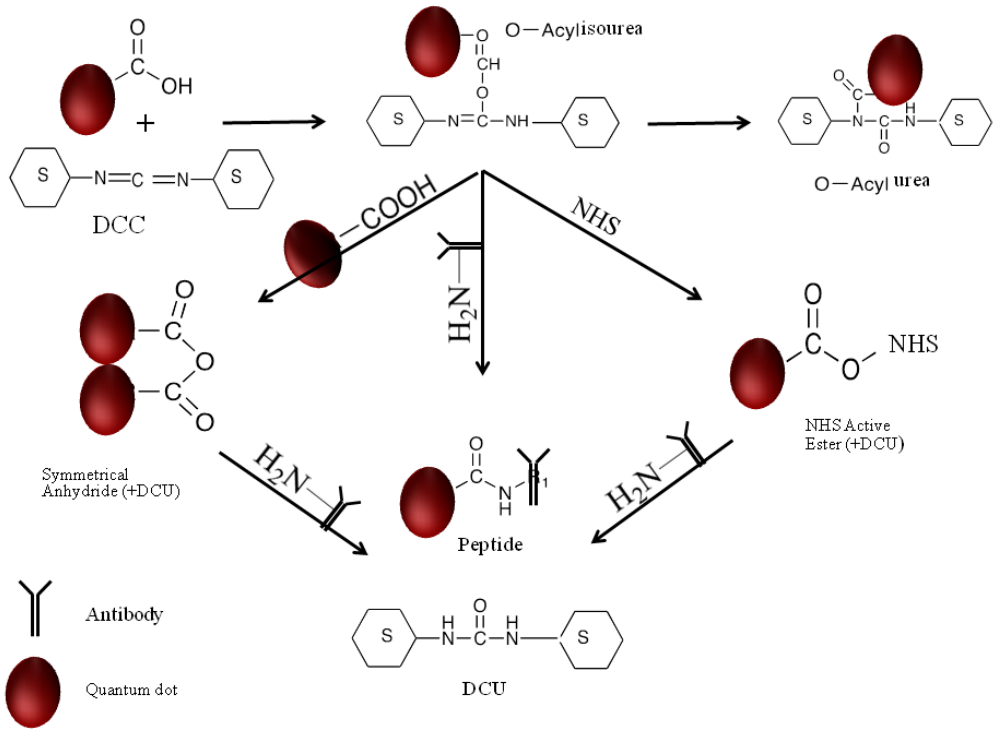

Figure 6.8: Mechanisms of conjugation using carbodiimide derivitives

6.3.5. Characterization of conjugated quantum dots and carbon nanotube (QD-CNT)

6.3.5.1. Emission characteristic of conjugated QD-CNT

Figure **6.9** compares the fluorescence spectra of uncoupled, NIR CdHgCoTe/MSA/MPOSS QD and coupled CNT-QD. As can be seen in this figure, the maximum emission of the uncoupled QD (solid line) is at NIR 800 nm. For CNT-conjugated QD, the maximum emission has shifted to 750 nm (dots), with a broad shoulder around 650 nm. This shifting is likely attributable to the background emissions from the CNT or aggregates forming to cross-linking in solution. However, an understanding of the detailed biophysics of these interactions will require further investigation.

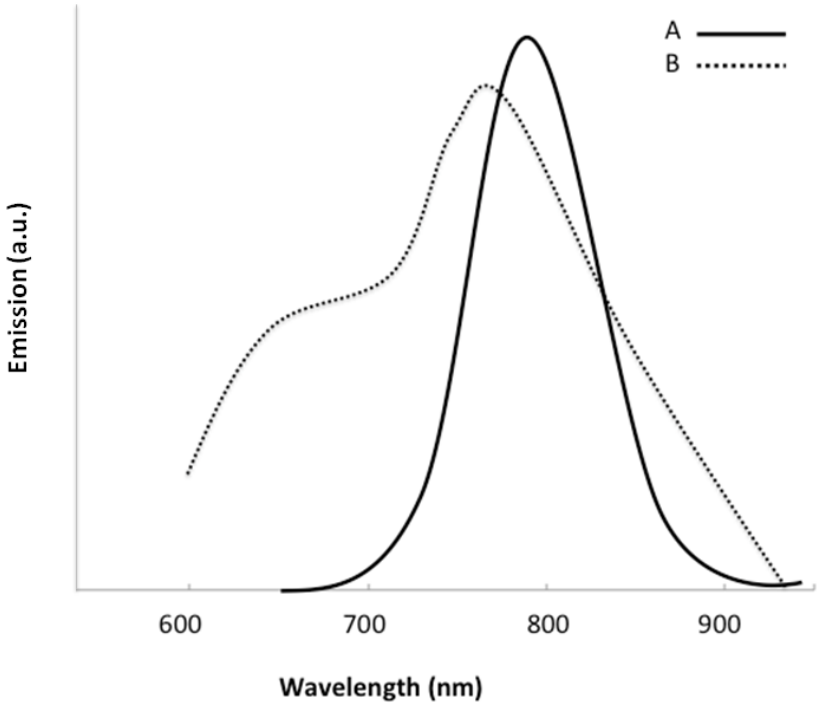

Figure 6.9: The fluorescent emission spectra of the uncoupled, NIR CdHgCoTe/MSA/MPOSS QD (A) and CNT-QD (B).
The maximum peak at 800 nm is consistent with specifications of this commercial QD. The blue shift from CNT-QD and a broad shoulder around 650 nm may result from the interactions and/or background emissions of CNT.

6.3.5.2. Transmission electron microscopy (TEM) of QD-CNT

The TEM images of CNT and CNT-QD are shown in figure **6.10**. The QD exhibits dark dots with an average particle size of 5–7 nm, randomly distributed on the surface of the CNTs (**Figure 6.10 b**). This suggests that coupling of CdHgCoTe/MSA/MPOSS QDs to CNT was successful. Many particle-like features can be observed on the sidewalls of the CNT bundles.

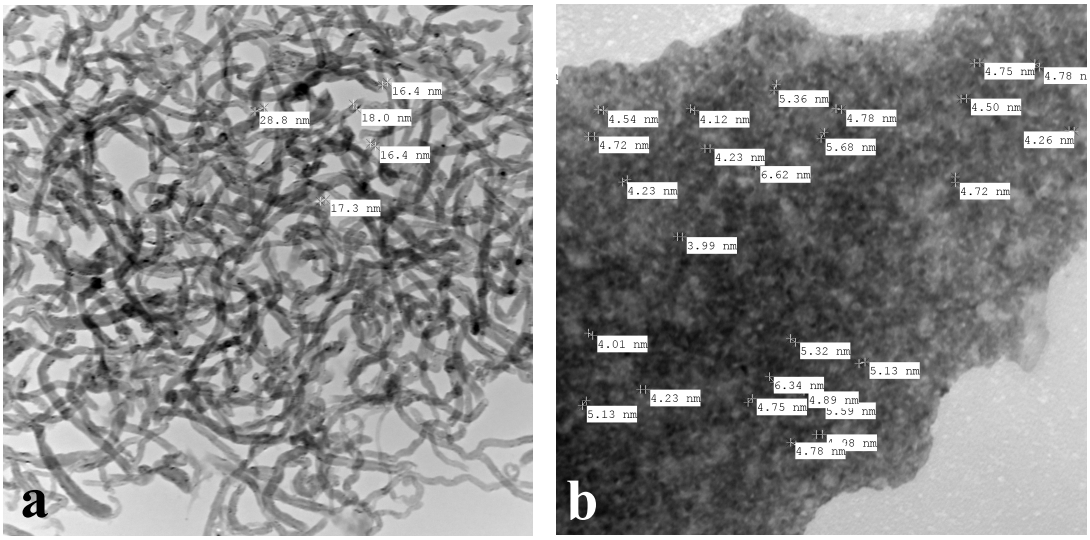

Figure 6.10: TEM images of CNT and QD-CNT. a) Uncoupled CNT and b) Coupled CNT with CdHgCoTe/MSA/MPOSS QDs with average size of 5 to 7 nm.

6.3.6. Conjugated QD-CNT photothermal induced immunogenic apoptosis

The aim of this experiment was to show that when QD-CNT is incubated with cell cultures and exposed to red light (630 nm) for 10 minutes, cell death (apoptosis) due to hyperthermia is initiated. Briefly, the set up consisted of incubating cultures in the presence of QD-CNT and exposing to light at 630 nm as illustrated in figure **6.11**. Figure **6.11 A** and **6.11 B** shows HUVEC cells when in the presence QD-CNT and stimulated by light with QD emitting at NIR (800 nm) and absorbed by CNT. There is absence of fluorescence when probed with QD-CRT antibodies. This is an indication that although cell death was initiated there is no evidence of CRT on cell surface of HUVEC primary cells. However, in figures **6.11 C** and **6.11 D** are the images of MCF-7 cancer cells when given the same treatment as described above. This time there was presence of CRT when probed by QD-CRT antibodies, a clear indication of cell undergoing apoptosis. Similarly, the above procedure was carried out for SW620 cancer cells, which also produced CRT when probed with QD-CRT antibodies. This phonemena appears to be specific for cancer cells only and not to normal cells. This indicates that hyperthermia induced by absorption of NIR emitted from QD to CNT with production of CRT on cancer cell surfaces. In principle this application can also be used for photodynamic treatment (PDT) by stimulating organic dyes for cancer cell

treatment. Figure **6.11 E** and **6.11 F** are the images of the SW620 cells when exposed to light in the presence of QD-CNT. The presence of CRT on all the cancer cells except normal cells is a clear indication that immunogenic apoptosis has occurred. Using QD-CNT as thermal inducers by NIR from QDs also produced CRT when excited by light Figure **6.11 (G, H, I, J)**. However, MCF-7 breast cancer cells exposed to CNT only (control) under illumination did not induce CRT protein (no fluorescence) with Anti-CRT indicating no cell death. (**Figure 6.11 G, H**). Similar results for SW620 exposed to CNT only were also obtained with no fluorescent indicated absence of apoptosis (**Figure 6.11 I, J**).

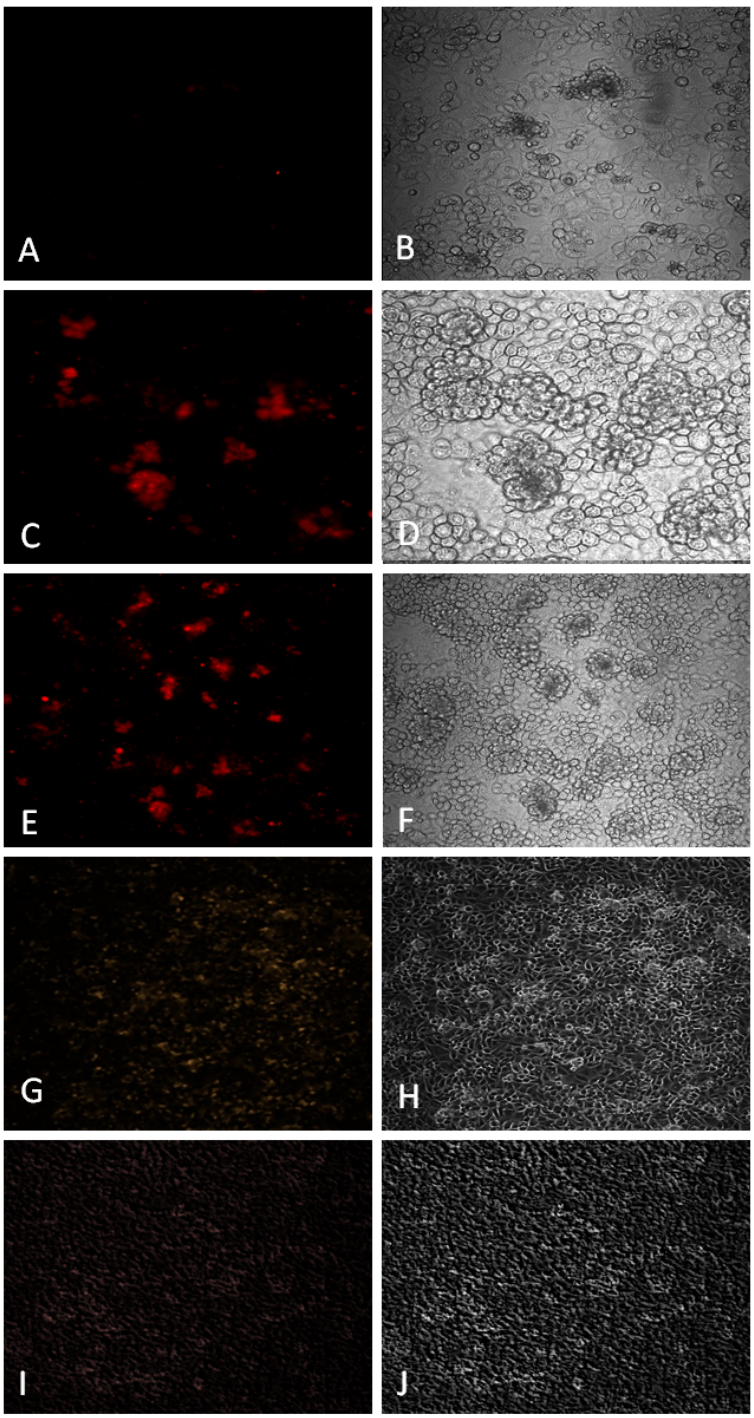

Figure 6.11: A, B) Fluorescent and DIC images of primary HUVECs exposed to conjugated QD-CNT. **C, D)** Fluorescent and DIC images of MCF-7 cells exposed to conjugated QD-CNT. **E, F)** Fluorescent and DIC images of SW620 cancer cells exposed to conjugated QD-CNT. **G, H)** Fluorescent and DIC images of MCF-7 breast cancer cells expose to CNT only. **I, J)** Fluorescent and DIC images of SW620 exposed to CNT only. Images of all cancer cells exposed to CNT only indicated absence of CRT proving cells have not undergone apoptosis as no QDs was present.

6.3.7. Biodistribution assessment of conjugated QD-CNT with confocal laser scanning microscopy (CLSM)

QDs and other nanomaterials offer great promise for biomedical applications in such areas as tumour research. However, for clinical applications the potential usefulness of such materials cannot be evaluated without knowledge of their biodistribution. NIR QDs was conjugated to CNT so as to trace their biodistribution in *in vivo* and *ex vivo* by emitted NIR light. Figure **6.12** is schematic representation of *in vivo* noninvasive detection of injected NIR QD-CNT

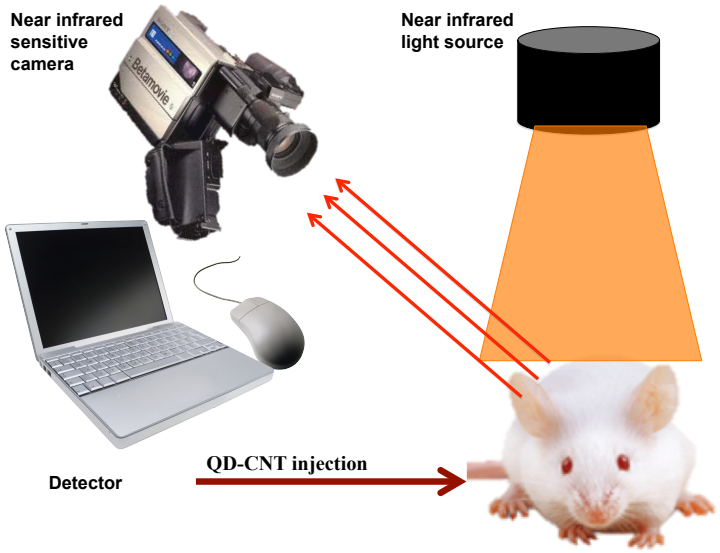

Figure 6.12: Schematic representation of a set up for detecting conjugated QD-CNT in a mouse. NIR sensitive camera with suitable filters can be used for detection.

A qualitative biodistribution was determined in mice, a relevant animal model. At 4 h after IP administration of QD-CNT (100 µg/ml) 600 µl, (mice n = 3 and control = 3) were sacrificed by CO_2. Figure **6.13 A** shows unconjugated CNT and QD conjugated CNT. This shows absence of fluorescence with the unconjugated CNT (control) compared to the QD-CNT. Figure **6.13 (B-D)** shows injected PBS/unconjugated CNT (CNT in PBS) and conjugated QD-CNT localized in liver and spleen.

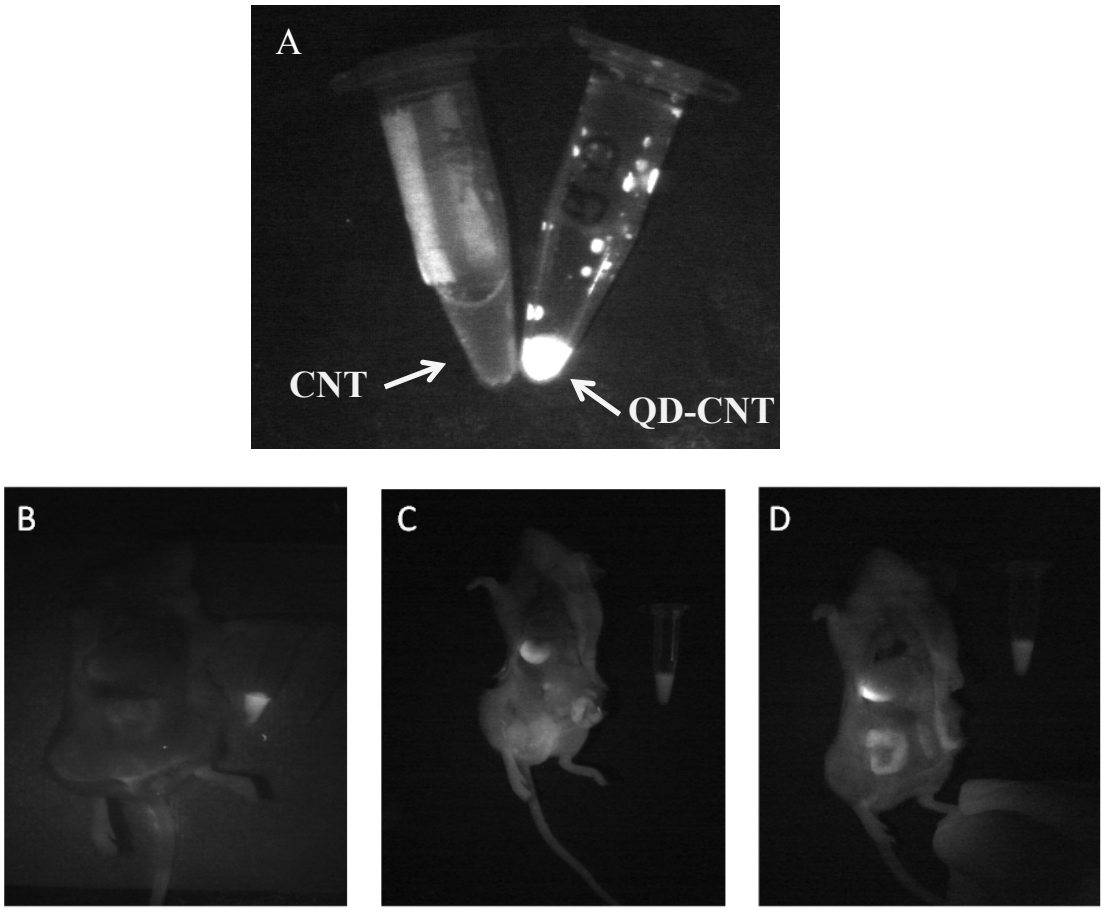

Figure 6.13: Images of mice injected with unconjugated CNT and conjugated QD-CNT in PBS. (A) CNT in PBS and conjugated QD-CNT in eppendorf (B) Mouse injected with unconjugated CNT, (C) Mouse injected with conjugated QD-CNT with liver accumulation of QD-CNT, (D) Mouse injected with QD-CNT with spleen showing NIR fluorescent.

To locate QD-CNT uptake in various organs, mice were sacrificed and brain, liver, spleen and lung were obtained from the dissected animal, and 20 μm-thick frozen sections prepared for *ex vivo* imaging. Fluorescence images of QD-CNT in various organs are shown below (**Figure 6.14-6.17**). The intensity and peak emission wavelength of QD-CNT in the tissues were the same as those in buffer. The strong NIR emissions under 630 nm support the conclusion that QD-CNT may provide significant advantages for deep tissue diagnosis. In each tissue, it can be demonstrated an intense fluorescence of QD-CNT at 800 nm excited at 630 nm compared to background. In the liver, the complex was observed in the central vein, parenchyma and hepatocytes (**Figure 6.15**). In the spleen, the QD-CNT was observed in both the red and white pulp (**Figure 6.14)**. The peak emission wavelength of QD-CNT was around 800 nm *in vitro* when excited by 630 nm from LTD light array. In the QD-CNT treated mice, the

highest emission of the complex was observed in the liver (**Figure 6.15**), as liver is the first organ to encounter any non-toxic/toxic material via the blood. However, other tissues have also shown the presence of the QD-CNT. Interestingly, a significant amount of QD-CNT was detected in the brain (**Figure 6.17**), which indicates permeation of QD-CNT through the blood brain barrier (BBB). It must be emphasized that the tested QD-CNT conjugate did not contain specific cell or organ targeting moieties. Therefore the observed biodistribution pattern following i.p. administration reflects non-specific binding and elimination for that time span. It is anticipated, however, that conjugating with specific targeting ligands such as peptides or antibodies will alter the biodistribution pattern.

In this study, it was investigated how QD-CNT is delivered into various organs of mice *in vivo* when administered intraperitoneally. Liver and spleen, the primary locations of the reticulum endothelial system (RES) are also the primary organs of QD uptake, as shown by the fluorescence. Detection of QDs coupled to CNT allowed their tracking with the possibility of drug delivery. This study was undertaken to show that it is possible to detect CNT, which is a good candidate for drug delivery with NIR CdHgCoTe/MSA/MPOSS QD as a tracker for biodistribution.

It can be concluded that the QD-CNT complex, with the highest signal was observed in the liver, followed by spleen, lungs and brain. Interestingly, signal were also detected in the brain (**Figure 6.17**), which can only mean that it has crossed the BBB. As it was not targeted the spectral profiles indicates there is a good distribution of the QD-CNT. This study did conduct a detail study of the constituent material (Cd^{2+} ion) distribution within the organs. This would have necessitated the use of a technique called inductively coupled plasma mass spectrometry (**ICP-MS**). This study investigated the distribution of QD-CNT following IP injection into mice as model system for determining the tissue localization of QD-CNT, employing confocal microscopy. It can be demonstrated that this delivery mode must have entered the systemic circulation and into the brain at 4 h after injection. This is a first evidence of QD-CNT nanocomposite entering the brain after IP injection. More studies as to the quantitation of QD-CNT and its constituent and elimination in *in vivo* need further investigation for future studies.

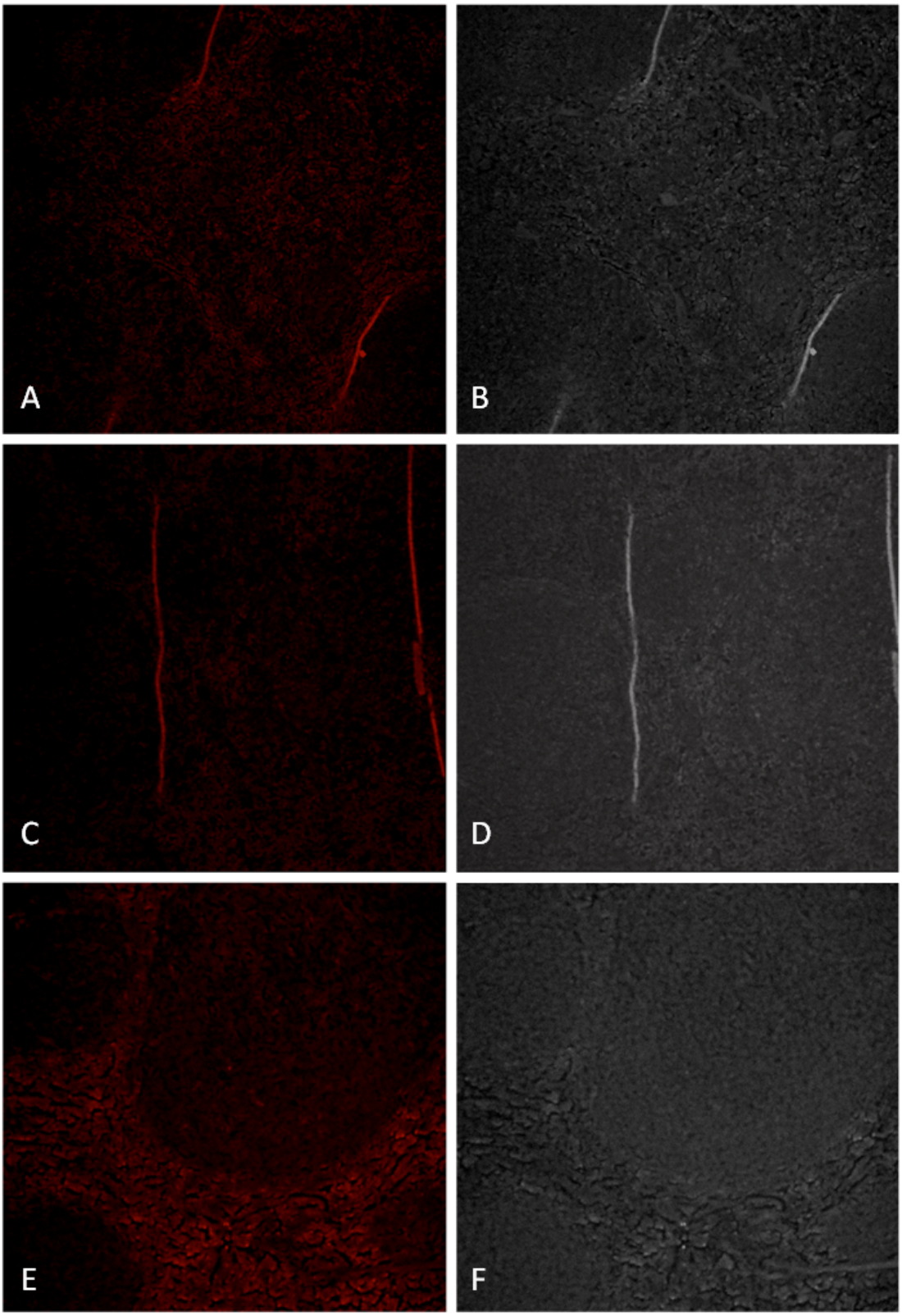

Figure 6.14: Confocal images of spleen exposed to NIR conjugated QD-CNT for 4 h incubation when administrated via IP.
A, C and D represent the different fluorescent images of spleen when exposed to conjugated NIR QD-CNT for 4 h as they show even distribution in the spleen tissues. B, D and F are the DIC images.

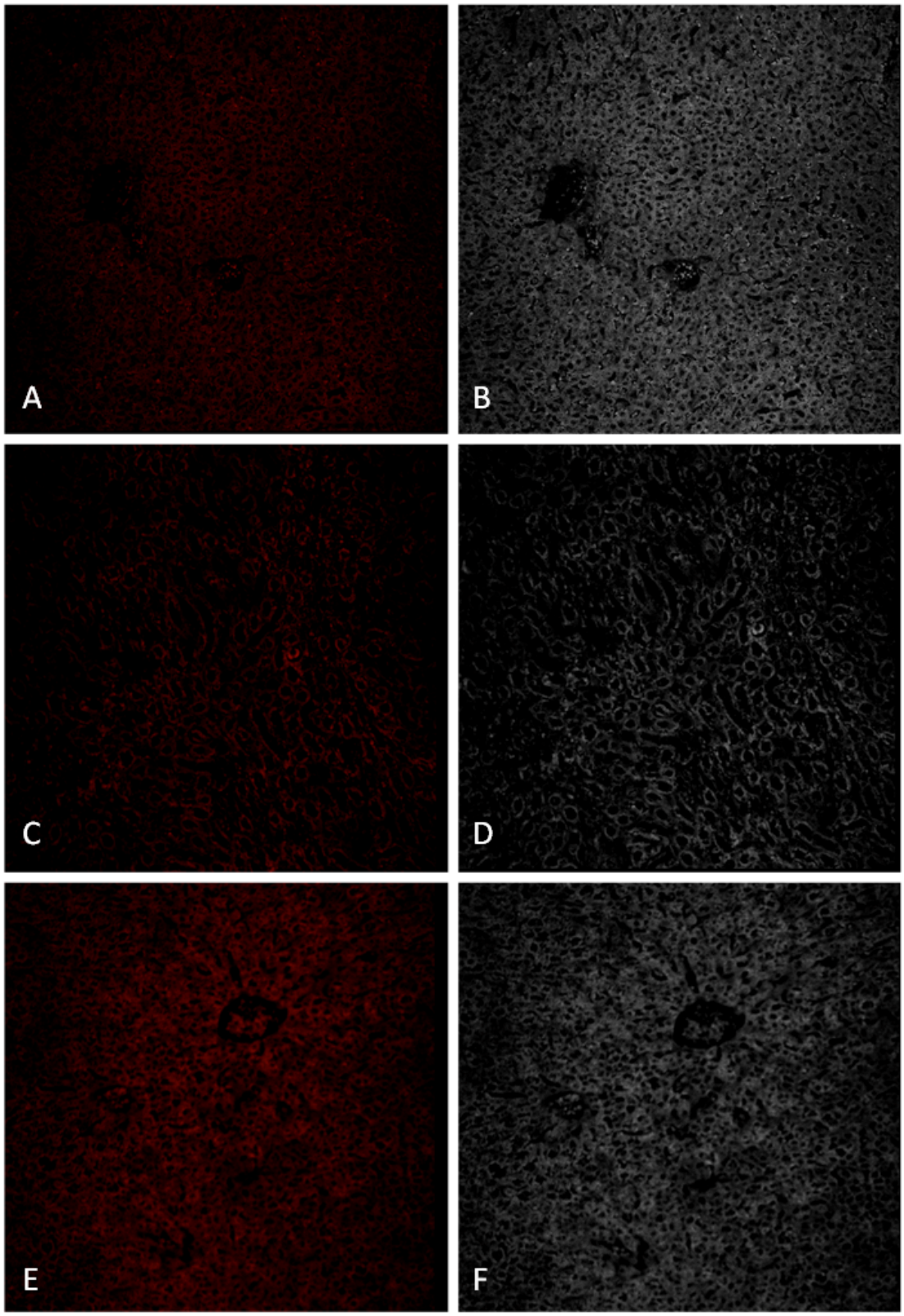

Figure 6.15: Confocal images of liver exposed to NIR conjugated QD-CNT for 4 h incubation when administrated via IP.
A, C and D represent the different fluorescent images of liver when exposed to conjugated QD-CNT for 4 h as they show strong fluorescent with even distribution in the liver tissues. B, D and F are the DIC images.

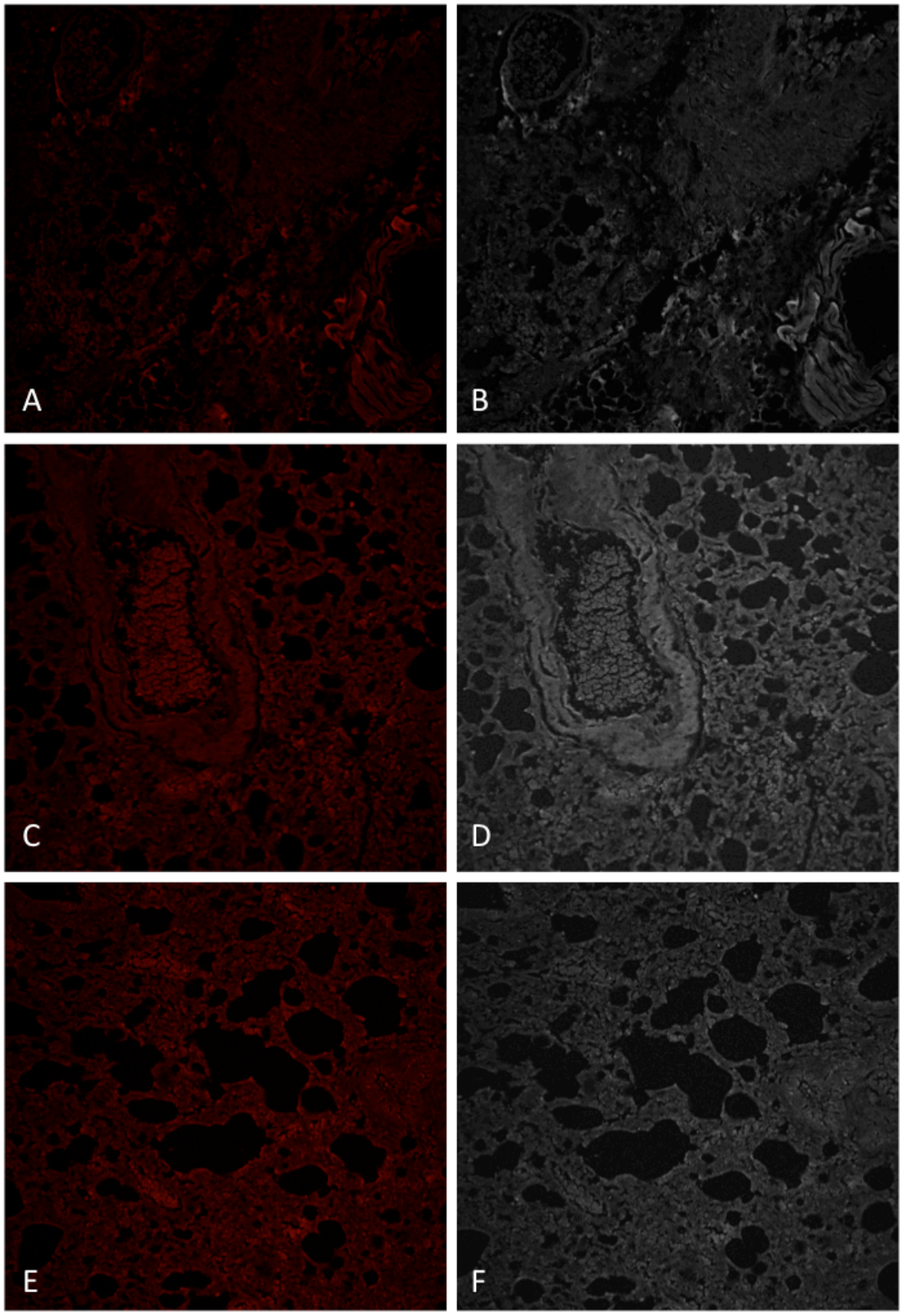

Figure 6.16: Confocal images of lung exposed to NIR conjugated QD-CNT for 4 h incubation when administrated via IP.
A, C and D represent the different fluorescent images of lung when exposed to conjugated QD-CNT for 4 h as they show even distribution in the lung tissues. B, D and F are the DIC images.

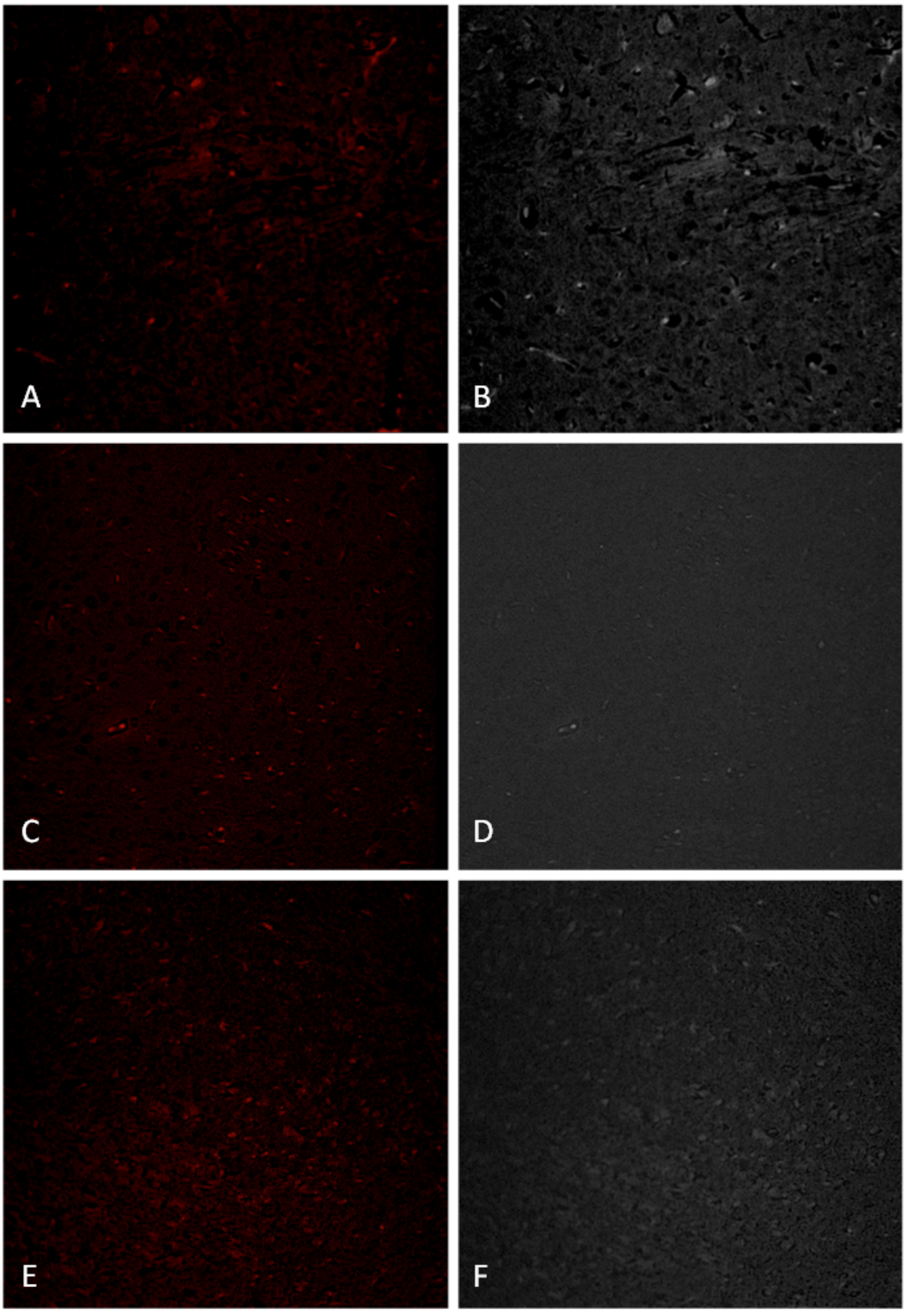

Figure 6.17: Confocal images of brain exposed to NIR conjugated QD-CNT for 4 h incubation when administrated via IP.
A, C and D represent the different fluorescent images of brain when exposed to conjugated QD-CNT for 4 h as they show even distribution in the brain tissue. B, D and F are the DIC images. However, the level of distribution is relatively less compared to other tissues.

6.4. Overall discussion

The possibility of conjugating QDs to biomolecules was first undertaken in 1998 and has since been applied as fluorescent probes for targeting and visualizing subcelluar and cellular membrane signal transducing molecules in cell study. There are many conjugation procedures for linking biomolecules to QDs depending on the surface linkers (Alivisatos et al., 2005, Alivisatos, 2004). Covalent linking of CdHgCoTe/MSA/MPOSS coated QDs using cross-linking agents N-hydroxysulfosuccinimide (NHS) and 1-ethyl-3(3-dimethylaminopropyl) carbodiimide hydrochloride (EDC) have been used with bovine serum albumin (BSA), as was stated earlier.

The present study describes the development and use of QDs Bioconjugated to specific antibodies and explored whether these bioconjugates could specifically and effectively target cancer cells undergoing immunogenic apoptosis. The bioconjuagte was designed and developed for noninvasive examination of NIR QD. The rationale for this study was to conjugate in aqueous buffer to produce Anti-CRT for detection of cancer cell apoptosis on exposure to Doxorubicin or Cd^{+2} ions in cell culture. Additionally, by conjugating NIR QD with CNT it could be tract as a drug delivery vehicle. It was also discovered that NIR emission by QDs was absorbed by CNT with thermal production in the vicinity or cancer cells. CNT stimulation directly by NIR to produce hyperthermia has been shown by other groups to be feasible in cancer treatments. This study has shown that NIR QDs conjugated to CNT can be localized with detection and treatment. CRT detection has implications in early detection of necrotic apoptosis in cancer cells when exposed to various anticancer compounds such as anthracyclin as an effective treatment in the prognosis of cancer. This is important as immunological participation may play an important part in cancer management.

6.4.1. Application of NIR quantum dots in noninvasive imaging of lymph nodes

The current tracers for sentinel lymph node biopsy (SLNB) including the blue dye and radiocolloid have various limitations like anaphylactic reaction to the dye and exposure of radioactivity to both patients and clinicians. QDs have potential application as a tool for imaging SLNs and guiding surgery. It was initially demonstrated, the visualization

of SLNs in an animal model via optical imaging of fluorescence emitted by QDs was feasible. This study represents a potential medical application of nanocrystals, a step forward in clinical application of SLNB in cancer surgery. SLNs are the foremost or group of nodes to be infiltrated by metastasizing cancer cells from a primary tumor. The advantage of QDs over blue dye is that SLN containing QDs, particularly NIR QDs can be visualized through the depth of tissue, even before the incision is made. Previous studies has been established that QDs injected into tumors drain to the SLNs rapidly (Ballou et al., 2007), which implicates that with tracking of QDs, it might facilitate the removal of the primary tumour and the SLN in a single surgery. For the future, the use of NIR QD imaging can make important contribution to the surgical management of cancer patients. It should have a major contribution in facilitating in SLNB of visceral cancers and SLMB in melanoma and breast cancer (**Figure 6.18**).

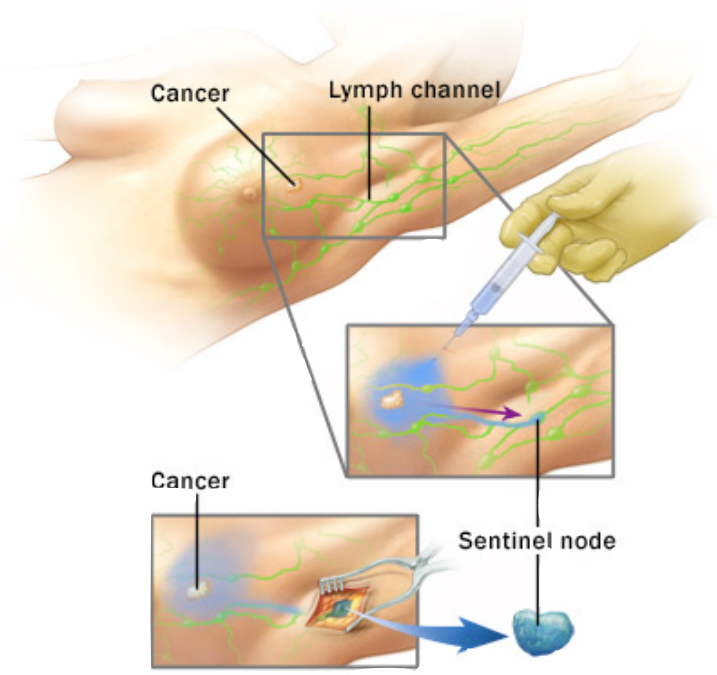

Figure 6.18: A schematic arrangement of QDs emitting in the NIR range have been developed as alternative probes for SLNB with set up for live NIR imaging system to track cancer in deep tissues.

Figure **6.19** shows similar strategy to figure **6.18** by using QDs to track the SLN. The CdHgCoTe/MSA/MPOSS QDs with emission wavelength of 800 nm were injected into the rat's paw to track the migration of lymphatic nodes, exposed to UV light after 10 minutes time frame.

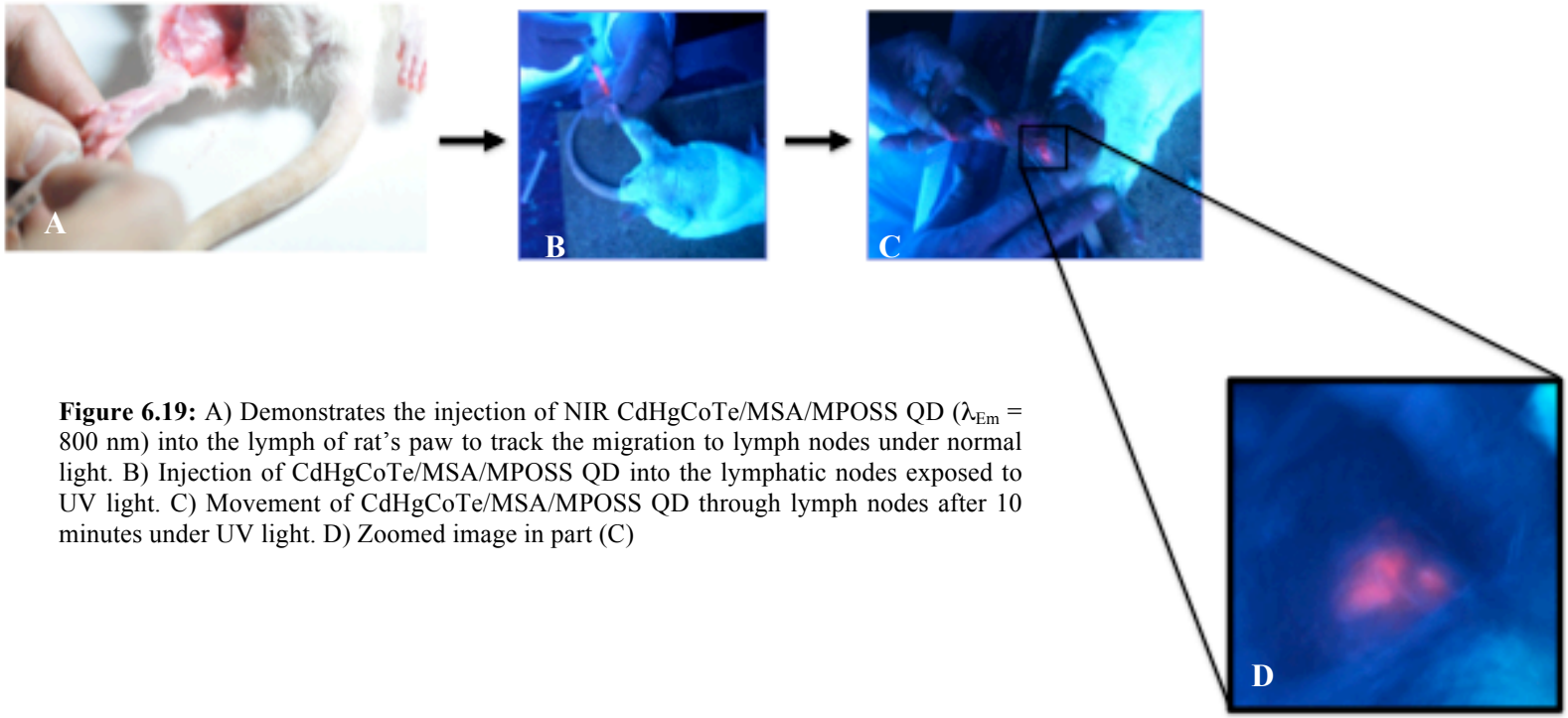

Figure 6.19: A) Demonstrates the injection of NIR CdHgCoTe/MSA/MPOSS QD (λ_{Em} = 800 nm) into the lymph of rat's paw to track the migration to lymph nodes under normal light. B) Injection of CdHgCoTe/MSA/MPOSS QD into the lymphatic nodes exposed to UV light. C) Movement of CdHgCoTe/MSA/MPOSS QD through lymph nodes after 10 minutes under UV light. D) Zoomed image in part (C)

6.4.2. Targeted NIR CdHgCoTe/MSA/MPOSS quantum dots to damaged liver in mice

NIR CdHgCoTe/MSA/MPOSS QDs were conjugated to a synthetic Lipid A antagonist using EDC and NHS. In this study mice were injected intraperitoneally with acetaminophen to induce liver damage with the expression of Toll Like Receptor 4 (TLR4). Mouse was anesthetized and 200 µl of conjugated NIR CdHgCoTe/MSA/MPOSS QD was injected via the mouse tail vain. This study was carried out in collaboration with the department of Hepathology, UCL, London (permitted, current study).

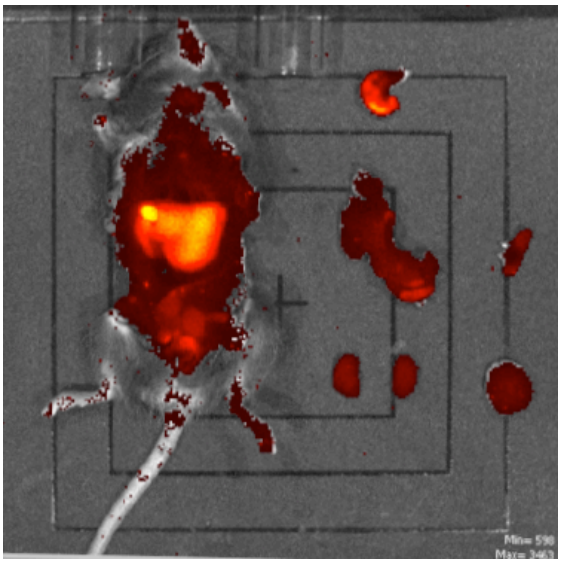

Figure 6.20: *In vivo* imaging of NIR QD-Lipid A antagonist at 4 h post-injection (pseudocoloured red). The NIR QD is localised in the damaged liver and detected by NIR emission.

Here, the NIR signal resulting from QD-Lipid A antagonist was clearly visible using the small animal IVIS system. NIR QD-Lipid A antagonist mainly targets the Toll-like receptor-4 in the liver expressed because of the damage. *Ex vivo* fluorescence of various organs indicated localization. However receptors were also detected in the spleen. This work is ongoing at the time of thesis submission.

6.4.3. Excretion and elimination of quantum dots

Finally, one theory is that as the particles are released from the lymph nodes and spleen, the Kupffer cells of the liver absorb them. The Kupffer cells then transport the QDs to the biliary system for their excretion. Some literature suggests that QD metabolism and

excretion is more complex and in fact depends heavily upon the chemistry of the QD in question. Further study of QD circulation and excretion *in vivo* will be the subject of intense investigation over the next several years.

6.4.4. Further study and investigation

Whether QDs have been found to accumulate in mouse organs such as spleen or liver after administration is something that needs to be investigated thouroghly. Little is known if and how QDs with a variety of sizes and surface chemistries will finally be cleared form biological body. However, there are some studies stating that if the hydrodynamic size of QDs was smaller than 5.5 nm, the particles were predominantly cleared from the mouse body through rapid and efficient urinary excretion; whereas QD nanocrystals coated with bigger molecules were associated with the adsorption of serum protein on surface, making them more than 15 nm bigger in hydrodynamic diameter, thereby precluding their renal excretion (Yu, 2008).

QDs are highly valuable to preclinical optical imaging. They can be used *in vitro* and *in vivo* for labeling and also to target tissue-specific cancer biomarkers to identify tumour cells in sentinel lymph nodes. In addition the QDs can be targeted as a fluorescent tags in cell biology. While ongoing toxicity and clearance studies remain to establish their clinical usefulness, current studies indicate potential applications of the QD (Smith et al., 2008b) as an image probe to study the binding and extravasation parameters of targeted nanoparticles in lymphatic node cancer.

6.5. Conclusion

Nanoparticles with contrast enhancing properties are necessary in the field of molecular imaging. QDs can be engineered with multiple components to form one single nanoparticle system which will allow the creation of nano-probes capable of several imaging techniques, namely multimodal imaging. Molecular imaging is dependent on early detection of various diseases and can be constructed to personalized therapy. While conventional imaging systems such as computer tomography (CT) and magnetic resonance imaging (MRI) facilitate visualization of anatomical and (patho)physiological outcome of the disease, molecular imaging is based on the molecular and cellular markers of the disease. This is dependent on disease-specific molecular targets as well as targeted nanoparticles. Furthermore, these nanocrystals should facilitate the visualization *in vivo* with high definition.

Recent research has led to nanoscaled, light-emitting QDs as a new class of fluorescent labels to be used in biology and medicine. These highly bright fluorescent and stable QD probes are well suited for detecting protein biomarkers on cells and clinical tissue application. This chapter has shown conjugation methods for different applications. One was, to detect the cancerous cells going under apoptosis and secondly non-targeted distribution, by fluorescence tracking with CNT. The work on conjugated QD-CNT has shown potential applications for cancer detection and localized photothermal therapy.

The main aim of this study was to demonstrate that QDs could be used for tracking as biological tools, with potential for biomedical applications. It can be demonstrated that cancer cells *in vitro*, when induced to undergo apoptosis will produce CRT and NIR CdHgCoTe/MSA/MPOSS QD conjugated with Anti-CRT will detect the protein.

This was successfully applied to cancer cells indicating a marker of early cell death. Confocal microscopy as tool can visualize this process with accuracy. This study has demonstrated that NIR QDs has the potential for targeted detection and therapy for markers in diseased organs. Despite the increasing number of publications on the potential use of semiconductor for imaging, cancer detection and therapy, there is still a lot of work to be done before this technique is clinically applicable due to safety concerns. With this current study and progress in the development, with significant

toxic reduction or semiconductor QDs, one can envisage the viable use in a clinical setting for the future.

Chapter 7
Summary, conclusions and future directions

7.1. Summary

The primary objectives of this thesis were to develop an environmentally safe and friendly synthesis method to design and develop water-soluble QDs with sustainable strong NIR emission, photostability and potentially for biomedical imaging applications. To specifically address these objectives, the studies undertaken were focused on achieving the following goals:

1. To establish a technique for aqueous synthesis using the multifunctional CdHgCoTe as a model system.
2. To develop the water-soluble CdHgCoTe QDs with novel hybrid surface chemistry to promote PL intensity, stability and biocompatibility.
3. To evaluate cytotoxicity test and establish the non-toxicity of the CdHgCoTe/MSA/MPOSS QDs and compare with toxicities of CdHgCoTe/MSA and toxic constituent parts Cd^{2+} and Hg^{2+} ions.
4. To develop and improve conjugation of the water soluble QDs with biomolecules and nanomaterials (CNT) for imaging and potential therapy of cancer cells.

7.1.1. Concluding remarks of current study

Chapter 4: Using CdHgCoTe/MSA/MPOSS as a model system, a practical simple one step and 'green' approach to synthesis method was developed to manufacture the QDs in aqueous buffer directly at a temperature at 100 °C under reflux. The QDs obtained exhibited an ultra small size of 5 nm diameters with spheroid structure. The QY obtained was around 90% highest ever achieved compared to any commercially produced cadmium-based QDs. Parameters such as different pH and coatings were studied to improve photoluminescence of the QDs. It was shown that this type of QDs synthesised at pH 7.0 produced strong PL intensity significantly. The soluble QDs displayed excellent photostability under UV irradiation for and in water or PBS buffer and also at +4 °C for 2 years. Introducing a novel hybrid coating MSA/MPOSS not only facilitated the dispersal of the QDs in aqueous environment, but also as a functional linker for conjugation to biomolecules or to nanomaterials via covalent bonding. The convenience of modification and the excellent PL properties in aqueous buffer and ease of manufacture paves the way for an economical approach for bulk

production of aqueous QDs, attractive for fluorescent probes for noninvasive, long-term imaging and tracking in biomedical systems.

Chapter 5: Using two cytotoxicity assays namely Alamar Blue and Neutral Red were carried out for the CdHgCoTe/MSA/MPOSS QDs on different human cancer cells (MCF-7, SW620, PC3) and human endothelial cells (HUVECs). The results showed that CdHgCoTe QDs with the hybrid coating MSA/MPOSS were non-toxic at 1 µg/mL and 100 µg/mL at 24 h. This was compared with the uncoated, CdHgCoTe/MSA QDs and the free metals Cd^{2+} and Hg^{2+}. It can be concluded that the cytotoxicity of the uncoated and MSA coated QDs and the extremely low toxicity of the CdHgCoTe/MSA/MPOSS were mainly due to the presence of suitable coatings preventing the release of toxic Cd^{2+} and Hg^{2+} respectively. The absence of significant toxicity of the hybrid coatings for QDs may pave the way in reducing the potential hazards to the environment and to human health and attractive for clinical *in vivo* applications.

Chapter 6: The developed novel surface chemistry of QDs was exploited for conjugation to ligands and biomaterials. The MSA/MPOSS coated QDs, the peptide bond can be created between the carboxyl group of MSA/MPOSS and the amino groups of biomolecules (antibodies) or via linkers to CNT using the coupling reagents EDC and NHS. As an example, the antibodies against the calcium binding protein (calreticulin) were successfully imaged with antibody conjugated QDs when applied to cancer cells undergoing immunogenic apoptosis. This was done by exposing cells to Doxorubicin and also to conjugated QD-CNT for photoinduction. For CNT with carboxyl groups a diamino linker (polyethylene glycol-PEG) can be used as a cross-linker to form covalent bond between the QDs carboxyl groups. The conjugated QD-CNT was used to track biodistribution *in vivo* and also for its hyperthermic induction in cancer cells thus inducing apoptosis.

In conclusion, a unique simple, cheap, environmentally friendly, aqueous synthesis method was developed to manufacture stable QDs in water directly by refluxing at 100 °C. Despite using toxic semiconductor materials Cd^{2+} and Hg^{2+} as starting materials, it can be shown for the first time that it can be detoxified by a novel hybrid coating which includes MSA and MPOSS, thus preserving its small size (5 nm), biocompatibility, excellent strong photoluminescence and biostability. The present developed QDs with

this kind of hybrid coatings have great potential for a noninvasive multimodal imaging applications due to its well-engineered coating material.

7.2. Future studies

Semiconductor based QDs with their intrinsic novel physico-chemical characteristics is a unique candidate for potential applications in nanomedicine. With its potential beneficial multifunctional role, there is great concern as to their exposure to humans and the repercussions to human health. Numerous studies and research have been conducted in order to understand the mechanism of interaction in a number of *in vitro* and *in vivo* systems, and a vast information base has been established regarding this interaction and its potential biological effects. The current approved nanoparticle systems have in certain cases improved the therapeutic index of drugs by enhancing drug efficacy by reducing drug toxicity. The term "theranostics" was coined defining current developments in specific, individualized therapies for a multitude of diseases, and to integrate diagnostic and therapeutic properties into a single entity. The need arose from the evidence that diseases such as cancers are heterogeneous, and all current treatments are effective for certain patient subpopulations and at certain stages of disease progression. The arrival of nanotechnology has offered the possibility to merge diagnosis and therapy closer. Nanoparticles in the arena of imaging and therapy have been explored separately and well documented that nanoparticle theranostics is almost a reality, whereby co-delivery of therapy and imaging is a possibility. It is fortunate that many nanomaterials are imaging agents and can be developed as theranostic agents by impacting with therapeutic functions on them. The main criterion for such combination of imaging and therapy is getting the optimum concentration at targeted area of the diseased organ. This common targeting criterion will bring the synergy effect with enhancement for both imaging and therapy.

Localization strategies are immense and to tailor targets, require appropriate surface chemistries. In cancer studies, it is a common approach to identify a biomarker that is specifically expressed on the membrane surface of cancer cells, and load the ligands with drugs to the target. In all these strategies, the unique size scale of the particles permits the EPR effect in tumour targeting. In all these applications, strategies have been applied to modify surfaces with appropriate coatings to achieve biocompatibility and long half live in bioapplications. Currently, many types of nanoplatforms are

undergoing intensive exploration for theranostic applications. All of these nanoplatforms have undergone development with easy synthesis with functional properties. These nanoparticles with reduced toxicity can incorporate unique optical or magnetic properties and have proved feasible with many successes. These have established an infra structure for further development, as apart from imaging it can also function as drug cargoes with suitable therapeutics. It has been demonstrated that therapeutics of multiform, including small molecules, proteins and DNA based can be conjugated onto nanoparticles as nanoplatforms. Due to its construct and with large surface to volume ratios, allows multi-functionality, which permits the evolution of all-in-one nano-system with desirable features.

Despite the rapid progress in this field, there is not an approved system for clinical use. Each system has its promises and advantages, however, has certain disadvantages to circumvent. The major concern is toxicity for QDs, and non-biodegradadable nature of CNTs. Alternatives are currently being explored and we have to date developed gold NIR QDs, which have shown to be promising in terms of application for theranostics. This is still in the experimental stages, since cadmium based QD work was undertaken for this thesis. QDs as drug carriers and with specific synthetic peptides as probes or antigens can be delivered to specific targets. As more suitable biomarkers are currently being discovered for diseased tissues, suitable ligands to these targets designed and synthesized with high efficiency. While this route is being explored and improved, it has been shown in this work that nanoparticle induced hyperthermia polarized within a selected region is possible and is being addressed in this laboratory with NIR gold QDs.

Finally in addition to achieving and evaluating the toxicity issues in multifunctional QDs, integrating imaging and therapy will be a great leap in combination therapy defined as “theranostics”. In concept and practicality, nanoparticle-based theranostic probes can deliver therapeutics to selected disease areas with imaging function for diagnosis while monitoring therapeutic response, in a multi-role tool. In this thesis, the works on QDs with its intrinsic positive qualities and ongoing development have shown the feasibility for potential clinical applications.

References

AKHTAR, R. S., LATHAM, C. B., SINISCALCO, D., FUCCIO, C. & ROTH, K. A. 2007. Immunohistochemical detection with quantum dots. *Methods Mol Biol,* 374**,** 11-28.

ALIVISATOS, A. P. 1996. Semiconductor Clusters, Nanocrystals, and Quantum Dots. *Science,* 271**,** 933-937.

ALIVISATOS, A. P. 2008. Birth of a nanoscience building block. *ACS Nano,* 2**,** 1514-6.

ALIVISATOS, A. P., GU, W. & LARABELL, C. 2005. Quantum dots as cellular probes. *Annu Rev Biomed Eng,* 7**,** 55-76.

ALIVISATOS, P. 2004. The Use of Nanocrystals in Biological Detection. *Nature Biotechnology,* 22**,** 47-52.

ALTINOGLU, E. I., RUSSIN, T. J., KAISER, J. M., BARTH, B. M., EKLUND, P. C., KESTER, M. & ADAIR, J. H. 2008. Near-infrared emitting fluorophore-doped calcium phosphate nanoparticles for in vivo imaging of human breast cancer. *ACS Nano,* 2**,** 2075-84.

APPENZELLER, T. 1991. The man who dared to think small. *Science,* 254**,** 1300.

ARYA, H., KAUL, Z., WADHWA, R., TAIRA, K., HIRANO, T. & KAUL, S. C. 2005. Quantum dots in bio-imaging: Revolution by the small. *Biochem Biophys Res Commun,* 329**,** 1173-7.

ASWATHY, R. G., YOSHIDA, Y., MAEKAWA, T. & KUMAR, D. S. 2010. Near-infrared quantum dots for deep tissue imaging. *Anal Bioanal Chem,* 397**,** 1417-35.

AUSTIN M. DERFUS, W. C. W. C., AND SANGEETA N. BHATIA 2004. Probing the Cytotoxicity of Semiconductor Quantum Dots. *Nano Lett,* 4**,** 11-18.

AUSTIN M. DERFUS, W. C. W. C., SANGEETA N. BHATIA 2003. Probing the Cytotoxicity of Semiconductor Quantum Dots. *NANO LETTER* 4**,** 11-18.

BAKALOVA, R., ZHELEV, Z., JOSE, R., NAGASE, T., OHBA, H., ISHIKAWA, M. & BABA, Y. 2005. Role of free cadmium and selenium ions in the potential mechanism for the enhancement of photoluminescence of CdSe quantum dots under ultraviolet irradiation. *J Nanosci Nanotechnol,* 5**,** 887-94.

BALLOU, B., ERNST, L. A., ANDREKO, S., HARPER, T., FITZPATRICK, J. A., WAGGONER, A. S. & BRUCHEZ, M. P. 2007. Sentinel lymph node imaging using quantum dots in mouse tumor models. *Bioconjug Chem,* 18**,** 389-96.

BALLOU, B., LAGERHOLM, B. C., ERNST, L. A., BRUCHEZ, M. P. & WAGGONER, A. S. 2004. Noninvasive imaging of quantum dots in mice. *Bioconjug Chem,* 15**,** 79-86.

BENOIT DUBERTRET, P. S., DAVID J. NORRIS, VINCENT NOIREAUX, ALI H. BRIVANLOU, ALBERT LIBCHABER 2002. In Vivo Imaging of Quantum Dots Encapsulated in Phospholipid Micelles. *sciencemeg,* 298.

BENTOLILA, L. A., MICHALET, X., PINAUD, F. F., TSAY, J. M., DOOSE, S., LI, J. J., SUNDARESAN, G., WU, A. M., GAMBHIR, S. S. & WEISS, S. 2005. Quantum dots for molecular imaging and cancer medicine. *Discov Med,* 5**,** 213-8.

BHARALI, D. J., KLEJBOR, I., STACHOWIAK, E. K., DUTTA, P., ROY, I., KAUR, N., BERGEY, E. J., PRASAD, P. N. & STACHOWIAK, M. K. 2005. Organically modified silica nanoparticles: a nonviral vector for in vivo gene delivery and expression in the brain. *Proc Natl Acad Sci U S A,* 102**,** 11539-44.

BIFENG PAN, D. C., RONG HE, FENG GAO, YAFEI ZHANG 2006. Covalent attachment of quantum dot on carbon nanotubes. *Chemical Physics Letters,* 417**,** 419-424.

BRUCHEZ, M., JR., MORONNE, M., GIN, P., WEISS, S. & ALIVISATOS, A. P. 1998. Semiconductor nanocrystals as fluorescent biological labels. *Science,* 281**,** 2013-6.

C. B. MURRAY, D. J. N., M. G. BAWENDI 1993. Synthesis and characterization of nearly monodisperse CdE (E = sulfur, selenium, tellurium) semiconductor nanocrystallites. *J. Am. Chem. Soc,* 115**,** 8706–8715.

CHAKRAVARTHY, K. V., DAVIDSON, B. A., HELINSKI, J. D., DING, H., LAW, W. C., YONG, K. T., PRASAD, P. N. & KNIGHT, P. R. 2011. Doxorubicin-conjugated quantum dots to target alveolar macrophages and inflammation. *Nanomedicine,* 7**,** 88-96.

CHALOUPKA K, M. Y., SEIFALIAN AM 2010. Nanosilver as a new generation of nanoproduct in biomedical applications. . *Trends Biotechnol (In Press)*.

CHAN, W. C. & NIE, S. 1998. Quantum dot bioconjugates for ultrasensitive nonisotopic detection. *Science,* 281**,** 2016-8.

CHAN, W. H., SHIAO, N. H. & LU, P. Z. 2006. CdSe quantum dots induce apoptosis in human neuroblastoma cells via mitochondrial-dependent pathways and inhibition of survival signals. *Toxicol Lett,* 167**,** 191-200.

CHEN FQ, G., D. 2004. Fluorescent CdSe/ZnS nanocrystal-peptide conjugates for long-term, nontoxic imaging and unclear targeting in living cells. . *Nano Lett,* 4**,** 1827-1832.

CHEN, H., CUI, S., TU, Z., JI, J., ZHANG, J. & GU, Y. 2011. Characterization of CdHgTe/CdS QDs for near infrared fluorescence imaging of spinal column in a mouse model. *Photochem Photobiol,* 87**,** 72-81.

CHEN, Z., CHEN, H., MENG, H., XING, G., GAO, X., SUN, B., SHI, X., YUAN, H., ZHANG, C., LIU, R., ZHAO, F., ZHAO, Y. & FANG, X. 2008. Bio-distribution and metabolic paths of silica coated CdSeS quantum dots. *Toxicol Appl Pharmacol,* 230**,** 364-71.

CHO, S. J., MAYSINGER, D., JAIN, M., RODER, B., HACKBARTH, S. & WINNIK, F. M. 2007. Long-term exposure to CdTe quantum dots causes functional impairments in live cells. *Langmuir,* 23**,** 1974-80.

CHO SJ, M. D., JAIN M, RÖDER B, HACKBARTH S, WINNIK FM. 2007. Long-term exposure to CdTe quantum dots causes functional impairments in live cells. . *Langmuir,* 23**,** 1974-1980.

CHOI, H. S., LIU, W., MISRA, P., TANAKA, E., ZIMMER, J. P., ITTY IPE, B., BAWENDI, M. G. & FRANGIONI, J. V. 2007. Renal clearance of quantum dots. *Nat Biotechnol,* 25**,** 1165-70.

CLAPP, A. R., GOLDMAN, E. R. & MATTOUSSI, H. 2006. Capping of CdSe-ZnS quantum dots with DHLA and subsequent conjugation with proteins. *Nat Protoc,* 1**,** 1258-66.

CLARKE, C. & SMYTH, M. J. 2007. Calreticulin exposure increases cancer immunogenicity. *Nat Biotechnol,* 25**,** 192-3.

CUENCA, A. G., JIANG, H., HOCHWALD, S. N., DELANO, M., CANCE, W. G. & GROBMYER, S. R. 2006. Emerging implications of nanotechnology on cancer diagnostics and therapeutics. *Cancer,* 107**,** 459-66.

CUI, D., PAN, B., ZHANG, H., GAO, F., WU, R., WANG, J., HE, R. & ASAHI, T. 2008. Self-assembly of quantum dots and carbon nanotubes for ultrasensitive DNA and antigen detection. *Analytical chemistry,* 80**,** 7996-8001.

DANESHVAR, H., NELMS, J., MUHAMMAD, O., JACKSON, H., TKACH, J., DAVROS, W., PETERSON, T., VOGELBAUM, M. A., BRUCHEZ, M. P. &

TOMS, S. A. 2008. Imaging characteristics of zinc sulfide shell, cadmium telluride core quantum dots. *Nanomedicine (Lond),* 3**,** 21-9.

DE MEL, A., OH, J. T., RAMESH, B. & SEIFALIAN, A. M. 2012. Biofunctionalized quantum dots for live monitoring of stem cells: applications in regenerative medicine. *Regen Med,* 7**,** 335-47.

DEEN, W. M., LAZZARA, M. J. & MYERS, B. D. 2001. Structural determinants of glomerular permeability. *Am J Physiol Renal Physiol,* 281**,** F579-96.

DELEHANTY, J. B., MATTOUSSI, H. & MEDINTZ, I. L. 2009. Delivering quantum dots into cells: strategies, progress and remaining issues. *Anal Bioanal Chem,* 393**,** 1091-105.

DELEHANTY JB, M. I., PONS T, BRUNEL FM, DAWSON PE, MATTOUSSI H. 2006. Self-assembled quantum dot-peptide bioconjugates for selective intracellular delivery. *Bioconjug Chem,* 17**,** 920-927.

DERFUS AM, C. W., BHATIA SN 2003. Probing the cytotoxicity of semiconductor quantum dots. *Nano Letter,* 4**,** 11-18.

DUBERTRET, B., CALAME, M. & LIBCHABER, A. J. 2001. Single-mismatch detection using gold-quenched fluorescent oligonucleotides. *Nat Biotechnol,* 19**,** 365-70.

DUBERTRET, B., SKOURIDES, P., NORRIS, D. J., NOIREAUX, V., BRIVANLOU, A. H. & LIBCHABER, A. 2002. In vivo imaging of quantum dots encapsulated in phospholipid micelles. *Science,* 298**,** 1759-62.

FARMER, D. B. & GORDON, R. G. 2006. Atomic layer deposition on suspended single-walled carbon nanotubes via gas-phase noncovalent functionalization. *Nano Lett,* 6**,** 699-703.

FISCHER, H. C., LIU, L. C., PANG, K. S. & CHAN, W. C. W. 2006. Pharmacokinetics of nanoscale quantum dots: In vivo distribution, sequestration, and clearance in the rat. *Advanced Functional Materials,* 16**,** 1299-1305.

FISCHER HC, L. L., PANG KS, CHAN WC. 2006. Pharmacokinetics of nanoscale quantum dots: In vivo distribution, sequestration, andclearance in the rat. *Adv Funct Mater,* 16**,** 1299–1305.

FRANGIONI, J. V. 2003. In vivo near-infrared fluorescence imaging. *Curr Opin Chem Biol,* 7**,** 626-34.

GAO, X., CHAN, W. C. & NIE, S. 2002. Quantum-dot nanocrystals for ultrasensitive biological labeling and multicolor optical encoding. *J Biomed Opt,* 7**,** 532-7.

GAO, X., CUI, Y., LEVENSON, R. M., CHUNG, L. W. & NIE, S. 2004. In vivo cancer targeting and imaging with semiconductor quantum dots. *Nat Biotechnol,* 22**,** 969-76.

GOPEE NV, R. D., WEBB P, COZART CR, SIITONEN PH, WARBRITTON AR, YU WW, COLVIN VL, WALKER NJ, HOWARD PC. 2007. Migration of intradermally injected quantum dots to sentinel organs in mice. *Toxicol Sci,* 98**,** 249–257.

GREEN, M. & HOWMAN, E. 2005. Semiconductor quantum dots and free radical induced DNA nicking. *Chem Commun (Camb)***,** 121-3.

GU, W., PELLEGRINO, T., PARAK, W. J., BOUDREAU, R., LE GROS, M. A., ALIVISATOS, A. P. & LARABELL, C. A. 2007. Measuring cell motility using quantum dot probes. *Methods Mol Biol,* 374**,** 125-31.

GU, W., PELLEGRINO, T., PARAK, W. J., BOUDREAU, R., LE GROS, M. A., GERION, D., ALIVISATOS, A. P. & LARABELL, C. A. 2005. Quantum-dot-based cell motility assay. *Sci STKE,* 2005**,** pl5.

HAN, M., GAO, X., SU, J. Z. & NIE, S. 2001. Quantum-dot-tagged microbeads for multiplexed optical coding of biomolecules. *Nat Biotechnol,* 19**,** 631-5.

HANAKI, K., MOMO, A., OKU, T., KOMOTO, A., MAENOSONO, S., YAMAGUCHI, Y. & YAMAMOTO, K. 2003. Semiconductor quantum dot/albumin complex is a long-life and highly photostable endosome marker. *Biochem Biophys Res Commun,* 302**,** 496-501.

HARDMAN, R. 2006. A toxicologic review of quantum dots: toxicity depends on physicochemical and environmental factors. *Environ Health Perspect,* 114**,** 165-72.

HILD, W. A., BREUNIG, M. & GOEPFERICH, A. 2008. Quantum dots - nano-sized probes for the exploration of cellular and intracellular targeting. *Eur J Pharm Biopharm,* 68**,** 153-68.

HOPPER, C. 2000. Photodynamic therapy: a clinical reality in the treatment of cancer. *Lancet Oncol,* 1**,** 212-9.

HOSHINO A, F. K., OKU T, SUGA M, SAKAKI YF, YASUHARA M 2004a. Physico- chemical properties and cellular toxicity of nanocrystal quantum dots depend on their surface modification. *Nano Lett* 4**,** 63-9.

HOSHINO A, F. K., OKU T, SUGA M, SASAKI YF, OHTA T, YASUHARA M, & SUZUKI K, Y. K. 2004. Physicochemical properties and cellular toxicity of nanocrystal quantum dots depend on theirsurface modification. *Nano Lett,* 4**,** 2163-2169.

HOSHINO, A., FUJIOKA, K., OKU, T., NAKAMURA, S., SUGA, M., YAMAGUCHI, Y., SUZUKI, K., YASUHARA, M. & YAMAMOTO, K. 2004a. Quantum dots targeted to the assigned organelle in living cells. *Microbiol Immunol,* 48**,** 985-94.

HOSHINO, A., HANAKI, K., SUZUKI, K. & YAMAMOTO, K. 2004b. Applications of T-lymphoma labeled with fluorescent quantum dots to cell tracing markers in mouse body. *Biochem Biophys Res Commun,* 314**,** 46-53.

HOSHINO A, H. K., SUZUKI K, YAMAMOTO K. 2004b. Applications of T-lymphoma labeled with fluorescent quantum dots to celltracing markers in mouse body. *Biochem Biophys Res Commun,* 314**,** 46-53.

HUIFENG QIAN, C. D., JINLIANG PENG, XIN QIU, YUHONG XU, JICUN REN 2007. High-quality and water-soluble near-infrared photoluminescent CdHgTe/CdS quantum dots prepared by adjusting size and composition. *J. Phys. Chem,* 111**,** 16852-16857.

HULL, E. L., NICHOLS, M. G. & FOSTER, T. H. 1998. Localization of Luminescent Inhomogeneities in Turbid Media with Spatially Resolved Measurements of cw Diffuse Luminescence Emittance. *Appl Opt,* 37**,** 2755-65.

IGA, A. M., ROBERTSON, J. H., WINSLET, M. C. & SEIFALIAN, A. M. 2007. Clinical potential of quantum dots. *J Biomed Biotechnol,* 2007**,** 76087.

IPE, B. I., LEHNIG, M. & NIEMEYER, C. M. 2005. On the generation of free radical species from quantum dots. *Small,* 1**,** 706-9.

JAISWAL, J. K., MATTOUSSI, H., MAURO, J. M. & SIMON, S. M. 2003. Long-term multiple color imaging of live cells using quantum dot bioconjugates. *Nat Biotechnol,* 21**,** 47-51.

JAISWAL JK, M. H., MAURO JM, SIMON SM. 2003. Long term multiple color imaging of live cells using quantum dot bioconjugates. *Nat Biotechnol,* 21**,** 47-51.

JAMIESON, T., BAKHSHI, R., PETROVA, D., POCOCK, R., IMANI, M. & SEIFALIAN, A. M. 2007. Biological applications of quantum dots. *Biomaterials,* 28**,** 4717-32.

JIN, T., YOSHIOKA, Y., FUJII, F., KOMAI, Y., SEKI, J. & SEIYAMA, A. 2008. Gd3+-functionalized near-infrared quantum dots for in vivo dual modal (fluorescence/magnetic resonance) imaging. *Chem Commun (Camb)***,** 5764-6.

JOHN P. ZIMMER, S.-W. K., SHUNSUKE ONISHI, EICHII TANAKA, JOHN V. FRANGIONI,AND MOUNGI G. BAWENDI 2000. Size Series of Small Indium Arsenide-Zinc Selenide Core-Shell Nanocrystals and Their Application to In Vivo Imaging. *J Am Chem Soc,* 128**,** 2526-2527.

JUNLING DUAN, L. S., JINHUA ZHAN One-Pot Synthesis of Highly Luminescent CdTe Quantum Dots byMicrowave Irradiation Reduction and Their Hg2+-Sensitive Properties. *Department of Chemistry, Shandong University, China*.

JUZENAS, P., CHEN, W., SUN, Y. P., COELHO, M. A., GENERALOV, R., GENERALOVA, N. & CHRISTENSEN, I. L. 2008. Quantum dots and nanoparticles for photodynamic and radiation therapies of cancer. *Adv Drug Deliv Rev,* 60**,** 1600-14.

KIDANE, A. G., BURRIESCI, G., EDIRISINGHE, M., GHANBARI, H., BONHOEFFER, P. & SEIFALIAN, A. M. 2009. A novel nanocomposite polymer for development of synthetic heart valve leaflets. *Acta Biomater,* 5**,** 2409-17.

KIM, S., LIM, Y. T., SOLTESZ, E. G., DE GRAND, A. M., LEE, J., NAKAYAMA, A., PARKER, J. A., MIHALJEVIC, T., LAURENCE, R. G., DOR, D. M., COHN, L. H., BAWENDI, M. G. & FRANGIONI, J. V. 2004. Near-infrared fluorescent type II quantum dots for sentinel lymph node mapping. *Nat Biotechnol,* 22**,** 93-7.

KIRCHNER, C., LIEDL, T., KUDERA, S., PELLEGRINO, T., MUNOZ JAVIER, A., GAUB, H. E., STOLZLE, S., FERTIG, N. & PARAK, W. J. 2005. Cytotoxicity of colloidal CdSe and CdSe/ZnS nanoparticles. *Nano Lett,* 5**,** 331-8.

KLARREICH, E. 2001. Biologists join the dots. *Nature,* 413**,** 450-2.

KNOLL, J. H. 2007. Human metaphase chromosome FISH using quantum dot conjugates. *Methods Mol Biol,* 374**,** 55-66.

KOMARALA, V. K., RAKOVICH, Y. P., BRADLEY, A. L., BYRNE, S. J., CORR, S. A. & GUN'KO, Y. K. 2006. Emission properties of colloidal quantum dots on polyelectrolyte multilayers. *Nanotechnology,* 17**,** 4117-22.

LAGERHOLM, B. C. 2007. Peptide-mediated intracellular delivery of quantum dots. *Methods Mol Biol,* 374**,** 105-12.

LAKOWICZ, J. R., GRYCZYNSKI, I., GRYCZYNSKI, Z., NOWACZYK, K. & MURPHY, C. J. 2000. Time-resolved spectral observations of cadmium-enriched cadmium sulfide nanoparticles and the effects of DNA oligomer binding. *Anal Biochem,* 280**,** 128-36.

LARSON, D. R., ZIPFEL, W. R., WILLIAMS, R. M., CLARK, S. W., BRUCHEZ, M. P., WISE, F. W. & WEBB, W. W. 2003. Water-soluble quantum dots for multiphoton fluorescence imaging in vivo. *Science,* 300**,** 1434-6.

LEVSKY, J. M. & SINGER, R. H. 2003. Fluorescence in situ hybridization: past, present and future. *J Cell Sci,* 116**,** 2833-8.

LI, L., QIAN, H. & REN, J. 2005. Rapid synthesis of highly luminescent CdTe nanocrystals in the aqueous phase by microwave irradiation with controllable temperature. *Chem Commun (Camb)***,** 528-30.

LIANG LI, H. Q., NENGHU FANG, JICUN REN 2006. Significant enhancement of the quantumyield of CdTenanocrystalssynthesised in aqueousphase by controlling the pH and concentrations of precursor solutions. *Luminescence,* 116**,** 59-66.

LIN, P., CHEN, J. W., CHANG, L. W., WU, J. P., REDDING, L., CHANG, H., YEH, T. K., YANG, C. S., TSAI, M. H., WANG, H. J., KUO, Y. C. & YANG, R. S. 2008. Computational and ultrastructural toxicology of a nanoparticle, Quantum Dot 705, in mice. *Environ Sci Technol,* 42**,** 6264-70.

LIU, L., ZHANG, J., SU, X. & MASON, R. P. 2008. In vitro and In vivo Assessment of CdTe and CdHgTe Toxicity and Clearance. *J Biomed Nanotechnol,* 4**,** 524-528.

LOCKMAN, P. R., MUMPER, R. J., KHAN, M. A. & ALLEN, D. D. 2002. Nanoparticle technology for drug delivery across the blood-brain barrier. *Drug Dev Ind Pharm,* 28**,** 1-13.

LONGMIRE, M., CHOYKE, P. L. & KOBAYASHI, H. 2008. Clearance properties of nano-sized particles and molecules as imaging agents: considerations and caveats. *Nanomedicine (Lond),* 3**,** 703-17.

LOVRIC, J., BAZZI, H. S., CUIE, Y., FORTIN, G. R., WINNIK, F. M. & MAYSINGER, D. 2005a. Differences in subcellular distribution and toxicity of green and red emitting CdTe quantum dots. *J Mol Med (Berl),* 83**,** 377-85.

LOVRIC, J., CHO, S. J., WINNIK, F. M. & MAYSINGER, D. 2005b. Unmodified cadmium telluride quantum dots induce reactive oxygen species formation leading to multiple organelle damage and cell death. *Chem Biol,* 12**,** 1227-34.

LOVRIC J, C. S., WINNIK FM, MAYSINGER D. 2005. Unmodified cadmium telluride quantum dots induce reactive oxygen speciesformation leading to multiple organelle damage and cell death. *Chem Biol,* 12**,** 1227-1234.

MALAM, Y., LOIZIDOU, M. & SEIFALIAN, A. M. 2009. Liposomes and nanoparticles: nanosized vehicles for drug delivery in cancer. *Trends Pharmacol Sci,* 30**,** 592-9.

MATTHEAKIS, L. C., DIAS, J. M., CHOI, Y. J., GONG, J., BRUCHEZ, M. P., LIU, J. & WANG, E. 2004. Optical coding of mammalian cells using semiconductor quantum dots. *Anal Biochem,* 327**,** 200-8.

MAYSINGER, D., LOVRIC, J., EISENBERG, A. & SAVIC, R. 2007. Fate of micelles and quantum dots in cells. *Eur J Pharm Biopharm,* 65**,** 270-81.

MEDINTZ, I. L., CLAPP, A. R., MATTOUSSI, H., GOLDMAN, E. R., FISHER, B. & MAURO, J. M. 2003. Self-assembled nanoscale biosensors based on quantum dot FRET donors. *Nat Mater,* 2**,** 630-8.

NANN, T. 2005. Phase-transfer of CdSe@ZnS quantum dots using amphiphilic hyperbranched polyethylenimine{. *Chem Communication***,** 1735–1736.

NIDA, D. L., RAHMAN, M. S., CARLSON, K. D., RICHARDS-KORTUM, R. & FOLLEN, M. 2005. Fluorescent nanocrystals for use in early cervical cancer detection. *Gynecol Oncol,* 99**,** S89-94.

OBEID, M., TESNIERE, A., GHIRINGHELLI, F., FIMIA, G. M., APETOH, L., PERFETTINI, J. L., CASTEDO, M., MIGNOT, G., PANARETAKIS, T., CASARES, N., METIVIER, D., LAROCHETTE, N., VAN ENDERT, P., CICCOSANTI, F., PIACENTINI, M., ZITVOGEL, L. & KROEMER, G. 2007. Calreticulin exposure dictates the immunogenicity of cancer cell death. *Nature Medicine,* 13**,** 54-61.

OBERDORSTER, G., MAYNARD, A., DONALDSON, K., CASTRANOVA, V., FITZPATRICK, J., AUSMAN, K., CARTER, J., KARN, B., KREYLING, W., LAI, D., OLIN, S., MONTEIRO-RIVIERE, N., WARHEIT, D. & YANG, H.

2005. Principles for characterizing the potential human health effects from exposure to nanomaterials: elements of a screening strategy. *Part Fibre Toxicol,* 2**,** 8.

OGAWA, K. & KOBUKE, Y. 2008. Recent advances in two-photon photodynamic therapy. *Anticancer Agents Med Chem,* 8**,** 269-79.

OHLSON, M., SORENSSON, J., LINDSTROM, K., BLOM, A. M., FRIES, E. & HARALDSSON, B. 2001. Effects of filtration rate on the glomerular barrier and clearance of four differently shaped molecules. *Am J Physiol Renal Physiol,* 281**,** F103-13.

ORNBERG, R. L. & LIU, H. 2007. Immunofluorescent labeling of proteins in cultured cells with quantum dot secondary antibody conjugates. *Methods Mol Biol,* 374**,** 3-10.

PATHAK, S., CHOI, S. K., ARNHEIM, N. & THOMPSON, M. E. 2001. Hydroxylated quantum dots as luminescent probes for in situ hybridization. *J Am Chem Soc,* 123**,** 4103-4.

PATOLSKY, F., GILL, R., WEIZMANN, Y., MOKARI, T., BANIN, U. & WILLNER, I. 2003. Lighting-up the dynamics of telomerization and DNA replication by CdSe-ZnS quantum dots. *J Am Chem Soc,* 125**,** 13918-9.

PELLEGRINO, T., PARAK, W. J., BOUDREAU, R., LE GROS, M. A., GERION, D., ALIVISATOS, A. P. & LARABELL, C. A. 2003. Quantum dot-based cell motility assay. *Differentiation,* 71**,** 542-8.

PELLEY, J. L., DAAR, A. S. & SANER, M. A. 2009. State of academic knowledge on toxicity and biological fate of quantum dots. *Toxicol Sci,* 112**,** 276-96.

PENG, Z. A. & PENG, X. 2001. Formation of high-quality CdTe, CdSe, and CdS nanocrystals using CdO as precursor. *J Am Chem Soc,* 123**,** 183-4.

PINAUD, F., MICHALET, X., BENTOLILA, L. A., TSAY, J. M., DOOSE, S., LI, J. J., IYER, G. & WEISS, S. 2006. Advances in fluorescence imaging with quantum dot bio-probes. *Biomaterials,* 27**,** 1679-87.

PINAUD, F., MICHALET, X., IYER, G., MARGEAT, E., MOORE, H. P. & WEISS, S. 2009. Dynamic partitioning of a glycosyl-phosphatidylinositol-anchored protein in glycosphingolipid-rich microdomains imaged by single-quantum dot tracking. *Traffic,* 10**,** 691-712.

POPESCU, M. A. & TOMS, S. A. 2006. In vivo optical imaging using quantum dots for the management of brain tumors. *Expert Rev Mol Diagn,* 6**,** 879-90.

R. ROSSETTI, L. B. 1982. Electron-Hole Recombination Emission as a Probe of Surface Chemistry in AqueousCdS Colloids. *J. Phys. Chem,* 86**,** 4470-2.

RAO, J., DRAGULESCU-ANDRASI, A. & YAO, H. 2007. Fluorescence imaging in vivo: recent advances. *Curr Opin Biotechnol,* 18**,** 17-25.

RIZVI, S. B., GHADERI, S., KESHTGAR, M. & SEIFALIAN, A. M. 2010. Semiconductor quantum dots as fluorescent probes for in vitro and in vivo bio-molecular and cellular imaging. *Nano Rev,* 1**,** 5161-76.

ROCKSBY, H. P. 1932. Color of selenium ruby glasses *J. Soc. Glass Technol,* 16**,** 171.

ROSEN, A. B., KELLY, D. J., SCHULDT, A. J., LU, J., POTAPOVA, I. A., DORONIN, S. V., ROBICHAUD, K. J., ROBINSON, R. B., ROSEN, M. R., BRINK, P. R., GAUDETTE, G. R. & COHEN, I. S. 2007. Finding fluorescent needles in the cardiac haystack: tracking human mesenchymal stem cells labeled with quantum dots for quantitative in vivo three-dimensional fluorescence analysis. *Stem Cells,* 25**,** 2128-38.

ROSENTHAL, S. J., CHANG, J. C., KOVTUN, O., MCBRIDE, J. R. & TOMLINSON, I. D. 2011. Biocompatible quantum dots for biological applications. *Chem Biol,* 18**,** 10-24.

RYMAN-RASMUSSEN, J. P., RIVIERE, J. E. & MONTEIRO-RIVIERE, N. A. 2007. Surface coatings determine cytotoxicity and irritation potential of quantum dot nanoparticles in epidermal keratinocytes. *J Invest Dermatol,* 127**,** 143-53.

SAMIA, A. C., CHEN, X. & BURDA, C. 2003. Semiconductor quantum dots for photodynamic therapy. *J Am Chem Soc,* 125**,** 15736-7.

SAMIA, A. C., DAYAL, S. & BURDA, C. 2006. Quantum dot-based energy transfer: perspectives and potential for applications in photodynamic therapy. *Photochem Photobiol,* 82**,** 617-25.

SCHIPPER, M. L., CHENG, Z., LEE, S. W., BENTOLILA, L. A., IYER, G., RAO, J., CHEN, X., WU, A. M., WEISS, S. & GAMBHIR, S. S. 2007. microPET-based biodistribution of quantum dots in living mice. *J Nucl Med,* 48**,** 1511-8.

SCHIPPER ML, C. Z., LEE SW, BENTOLILA LA, IYER G, RAO J, CHEN X, WU AM, WEISS S, GAMBHIR SS. 2007. microPET-based biodistribution of quantum dots in living mice. *J Nucl Med,* 48**,** 1511-1518.

SCHROEDER, J. E., SHWEKY, I., SHMEEDA, H., BANIN, U. & GABIZON, A. 2007. Folate-mediated tumor cell uptake of quantum dots entrapped in lipid nanoparticles. *J Control Release,* 124**,** 28-34.

SEIFALIAN, A. M., SALACINSKI, H. J., PUNSHON, G., KRIJGSMAN, B. & HAMILTON, G. 2001. A new technique for measuring the cell growth and metabolism of endothelial cells seeded on vascular prostheses. *J Biomed Mater Res,* 55**,** 637-44.

SHAH, B. S., CLARK, P. A., MOIOLI, E. K., STROSCIO, M. A. & MAO, J. J. 2007. Labeling of mesenchymal stem cells by bioconjugated quantum dots. *Nano Lett,* 7**,** 3071-9.

SHI, L., DE PAOLI, V., ROSENZWEIG, N. & ROSENZWEIG, Z. 2006. Synthesis and application of quantum dots FRET-based protease sensors. *J Am Chem Soc,* 128**,** 10378-9.

SHIOHARA A, H. A., HANAKI K, SUZUKI K, YAMAMOTO K. 2004. On the cyto-toxicity caused by quantum dots. *Microbiol Immunol,* 48**,** 669-675.

SHIOHARA, A., HOSHINO, A., HANAKI, K., SUZUKI, K. & YAMAMOTO, K. 2004. On the cyto-toxicity caused by quantum dots. *Microbiol Immunol,* 48**,** 669-75.

SHIRIN GHADERI, B. R., MARELINA LOIZIDOU, SHI-YU YANG, ALEXANDER SEIFALIAN 2012. Development and in vitro Toxicity Assessment of Next Generation Biocompatible Near infrared Quantum Dots for Biomedical Application. *Journal of nanoscience and nanotechnology (JNN)*.

SINHA, R., KIM, G. J., NIE, S. & SHIN, D. M. 2006. Nanotechnology in cancer therapeutics: bioconjugated nanoparticles for drug delivery. *Mol Cancer Ther,* 5**,** 1909-17.

SMITH, A. M., DUAN, H., MOHS, A. M. & NIE, S. 2008a. Bioconjugated quantum dots for in vivo molecular and cellular imaging. *Adv Drug Deliv Rev,* 60**,** 1226-40.

SMITH, A. M., DUAN, H., RHYNER, M. N., RUAN, G. & NIE, S. 2006. A systematic examination of surface coatings on the optical and chemical properties of semiconductor quantum dots. *Phys Chem Chem Phys,* 8**,** 3895-903.

SMITH, B. R., CHENG, Z., DE, A., KOH, A. L., SINCLAIR, R. & GAMBHIR, S. S. 2008b. Real-time intravital imaging of RGD-quantum dot binding to luminal endothelium in mouse tumor neovasculature. *Nano Lett,* 8**,** 2599-606.

SO, M. K., XU, C., LOENING, A. M., GAMBHIR, S. S. & RAO, J. 2006. Self-illuminating quantum dot conjugates for in vivo imaging. *Nat Biotechnol,* 24**,** 339-43.

STROH, M., ZIMMER, J. P., DUDA, D. G., LEVCHENKO, T. S., COHEN, K. S., BROWN, E. B., SCADDEN, D. T., TORCHILIN, V. P., BAWENDI, M. G., FUKUMURA, D. & JAIN, R. K. 2005. Quantum dots spectrally distinguish multiple species within the tumor milieu in vivo. *Nature Medicine,* 11**,** 678-82.

SU, W., HUANG, X., LI, J. & FU, H. 2002. Crystal of semiconducting quantum dots built on covalently bonded t5 [in(28)cd(6)s(54)](-12): the largest supertetrahedral cluster in solid state. *J Am Chem Soc,* 124**,** 12944-5.

SU Y, H. Y., LU H, SAI L, LI Q, LI W, WANG L, SHEN P, HUANG Q, FAN C. 2009. The cytotoxicity of cadmium based, aqueous phase -synthesised, quantum dots and its modulation by surface coating.. *Biomaterials,* 30**,** 19-25.

TANG M, X. T., ZENG J, WANG H, LI C, YIN S, YAN D, DENG H, LIU J, WANG M, CHEN J, RUAN DY. 2008. Unmodified CdSe quantum dots induce elevation of cytoplasmic calcium levels and impairment of functional properties of sodium channels in rat primary culturedhippocampal neurons. . *Environ Health Perspect,* 116**,** 915-922.

THORNE, R. G. & NICHOLSON, C. 2006. In vivo diffusion analysis with quantum dots and dextrans predicts the width of brain extracellular space. *Proc Natl Acad Sci U S A,* 103**,** 5567-72.

THURSTON, D. E. 2006. DNA- Interactive Agents. *Chemistry and Pharmacology of Anticancer Drugs.* CRC Press.

TONKS, N. K. 2005. Redox redux: revisiting PTPs and the control of cell signaling. *Cell,* 121**,** 667-70.

UYEDA, H. T., MEDINTZ, I. L., JAISWAL, J. K., SIMON, S. M. & MATTOUSSI, H. 2005. Synthesis of compact multidentate ligands to prepare stable hydrophilic quantum dot fluorophores. *J Am Chem Soc,* 127**,** 3870-8.

VOURA, E. B., JAISWAL, J. K., MATTOUSSI, H. & SIMON, S. M. 2004. Tracking metastatic tumor cell extravasation with quantum dot nanocrystals and fluorescence emission-scanning microscopy. *Nature Medicine,* 10**,** 993-8.

WANG L, N. D., SELVARASAH S, DOKMECI MR, CARRIER RL. 2008. Toxicity of CdSe Nanoparticles in Caco-2 Cell Cultures.. *J Nanobiotechnology,* 6**,** 11.

WANG, S. & MARCHANT, R. E. 2004. Fluorocarbon Surfactant Polymers: Effect of Perfluorocarbon Branch Density on Surface Active Properties. *Macromolecules,* 37**,** 3353-3359.

WANG, X. S., DYKSTRA, T. E., SALVADOR, M. R., MANNERS, I., SCHOLES, G. D. & WINNIK, M. A. 2004. Surface passivation of luminescent colloidal quantum dots with poly(dimethylaminoethyl methacrylate) through a ligand exchange process. *J Am Chem Soc,* 126**,** 7784-5.

WELLER., H. 1993. Colloidal Semiconductor Q-Particles: Chemistry in the Transition Region Between Solid State and Molecules. *Chem Int Ed Eng,* 32**,** 42-53.

WENG, J. & REN, J. 2006. Luminescent quantum dots: a very attractive and promising tool in biomedicine. *Curr Med Chem,* 13**,** 897-909.

WHALEY, S. R., ENGLISH, D. S., HU, E. L., BARBARA, P. F. & BELCHER, A. M. 2000. Selection of peptides with semiconductor binding specificity for directed nanocrystal assembly. *Nature,* 405**,** 665-8.

WILLIAMS, Y., BYRNE, S., BASHIR, M., DAVIES, A., WHELAN, A., GUN'KO, Y., KELLEHER, D. & VOLKOV, Y. 2008. Comparison of three cell fixation methods for high content analysis assays utilizing quantum dots. *J Microsc,* 232**,** 91-8.

WOLL AR, R. P., LAGALLY MG 2002. Quantum Dots. *Int. J. High Speed Electron,* 12**,** 45-78.

WOODWARD JD, K. S., MIRZADEH S, DAI S, WALL JS, RICHEY T, & AVENELL J, R. A. 2007. In vivo SPECT/CT imaging and biodistribution using radioactive (CdTe)-Te-125m/ZnSnanoparticles. *Nanotechnology,* 18**,** 175103-175108.

WU, X., LIU, H., LIU, J., HALEY, K. N., TREADWAY, J. A., LARSON, J. P., GE, N., PEALE, F. & BRUCHEZ, M. P. 2003. Immunofluorescent labeling of cancer marker Her2 and other cellular targets with semiconductor quantum dots. *Nat Biotechnol,* 21**,** 41-6.

XIAO, Y. & BARKER, P. E. 2004. Semiconductor nanocrystal probes for human metaphase chromosomes. *Nucleic Acids Res,* 32**,** e28.

XING, Y., XIA, Z. & RAO, J. 2009. Semiconductor quantum dots for biosensing and in vivo imaging. *IEEE Trans Nanobioscience,* 8**,** 4-12.

XIONG, L., CHEN, Z., TIAN, Q., CAO, T., XU, C. & LI, F. 2009. High contrast upconversion luminescence targeted imaging in vivo using peptide-labeled nanophosphors. *Analytical chemistry,* 81**,** 8687-94.

YAGHINI, E., SEIFALIAN, A. M. & MACROBERT, A. J. 2009. Quantum dots and their potential biomedical applications in photosensitization for photodynamic therapy. *Nanomedicine (Lond),* 4**,** 353-63.

YAO HE, L.-M. S., HAO-TING LU, MEI HU, WEN-YONG LAI, QU-LI FAN, & LIAN-HUI WANG, W. H. 2007. Microwave-Assisted Synthesis of Water-Dispersed CdTeNanocrystals with High Luminescent Efficiency and Narrow SizeDistribution. *Chem. Mater,* 19**,** 359-365.

YAO HE, L.-M. S., HAO-TING LU, MEI HU, WEN-YONG LAI, QU-LI FAN, LIAN-HUI WANG, AND WEI HUANG 2007. Microwave-Assisted Synthesis of Water-Dispersed CdTe Nanocrystals with High Luminescent Efficiency and Narrow Size Distribution. *Chem. Mater,* 19.

YING, E., LI, D., GUO, S., DONG, S. & WANG, J. 2008. Synthesis and bio-imaging application of highly luminescent mercaptosuccinic acid-coated CdTe nanocrystals. *PLoS One,* 3**,** e2222.

YU, W. W. 2008. Semiconductor quantum dots: synthesis and water-solubilization for biomedical applications. *Expert Opin Biol Ther,* 8**,** 1571-81.

ZHANG, B., BOWERMAN, N. A., SALAMA, J. K., SCHMIDT, H., SPIOTTO, M. T., SCHIETINGER, A., YU, P., FU, Y. X., WEICHSELBAUM, R. R., ROWLEY, D. A., KRANZ, D. M. & SCHREIBER, H. 2007. Induced sensitization of tumor stroma leads to eradication of established cancer by T cells. *J Exp Med,* 204**,** 49-55.

ZHANG, C. Y., YEH, H. C., KUROKI, M. T. & WANG, T. H. 2005. Single-quantum-dot-based DNA nanosensor. *Nat Mater,* 4**,** 826-31.

ZHANG, H., YEE, D. & WANG, C. 2008a. Quantum dots for cancer diagnosis and therapy: biological and clinical perspectives. *Nanomedicine (Lond),* 3**,** 83-91.

ZHANG, L. W., YU, W. W., COLVIN, V. L. & MONTEIRO-RIVIERE, N. A. 2008b. Biological interactions of quantum dot nanoparticles in skin and in human epidermal keratinocytes. *Toxicol Appl Pharmacol,* 228**,** 200-11.

ZHANG T, S. J., GERION D, DING L, ELBOUDWAREJ O, COOKE PA, GRAY JW, ALIVISATOS AP, CHEN FF. 2006. Cellular effect of high doses of silica-coated quantum dot profiled with high throughput geneexpression analysis and high content cellomics measurements.. *Nano Lett,* 6**,** 800-808.

ZHANG Y, C. W., ZHANG J, LIU J, CHEN G, POPE C. 2007. In vitro and in vivo toxicity of CdTe nanoparticles. . *J Nanosci Nanotechnol,* 7**,** 497–503.

ZHAO, Y., YE, M., CHAO, Q., JIA, N., GE, Y. & SHEN, H. 2009. Simultaneous detection of multifood-borne pathogenic bacteria based on functionalized quantum dots coupled with immunomagnetic separation in food samples. *J Agric Food Chem,* 57**,** 517-24.

ZHENG, J., NICOVICH, P. R. & DICKSON, R. M. 2007. Highly fluorescent noble-metal quantum dots. *Annu Rev Phys Chem,* 58**,** 409-31.

ZHOU, M. & GHOSH, I. 2007. Quantum dots and peptides: a bright future together. *Biopolymers,* 88**,** 325-39.

ZIMMER, J. P., KIM, S. W., OHNISHI, S., TANAKA, E., FRANGIONI, J. V. & BAWENDI, M. G. 2006. Size series of small indium arsenide-zinc selenide core-shell nanocrystals and their application to in vivo imaging. *J Am Chem Soc,* 128**,** 2526-7.

ZIMMER JP, K. S., OHNISHI S, TANAKA E, FRANGIONI JV, BAWENDI MG. 2006. Size series of small indium arsenide-zinc selenide core-shell nanocrystals and their application to in vivo imaging. *J Am Chem Soc,* 128**,** 2526–2527.

ZITZMANN, S., EHEMANN, V. & SCHWAB, M. 2002. Arginine-glycine-aspartic acid (RGD)-peptide binds to both tumor and tumor-endothelial cells in vivo. *Cancer Research,* 62**,** 5139-5143.

Appendices

1. Cobalt Doped Quantum Dots for Multiplex Imaging (MRI)

The success of biocompatible QD synthesis doped with cobalt for multimodality MRI and photoluminescence offers the integration into a single probe.

Multiplex imaging using contrast agents based on water soluble highly luminescent and NIR QDs incorporating magnetic nanoparticles offers a novel class of materials for bio-imaging. Incorporating three functionalities in a single nanocrystal offers a sensitive imaging agent for three powerful and complementary imaging techniques (fluorescence and NIR) and magnetic resonance (MRI).

The development of a one-pot synthesis where all three functionalities (fluorescence, infrared and paramagnetic ions can be integrated into QDs (CdTeCoHg). This approach has demonstrated the potential use of QDs for bio-imaging in cancer studies. In addition using the novel surface chemistry, potential drug delivery and targeting can be applied (Popescu and Toms, 2006, Daneshvar et al., 2008) (**Figure A.1**). In image-guided surgical applications, a surgeon relies on information gathered from preoperative MRI or sometimes CT. The development of dual-modality contrast agents that can be visualized by standard imaging techniques such as MRI in preoperative image acquisition and by optical techniques during surgery such as tumor localization has obvious advantages.

The current water-soluble NIR QD containing paramagnetic particles can be detected and visualized by MRI and has potential modifications that could optimize imaging in clinically relevant system such as MRI.

In image-guide surgery applications, a surgeon relies on information gathered from preoperative MRI or sometimes CT. The development of dual-modality contrast agents that can be visualized by standard imaging techniques such as MRI in preoperative image acquisition and by optical techniques during surgery such as tumor localization has obvious advantages.

Finally, our current water-soluble QD containing paramagnetic particles can be detectable and visualized by MIR and has potential modifications that could optimize imaging in clinically relevant system such as MRI.

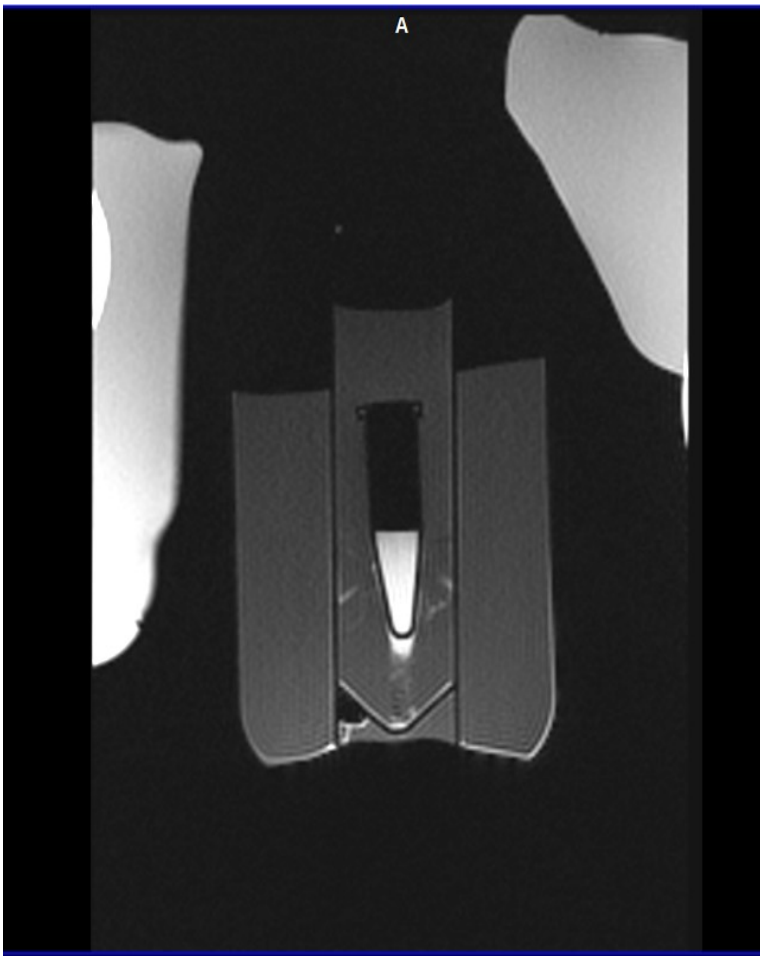

Figure A.1: Agra phantom of QD was developed and imaged with MRI.
The electron dense core of the CdCoTe/MSA and cobalt containing in the structure of QD, made the detection of the QD phantoms possible with MRI

2. Phantom Design

Synthesised CdCoTe/MSA QD with emission wavelength of 630 nm was diluted into 1 μM concentration in phosphate-buffer saline and was placed in 1.5 mL eppendorf tube. The QD-containing tube was then packed in plastic container contacting agar to mimic the density of human tissues. The images were carried out at Royal Holloway University, MRI unit (Siemens).

In conclusion this preliminary data revealed interesting data and will be applicable for development of multimodal imaging application.